Study of Quantum Transport at the Metal-Insulator Transition in Falicov-Kimball Model within Alloy Analogy

By

Prosenjit Haldar

PHYS10201204006

The Institute of Mathematical Sciences, Chennai

A thesis submitted to the

Board of Studies in Physical Sciences

In partial fulfillment of requirements

For the Degree of

DOCTOR OF PHILOSOPHY

of

HOMI BHABHA NATIONAL INSTITUTE

August, 2017

STATEMENT BY AUTHOR

This dissertation has been submitted in partial fulfillment of requirements for an advanced degree at Homi Bhabha National Institute (HBNI) and is deposited in the Library to be made available to borrowers under rules of the HBNI.

Brief quotations from this dissertation are allowable without special permission, provided that accurate acknowledgement of source is made. Requests for permission for extended quotation from or reproduction of this manuscript in whole or in part may be granted by the Competent Authority of HBNI when in his or her judgement the proposed use of the material is in the interests of scholarship. In all other instances, however, permission must be obtained from the author.

Prosenjit Haldar

DECLARATION

I, hereby declare that the investigation presented in the thesis has been carried out by me. The work is original and has not been submitted earlier as a whole or in part for a degree / diploma at this or any other Institution / University.

Prosenjit Haldar

List of Publications arising from the thesis

This thesis is based on the following publications:

Published:

(1) **P. Haldar**, Mukul S. Laad, S. R. Hassan, "Quantum critical transport at a continuous metal-insulator transition", Phys. Rev. B **94**, 081115 (R) (2016).

(2) **P. Haldar**, Mukul S. Laad, S. R. Hassan, "Real-space cluster dynamical mean-field approach to the Falicov-Kimball model: An alloy-analogy approach", Phys. Rev. B **95**, 125116 (2017).

Sent for Publication:

(1) **P. Haldar**, Mukul S. Laad, S. R. Hassan, Madhabi Chand, Pratap Raychaudhuri, "Quantum Critical Magneto-transport at a Continuous Metal-Insulator Transition ", Submitted to Phys. Rev. B.

(2) **P. Haldar**, Mukul S. Laad, S. R. Hassan, "Thermal Transport across a Continuous Metal-Insulator Transition", Submitted to Phys. Rev. B.

(3) **P. Haldar**, Mukul S. Laad, S. R. Hassan, "Universal Dielectric Response Across A Continuous Metal-Insulator Transition", Preparing for Submitting to Phys. Rev. B.

Prosenjit Haldar

DEDICATIONS

To my chhoto-didi (Chhandita) who
sacrifices a lot for me

ACKNOWLEDGEMENTS

After five very eventful years, I would like to thank all who have paved the path of achieving such a milestone with all their help, support and criticism!

Foremost, I am deeply grateful to my friend, philosopher and supervisor Prof. S. R. Hassan who guided me throughout my whole PhD work in both academic and non-academic issues. He has been an inspiring teacher, a hands-on supervisor and a caring mentor. He always stands by me at my ups and downs during Ph.D. I hope to carry with me his sincere and honest approach to science.

I would like to convey a special thank to Prof. R. Shankar who has been a steady and constant inspiration to me. I always enjoyed discussing with him. I feel very lucky to get opportunity to work with him.

I am very grateful to Prof. M. S. Laad who appeared to me like my elder brother. I have learnt a lot from him while working with him in last two and half years.

I am indebted to Prof. G. Baskaran and Prof. R. Ganesh with whom I have had some of the most useful discussions. I would also like to thank two of my experimentalist collaborators Prof. Pratap Raychaudhuri and Dr. Madhavi Chand at TIFR, Mumbai, who have made the thesis possible.

A sincere gratitude to Prof. Arti Garg at SINP, Kolkata whom I have visited last year. I would like to thank other members of my Doctoral Committee, Prof. Bala Sathiapalan, Prof. Ronojoy Adhikary and Prof. Sibasish Ghosh for their constant encouragement and support.

I sincerely thank all the course instructors in my Ph.D. course-work, Prof. Nemani Suryanarayana, Prof. Rajesh Ravindran, Prof. Ramesh Anishetty, Prof. M.V.N. Murthy, Prof.

Purusattam Ray for delivering such great lectures and the members of my Monitoring Committee, Prof. Indumathi D, Prof. Sujay Ashok and Prof. Sanatan Digal. Special thanks to Prof. Indumathi D and Prof. Purusattam Ray for standing by me at my tough times during Ph.D. I also thank all the faculty members of IMSc for creating such a wonderful research environment.

I am really grateful to all the group members of condensed matter physics at IMSc for their help and cooperation, especially to, Arya S, Jesrael K. Mani, Shanu Karmakar, Subhankar Khatua, Srivastava N.S. I have enlarged my knowledge by fruitful discussions with them. I would like to thank all the Ph.D. students at IMSc for making my graduate study prosperous and really enjoyable. A few special of them are Rajesh Singh who helped me a lot at my beginning stage of learning numerical computations, Atanu Bhatta, Arnab Priya Saha and Amlan Chakraborti who have been mentally supporting me throughout my entire graduate study.

I would like to thank the computer staff, the library staff for providing help at all the time during my research and administration, other non-academic stuff for making my stay at the Institute pleasant and enjoyable.

I would also like to thank all my family members, especially my mother, my elder sisters and my late father for their sacrifices and encouragement in building up my academic career. I thank my fiancé, Puja Mondal for constantly supporting me in last five years.

Last but not the least, I would like to express my love to all my friends and relatives for their help, love and support to me since my childhood.

Contents

Synopsis

Continuous Mott transitions are a rarity in condensed matter. In contrast to their generic first-order character, the Mott transition in the spinless Falicov-Kimball Model (FKM) is continuous, and hence expected to be one of the few models that rigorously display "Mott quantum criticality". Many studies, including Dynamical Mean Field Theory (DMFT) [38] and its cluster extensions [61] have been used in this context.

In another vein, the FKM is also long known to be isomorphic to a binary-alloy Anderson disorder model, where the quantum criticality associated with the metal-insulator transition (MIT) has also been extensively studied.

On both counts above, however, the important question of the role of short-range spatial correlations on the (DMFT) MIT has long been an open and important issue. Usually, the problem is complicated because of involved numerics, which many times also obscures physical insight. This is especially so in the strong coupling limit, where perturbation theory breaks down.

This thesis discusses the five parts - (a) Study of Falicov-Kimball Model (FKM) within alloy analogy using cluster DMFT (CDMFT) technique (b) Study of quantum criticality of dc conductivity at a continuous metal-insulator transition (c) Study of quantum criticality of magneto-transport at a continuous metal-insulator transition (d) Thermal transport across a continuous metal-insulator transition and (e) Optical conductivity and universal

dielectric response at the continuous metal-insulator transition

Real-Space Cluster-Dynamical Mean Field Approach to the Falicov-Kimball Model: An alloy-analogy approach

The Hamiltonian for the spin-less FKM is given as,

$$H_{FK} = -t \sum_{\langle ij \rangle} c_i^\dagger c_j + \mu \sum_i c_i^\dagger c_i + U \sum_i n_{id} n_{ic}$$

$c_i(c_i^\dagger), c_i(c_i^\dagger)$ are the fermion annihilation (creation) operators in dispersive band(c) and the non-dispersion state(d) respectively, t is the one electron hopping integral and U is the onsite repulsion between c and d electrons. Since, $n_{id} = 0, 1$, $v_i = U n_{id}$ can be viewed as a static disorder potential for the c-fermions with binary distribution given as, $P(v_i) = (1-x)\delta(v_i - v_A) + x\delta(v_i - v_B)$ with $v_A = 0$ and $v_B = U$. The short range order (SRO) between nearest neighbour disorder is: $f_{ij} = \langle v_i v_j \rangle - \langle v_i \rangle \langle v_j \rangle = C$, a constant parameter.

The FKM has been studied in details within alloy approximation using analytic cluster extensions of DMFT (CDMFT) exact-to-order-1/d, where d is the system dimensionality. The short range spatial correlations also considered explicitly in the CDMFT technique. So our scheme allows direct physical insight to be gained at much more modest numerical cost. It can also be used as an advanced approximation supplanting Coherent Potential Approximation (CPA) for disordered binary alloys in the context of ab-initio electronic structure calculations for disordered systems.

We calculated local Green function, self energy with no violation of the causality. We also computed cluster momentum dependent Green function, self energy and two particle irreducible vertex function. The vertex function shows clear non-analyticities before the band splitting transition of the Hubbard type occurs, signalling onset of an unusual type of localization at the strong coupling. We also studied effect of SRO on the MIT by applying

finite "antiferro alloy" SRO, $f_{0\alpha} = \langle x_0 x_\alpha \rangle - \langle x_0 \rangle \langle x_\alpha \rangle = -0.15$. We found MIT occurs at lower value of U compare to fully random case ($f_{0\alpha} = 0$).

However, our cluster extension also allows us to study two-particle response function related to density fluctuations in detail. We find that this shows anomalous power-law behaviour at strong coupling BEFORE the MIT occurs. More implications of this result is used to study the long-time response to a sudden local quench. from which we propose that the localization at strong coupling is of a novel type, and that it may be related to a kind of many-body localization. However, we have not studied this aspect, which we have left for the future.

Quantum Criticality of DC Conductivity across the Continuous Metal-Insulator Transition

Across continuous MITs, transport properties, in particular, electrical transport, is expected to reveal the quantum criticality in an especially clear way, as has long been known in the case of the Anderson disorder model. On the other hand, such quantum criticality remains to be investigated in models with electronic correlations, especially ion strong-coupling regimes, where no perturbative solutions are expected to work. These problems supply the motivation for our present work, which studies "Mott" quantum criticality across the MIT in a simplest model for correlated fermions, namely FKM.

Using our recently developed exact-to-order 1/d cluster-DMFT technique, we present an exact description of the transport quantum criticality for the FKM. The main features that stand out are:

(i) dc resistivity exhibits striking features with increasing correlations, going over from a "dirty Fermi liquid" at small U, via an unusual bad metal at intermediate U, to a bad-insulator-like or very bad metal for U close to the critical value where the continuous Mott

transition occurs in CDMFT.

(ii) upon careful scaling, we find that clear mirror-symmetry of scaled resistivity, driven by unusual form of the beta-function (or Gell-Mann-Low function in field theory) of the form $\beta(g) \sim log(g)$, with g is a scaled conductance, obtains. This is very different from the form expected at a non-interacting Anderson transition. We find that a scenario of Mott-like quantum criticality naturally accounts for these findings. More consequences of this analysis are: (1) novel symmetry relations between the conductivity and resistivity on the two sides of the MIT, (2) clear emergence of a low-energy scale (T_0), which vanishes precisely at the MIT as a power law on both sides of the Mott QCP, (3) extraction of the critical exponents z and ν from microscopic calculations, which seem to be in the right value range compared to experiment.

It can also be used for analysing experimental results in a variety of interesting systems: in particular, the close similarity between our results and the famous experiments of Kravchenko et al (in 1995) lend support to this argument.

Quantum Critical Magneto-transport at the Continuous Metal-Insulator Transition

We study magneto-transport and the issue of Mott quantum criticality reflected in magneto-transport studies across a continuous MIT, which has long been an interesting issue in the literature. In perturbative approaches to Anderson disorder problems, the Hall constant is T-independent and non-critical at the MIT. However, a range of real materials like GeSb and P-doped Si do exhibit both, the critical scaling of the Hall constant, as well as breakdown of the weak localization predictions, at the MIT. This necessitates either introduction of electron electron interactions, or consideration of non-perturbative approaches to solve the strong scattering problem. Using our recently developed exact-to-order 1/d

cluster-DMFT technique, we present an exact description of the transport quantum criticality for the FKM. The main features that stand out are:

(i) the off-diagonal conductivity shows clear and anomalous behaviour near the MIT. Correspondingly, the Hall constant exhibits striking T-dependence, at variance with perturbative predictions. Since we nevertheless find that (1) $R_H(T)$ is finite in the metal, but (2) diverges in the insulator, the issue is whether an underlying quantum criticality also underpins off-diagonal conductivity and Hall effect. (ii) To test this, we perform a scaling procedure for the Hall conductivity in a way similar to that used for the dc transport in earlier works. A remarkable finding of this work is that the "mirror symmetry" and Mott-like beta-function, features characteristic of Mott criticality, are also cleanly reflected in the scaled magneto-conductivity around the continuous MIT. This leads to other very interesting consequences, which we also find to excellent precision: (1) satisfaction of a rigorous "symmetry" arguments relating the scaled off-diagonal conductivity to its inverse across the MIT, and (2) universal scaling behaviour for the scaled off-diagonal conductivity as a function of an appropriately chosen "scaling function".

Moreover we found $\frac{\Delta R_H/R_H}{\Delta\rho_{xx}/\rho_{xx}}$ achieves values between 0.5 and 0.8 close to the MIT whcih is largly contradict to the prediction of weak localization theory (in weak localization theory the ratio to be equals to 2). But out calculated ratio is in good accord with the recent study by Chand *et. al.* on NbN [23] in strongly disorder region where they found the ratio to be 0.69. Motivated by this we re-analysed their data and study the quantum criticality near the critical point ($k_F l \sim 1$). We found the universal scaling function for both diagonal and off-diagonal conductivity and the quantum critical exponent $z\nu$ to be 1.285 which is very close to our theoretical value. This provides good experimental support to our formalism and results, showing that such features are characteristic of a "strong scattering" regime, where perturbative theories are inadequate.

Thermal Transport across the Continuous Metal-Insulator Transition

Like electrical conductivity and Hall conductivity thermal transport is also play an vital role in numerous applications of thermoelectric materials. The control of these properties is a key goal in material design which motivates us to study thermal transport of the system with binary disorder potential or equivalent FKM.

On the otherhand according to Wiedemann-Franz (WF) law in metals at low tempare-ture the electrical conductivity ($\sigma_{xx}(T)$) and thermal conductivity ($K(T)$) related via the universal Lorentz number, $L_0 = \frac{K(T)}{T\sigma_{xx}(T)} = \frac{\pi^2 k_B^2}{3e^2}$ as long as interactions between electrons preserve their fermion-quasiparticle character. We study thermal transport and the fate of the WF law close to a continuous MIT in the FKM using CDMFT technique within alloy analogy approximation. Surprisingly, as for electrical transport, we find robust and novel quantum critical scaling in thermal transport (thermopower, thermal conductivity and Lorentz number) across the MIT. We have also calculated corresponding quantum critical exponent and show that, $\beta_{th}(s) = d[log(s)]/d[log(T)] \approx log(s)$ on both sides of QCP as found in conductivity tensor. Here, $s = S(T)/S_c(T)$ with S(T) is the thermopower and $S_c(T)$ is the thermopower at the MIT.

We unearth the deeper reasons for these novel findings in terms of (i) the specific structure of energy-current correlations for the FKM and (ii) the microscopic electronic processes which facilitate energy transport while simultaneously blocking charge transport close to the MIT. However, within CDMFT, we also find that the WF law survives at $T \longrightarrow 0$ in the incoherent metal right up to the MIT, even in absence of Landau quasiparticles. Finally, we discussed Thomson co-efficient (τ_{th}) and electronic specific heat $\gamma_e = \frac{dS(T)}{dT}$ as a function of U across the MIT with $\gamma_e(T)$ diverges at the MIT.

Universal Dielectric Response across the Continuous MIT

A wide range of disordered materials, including doped (weakly and strongly correlated) semiconductors, molecular and ionic liquids and glasses, show "Universal Dielectric Response " (UDR), followed by a superlinear power-law increase in their optical responses over exceptionally broad frequency ranges, covering the range from ultra-low (mHz) to phonon (THz) regimes. Motivated thereby, we investigate the optical response of the FKM across the continuous MIT using CDMFT. Surprisingly, we find that all the above features emerge quite naturally in the quantum critical region associated with the continuous MIT. We argue that these novel features are linked to emergence of a strongly correlated electronic glassy dynamics close to the MIT, explaining the similarity between optical responses of correlated electronic matter and canonical glass formers.

Conclusion

To conclude, we extend the formalism of single site DMFT to two site Cluster-DMFT and study the continuous metal to insulator transition in the Falicov-Kimball Model within alloy analogy on the high dimensional bethe lattice. Our scheme goes beyond extant schemes by (i) computing effects of spatial correlations on the MIT to exact-to-order-1/d, where d is the system dimensionalty (ii) it can be easily adapted to real electronic structure computations for strongly disordered real binary alloys, and (iii) it throws light on the unusual character of localization near a continuous MIT. We also reveal on the quantum criticality of the dc transport properties near the MIT through the "mirror symmetry" and β-function analysis across MIT. At the end we compare our theoretical result with the experimental data on NbN materials.

List of Figures

Chapter 1

Introduction

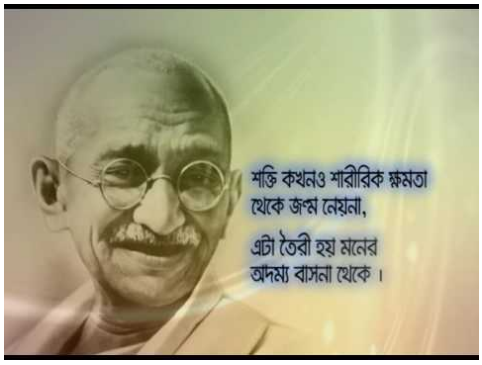

Condensed matter physics is largely a subject of understanding the properties of materials in the solid, liquid and gas phases. Nonetheless, compared to liquid and gases it is the physics of the solids [9, 76, 94, 95, 115] that advanced very steeply. The reason is that solid has a large scope of applications which attract people to contribute more on the process of the development of this field. The birth of the theoretical solid state physics was followed by the description of the properties of metals by P. Drude [30] in 1900. The theory was further developed by H. A. Lorentz [70] who put forward more precise description of the conduction properties of metals. The discovery of superconductivity by H. K. Onnes [89] in 1911, made people to forage for new theoretical descriptions of this physical properties of solids.

With the advent of the quantum mechanics the new theory was proposed that qualitatively as well as quantitatively explained a wide range of phenomena with its spectacular success. By the end of 1920s people came to know about two distinct classes of particles: fermions and bosons. Particles with half-integer spins, like electrons, are fermions described by Fermi-Dirac statistics, while bosons are particles with integer spins, described

by Bose-Einstein statistics. Then within ten years people like B. Bethe, F. Bloch, L. Brillouin brought about a dramatic changes in the theoretical foundation of solid state physics. The theory explains thermal properties in crystals, conduction and optical properties through the quantum mechanical treatment of electronic states and the theory of magnetic phenomena with the identification of the exchange interaction. Although it failed to explain the physical mechanism of superconductivity.

The theory of superconductivity was finally proposed by J. Bardeen, L. N. Cooper and J. R. Schrieffer [12] in 1957. Incorporating quantum field theory (QFT) with quantum mechanics, they identified that it is the phonon mediated interaction between electrons which is responsible for superconductivity. For the first time, they gave the microscopic description of superconductivity that gained a new momentum to the experimental and theoretical study of superconductivity.

In the 1960s magnetism became the hottest research topic in the solid state physics community. In one hand quantum mechanical treatment gave important progress in studying magnetism in metals and on the other hand QFT provides a more precise solution for the model of magnetism based on localized magnetic moments. In 1963, J. Hubbard and M. C. Gutzwiller independently proposed a simple model [1, 45] that was expected to give a theoretical description of ferromagnetic behaviour caused by non-localized electrons. This Hubbard model and its generalizations gave a tremendous boost in the study of both magnetism as well as metal-insulator transition.

The study of disordered systems, amorphous systems and glassy systems [27] have recently gained an intense interest in the field of solid state physics. This system have a myriad of applications in designing new materials in the field of engineering and technology. Disorder has a prominent role to play in transport properties of materials - even weak disorder can make qualitative differences in the transport properties of materials. The most interesting phenomena of disorder physics is Anderson Localisation or Anderson metal-insulator transition [5, 118], first coined by P. W. Anderson in 1958, for which

he was awarded Nobel prize in 1977. He showed the absence of diffusion of electrons in 1D and 2D systems with any arbitrary weak disorder. The extended states (Bloch states) near the Fermi surface becomes localized due to multiple scattering (Quantum Interference) of the disorder. The diffusion of electrons near the Fermi level is only possible for dimension $D \geq 3$ for parameter W small compared to the bare bandwidth ($\sim 2zt$) and the system behaves as metal, where W characterizes the disorder of the system. When W exceeds a critical value, the electrons diffusion stops and the system shows insulating behaviour although the density of states near the Fermi level is non-vanishing. This is known as Anderson Metal-Insulator Transition.

Binary alloy represents another class of disordered systems. This system breaks the lattice translational symmetry making its theoretical description very difficult unlike the crystalline solid where the discrete translational symmetry is intact. The people have incorporated different techniques to solve the alloy problem like, Averaged T -Matrix Approximation, Coherent Potential Approximation (CPA) [116] etc. Binary alloy shows the Metal-Insulator Transition (MIT) by changing the composition of the alloy or strength of the disorder potential. Unlike the Anderson insulator, here the insulating state is characterised by the gap in the single particle state (band splitting). The MIT is second order in nature i.e. the density of state at the Fermi energy vanishes continuously at the critical point.

It is interesting to study quantum criticality at the metal-insulator transition. In binary alloy MIT is observed at $T = 0$ as it is a quantum phase transition [100] unlike classical (Landau) phase transition at finite temperature ($T \neq 0$). But all experimental results are obtained at non zero temperature although very low temperature (T) and there is no perfect order parameter for MIT, makes it more difficult to study quantum criticality at the MIT. One possible solution is to formulate theory for quantum phase transition that describes the effect of the quantum critical point (singularity at T=0) on various physical properties at finite temperature ($T \neq 0$). So, working away from the quantum critical point one could

understand the thermodynamic and dynamic properties of the system over a broad range of values of coupling constant (g) and temperature (T) .

In this thesis, I investigate the quantum critical transport (both dc as well as ac transport) in binary disordered model. Binary disordered model is isomorphic to Falicov-Kimball Model and Falicov-Kimball model can be solved exactly within Dynamical Mean Field Theory (DMFT) and in our newly developed Cluster DMFT approximations. I have studied the binary disordered model by solving Falicov-Kimball Model within alloy analogy using both DMFT as well as Cluster DMFT.

Chapter-wise summary of my thesis:

- In Chapter 2, I start with an introduction to metal-insulator transition (MIT) and give a brief about different types of MITs.

- Then I provide a short account of Dynamical Mean Field Theory (DMFT) and its cluster extensions in Chapter 3.

- In Chapter 4, I talk about Falicov-Kimball model (FKM) and how it can be solved exactly within single-site DMFT approximation in details.

- After that, I describe in details our newly developed Cluster Dynamical Mean Field Theory (CDMFT) technique in FKM within alloy analogy approximation in Chapter 5. I show the MIT in this model and how the critical point change with the short range order between the nearest neighbour disorder.

- In Chapter 6, I present dynamical charge susceptibility in FKM using Cluster DMFT technique. I also discuss the response of the system to a sudden local quench.

- In Chapter 7, I study the quantum criticality of dc conductivity tensor at the continuous metal-insulator transition in FKM using Cluster DMFT technique. I also compare our result with the result of single-site DMFT. I compare our quantum

critical exponent with that of the experimentally determined critical exponent of disorder NbN.

- I extend the idea of quantum criticality to thermal transport and present that thermal transport coefficients also show quantum critical behaviour across the MIT in Chapter 8.

- In Chapter 9, I discuss the optical conductivity and dielectric response of the FKM within Cluster DMFT and I compare our result with the experimental results.

- I conclude my thesis with some future directions and open issues in Chapter 10

Chapter 2

Metal-Insulator Transitions and Quantum Criticality

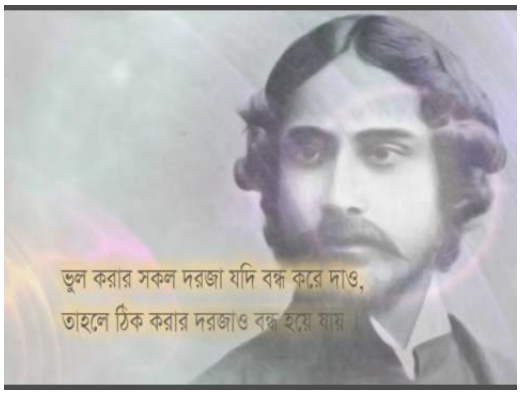

In this chapter, I introduce different types of metal-insulator transition (MIT). Then I talk about the idea of Quantum Phase Transition and how it is different from Landau type phase transition. At the end, I briefly discuss recent theoretical and experimental works on quantum criticality at the MIT.

In condensed matter theory metal-insulator transition (MIT) [50, 27] is one of the oldest but fascinating problems which have attracted a lot of attention even today. First sucessful theoretical description of the MIT was the band theory explanation based on weakly interacting electron system. But this simple theories [9] described the phenomenon well for the materials which are either good metals(e.g. gold, copper) or good insulators(e.g. silicon, germenium) and physical properties of this materials is too stable to meet the needs of modern technology or to get interesting phenomena. So to extract

novel and interesting physics, one needs to study the materials that properties can be changed by tuning (e.g. doping, pressure). Most recent example of this type of materials is doped semiconductor which led to the discovery of the transistor, MOSFET and others integrated circuits. Band picture fails to provide theoretical description of this materials. So people search for different mechanism which can drives the system from metal to insulator or vice versa. In the following sections I discuss about different types of MIT and different mechanism associated with different MITs.

2.1 Different types of Metal-Insulator Transition

Metal-insulator transition can be of two types [15] - one type of transition happen due to the structural changes of the lattice which leads to the separation of conduction and valance bands. Another type of metal-insulator transition is due to electronic distribution. The second category of MIT is the most general MIT. This MIT is further divided into three categories of insulators (shown in Fig 2.1) : Band Insulator due to ordering ordering transition, Mott Insulator due to electron electron interaction, Anderson Insulator due to strong disorder. There is another type of insulator arising due to electron electron correlation and also disorder called Many Body Localization (MBL).

2.1.1 Band Insulator

According to the band theory of solid [9], one can calculate the electronic band structure of the materials. Now if the highest occupied electronic state i.e. Fermi level lies within a band gap then all bands are either full or empty, it takes finite enregy ($\sim$ band gap) to excite the electron to the lowest accessible state in order to carry elctrical current, then the material is an insulator (Band Insulator). Otherwise, if the Fermi level lies inside the band this band is partially filled, electron can carry current without supply of any energy, then material behaves as metal. When the system undergoes some ordering transition, it

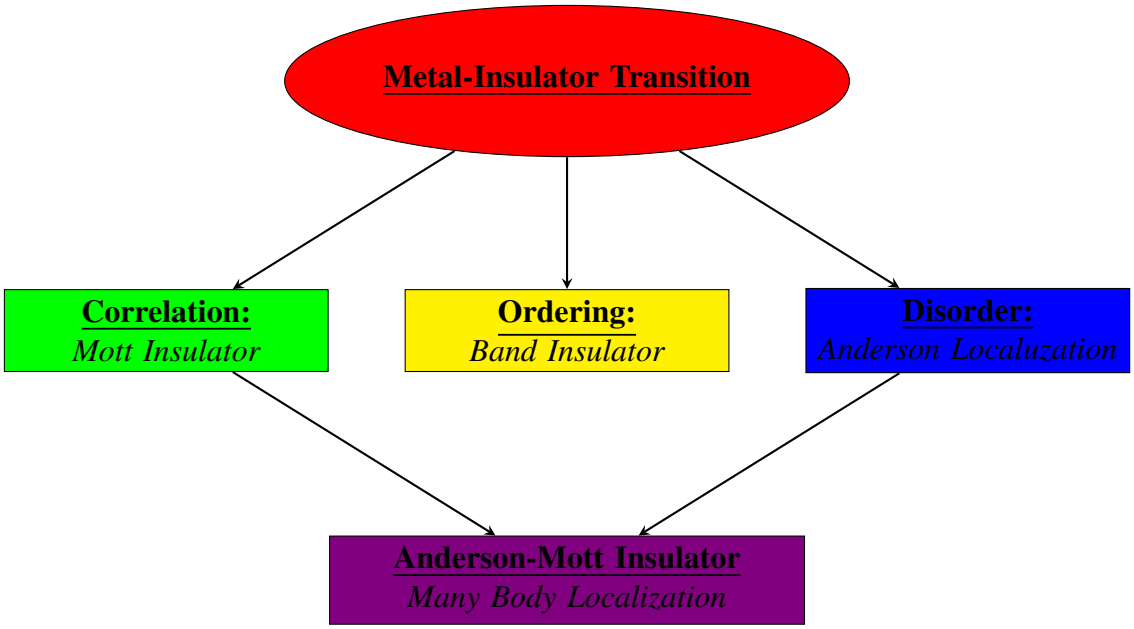

Figure 2.1: Three Basic Insulators: Mott Insulator, Band Insulator, Anderson Insulator. Many Body Localization (Mott-Anderson Insulator) is a Challenging Problem!

is possible to induce a gap at the Fermi surface and the system shows metal to insulator transition. This odering transition corresponds to the some kind of Fermi surface instability where a charge-density-wave(CDW) or spin-density-wave(SDW) [43] formation leads to unit cell doubling. As for example the Slater theory [114] of itinerant antiferromagnets, where the gap opens due to the magnetic ordering.

The band theory of solid is based on the assumption that all the electron-electron interaction and electron-impurity interaction is approximated by an effective potential i.e. pseudopotential and elctron is moving free in the pseudopoentials. But this assumption is valid only if kinetic energy of this electron is dominant compare to any other energy scale in this problem. A useful method is calculation of r_s number: $r_s = \frac{E_c}{E_F}$, E_c is the average coulomb energy per particle and E_F is the Fermi energy. For low value of r_s number the band theory is applicable. Even for good metal if this r_s number is between 3 and 5, the band theory should not work. However, there are other important facts [9] that minimize the role of interaction:

- in metal due to screening the strength of the electron-electron or electron-impurity

interactions renormalized to a significant degree.

- the Hartree and exchange part of the coulomb energy contribute to pseudo-potential and only "correlation" energy gives rise to many-body effects.
- the Pauli exclusion principle reduces the phase space of the electron-electron interaction

As a result the effect of the elctron-elctron interaction and electron-impurity interaction is treated as perturbation where the dominant energy scale is the kinectic energy, known as "Fermi liquid" described by Landau's Fermi Liquid Theory [63, 64].

This theory fails to describe the system close to the metal-insulator transition. This situation found in:

- Narrow band materials such as transition-metal oxide V_2O_3.
- Doped semiconductors such as Si:P or diluted two-dimensional electron gas.
- Doped Mott insulators such as high-T_c cuprate $La_{2-x}Sr_xCuO_4$.

In all these materials, the potential energy due to the electron-electron and electron-impurity interaction becomes comparable to the Fermi energy and the ground state of the system undergoes sudden and dramatic changes - the electrons become bound or localized. As a result the material does not conduct current and behaves as insulator although band theory does not predict any gap at the Fermi surface.

2.1.2 Correlation driven Mott Insulator

In contrast to the band theory many materials with an odd number of electrons behaves as insulator in the experiments. Such materials(e.g. transition metal oxides) have antifferomagnetic ground state. Slater proposed spin density wave [114] formation is origin

of this insulating behaviour. According to the Slater [114] such insulating behaviour would disappear above Neel temperature($\sim 10^2 K$). Surprisingly in most of the antiferromagnetic oxides this insulating behaviour survive at temperature even higher than Neel temperature, ruling out Slater's weak coupling mechanism.

It was Mott [82] and Hubbard [1], first came to explain this issues by proposing the strong coloumb repulsion between electrons occupying the same orbital is the cause of this insulating behaviour. In this description the electron tunnel between near neighbour with strong onsite coulomb repulsion, as described by Hubbard Hamiltonian [83],

$$H_{HUB} = -\sum_{\langle ij\rangle\sigma}(tc^{\dagger}_{i\sigma}c_{j\sigma} + h.c.) + \sum_{j\sigma}\epsilon_j c^{\dagger}_{j\sigma}c_{j\sigma} + U\sum_{j} c^{\dagger}_{j\uparrow}c_{j\uparrow}c^{\dagger}_{j\downarrow}c_{j\downarrow} \tag{2.1}$$

Here, the operator $c^{\dagger}_{i\sigma}$ creates an electron of spin σ in the i-th orbital, t is tunnelling amplitude describing the nearest neighbour inter-orbital hybridization, ϵ_j represents the corresponding site energy and U describes the onsite Coulomb repulsion.

When the lattice is at half filling(i.e. one electron per site) the electron can move from one site to another only if electrons have enough kinetic energy($E_K \sim t$) to overcome the Coulomb energy U. In the narrow band limit $t \ll U$, the electron do not have enough kinetic energy to overcome U and electron becomes localized to a particular site leading to a gap in the single-particle excitation spectrum, behaves as an Mott insulator. The phase diagram of Hubbard model at half filling using DMFT is shown in Fig 2.2. The gap $E_g \approx U - B$(here $B = 2zt$, z is the coordination of the lattice) is the energy need to supply from outside to overcome Coulomb energy U so that electron can move from one side to another. In Mott insulator at half filling every site is singly occupied and so electron behaves as spin 1/2 local magnetic moment. This local magnetic moments interact through magnetic super-exchange of order $J \sim \frac{U}{t_{ij}^2}$. As a result, a magnetic ordering establishes at a temperature of order $T_J \sim J$. The magnetic ordering ceases at temperature higher than T_J, however the insulating behaviour exists upto much higher temperatures $T_{MOTT} \sim E_g$ than T_J. For oxide the typical value of $T_{Mott} \sim E_g \sim 10^3 - 10^4 K$ while magnetic ordering

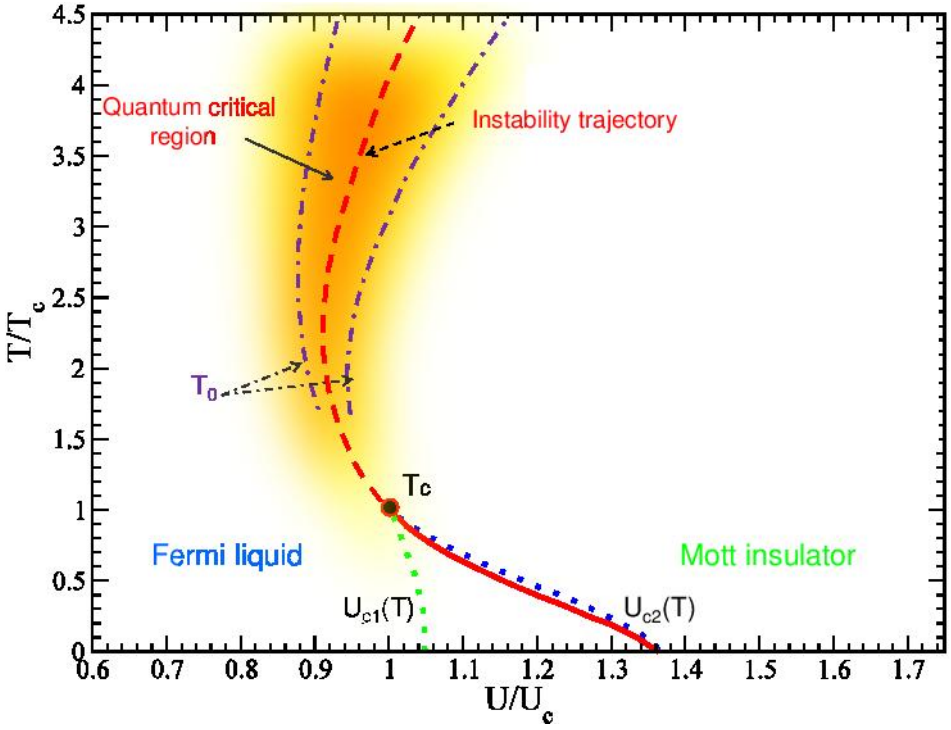

Figure 2.2: The phase diagram of fully frustrated Hubbard model at half filling using DMFT technique, T_c is the critical point below which first order phase transition happen, shaded region showing quantum critical like scaling("hidden quantum criticality"),red dotted line above T_c is the instability line, T_0 is the crossover temperature

emerges upto temperature of order $T_J \sim 100 - 300K$.

When the kinetic energy (t) and Coulomb energy (U) are comparable to each other, the system is near the Mott transition. Experimentally, for this materials one can tuned the bandwidth(B$\sim 2zt$) by modifying the orbital overlap t to drive the system from metallic to insulating and vice versa. For example in transition metal oxide, it is possible to change their metal or insulating properties by applying external hydrostatic pressure. Unfortunately, theoretically it is very difficult to study the system in the vicinity of Mott transition as the perturbation theory fails to describe the system in this regions. Though after a research effort people have found some theoretical tools which can qualitatively describe the properties of the system close to the Mott transition.

2.1.3 Disorder Driven MIT

Random impurity in a metal scattered the mobile elctron randomly and mean free path of the elctron decreases as a consequence decrease in the conductivity. In ordinary metal, the kinetic energy of the mobile elctron is so large compare to the random poetntial due to impurity that the later can be treated as a small perturbation. In this case, one can apply classical drude theory [30] where the conductivity is written as,

$$\sigma \approx \sigma_0 = \frac{ne^2\tau_{tr}}{m} \tag{2.2}$$

where, n is the carrier concentration, e is the electron charge, m is band mass and τ_{tr}^{-1} is the scattering rate. According to the Matthiessen's rule [9], the scattering rate takes additive contribution from different scattering channels i.e.,

$$\tau_{tr}^{-1} = \tau_{el}^{-1} + \tau_{ee}^{-1}(T) + \tau_{ep}^{-1}(T) + - - -- \tag{2.3}$$

Here, τ_{el}^{-1} is the elastic scattering rate, $\tau_{ee}^{-1}(T)$ is the inelastic electron-electron scattering rate and $\tau_{ep}^{-1}(T)$ is the inelastic electron-phonon scattering rate. The resistivity $\rho = \sigma^{-1}$ is a monotonically increasing function of temperature(T) is given by,

$$\rho(T) \approx \rho_0 + AT^n \quad with\ A > 0 \tag{2.4}$$

The value of exponent n depends on the scattering processes i.e. n=1 for electron-phonon scattering process, n=2 for electron-electron scattering processes etc. $\rho_0 = \sigma^{-1}(T = 0)$ is the coming from elastic scattering.

Now if the impurity density is large enough so that the impurity potential is comparable with the Fermi energy, then the semi classical description fails and the electrons make bound state with the impurity i.e. localized by the impurity. This leads to a continuous metal-insulator transition at T=0, since at finite temperature there is always a probability proportional to Bolzmann weight that an electron can overcome the impurity potential. Hence, in low temperature limit a continuous metal-insulator transition occurred where the conductivity vanishes in a power law fashion,

$$\sigma(T = 0) \sim (n - n_c)^{\mu}, \tag{2.5}$$

the μ is the conductivity exponent, the value of which depends on the characteristic length-scale for disorder.

The simplest example of disorder driven MIT is binary alloy. Consider a binary alloy (A_xB_{1-x}) as shown in Fig 2.3 of two types of atoms A and B with composition of atom A as x and that of B as (1-x). Atom A or B occupy randomly on a regular lattice site. The onsite energy differences between Atom A and B is $v_A - v_B = U$. The alloy shows MIT at a critical $U = U_c$ with fixed x. Similarly, by changing x with fixed U one can observed MIT.

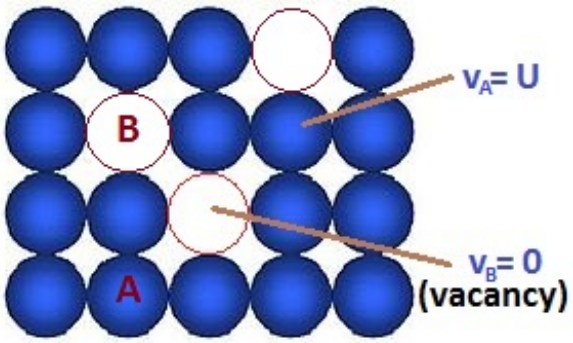

Figure 2.3: Binary alloy on a two dimensional lattice. If the lattice point is occupied by atom A it has an onsite energy $v_A = U$ and if it is unoccupied by the atom it has onsite energy $v_B = 0$

Anderson Localization:

Another interesting phenomena in the disorder system is Anderson Localization. The possibility of Anderson localisation in presence of strong disorder was first demonstrated by Anderson in 1958 [5]. According to Anderson's arguments sufficiently strong disorder is able to localize all electronics states within narrow bandwidth. At weak disorder the electronic states at the edge of the band are expected to be localized whereas the states at the middle of the band remain extended. The line that separate the extended from the localized states is called the "mobility edge(E_c)" as shown in Fig 2.4. As the disorder strength is increased, the position of the mobility edge is shifted towards the middle of the band. For sufficiently strong disorder, the mobility edge crosses the Fermi energy(E_F) leads to localization of all the electronic states close to the Fermi level - the system undergoes an Anderson metal insulator transition. The actual mechanism behind the localization of electron states is the destructive quantum interference of the electrons scattered by the disorder.

Let us consider the Hamiltonian of the form:

$$H = \sum_i \epsilon_i c_i^\dagger c_i + \sum_{i \neq j} (t_{ij} c_i^\dagger c_j + h.c.) \tag{2.6}$$

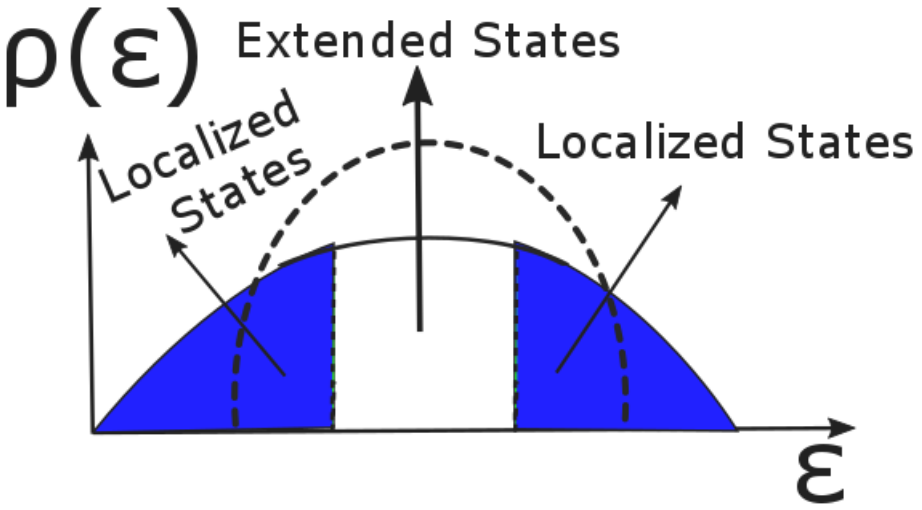

Figure 2.4: Electronic density of states of a disordered system with the mobility edge that separated the extended states at the middle of the band from the localized states at the tails of the band. Dashed line indicates the density of states in the absence of disorder.

Disorder in the system can be introduced in two way. Firstly, the diagonal term ϵ_i can choose a few discrete values randomly over an energy range known as diagonal disorder. Secondly, the hopping amplitude t_{ij} can take any random values known as off-diagonal disorder. For simplicity, I consider only the diagonal disorder with constant nearest-neighbour hopping amplitude t. The onsite energy ϵ_i has a uniform distribution over a energy range W with probability distribution $P(\epsilon_i)$ is given as,

$$P(\epsilon_i) = \begin{cases} \frac{1}{W}, & \text{if } \mid \epsilon_i \mid \leq \frac{W}{2} \\ 0, & \text{otherwise} \end{cases} \tag{2.7}$$

In 1D and 2D, for any value of W all the states will be localized and the system behaves as an insulator although non-vanishing density of states at the Fermi level. Anderson showed that for three dimension the system shows metallic behaviour as long as W is very small compares to the bare band-width($= 2zt$). As soon as W exceeds a critical value ($\equiv 10zt$) all the electrons states become localized. This localization owing to the presence of disorder is known as Anderson localization and the system behaves as an insulator.

2.1.4 Many Body Localization: Effect of Interaction in Disorder System

In the previous section, I have discussed about single-body (Anderson) localization in a non-interacting system, a single electron state becomes localized due to destructive interference with itself. This interference is induced by the presence of disorder.

Now by turning on interactions one can bring the realm of many-body physics, as single-particle states are not enough to describe the system any more. Now, if the behaviour similar to Anderson localization is observed in this many-body system (like many body mobility edge), one say that this system has many-body-localized states or is in the many-body-localized (MBL) regime.

Another reasonable way, one can argue that the many-body localization is present in a many-body system for which the Eigenstate thermalization hypothesis does not hold. Alternatively, a fully many-body localized system is a system where all the many-body eigenstates of the Hamiltonian are localized. On technical level, this is quite complicated and still a challenging problem! I am not going in details as this is out of the scope of my thesis. Interested reader may go through the following references [86, 71].

2.2 Quantum Phase Transitions

Quantum Phase Transition (QPT) [100] is a phase transition between different quantum phases at zero temperature unlike classical phase transition (Landau type) occurs at nonzero temperature due to thermal fluctuations. This is the abrupt change in the ground state of the Hamiltonian due to quantum fluctuation at T=0. Near zero temperature ($T \rightarrow 0$), the quantum fluctuation dominates over thermal fluctuations. At finite temperature ($T \neq 0$), quantum fluctuations is suppressed by thermal fluctuations - so only classical phase transition is possible. In my thesis, my discussion is limited to second

order (continuous) of quantum phase transitions.

2.2.1 MIT at the Critical Point

According to the Mott's earlier argument [83], the metal-insulator transition is discontinuous i.e. first order where a *minimum metallic conductivity* (σ_{min}) exists on the metallic side even at T=0. His argument is based on the Drude's picture, where the increasing disorder will imply decreasing in elastic mean free path($l = v_F \tau_{tr}$) and vice versa. The minimum possible value of the mean free path (l) cannot be shorter than the inter atomic distant or lattice spacing (a). Hence the metallic conductivity is bounded from below by "Mott limit"

$$\sigma \geq \sigma_{min} = \frac{ne^2 a}{m v_F} \tag{2.8}$$

For two-dimensional system, the minimum metallic conductivity σ_{2D} have a universal value with no length scale in it,

$$\sigma_{2D}^{min} \approx 0.1 \frac{e^2}{\hbar} \approx 3 \times 10^{-5} \Omega^{-1} \tag{2.9}$$

However, as shown in fig 2.5, the conductivity of silicon doped with phosphorus ($Si : P$) as a function of the dopant concentration when extrapolated to $T \longrightarrow 0$ limit, the conductivity starts to decrease rather sharply when it come close to the minimum metallic conductivityσ_{min} - even one can measure conductivities which are orders of magnitude smaller than the σ_{min}. The metal-insulator transition is extremely sharp(conductivity vanishes in power law fashion), but continuous i.e. second order.

For MIT, there is no order parameter though the system show clearly critical behaviour at T=0. As conductivity vanishes at $T \longrightarrow 0$ in insulating phase and remains finite in metallic phase, one can consider conductivity plays a role similar to the order parameter. So one can defined scaled conductivity like an order parameter to study quantum criticality

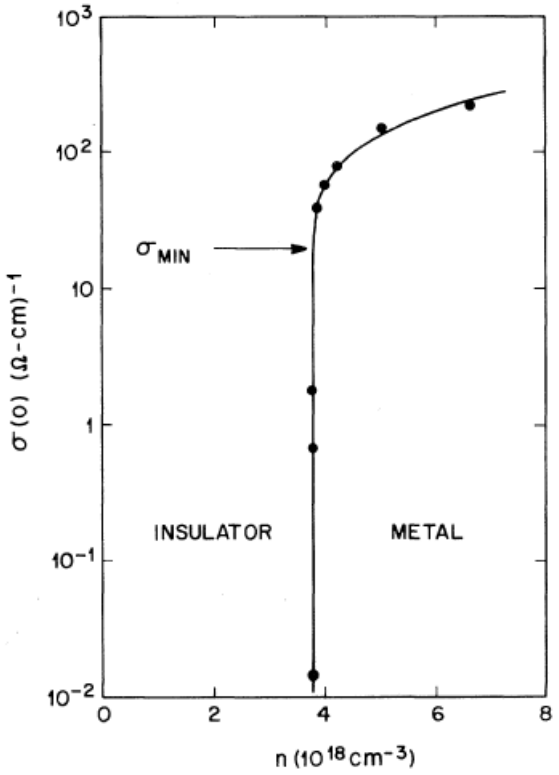

Figure 2.5: Zero-temperature conductivity of metallic P-doped Si as a function of the donor density, taken from [33]

at MIT.

2.2.2 Scaling theory of disorder-driven MIT

The scaling behaviour around the critical point is demonstrated by β function formalism. The original work described by the "gang of four" (Abrahams, Anderson, Licciardello and Ramakrishnan) in 1979 [3]. The $\beta-$ function describes how the conductance changes with the effective system size. In principle, one could take a finite size of disorder material and measure the conductance. If the experiment is repeated for different system size one could experimentally determine the conductance depends on the system size.

In a good metal, disorder is weak and conductivity is large so that one can use Drude theory to find the conductance. For metal, conductance will increase with the effective system size L. From Ohm's law, conductance g then scale with the system size L given as,

$$g_{met}(L) = \sigma L^{d-2} \qquad d > 2 \tag{2.10}$$

where σ is the conductivity. In the opposite limit of strong disorder, all the electrons to form bound states with impurities. If ξ is the characteristic length scale of this bound states, then the conductance will decrease exponentially with the size of the system L,

$$g_{ins}(L) \sim exp{-L/\xi} \tag{2.11}$$

According to the Gell-mann law the "β"-function is defined by,

$$\beta(g) = \frac{d(lng)}{dlnL} \tag{2.12}$$

"β(g)" does not explicitly depends on L, is a function of g only. It is a smooth(analytical) function near the transition. The quantity is expected to be positive in a metal and negative in the insulator. Hence, zero of the "β" function shows the metal-insulator transition.

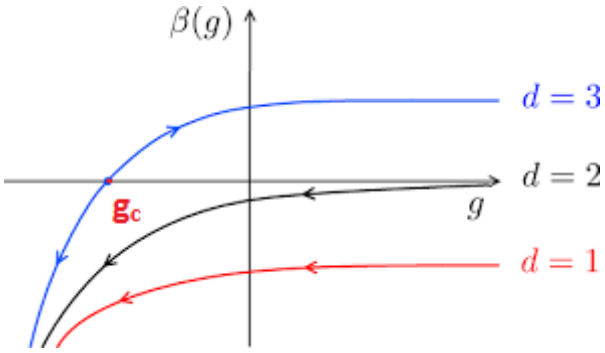

Figure 2.6: Scaling Analysis at MIT : β function of the localization problem for dimensions d = 1, 2, and 3

So in ohmic metal one find,

$$\beta_{met} = d - 2 \tag{2.13}$$

while for localized insulator,

$$\beta_{ins} = ln(g) \tag{2.14}$$

The plot of β-function for dimensions d=1,2 and 3 is shown in Fig 2.6. Since, $\beta_{met} > 0$ and $\beta_{ins} < 0$, β is a smooth function implies that β must change sign at some finite value of the conductance $g = g_c$ which corresponds to the critical point. So close to the critical point one can write β as,

$$\beta(g) \approx sln(g/g_c) \tag{2.15}$$

where, $s = \beta'(g_c)$ is the slope of the β-function near the critical point(g_c). Define a variable $t = ln\frac{g}{g_c}$. Now differentiating the β-function equation [28] I obtain,

$$\frac{d(lnt)}{dlnL} \approx s, \tag{2.16}$$

Integrating the above equation from the microscopic cut-off l to the sample size L and write

$$t(L) = t_0(L/l)^s. \tag{2.17}$$

This integration has to be carried out upto the correlation lengthscale i.e. $L = \xi$ such that

the renormalized distance to the transition $\delta g(L) = (g(L) - g_c)/g_c \approx t(L) \sim O(1)$. Since at short scale $t_0 = t(l) \sim \delta g_0 \sim \delta X$, I have

$$\xi \sim t_0^{1/s} \sim \delta n^{1/s} \tag{2.18}$$

Here X is the tuning parameter. Thus, the correlation length exponent

$$\nu = \frac{1}{s} \tag{2.19}$$

Substituting this I have the length scale dependence conductance as:

$$g(L) \approx g_c exp[A\delta X(L/l)^{1/\nu}] \tag{2.20}$$

2.2.3 Phenomenological scaling formulation:

A phenomenological scaling analysis is proposed for quantum criticality [100] to understand quantum critical phenomena and corresponding critical exponent. If the scaling analysis is valid then a single correlation length characterizing the system is $\xi \sim \delta X^{-\nu}$, where $\delta X = \frac{X - X_c}{X_c}$ is the dimensionless distant from the critical value (X_c) and ν is the correlation length exponent. If z is "dynamical exponent" of the system then the time scale corresponding to the correlation length is given by $\tau_z \sim \xi^z$. Using Heisenberg Uncertainty Principle, the corresponding energy (temperature) scale is of the form,

$$T_0 \sim \frac{\hbar}{\tau_{xi}} \sim \delta X^{\nu z} \tag{2.21}$$

At non-zero temperature, the length scale (L) is related to the temperature scale (T) through the dynamical exponent (z) as $T \sim L^z$. Using this and Eq. 2.21 I obtain from

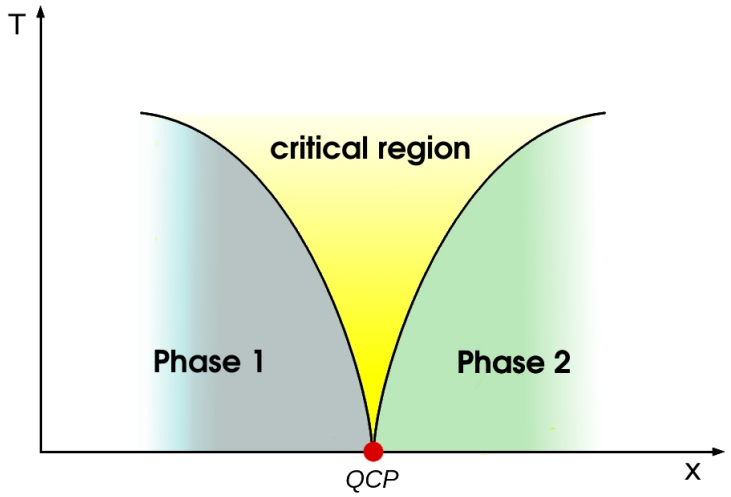

Figure 2.7: Cartoon representing a typical phase diagram in the vicinity of a quantum critical point, taken from [85]. Here, T is the temperature and X is the tuning parameter

Eq. 2.20 the temperature dependence of the conductance is,

$$g(\delta X, T) \approx g_c exp[sgn(\delta X) A (\frac{T_0}{T})^{1/\nu z}] \tag{2.22}$$

Hence the scaling temperature T_0 vanishes at the critical point $X = X_c$ with exponent νz. This scaling temperature T_0 is called the crossover temperature. Here, A is a dimensionless constant of order one. If the scaling conductance, $g^*(\delta X, T) = g(\delta X, T)/g_c$ then,

$$g^*(\delta X, T) \approx 1/g^*(-\delta X, T) \tag{2.23}$$

i.e. there is a mirror symmetry on log scale between metallic and insulating branch with $g^*(\delta X = 0, T) = 1$! The crossover temperature T_0 determined the boundary of the quantum critical region(shown in Fig 2.7) where the mirror symmetry between metallic ($\delta X < 0$) and insulating branch ($\delta X > 0$) exists,

For MIT there is no order parameter, though the system show clearly critical behaviour at T=0. As conductivity is vanishes at $T \longrightarrow 0$ in insulating phase and remains finite in metallic phase, one can consider conductivity plays a role similar to the order parameter.

So like order parameter in second order phase transition one can write conductivity in the scale invariant form given as,

$$\sigma(\delta n, T) = b^{-\mu/\nu} f_\sigma(b^{1/\nu}\delta n, b^z T). \tag{2.24}$$

Here, T is the temperature, b is the length rescaling factor and μ is the conductivity exponent, I identify tuning parameter X as the number density of electrons (n) i.e. $X \equiv n$. At T=0, behaviour of $\sigma(T = 0) \sim \delta n^\mu$ and choosing $b = \delta n^{-\nu} \sim \xi$. Then the scaling form is:

$$\sigma(T) = \delta n^\mu \tilde{\phi}_\sigma(\frac{T}{\delta n^{z\nu}}) \tag{2.25}$$

where, $\tilde{\phi}_\sigma(y) = f_\sigma(1, y)$. Finite temperature correction in the metallic phase are obtained by expanding:

$$\tilde{\phi}_\sigma(y) \approx 1 + a y^\alpha, \tag{2.26}$$

and the low temperature conductivity of the form:

$$\sigma(\delta n, T) \approx \sigma_0(\delta n) + m_\sigma(\delta n) T^\alpha \tag{2.27}$$

Where, $\sigma_0(\delta n) \sim \delta n^\mu$, and $m_\sigma(\delta n) \sim \delta n^{\mu - \alpha\nu z}$. Since the form of the scaling function $\phi_\sigma(y)$ is independent of δn, the value of the exponent α is universal in the entire metallic phase and for weak disorder can be calculated by using perturbation theory. For example, the interaction corrections in d=3 [67] lead to $\alpha = 1/2$.

The temperature dependence at the critical point (in the critical region) can be obtained if I put $\delta n = 0$ and $b = T^{-1/z}$, gives

$$\sigma_c(T) = \sigma(\delta n = 0, T) \sim T^{\mu/\nu z} \tag{2.28}$$

So I can write,

$$\sigma(n, T) = T^{\mu/\nu z} \phi_\sigma(T/T_0(n)), \tag{2.29}$$

where, $\phi_\sigma(x) = x^{\mu/\nu z}\tilde{\phi}_\sigma(x)$, and the crossover temperature $T_0(\delta n) \sim \delta n^{\nu z}$.

2.2.4 Experimental Evidence of Quantum Criticality:

To demonstrate experimentally quantum criticality, one must follow the procedure given below:

- Plot $\sigma(\delta n, T)$ vs. T for several carrier concentration on both side of the transition point. The critical curve(separatrix) shows the power-law behaviour $\sigma_c \sim T^x$ and one can identify the critical concentration ($n = n_c$) which looks like straight line when the data are plotted in log-log scale.

- From the slope of the $\sigma_c(T)$ in log-log scale, one can find the critical exponent $x = \frac{\mu}{\nu z}$.

- Then plot $\phi_\sigma(T/T_0(\delta n)) = \sigma(\delta n, T)/\sigma_c(T)$ as a function of $T/T_0(\delta n)$. T_0 is the crossover temperature such that at critical point $T_0 = 0$. T_0 is determined in such a way that all the curves of the scaling function $\phi_\sigma(y)$ fall on either of the two branches(metallic or insulating).

- Plot $T_0(\delta n)$ as a function of δn on log-log scale and calculate critical exponent νz. The exponent νz is expected to be same on both sides. Then one can calculate conductivity exponent from $\mu = x\nu z$.

- One can do cross check by extrapolating the metallic curves $\sigma(\delta n, T)$ to $T \longrightarrow 0$ and then determines the exponent μ from the relation $\sigma(\delta n, T = 0) \sim \delta n^\mu$.

2.2.5 Past Experimental Evidence:

The metal-insulator transition is driven by quantum fluctuation i.e. the transition is appeared at T=0 where the thermal fluctuation dies out. Although experimental evidences

of this are limited I would like to emphasize a few experiment evidences.

- **Doped semiconductors such as Si:P**

  In this experiment, MIT critical behaviour is carefully studied [113]. When the conductivity is extrapolated to T=0 shows a sharp critical behaviour [90, 91] of the form $\sigma \sim (n - n_c)^{\mu}$ with the critical exponent $\mu \approx 1/2$ for uncompensated samples (half filled impurity band) and conductivity exponent $\mu = 1$ for heavily compensated samples of Si:P,B or in presence of strong magnetic field. Such dramatic difference between these cases is seen over an extremely broad concentration range upto several times of the critical density.

- **Two-dimensional metal-insulator transitions**

  In several two-dimensional electron gas (2DEG) such as silicon MOSFET, a sharp metal-insulator transition reported [59, 96, 4]. There are some controversies regarding the driving force of the transition. Some debates also going on the nature of the transition. Remarkably, in some experiments describing the scaling freature of the resitivity near the transition at low temperature, also found the mirror symmetry [59, 96] between both sides of the transition ("duality") [28] which shows (in Fig 2.8) a strong evidence of "Quantum Criticality" [112]. This critical behaviour extends to relatively high temperature, comparable to the Fermi temperature [4].

- **High temperature anomalies-Mooij correlation**

  Mooij [81] for the first time pointed out that similar MIT transition has been observed in systems [67] driven by disorder with fixed electron density. In recent study [111], the temperature coefficient of the resistivity(TCR) is found to change sign, indicating the crossover from metallic($d\rho/dT > 0$) to insulating ($d\rho/dT > 0$) transport, around the values of the resistivity close to the "Mott limit" $\rho_c = 1/\sigma_{min}$. This behaviour is consistent with the Mott's idea that as the temperature increases the resistivity approaches to a saturation [34] value as the mean-free-path becomes

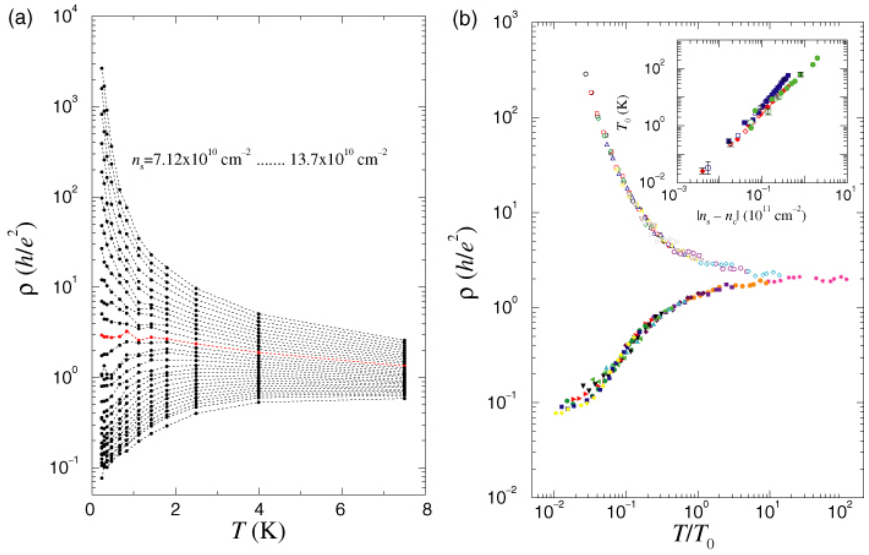

Figure 2.8: The resistivity curves (a) for a two-dimensional electron system in silicon [59] show a dramatic metal-insulator crossover as the density is reduced below $n_c \sim 1011 cm^{-2}$ (b) displays the scaling behaviour, which seems to hold over a comparable temperature range. The remarkable "mirror symmetry" [28] of the scaling curves seems to hold over more then an order of magnitude for the resistivity ratio

comparable to the atomic scale.

- **High temperature violation of the Mott limit**

  The most surprising behaviour was first observed in cuprate superconductors [49] where Mott limit violates. This bhaviour is explained by non-Fermi liquid physics and strongly correlation effects. Futher study of organic Mott system [68] and transition metal oxides such as V_2O_3 [69] shows the violation of Mott limit at temperature exceeding Fermi-liquid coherent scale T^* and was observed to coincide with the suppression of the corresponding Drude peak in the optical conductivity. Similarly to the resistivity saturation, "bad metal" behaviour seems to emerges only in the high temperature incoherent region where local scattering process dominates.

- **Quantum criticality of Mott transition in organic materials**

  In the very recent experimental studies [39, 102], the evidence for the quantum critical nature of the Mott instability was investigated. In one study [39], the electron transport of three organic systems with different ground states under continuously

controlled pressure was studied. The resistivity obeys the material-independent quantum-critical scaling relation bifurcating into a Fermi liquid or Mott insulator, irrespective of the ground states. Electrons on the verge of becoming delocalized behave like a strange quantum-critical fluid before becoming a Fermi liquid. In another study [102], they presented the electron transport properties in the vicinity of a doping-driven Mott transition. They showed a continuous metal-insulator transition (MIT) as electron doping proceeds.

All these experiments suggest that there are many interesting issues in many body metal-insulator transition(MIT) that need to be studied with appropruate theoretical tools. Unfrotunately the well known theory is failed due to the lack of order parameter formulation. Recently, an alternative formulation has been developed based on Dynamical Mean Field Theory(DMFT) [41]. Complementary to the phenomenological theory, this formalism provides some striking result for disordered systems consistent with the experimental result. In the following chapters I will describe this method in details and extensions of this formalism.

Chapter 3

Dynamical Mean Field Theory and Its Extensions

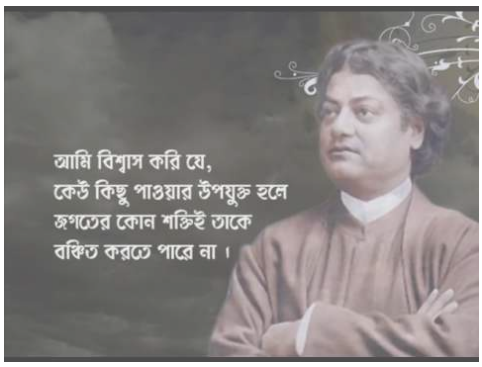

Before going into the details of my thesis problems, here I will give a brief idea of Dynamical Mean Field Theory (DMFT) and its extensions. In this chapter, we talk about the basic concept of single site DMFT and then we will describe two types of Cluster extension of DMFT - (a) Real Space Cluster Extension (Cluster DMFT) and (b) Momentum Space Cluster Extension (Dynamical Cluster Approximation)

The numerical implementation of strongly correlated systems is an interesting area of research in modern day physics. Unfortunately there is no suitable method to solve standard many-body problems in strongly correlated region: Exact diagonalization methods are applicable to problems with small number of sites as the basis of the Hilbert spaces grows exponentially with the no. of sites. The Quantum Monte Carlo method has sign problems, fails at low temperatures. Standard DMRG method also limited to one

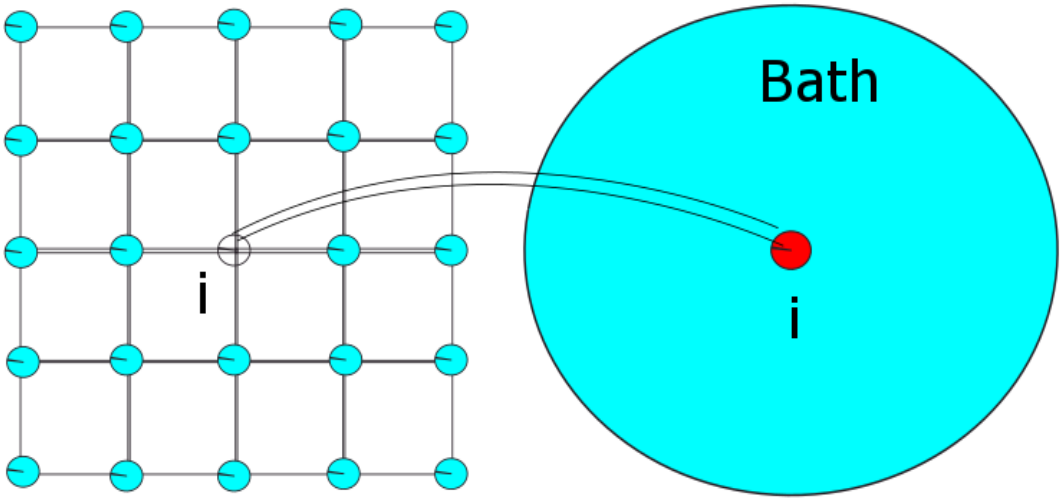

Figure 3.1: In DMFT the full lattice problem is mapped to an single site lattice (say $'i'$) problem embedding in an effective medium

dimensional system.

A useful numerical approach to treat fermionic systems in strongly correlated region is Dynamical Mean Field Theory (or DMFT). The development of this field was started by Muller-Hartmann and Metzner and Vollhardt [77] while the insights were developed by by Georges, Kotliar and co-workers [41]. All the results presented here have been obtained using Cluster-Dynamical Mean Filed Theory (CDMFT) which is a cluster extension of the single site DMFT. We therefore give a brief overview of single site DMFT and its extension to Cluster-DMFT. The interested reader may go through an introductory article [57], an extensive review [41] as well as thesis and lecture note [56, 44] on DMFT and the Cluster DMFT [75].

3.1 Single-site DMFT

The basic ideas of DMFT come from the original classical Weiss mean field theory of magnetism [42]. It focuses on a single lattice site and the effect of all the other degrees of freedom is included in a self-consistently determined "effective medium" [41]. In con-

trast to the Weiss mean field theory, in DMFT the environment can not be determined by a static field, but must contain a dynamic "bath function"($\Delta_i(\omega)$) which takes into account the dynamics of the electrons on a given site due to the environment. Hence, in DMFT the complicated full lattice problem is mapped to an effective single site problem. The calculation then reduces to solving an appropriate quantum impurity problem supplemented by a self-consistently determined bath function $\Delta(\omega)$. The precise form of DMFT equation will be different for electron-electron interaction or interaction with disorder or for both.

The first derivation of dynamical mean field theory is known under the name of "cavity method" [41]. The idea is to focus on a given site, say $'i'$ and integrate out all degrees of freedom associated with other lattice sites so that one can define an effective dynamics for the selected site $'i'$ as shown in Fig 3.1. The total Hamiltonian can be split into:

$$H = H_i + H_{hyb} + H^{(0)} \tag{3.1}$$

where, H_i is the term that corresponds to site $'i'$, $H^{(0)}$ is the Hamiltonian of the lattice by removing a single site $'i'$ and its adjacent bonds (i.e. a cavity is created surrounding $'i'$), H_{hyb} is the hybridization term that corresponds to the site i and the cavity lattice. For a general lattice the relation between the full lattice green function and the cavity green function is given by,

$$G^{(0)}_{lm} = G_{lm} - \frac{G_{li}G_{im}}{G_{ii}} \tag{3.2}$$

where, $G_{lm}, G^{(0)}_{lm}$ are the full lattice green function and cavity green function, respectively. The cavity green function $G^{(0)}$ is related to the effective local green function corresponding to the site $'i'$ with suitable self-consistency. The spectral part of the cavity green function gives the information of metal-insulator transition (MIT), hence can serve as an order parameter for MIT. According to the Fermi-golden Rule, the transition rate to a neighbouring site is proportional to the density of the final states. Hence an insulating behaviour leads to a gap in the spectral part at Fermi energy. In Hubbard model such a gap is a direct consequence of the strong onsite electron-electron Coulomb repulsion and

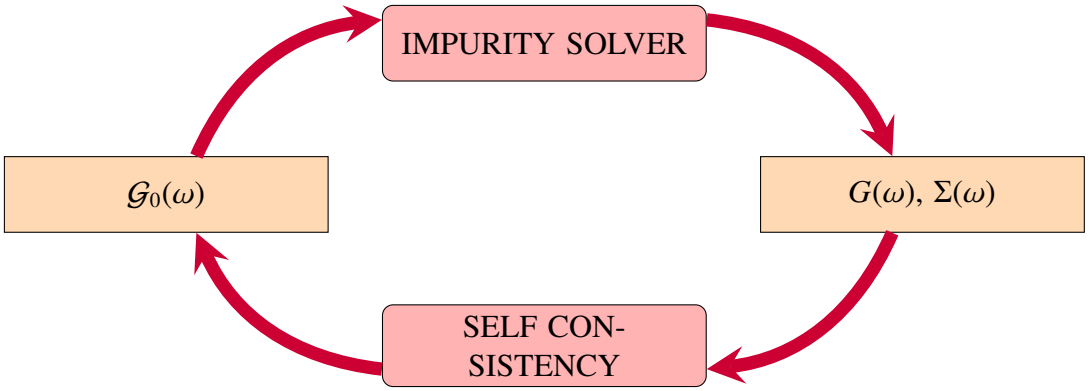

Figure 3.2: DMFT Self-Consistency loop. For a given $\mathcal{G}_0(\omega)$ solving the impurity problem one can get interacting Green's function $G(\omega)$ and Self-energy $\Sigma(\omega)$. This is in self-consistency condition to produce a new bath Green's function $\mathcal{G}_0(\omega)$. Iterations goes on until convergence is achieved

is same for every lattice site.

In case of the Anderson insulator (disorder induced localization) [5] the average of the spectral part has no gap in the insulating state and hence cannot serve as an order parameter for Anderson localization. In this case we consider the "typical spectral function" [7] as an order parameter. This typical spectral function has a gap at the Fermi surface in the Anderson insulating state. The relation between the typical spectral function and average spectral part [25] as,

$$\Delta_{typ} = exp\langle ln(\Delta_i)\rangle \tag{3.3}$$

The average is taken over the distribution of the disorder. In the presence of disorder we go from normal metal(Fermi liquid) to a non Fermi liquid metal and then finally to an insulator.

Some of the physical aspects of DMFT are as follows:

- This approach is an approximate scheme where problems of infinite length scale are mapped to a single lattice site with infinite time scale. In the limit of infinite coordination number, the method is exact as in this limit the spatial correlation vanishes.

- In the metallic region, DMFT reproduces the Fermi liquid behaviour of metal both in the low-temperature and the high temperature incoherent regime.

- From the local green function one can have local self-energy $\Sigma_{ii}(\omega)$, from which one can calculate the effective mass of the quasi-particle $m^* = 1 - (\delta\Sigma_{ii}/\delta\omega)_{\omega=0}$ and the inelastic scattering rate $\tau_{in}^{-1}(\omega) = -Im\Sigma_{ii}(\omega = 0)$. With disorder these quantities display spatial fluctuations [80] and an appropriate distribution function is necessary to characterize them.

- As DMFT ignores spatial fluctuations it cannot describe the phenomena which are described by long wavelength spatial fluctuations.

Though there are some limitations, DMFT has come to be most powerful technique to understand system in the strongly correlated regime with many successful applications [56].

In the following section I discuss two extension of the DMFT- CDMFT (Cluster Dynamical Mean Field Theory) and DCA (Dynamical Cluster Approximation).

3.2 Cluster Extensions of DMFT

It is shown from single site DMFT that in the limit of infinite coordination number the lattice model can be exactly mapped to a single site impurity model where the lattice Green function is related to the impurity Green function via a suitable self-consistency condition. Although the mapping is not exact for a lattice with finite coordination number, one can use this as an approximation. So in this approximation one assume the momentum-dependent (non-local) self-energy by local self energy i.e. $\Sigma(k, \omega) \approx \Sigma(\omega)$. But for certain physical phenomena the inter-site correlation becomes relevant for example the super-exchange in Hubbard model. In such cases, single site DMFT approximation is unable to describe the physics in such cases.

Therefore, recently several attempts have been made to extend DMFT approximation

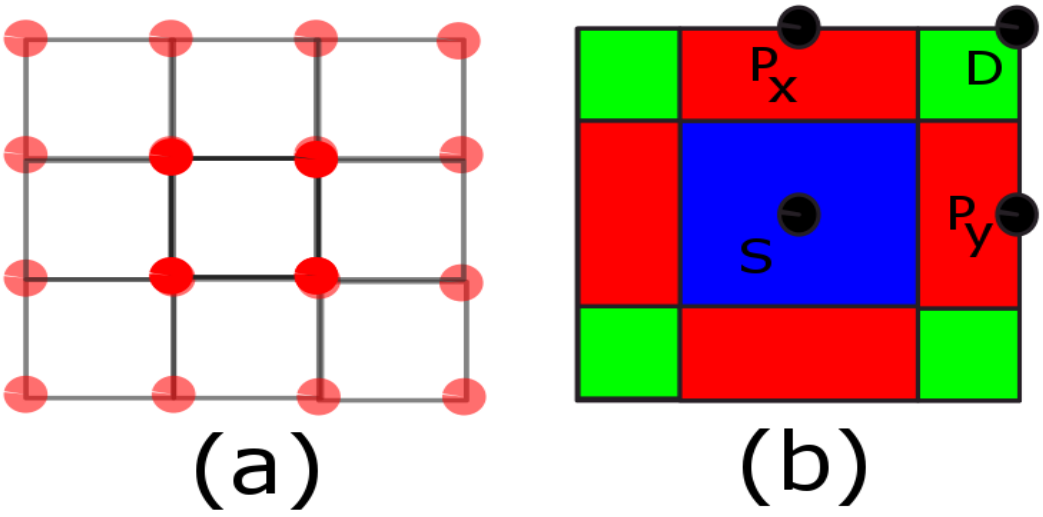

Figure 3.3: Two types of cluster extension of DMFT (a) Real space Cluster DMFT (CDMFT) with four site square as cluster impurity and (b) Momentum space Cluster DMFT (DCA) [93] with four cluster momentum plaquette (S, P_x, P_y and D)

to include inter-site correlations. Considers instead of focusing on a single site, within cluster-DMFT one consider a cluster of sites as 'impurity' and solves the model of cluster Anderson impurities embedded in a bath with a self- consistency condition at the cluster level. Hence the self-energy becomes momentum dependent i.e. $\Sigma(\vec{K}, \omega)$ with the number of $\vec{K}$ values is dependent on the number of sites in the impurity cluster.

In the following subsections I discuss two widely used cluster schemes - CDMFT (Cellular Dynamical Mean Field Theory) and DCA (Dynamical Cluster Approximations). Figures 3.3(a) and Fig 3.3(b) depict these methods schematically.

3.2.1 Cluster Dynamical Mean Field Theory(CDMFT)

In CDMFT a real space cluster is treated as impurity embedded by cluster of baths as shown in Fig 3.3(a). For a lattice of infinite extent, we choose a large subset of the lattice as a cluster which obeys all the symmetries of the lattice (e.g. for a two dimensional lattice a suitable cluster would be 2×2 cluster) and then map the full lattice to a super-lattice where the cluster is treated as a basis. The super-lattice has all the symmetries

of the original lattice. Now choose one site in the super-lattice as the impurity and rest of them as the bath and map it to an Anderson impurity problem. Hence the impurity green function will be a matrix green function($\hat{G}_{imp}(\omega)$) and the bath function ($\hat{\Delta}(\omega)$) is connected with the lattice Green function with self-consistent matrix equations.

Let us consider a lattice of sites N and make a super-lattice of clusters with N_c sites. Let, $\tilde{\mathbf{x}}$ be the lattice vector of the cluster from the origin in the super-lattice. Then a lattice point $\mathbf{x}$ in the original lattice is given as, $\mathbf{x} = \tilde{\mathbf{x}} + \mathbf{X}$, where $\mathbf{X}$ is the vector from the cluster to the lattice point. In reciprocal space the original Brillouin zone is divided into N_c number of super-lattice Brillouin zones with $\mathbf{k} = \tilde{\mathbf{k}} + \mathbf{K}$, where $\mathbf{k}, \tilde{\mathbf{k}}$ are the reciprocal lattice vectors in the original lattice BZ and super-lattice BZ, $\mathbf{K}$ in cluster momentum.

Splitting the hopping and the self-energy into intra-cluster and inter-cluster part one has,

$$\mathbf{t}(\tilde{\mathbf{x}}_\mathbf{i} - \tilde{\mathbf{x}}_\mathbf{j}) = \mathbf{t_c}\delta_{\tilde{\mathbf{x}}_\mathbf{i},\tilde{\mathbf{x}}_\mathbf{j}} + \delta\mathbf{t}(\tilde{\mathbf{x}}_\mathbf{i} - \tilde{\mathbf{x}}_\mathbf{j}) \tag{3.4}$$

$$\mathbf{\Sigma}(\tilde{\mathbf{x}}_\mathbf{i} - \tilde{\mathbf{x}}_\mathbf{j}, i\omega_n) = \mathbf{\Sigma_c}(\mathbf{i}\omega_\mathbf{n})\delta_{\tilde{\mathbf{x}}_\mathbf{i},\tilde{\mathbf{x}}_\mathbf{j}} + \delta\mathbf{\Sigma}(\tilde{\mathbf{x}}_\mathbf{i} - \tilde{\mathbf{x}}_\mathbf{j}, i\omega_n) \tag{3.5}$$

where, all bold quantities are of size $N_c \times N_c$. Expanding the Green function one has,

$$\begin{aligned}\mathbf{G}(\tilde{\mathbf{x}}_\mathbf{i} - \tilde{\mathbf{x}}_\mathbf{j}, i\omega_n) &= \mathbf{g}(i\omega_n)\delta_{\tilde{x}_i,\tilde{x}_j} \\ &+ \mathbf{g}(i\omega_n)\sum_l [\delta\mathbf{t}(\tilde{\mathbf{x}}_\mathbf{i} - \tilde{\mathbf{x}}_\mathbf{j}) + \delta\mathbf{\Sigma}(\tilde{\mathbf{x}}_\mathbf{i} - \tilde{\mathbf{x}}_\mathbf{j}, i\omega_n)\mathbf{G}(\tilde{\mathbf{x}}_\mathbf{i} - \tilde{\mathbf{x}}_\mathbf{j}, i\omega_n)]\end{aligned} \tag{3.6}$$

where, $\mathbf{g}$ is the Green function restricted to the cluster, defined as:

$$\mathbf{g} = [(i\omega_n + \mu) - \mathbf{t}_c - \mathbf{\Sigma}_c(i\omega_n)]^{-1} \tag{3.7}$$

In momentum space this equation simplifies to:

$$\mathbf{G}(\tilde{\mathbf{k}}, i\omega_n) = \mathbf{g}(i\omega_n) + \mathbf{g}(i\omega_n)[\delta\mathbf{t}(\tilde{\mathbf{k}}) + \delta\mathbf{\Sigma}(\tilde{\mathbf{k}}, i\omega_n)]\mathbf{G}(\tilde{\mathbf{k}}, i\omega_n). \tag{3.8}$$

In DMFT, the self-energy is chosen to be local. Similarly in CDMFT the self-energy of the cluster super-lattice is local i.e. $\delta\mathbf{\Sigma} = 0$, then one has,

$$\begin{aligned} \mathbf{G}(\tilde{\mathbf{k}}, i\omega_n) &= \mathbf{g}(i\omega_n) + \mathbf{g}(i\omega_n)\delta\mathbf{t}(\tilde{\mathbf{k}})\mathbf{G}(\tilde{\mathbf{k}}, i\omega_n) \\ &= [\mathbf{g}^{-1}(i\omega_n) - \delta\mathbf{t}(\tilde{\mathbf{k}})^{-1}]^{-1} \end{aligned} \tag{3.9}$$

the "coarse gaining" of the cluster Green function is given as:

$$\bar{\mathbf{G}}(i\omega_n) = \frac{N_c}{N} \sum_{\tilde{\mathbf{k}}} \mathbf{G}(\tilde{\mathbf{k}}, i\omega_n). \tag{3.10}$$

and the Weiss function in CDMFT is given as:

$$\mathcal{G}^{\mathbf{0}}(i\omega_n) = [\bar{\mathbf{G}}^{-1}(i\omega_n) + \mathbf{\Sigma}_c(i\omega_n)]^{-1} \tag{3.11}$$

A sketch of the self-consistency loop is shown in the flowchart (Fig 3.4) next page:

Figure 3.4: Cluster DMFT Algorithm Flow Diagram

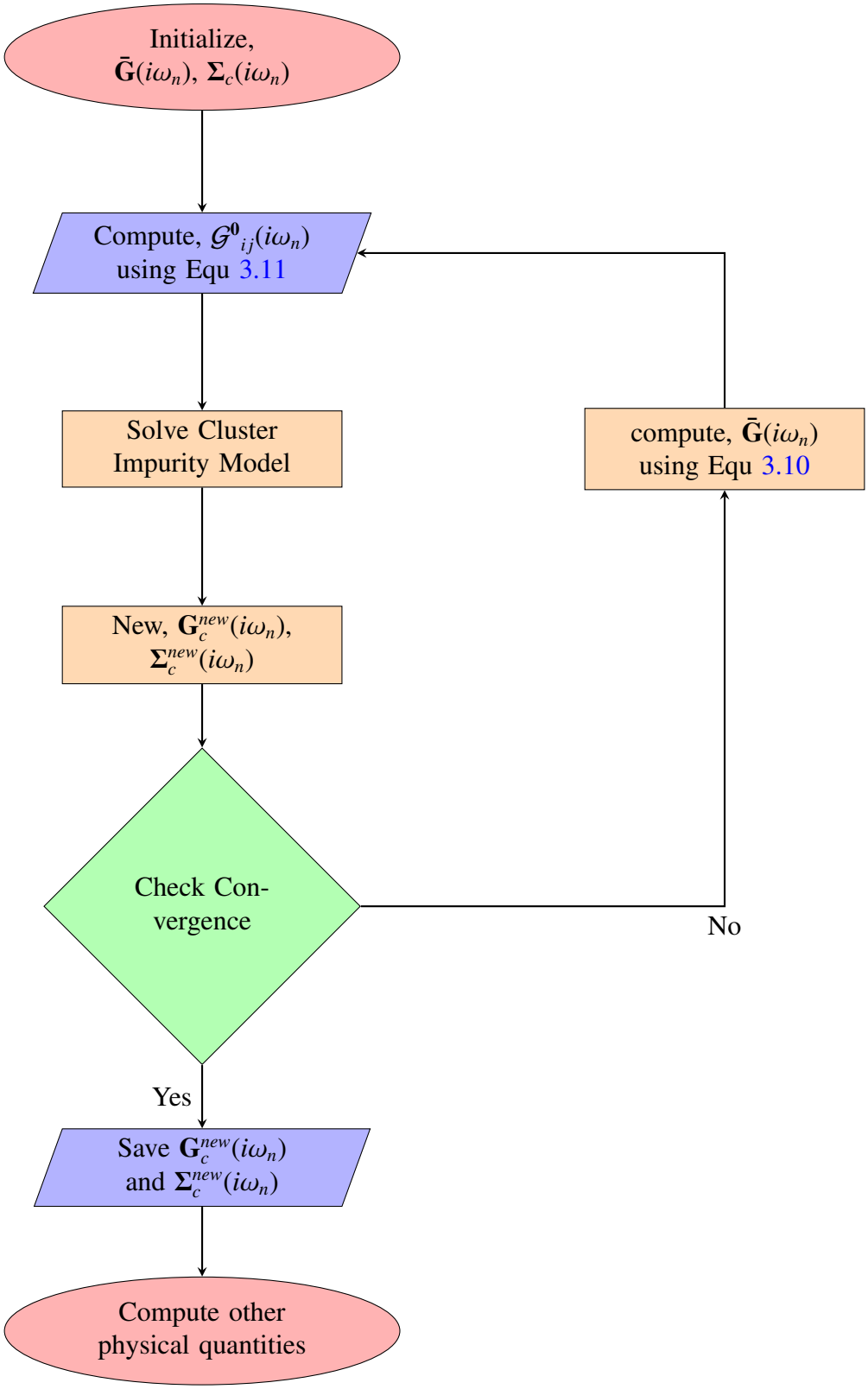

3.2.2 Dynamical Cluster Approximation (DCA)

In this method [93] the full lattice Brillouin zone(BZ) is divided into N_c patches with equal size as shown in Fig 3.3(b). Each patch is chosen in such a way that center of the is the reciprocal lattice vector of the real space cluster. The patch function is defined by:

$$\phi_{\mathbf{K}}(\mathbf{k}) = \begin{cases} 1, & \text{if } \mathbf{k} \text{ is in patch } \mathbf{K} \\ 0, & \text{otherwise.} \end{cases} \tag{3.12}$$

so that one can restrict the momentum sums inside the $\mathbf{K}^{th}$ patch. The approximation of DCA is to choose a constant self-energy on each patch but different in different patches i.e.:

$$\Sigma(\mathbf{k}, i\omega_n) \approx \Sigma_c(\mathbf{K}, i\omega_n) \tag{3.13}$$

Since the self-energy is a function of the Green function, the cluster self-energy is also a function of the coarse grained Green function, $\Sigma_c(\mathbf{K}, i\omega_n) = \Sigma_c[\bar{G}(\mathbf{K}, i\omega_n)]$. The coarse grained Green function $\bar{G}(\mathbf{K}, i\omega_n)$ is:

$$\bar{G}(\mathbf{K}, i\omega_n) = \frac{N_c}{N} \sum_{\mathbf{k}} \phi_{\mathbf{K}}(\mathbf{k}) G(\mathbf{k}, i\omega_n) = \frac{N_c}{N} \sum_{\mathbf{k}} \phi_{\mathbf{K}}(\mathbf{k}) \frac{1}{i\omega_n - \epsilon_k + \mu - \Sigma^{DCA}(\mathbf{k}, i\omega_n)} \tag{3.14}$$

The DCA self-energy $\Sigma^{DCA}(\mathbf{k}, i\omega_n)$ is:

$$\Sigma^{DCA}(\mathbf{k}, i\omega_n) = \sum_{\mathbf{K}} \phi_{\mathbf{K}}(\mathbf{k}) \Sigma_c(\mathbf{K}, i\omega_n) \tag{3.15}$$

Then the corresponding non-interacting Green function is given as:

$$\mathcal{G}^0(\mathbf{K}, i\omega_n) = [\bar{G}^{-1}(\mathbf{K}, i\omega_n) + \Sigma_c(\mathbf{K}, i\omega_n)]^{-1} \tag{3.16}$$

This non-interacting Green function $\mathcal{G}^0(\mathbf{K}, i\omega_n)$ is fed back to the cluster impurity solver. The impurity solver gives the interacting cluster Green function $G_c(\mathbf{K}, i\omega_n)$. Then we

calculate the cluster self-energy $\Sigma_c(\mathbf{K}, i\omega_n)$ using Dyson's equation,

$$\Sigma_c(\mathbf{K}, i\omega_n) = \mathcal{G}_0^{-1}(\mathbf{K}, i\omega_n) - G_c^{-1}(\mathbf{K}, i\omega_n) \tag{3.17}$$

The new cluster self-energy is fed back in equation(3.15) and iterated till self-consistently is attained. The iteration stops when the $\Sigma_c(\mathbf{K}, i\omega_n)$ converges.

Chapter 4

Falicov-Kimball Model and Dynamical Mean Field Theory

In this chapter, I will present a review on Falicov-Kimball Model. I will first show how it is related with Binary Disordered Alloy and then exact solution within DMFT approximation.

The "Falicov-Kimball model" was first introduced by Hubbard and Gutzwiller in 1963-65 as a simplification of the Hubbard model. Falicov and Kimball [32] introduced in 1969 a model that included a few extra complications, in order to investigate metal-insulator phase transitions in rare-earth materials and transition-metal compounds. Experimental data suggested that this transition is due to the interactions between electrons in two electronic states: non-localized states (itinerant electrons), and states that are localized around the sites corresponding to the metallic ions of the crystal (static electrons). Brandt and Mielsch [18, 19, 20] for the first time exactly solve this model

analytically in infinite dimensions.

4.1 Hamiltonian of FKM Model

The Falicov-Kimball Model involve spinless conduction electrons and localized electrons or ions. The Hamiltonian is:

$$H = -t\sum_{\langle ij\rangle}(c_i^\dagger c_j + h.c.) + \sum_i \epsilon_f f_i^\dagger f_i - \mu\sum_i (c_i^\dagger c_i + f_i^\dagger f_i) + U\sum_i c_i^\dagger c_i f_i^\dagger f_i \tag{4.1}$$

Here, $c, c^\dagger$ are the annihilation and creation operators corresponding to the conduction electrons respectively, t is the kinetic term of c-electrons, ϵ_f is the site energy of f-electrons, μ is the chemical potential, U is the on site interaction of c and f electrons. Let us mention that Falicov-Kimball model has been used by several authors to devise approximations to the solution of the $d = \infty$ Hubbard model. Here the number density of localized f electrons is determined by statistical average. If I consider Hubbard model with one of the spin species as moving(conduction electrons) in the background of the other one(localized electrons), considered frozen and static then Hubbard model and Falicov-Kimball Model are equivalent.

4.2 Exact Solution of FKM

Brandt and Mielsch [18] first showed that FKM model can be solved exactly in infinite dimension [127] by analytical methods. In this method the full lattice problem is mapped to a exactly solvable atomic problem with a time dependent field in the conduction electron as perturbation. Then the corresponding generalized partition function is given by,

$$Z = Tr_{\{c,f\}}[Exp(-\beta H_{at})S(\lambda)] \tag{4.2}$$

where, H_{at} is the atomic Hamiltonian given as,

$$H_{at} = Uc^{\dagger}cf^{\dagger}f + E_f f^{\dagger}f - \mu(c^{\dagger}c + f^{\dagger}f) \tag{4.3}$$

$$S(\lambda) = T_{\tau}Exp\left[-\int_0^{\beta} d\tau \int_0^{\beta} d\tau' \lambda(\tau,\tau')d^{\dagger}(\tau)d(\tau')\right] \tag{4.4}$$

here, $\lambda(\tau,\tau^{'})$ is the generalized time-dependent field which can be written in Fourier transform form as,

$$\lambda(\tau,\tau') = \frac{1}{\beta}\sum_n Exp[-i\omega_n(\tau-\tau')]\lambda_n \tag{4.5}$$

ω_n is the Matsubara frequency given as,

$$\omega_n = \frac{(2n+1)\pi}{\beta} \tag{4.6}$$

Now the Green function of the conduction electron is:

$$G(\tau,\tau') = \frac{1}{Z}Tr_{\{c,f\}}[-Exp(-\beta H_{at})S(\lambda)c(\tau)c^{\dagger}(\tau')] \tag{4.7}$$

The green function is related with the partition function as:

$$G(\tau,\tau') = -\frac{1}{Z}\frac{dZ}{d\lambda(\tau,\tau')} = -\frac{dlnZ}{d\lambda(\tau,\tau')} \tag{4.8}$$

Now in the Fourier space of $G(\tau,\tau')$ is:

$$G(i\omega_n) = -\frac{dlnZ}{d\lambda_n} \tag{4.9}$$

Now I know that for atomic FK model the number of f electrons is constant of motion i.e. is either 0 or 1 while the c-electron number can take any value between 0 and 1. Indeed the two Hilbert subspace of f-electrons $f^{\dagger}f = 0$ and $f^{\dagger}f = 1$ evolve independently under the dynamics of the c-electrons. Hence trace can be performed separately for $n_f = 0$ and

$n_f = 1$ subspaces. Hence the partition function is:

$$\begin{aligned} Z &= Tr_{\{c\}}[Exp(-\beta H_{at})S(\lambda)]_{f^\dagger f=0} + Tr_{\{c\}}[Exp(-\beta H_{at})S(\lambda)]_{f^\dagger f=1} \\ &= Z_0 + Z_1 \end{aligned} \tag{4.10}$$

For $n_f = 0$ subspace the atomic Hamiltonian becomes:

$$H_{at} = -\mu c^\dagger c \tag{4.11}$$

Then the partition function corresponds to the $n_f = 0$ subspace as,

$$Z_0 = 2\prod_n \frac{i\omega_n + \mu - \lambda_n}{i\omega_n} \tag{4.12}$$

Similarly, for $n_f = 1$ subspace the atomic Hamiltonian becomes:

$$H_{at} = (U - \mu)c^\dagger c + (E_f - \mu) \tag{4.13}$$

Hence the partition function becomes the same as Z_0 with μ will be replaced by $\mu - U$ and multiplied by a pre-factor $Exp[-\beta(E_f - \mu)]$. Hence,

$$Z_1 = 2Exp[-\beta(E_f - \mu)]\prod_n \frac{i\omega_n + \mu - \lambda_n}{i\omega_n} \tag{4.14}$$

Hence the full partition function becomes:

$$\begin{aligned} Z &= 2\prod_n \frac{i\omega_n + \mu - \lambda_n}{i\omega_n} + 2Exp[-\beta(E_f - \mu)]\prod_n \frac{i\omega_n + \mu - \lambda_n}{i\omega_n} \\ &= 2Exp\left\{\sum_n [ln(i\omega_n + \mu - \lambda_n) - ln(i\omega_n)]e^{i\omega_n 0^+}\right\} + \\ 2 \quad &Exp\left\{-\beta(E_f - \mu) + \sum_n [ln(i\omega_n + \mu - U - \lambda_n) - ln(i\omega_n)]e^{i\omega_n 0^+}\right\} \end{aligned} \tag{4.15}$$

By differentiating logarithmic Z of w.r.t. λ_n (See Appendix B) I have the green function as,

$$G(i\omega_n) = \frac{w_0}{i\omega_n + \mu - \lambda_n} + \frac{w_1}{i\omega_n + \mu - U - \lambda_n} \tag{4.16}$$

with $w_0 = \frac{Z_0}{Z} = 1 - w_1$ and,

$$w_1 = \frac{Z_1}{Z} = \frac{2}{Z} Exp\left\{-\beta(E_f - \mu) + \sum_n [ln(i\omega_n + \mu - U - \lambda_n) - ln(i\omega_n)]e^{i\omega_n 0^+}\right\} \tag{4.17}$$

w_0 is interpreted as the average conduction electron per site whereas, w_1 is the average of the f-electron per site.

The non interacting green function is interpreted as,

$$\mathcal{G}^{-1}(i\omega_n) = i\omega_n + \mu - \lambda_n \tag{4.18}$$

Then define self energy Σ_n as,

$$G^{-1}(i\omega_n) = (\mathcal{G}(i\omega_n)^{-1} - \Sigma(i\omega_n))^{-1} \tag{4.19}$$

Combining the above two equations I have,

$$\Sigma_n = w_1 U + w_0 w_1 U_n^2 (\mathcal{G}_n - w_0 G_n)^{-1} \tag{4.20}$$

This self energy depends on λ_n. Expressing λ_n in terms of G_n and using $w_0 = 1 - w_1$ one have,

$$\Sigma_n(G_n) = \frac{U}{2} - \frac{1}{2G_n} + \sqrt{\left(\frac{U}{2} - \frac{1}{2G_n}\right)^2 + w_1 \frac{U}{G_n}} \tag{4.21}$$

where, w_1, Σ_n is both functions of G_n.For constant w_1 the result will be similar with the coherent potential approximation(CPA) self energy of random binary alloy where the w_1 is constant fixed from outside.

In order to calculate lattice green function one can write the Dyson's equation for lattice

green function:

$$(i\omega_n + \mu - \Sigma_n^{ii}(G_n^{ii}))G_n^{il} - \sum_m t_{im} G_n^{ml} = \delta_{il} \tag{4.22}$$

I assume that Σ^{ii} is independent of site and for $d = \infty$ the self energy is local. Hence the Fourier transform of lattice green function:

$$G_n(k) = \frac{1}{i\omega_n + \mu - \Sigma_n - \epsilon_k} \tag{4.23}$$

Thus the local lattice green function becomes:

$$G_n^{ii} = \sum_k \frac{1}{i\omega_n + \mu - \Sigma_n - \epsilon_k} = \int_{-\infty}^{\infty} d\epsilon \frac{\rho_0(\epsilon)}{i\omega_n + \mu - \epsilon - \Sigma(i\omega_n)} \tag{4.24}$$

4.3 Properties of FKM Model:

In this section, I will discuss some of the general feature of the Falicov-Kimball Model(FKM):

- At half filling $n_c + n_f = 1$, the model display a metal insulator transition [121, 122] at critical U, $U_c = D$ i.e. for $U < U_c$ the system is metal and for $U > U_c$ the system is insulator.
- If the number of electron per side $n_f = 0$ or 1, the model reduces to non interacting Fermi gas.
- If n_f is in between 0 and 1, f-electrons acts like a disorder scatterer with an annealed average over disorder (more details discussion in next section). This disorder produces a finite lifetime even at the Fermi surface, the quasi-particle picture breaks down. The system behaves like an non Fermi liquid. Although, for small U the system behaves like a "dirty Fermi liquid".
- Hence the unlike Hubbard model the model exhibits three phases: (a) dirty Fermi liquid metal b) non-Fermi liquid metal and (c) insulator.

- For half filling at low temperature, the $d = \infty$ FK Model display CDW ordering phase in all bipartite lattice as a function of U. It had shown analytically [123] $T_c \sim 1/U$ for large U, while $T_c \sim U^2 ln(1/U)$ for small U.

- Lastly, the f-electron spectral function has a x-ray edge singularity. I will not provide here detail discussion of f-electron spectrum as it is out of scope of present thesis. Interested reader may go through the following articles [110, 21, 52].

4.3.1 Binary Disorder Alloy as FKM

Here I show that binary disorder alloy model Hamiltonian can be mapped to Falicov-Kimball Model Hamiltonian. The Hamiltonian for binary disordered alloy is given by,

$$H_{binary} = -t \sum_{\langle ij \rangle} (c_i^\dagger c_j + h.c.) - \mu \sum_i c_i^\dagger c_i + \sum_i v_i c_i^\dagger c_i \tag{4.25}$$

Where, v_i is the disordered potential at site i, for binary alloy v_i have one of the two possible values either U or 0. The probability distribution of disorder potential,

$$P(v_i) = \begin{cases} x, & \text{if } v_i = U \\ 1 - x, & \text{if } v_i = 0 \end{cases} \tag{4.26}$$

Hence one can write $v_i = U x_i$, where x_i is either 0 or 1 with $\langle x_i \rangle \equiv x$. Now if I promoted x_i as an operator it satisfied all the commutation relations as the fermion number operator does. So one can think x_i as $x_i \equiv n_i^f = f_i^\dagger f_i$. Then the Hamiltonian is,

$$H_{binary} = -t \sum_{\langle ij \rangle} (c_i^\dagger c_j + h.c.) - \mu \sum_i c_i^\dagger c_i + U \sum_i f_i^\dagger f_i c_i^\dagger c_i \tag{4.27}$$

This is the Falicov-Kimball Model (FKM) with site energy of f-electrons $\epsilon_f = \mu$. There is no kinetic term corresponding to f-electrons, so it is called localized electrons. One more thing that should mention that disorder average $\langle x_i \rangle$ for binary alloy is fixed from

outside i.e. quenched, whereas the average f-electrons i.e. $\langle n_f \rangle$ is calculated statistically i.e. annealed. So one can think binary disordered alloy model as Falicov-Kimball Model with quenched average over f-electrons instead of annealed. In this thesis, I consider the quenched average of f-electrons $\langle n_f \rangle$.

4.4 DMFT approach to Falicov-Kimball Model within Alloy Analogy

Consider the Falicov Kimball Model(FKM) or Binary Disordered Alloy Model on bethe lattice of infinity coordination number(i.e.$d = \infty$). The Hamiltonian is:

$$H = -t \sum_{\langle ij \rangle, \sigma} (c_i^\dagger c_j + h.c.) - \mu \sum_{i,\sigma} c_i^\dagger c_i + \sum_i v_i c_i^\dagger c_i \tag{4.28}$$

I assume that the distribution of disorder in binary alloy is:

$$P(v_i) = (1 - x)\delta(v_i) + x\delta(v_i - U) \tag{4.29}$$

Then $v_i = U n_i^f$ with n_i^f is 0 or 1. This model is not a Fermi-liquid for $\langle n^f \rangle \neq 0$ or 1, as for $\langle n^f \rangle = 0$ or 1 the model is an noninteracting problem.Because f-electrons act as an annealed disorder scatterer and the scattering produces finite lifetime at the Fermi surface. So no quasi-particle exists and Fermi-liquid theory breaks down. Although for small disorder one can think this model as "dirty Fermi liquid".

Using DMFT technique one can mapped the Hamiltonian to a impurity problem embedding with an "effective medium" given by,

$$H_{imp} = U \sum_\sigma n_0^f c_{0\sigma}^\dagger c_{0\sigma} - \mu \sum_\sigma c_{0\sigma}^\dagger c_{0\sigma} + \sum_{k,\sigma} (\epsilon_k - \mu) c_{k,\sigma}^\dagger c_{k\sigma} + \sum_{k,\sigma} (t e^{ik.R_0} c_{k\sigma}^\dagger c_{0\sigma} + h.c.) \tag{4.30}$$

where, 0 denotes the impurity site, first term is the impurity potential due to disorder, μ is

the chemical potential, third term is the dispersion of the effective medium (bath), fourth term is the hybridization term between the impurity and the effective medium (conduction electron bath function) that has to be self consistently determined by a suitable embedding procedure.

Now I will calculate the impurity green function, i.e. $G_{00}(\omega) = \langle c_0; c_0^\dagger \rangle, G_{k0}(\omega) = \langle c_k; c_0^\dagger \rangle$ with the technique of Equation of Motion (EOM).Using the identity:

$$\omega \langle \hat{A}; \hat{B} \rangle = \langle [\hat{A}, \hat{B}]_\pm \rangle + \langle [[\hat{A}, \hat{H}]; \hat{B}]_\pm \rangle \tag{4.31}$$

Here, $\hat{A}$ and $\hat{B}$ are fermionic or bosinic operators and anticommutator and commutator are respectively for fermionic and bosonic operators.

EOM for $G_{00}(\omega)$:

$$(\omega + \mu) G_{00}(\omega) = 1 + \sum_k t_k G_{k0} + v \langle n_0^f c_0; c_0^\dagger \rangle \tag{4.32}$$

Notice the appearance of the higher order green function. Using EOM one can calculate the higher order green function and close the loop. For $\langle n_0^f c_0; c_0^\dagger \rangle$,

$$(\omega + \mu - U) \langle n_0^f c_0; c_0^\dagger \rangle = \langle n_0^f \rangle + \sum_k t_k \langle n_0^f c_k; c_0^\dagger \rangle \tag{4.33}$$

EOM for G_{k0},

$$G_{k0}(\omega) = \frac{t_k^*}{(\omega + \mu - \epsilon_k)} G_{00}(\omega) \tag{4.34}$$

EOM for $\langle n_0^f c_k; c_0^\dagger \rangle$,

$$\langle n_0^f c_k; c_0^\dagger \rangle = \frac{t_k^*}{(\omega + \mu - \epsilon_k)} \langle n_0^f c_0; c_0^\dagger \rangle \tag{4.35}$$

where, I have used $(n_0^f)^2 = n_0^f$. Closing the above four equation the local green function is given as:

$$G_{00}(\omega) = \frac{1 - \langle n_0^f \rangle}{\omega + \mu - \Delta(\omega)} + \frac{\langle n_0^f \rangle}{\omega + \mu - U - \Delta(\omega)} \tag{4.36}$$

where, $\Delta(\omega)$ is a bath function given as,

$$\Delta(\omega) = \sum_k \frac{\mid t_k \mid^2}{\omega + \mu - \epsilon_k} \tag{4.37}$$

$\Delta(\omega)$ is related with the lattice green function with suitable self consistency condition. For any general lattice the consistency condition is:

$$\Delta(\omega) = \int_{-\infty}^{\infty} \frac{\rho_0(\epsilon) d\epsilon}{\omega + \mu - \epsilon_k - \Sigma_k(\omega)} \tag{4.38}$$

For bethe lattice with infinite coordination number the self energy is local i.e. $\Sigma_k(\omega) = \Sigma_{ii}(\omega)$. The self consistency condition is:

$$\Delta(\omega) = t^2 G_{00}(\omega) \tag{4.39}$$

The non-interacting Weiss Green function is given as:

$$\mathcal{G}^{-1}(\omega) = \omega + \mu - \Delta(\omega) \tag{4.40}$$

Using Dyson's equation the self energy is given as:

$$\Sigma_{00}(\omega) = \mathcal{G}^{-1}(\omega) - G_{00}^{-1}(\omega) \tag{4.41}$$

Hence for bethe lattice with infinite coordination the self energy has the form:

$$\Sigma_{00}(\omega) = U\langle n_0^f \rangle + \frac{U^2 \langle n_0^f \rangle (1 - \langle n_0^f \rangle)}{\omega - U(1 - \langle n_0^f \rangle) - t^2 G_{00}(\omega)} \tag{4.42}$$

The algorithm of the DMFT self-consistency loop is shown in the flowchart 4.1:

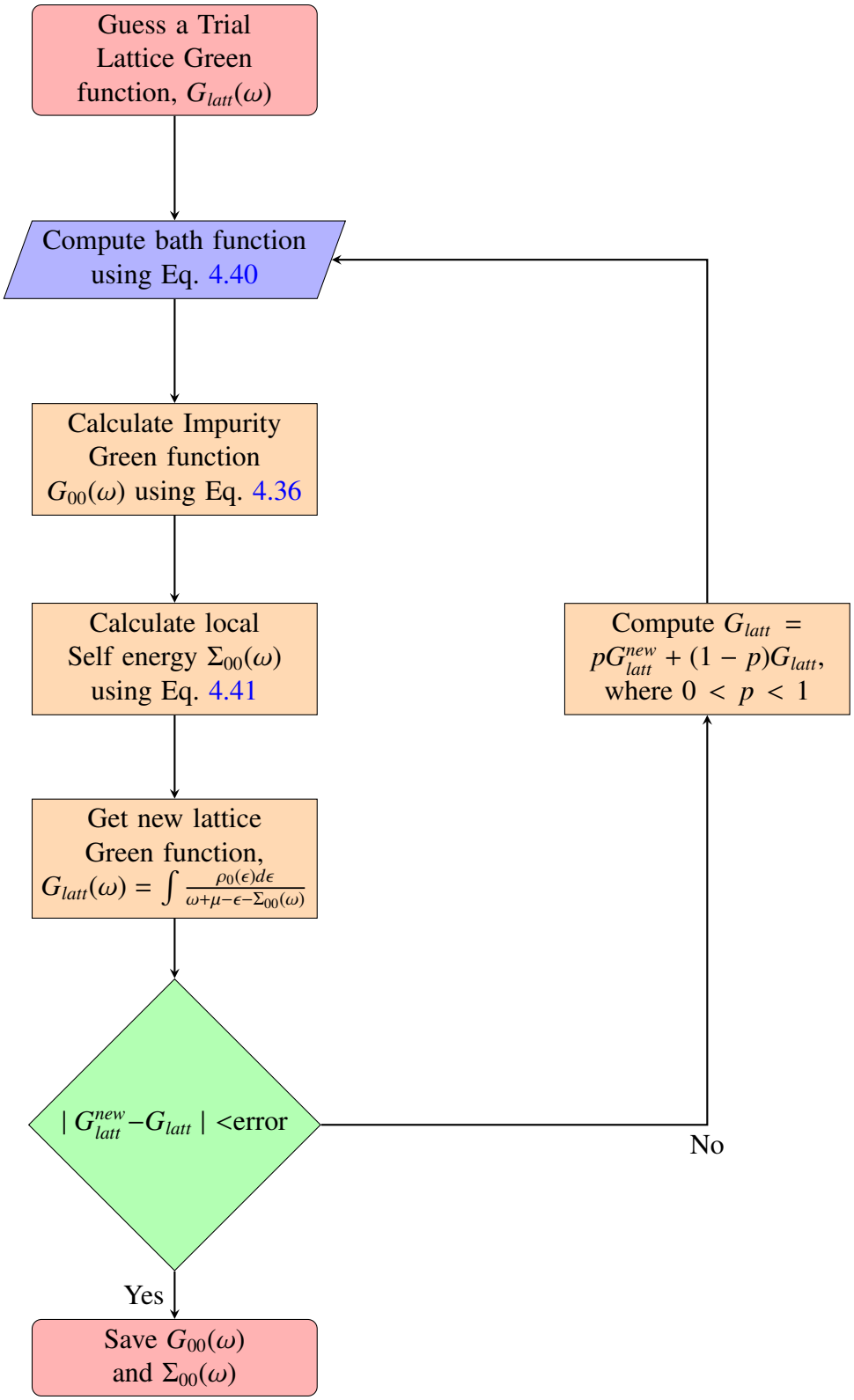

Figure 4.1: Algorithm of the single-site DMFT self-consistency loop

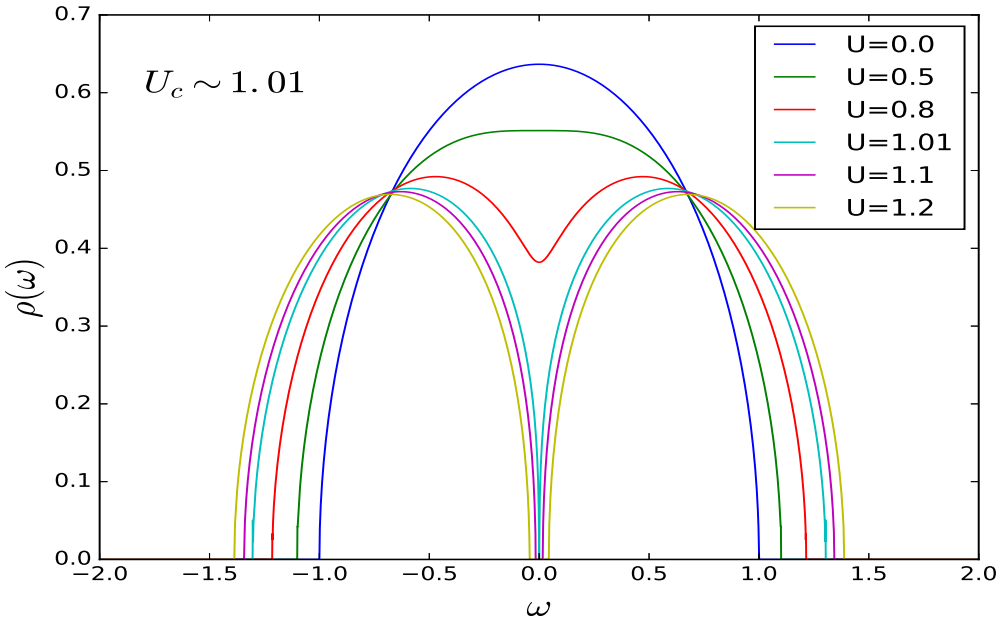

Figure 4.2: The local density of states (LDOS) of the binary disorder alloy model for p-h symmetry case. A clear continuous band-splitting transition is seen at $U_c = 1.01$ (cyan curve).

4.5 Results and Discussions:

Following the algorithm as describe in the above flowchart I have calculated the local green function $G_{00}(\omega)$ for bethe lattice with infinite coordination number ($d = \infty$) with bare half-bandwidth is unity. The convergence has been achieved upto the error of 10^{-5}. The spectral function is given as, $A(k,\omega) = -\frac{1}{\pi}G(k,\omega)$. For infinite dimensional bethe lattice Green function as well as self-energy are local. Hence the spectral density is given as, $A(\omega) = -\frac{1}{\pi}G_{00}(\omega)$. In Fig 4.2 the local DOS is shown for different disorder strength (U) for $\langle n_0^f \rangle = 0.5$ i.e. particle-hole symmetric case. It shows a continuous metal-insulator transition (MIT) at the critical disorder strength $U_c = 1.01$ (cyan curve). Fig 4.3 shows the real part of the local self energy ($\Sigma(\omega)$) and Fig 4.4 shows the imaginary part of the local self energy ($\Sigma(\omega)$) as a function of disorder strength (U) on both sides of the critical curve. Self-energy shows the non-Fermi-Liquid characteristic in the metallic state. Imaginary part of the self-energy shows the quadratic behaviour but with wrong sign and at zero

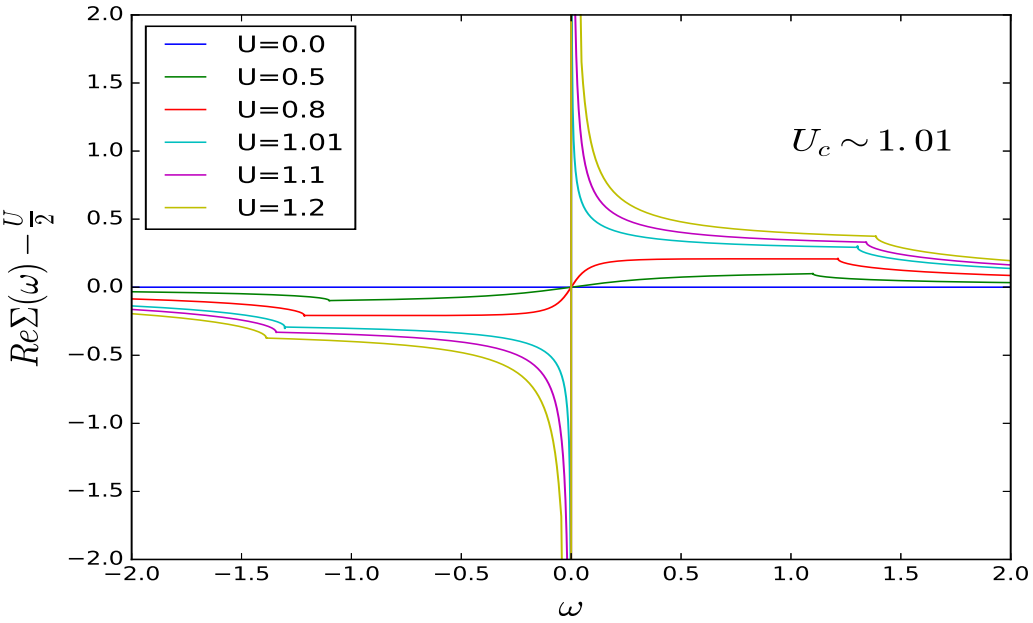

Figure 4.3: Real part of the local self-energy of binary disorder model for the same parameter value as in Fig 4.2. It shows discontinuity at ω=0 at critical U=1.01 (cyan curve)

temperature the intercept at $\omega = 0$ does not go to zero. The real part of the self energy is linear but the slope has the wrong sign near ω. In the insulating state the imaginary part of the self-energy diverges as well as the real part shows discontinuity at $\omega = 0$ which is responsible for the opening of the gap at $\omega = 0$.

4.6 Summary

To summarize, I have reviewed the FKM model and how it is related with the binary disorder alloy within some restrictions. I also show that both FKM and binary disorder model can be solved exactly within single-site DMFT. I also presented the continuous metal-insulator transition (MIT) in this model on infinite dimensional bethe lattice and analysis the properties of single-particle propagator (both Green function and self-energy) across the MIT. From the next chapter, I will start discussing about the main part of my thesis problem where I will extend this DMFT technique to the two-site cluster level and

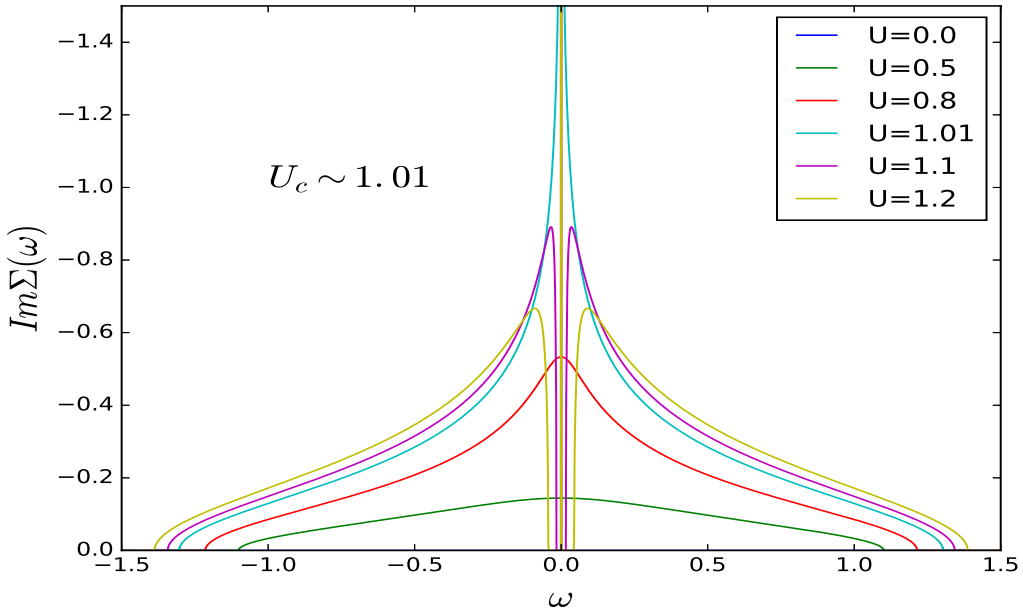

Figure 4.4: Imaginary part of the local self-energy of binary disorder model for the same parameter value as in Fig 4.2. It shows singularity at ω=0 at critical U=1.01 (cyan curve)

will apply this technique to study the quantum transport in the FKM within alloy analogy.

Chapter 5

Solution of FKM within Alloy Analogy Using Cluster DMFT

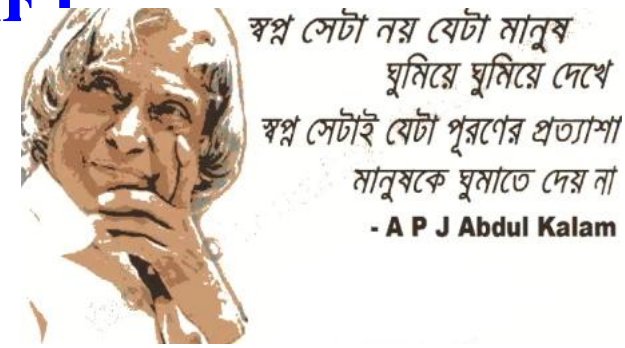

This chapter is devoted to discuss the solution of Falicov Kimball Model (FKM) or equivalently Anderson disorder problem with binary alloy distribution taking into account the short range order (SRO). The Hamiltonian is solved using cluster Dynamical mean field Theory (C-DMFT) technique which treated inter-site correlation($\frac{1}{d}$) exactly. In results and discussions, I will show the local propagator as well as cluster momentum propagator, self energy and two-particle cluster momentum vertex function and discuss their analytical properties and behaviour across the MIT.

5.1 Introduction

Single-site DMFT or equivalently Coherent Potential Approximation (CPA) falls short in describing Anderson Localization (AL) [5], since for this technique non-

local self-energy vanishes and the local self-energy cannot take into account for the coherent back-scattering process that is responsible for AL. One way to include the non-local correlation is several numerical based cluster approaches [79, 53, 99] that has been applied with mixed success. The major difficulty of these methods is the time taken to solve this model grows exponentially with the number of lattice sites within the cluster. This rises a big challenge to solve the model in three dimensional lattice with large lattice sites.

To solve the issue of finite lattice I have adopted cluster extension of DMFT that treats intra-cluster (1/d, d=spatial dimension) correlations exactly to solve binary disordered problem or equivalent Falicov-Kimball Model. I extend earlier developed two-site cluster DMFT [62] to take into account non-local self-energy.

5.2 Model and Solution

The Hamiltonian for Anderson disorder model or equivalently Falicov-Kimball model (FKM) is given as,

$$H = -t \sum_{\langle i,j\rangle,\sigma} (c^{\dagger}_{i\sigma} c_{j\sigma} + h.c.) - \mu \sum_{i,\sigma} c^{\dagger}_{i\sigma} c_{i\sigma} + \sum_{i\sigma} v_i n_{i\sigma} \tag{5.1}$$

with $v_i = U x_i$. Here, I assume the binary distribution of disorder i.e.,

$$P(v_i) = (1 - x)\delta(v_i) + x\delta(v_i - U) \tag{5.2}$$

as defined in the previous chapter (Chapter 4). I also consider Short Range Order (SRO) f_{ij} between nearest neighbour disorder as a constant parameter, defined as:

$$f_{ij} = \langle v_i v_j \rangle - \langle v_i \rangle \langle v_j \rangle \tag{5.3}$$

In real materials this SRO is strongly depends on the x, temperature and other physical variables.

Now using C-DMFT technique the Hamiltonian can be mapped to an effective Anderson impurity model with impurity as a two sites cluster embedding by an effective dynamical bath with cluster self-energy.

The Hamiltonian for the impurity model is given as:

$$H_{imp} = H_{\mu} + H_U + H_{bath} + H_{hyb} \tag{5.4}$$

where, H_{μ}, H_U are terms corresponds to impurity, H_{bath} is the bath Hamiltonian and H_{hyb} is the hybridization term between the impurity and the bath. Each of these terms is given as:

$$\begin{aligned} H_{\mu} &= -\mu \sum_{i\in\{0,\alpha\}\sigma} c^{\dagger}_{i\sigma} c_{i\sigma} \\ H_U &= U \sum_{i\in\{0,\alpha\}\sigma} x_i n_{i\sigma} \\ H_{bath} &= \sum_{k,\sigma} \epsilon_{k,\sigma} c^{\dagger}_{k,\sigma} c_{k,\sigma} \\ H_{hyb} &= \sum_{k,i\in\{0,\alpha\},\sigma} (v_{ki} c^{\dagger}_{i\sigma} c_{k\sigma} + h.c.) \end{aligned} \tag{5.5}$$

where $0, \alpha$ are the two sites of the cluster impurity.

Now the cluster Green function is defined as:

$$\hat{\mathbf{G}} = \begin{pmatrix} G_{00}(\omega) & G_{0\alpha}(\omega) \\ G_{0\alpha}(\omega) & G_{00}(\omega) \end{pmatrix}$$

where, $G_{00}(\omega)$ is the diagonal Green function define as, $G^{\sigma}_{00}(\omega) := \langle c_{0\sigma}; c^{\dagger}_{0\sigma} \rangle$ and $G_{0\alpha}(\omega)$ is the off-diagonal Green's function define as, $G^{\sigma}_{0\alpha}(\omega) := \langle c_{0\sigma}; c^{\dagger}_{\alpha\sigma} \rangle$. Here, σ is the spin

indices, i.e. $\sigma \in \{\uparrow, \downarrow\}$. Using the identity (proof is given in Appendix A):

$$\omega\langle\hat{A};\hat{B}\rangle = \langle[\hat{A},\hat{B}]_{\pm}\rangle + \langle[[\hat{A},\hat{H}];\hat{B}]_{\pm}\rangle \tag{5.6}$$

The Equation of Motion (EQM) for $G^{\sigma}_{00}(\omega)$ is:

$$\omega G^{\sigma}_{00}(\omega) = 1 - tG^{\sigma}_{\alpha 0}(\omega) + U < x_0 c_{0\sigma}; c^{\dagger}_{0\sigma} > + \sum_k v_{k0} G^{\sigma}_{k0} \tag{5.7}$$

The EQM for off-diagonal Green function $G^{\sigma}_{0\alpha}(\omega)$ is:

$$\omega G^{\sigma}_{\alpha 0}(\omega) = U < x_\alpha c_{\alpha\sigma}; c^{\dagger}_{0\sigma} > -tG^{\sigma}_{00}(\omega) + \sum_k v_{k\alpha} G^{\sigma}_{k0}(\omega) \tag{5.8}$$

EOM for $G^{\sigma}_{k0}(\omega)$ is:

$$\begin{aligned} \omega\langle c_{k\sigma}; c^{\dagger}_{0\sigma}\rangle &= \epsilon_k\langle c_{k\sigma}; c^{\dagger}_{0\sigma}\rangle + \sum_{i\in\{0,\alpha\}} v^{*}_{ki}\langle c_{i\sigma}; c^{\dagger}_{0\sigma}\rangle \\ \Rightarrow G^{\sigma}_{k0}(\omega) &= \sum_{i\in\{0,\alpha\}} \frac{v^{*}_{ki}}{\omega - \epsilon_k} G^{\sigma}_{i0} \end{aligned} \tag{5.9}$$

Define, $\Delta_{00}(\omega) = \sum_k \frac{|v_{k0}|^2}{\omega-\epsilon_k}$ and $\Delta_{\alpha 0}(\omega) = \sum_k \frac{v_{k0}v^{*}_{k\alpha}}{\omega-\epsilon_k}$. Solving above three equations one gets,

$$G^{\sigma}_{00}(\omega) = \frac{1 + U < x_0 c_{0\sigma}; c^{\dagger}_{0\sigma} > + (\frac{U}{-t+\Delta_{\alpha 0}(\omega)}) F_2(\omega) < x_\alpha c_{\alpha\sigma}; c^{\dagger}_{0\sigma} >}{\omega - \Delta_{00} - F_2(\omega)} \tag{5.10}$$

$$G^{\sigma}_{\alpha 0}(\omega) = \left[\frac{U(\omega - \Delta_{00}(\omega)) < x_\alpha c_{\alpha\sigma}; c^{\dagger}_{0\sigma} > + (-t + \Delta_{\alpha 0}(\omega))(1 + U < x_0 c_{0\sigma}; c^{\dagger}_{0\sigma} >)}{(\omega - \Delta_{00}(\omega))(\omega - \Delta_{00}(\omega) - F_2(\omega))}\right] \tag{5.11}$$

Here, $F_1(\omega) \equiv \frac{(-t+\Delta_{\alpha 0}(\omega))^2}{\omega - U - \Delta_{00}(\omega)}$ and $F_2(\omega) \equiv \frac{(-t+\Delta_{\alpha 0}(\omega))^2}{\omega - \Delta_{00}(\omega)}$.

Similarly, using EOM one can calculate higher order Green function. The EOM for $< x_0 c_{0\sigma}; c^{\dagger}_{0\sigma} >$ is:

$$(\omega - U) < x_0 c_{0\sigma}; c^{\dagger}_{0\sigma} > = < x_0 > -t < x_0 c_{\alpha\sigma}; c^{\dagger}_{0\sigma} > + \sum_k v_{k0} < x_0 c_{k\sigma}; c^{\dagger}_{0\sigma} > \tag{5.12}$$

The EOM for $< x_0 c_{k\sigma}; c^{\dagger}_{0\sigma} >$ is:

$$\begin{aligned}
\omega\langle x_0 c_{k\sigma}; c^{\dagger}_{0\sigma}\rangle &= \epsilon_k\langle x_0 c_{k\sigma}; c^{\dagger}_{0\sigma}\rangle + \sum_{i\in\{0,\alpha\}} v^{*}_{ki}\langle x_0 c_{i\sigma}; c^{\dagger}_{0\sigma}\rangle \\
\langle x_0 c_{k\sigma}; c^{\dagger}_{0\sigma}\rangle &= \sum_{i\in\{0,\alpha\}} \frac{v^{*}_{ki}}{\omega-\epsilon_k}\langle x_0 c_{i\sigma}; c^{\dagger}_{0\sigma}\rangle
\end{aligned} \tag{5.13}$$

The EOM for $< x_0 c_{\alpha\sigma}; c^{\dagger}_{0\sigma} >$ is:

$$\omega < x_0 c_{\alpha\sigma}; c^{\dagger}_{0\sigma} >= U < x_0 x_\alpha c_{\alpha\sigma}; c^{\dagger}_{0\sigma} > -t < x_0 c_{0\sigma}; c^{\dagger}_{0\sigma} > + \sum_k v_{k\alpha} < x_0 c_{k\sigma}; c^{\dagger}_{0\sigma} > \tag{5.14}$$

The EOM for $< x_0 x_\alpha c_{\alpha\sigma}; c^{\dagger}_{0\sigma} >$ is:

$$(\omega - U) < x_0 x_\alpha c_{\alpha\sigma}; c^{\dagger}_{0\sigma} >= -t < x_0 x_\alpha c_{0\sigma}; c^{\dagger}_{0\sigma} > + \sum_k v_{k\alpha} < x_0 x_\alpha c_{k\sigma}; c^{\dagger}_{0\sigma} > \tag{5.15}$$

The EOM for $< x_0 x_\alpha c_{k\sigma}; c^{\dagger}_{0\sigma} >$ is:

$$\begin{aligned}
\omega < x_0 x_\alpha c_{k\sigma}; c^{\dagger}_{0\sigma} > &= \epsilon_k < x_0 x_\alpha c_{k\sigma}; c^{\dagger}_{0\sigma} > + \sum_{i\in\{0,\alpha\}} v^{*}_{k\alpha} < x_0 x_\alpha c_{i\sigma}; c^{\dagger}_{0\sigma} > \\
\Rightarrow < x_0 x_\alpha c_{k\sigma}; c^{\dagger}_{0\sigma} > &= \sum_{i\in\{0,\alpha\}} \frac{v^{*}_{k\alpha}}{\omega-\epsilon_k} < x_0 x_\alpha c_{i\sigma}; c^{\dagger}_{0\sigma} >
\end{aligned} \tag{5.16}$$

The EOM for $< x_0 x_\alpha c_{0\sigma}; c^{\dagger}_{0\sigma} >$ is:

$$(\omega - U) < x_0 x_\alpha c_{0\sigma}; c^{\dagger}_{0\sigma} >= \langle x_0 x_\alpha\rangle - t < x_0 x_\alpha c_{\alpha\sigma}; c^{\dagger}_{0\sigma} > + \sum_k v_{k0} < x_0 x_\alpha c_{k\sigma}; c^{\dagger}_{0\sigma} > \tag{5.17}$$

Here $\langle x_0 x_\alpha\rangle \equiv \langle x_\alpha x_0\rangle = \langle x_{0\alpha}\rangle$. Solving the above equations the expression for $\langle x_0 c_{0\sigma}; c^{\dagger}_{0\sigma}\rangle$ is:

$$< x_0 c_{0\sigma}; c^{\dagger}_{0\sigma} >= \frac{< x_0 > - < x_{0\alpha} >}{\omega - U - \Delta_{00}(\omega) - F_2(\omega)} + \frac{< x_{0\alpha} >}{\omega - U - \Delta_{00}(\omega) - F_1(\omega)} \tag{5.18}$$

The EOM for $< x_\alpha c_{\alpha\sigma}; c^\dagger_{0\sigma} >$ is:

$$(\omega - U) < x_\alpha c_{\alpha\sigma}; c^\dagger_{0\sigma} >= -t < x_\alpha c_{0\sigma}; c^\dagger_{0\sigma} > + \sum_k v_{k\alpha} < x_\alpha c_{k\sigma}; c^\dagger_{0\sigma} > \tag{5.19}$$

The EOM for $< x_\alpha c_{k\sigma}; c^\dagger_{0\sigma} >$ is:

$$\begin{aligned} \omega < x_\alpha c_{k\sigma}; c^\dagger_{0\sigma} > &= \epsilon_k < x_\alpha c_{k\sigma}; c^\dagger_{0\sigma} > + \sum_{i\in\{0,\alpha\}} v^*_{ki} < x_\alpha c_{i\sigma}; c^\dagger_{0\sigma} > \\ < x_\alpha c_{k\sigma}; c^\dagger_{0\sigma} > &= \sum_{i\in\{0,\alpha\}} \frac{v^*_{ki}}{\omega - \epsilon_k} < x_\alpha c_{i\sigma}; c^\dagger_{0\sigma} > \end{aligned} \tag{5.20}$$

The EOM for $< x_\alpha c_{0\sigma}; c^\dagger_{0\sigma} >$ is:

$$\omega < x_\alpha c_{0\sigma}; c^\dagger_{0\sigma} >=< x_\alpha > + U < x_\alpha x_0 c_{0\sigma}; c^\dagger_{0\sigma} > - t < x_\alpha c_{\alpha\sigma}; c^\dagger_{0\sigma} > + \sum_k v_{k0} < x_\alpha c_{k\sigma}; c^\dagger_{0\sigma} > \tag{5.21}$$

Solving the above equations the expression for $\langle x_\alpha c_{\alpha\sigma}; c^\dagger_{0\sigma}\rangle$ is:

$$< x_\alpha c_{\alpha\sigma}; c^\dagger_{0\sigma} >= \frac{F_1(\omega)}{-t + \Delta_{\alpha 0}(\omega)} \left[\frac{< x_\alpha > - < x_{0\alpha} >}{\omega - \Delta_{00}(\omega) - F_1(\omega)} + \frac{< x_{0\alpha} >}{\omega - U - \Delta_{00}(\omega) - F_1(\omega)} \right] \tag{5.22}$$

Using the four equations I have the final expressions for diagonal and off-diagonal Green function:

$$\begin{aligned} G_{00}(\omega) &= \frac{1 - \langle x_0\rangle - \langle x_\alpha\rangle + \langle x_{\alpha 0}\rangle}{\omega - \Delta_{00}(\omega) - F_2(\omega)} + \frac{\langle x_0\rangle - \langle x_{\alpha 0}\rangle}{\omega - v - \Delta_{00}(\omega) - F_2(\omega)} \\ &+ \frac{\langle x_\alpha\rangle - \langle x_{\alpha 0}\rangle}{\omega - \Delta_{00}(\omega) - F_1(\omega)} + \frac{\langle x_{\alpha 0}\rangle}{\omega - v - \Delta_{00}(\omega) - F_1(\omega)} \end{aligned} \tag{5.23}$$

$$\begin{aligned} G_{\alpha 0}(\omega) &= \frac{F_2}{(-t + \Delta_{\alpha 0}(\omega))} \left[\frac{1 - \langle x_0\rangle - \langle x_\alpha\rangle + \langle x_{\alpha 0}\rangle}{\omega - \Delta_{00}(\omega) - F_2(\omega)} + \frac{\langle x_0\rangle - \langle x_{\alpha 0}\rangle}{\omega - v - \Delta_{00}(\omega) - F_2(\omega)} \right] \\ &+ \frac{F_1}{(-t + \Delta_{\alpha 0}(\omega))} \left[\frac{\langle x_\alpha\rangle - \langle x_{\alpha 0}\rangle}{\omega - \Delta_{00}(\omega) - F_1(\omega)} + \frac{\langle x_{\alpha 0}\rangle}{\omega - v - \Delta_{00}(\omega) - F_1(\omega)} \right] \end{aligned} \tag{5.24}$$

Here the bath function $\hat{\mathbf{\Delta}}(\omega)$ is a 2×2 matrix,

$$\hat{\mathbf{\Delta}}(\omega) = \begin{pmatrix} \Delta_{00}(\omega) & \Delta_{0\alpha}(\omega) \\ \Delta_{0\alpha}(\omega) & \Delta_{00}(\omega) \end{pmatrix}$$

5.2.1 Calculation of self-energy:

The self-energy is in 2×2 matrix form:

$$\hat{\mathbf{\Sigma}}(\omega) = \begin{pmatrix} \Sigma_{00}(\omega) & \Sigma_{0\alpha}(\omega) \\ \Sigma_{0\alpha}(\omega) & \Sigma_{00}(\omega) \end{pmatrix}$$

The non-interacting Weiss Green function is:

$$\hat{\mathcal{G}}(\omega) = \left[(\omega + \mu)\mathbb{I} - \hat{\mathbf{T}} - \hat{\mathbf{\Delta}}(\omega)\right]^{-1} \tag{5.25}$$

Here $\mathbb{I}$ is the 2×2 identity matrix and $\hat{\mathbf{T}}$ is of form:

$$\hat{\mathbf{T}} = \begin{pmatrix} 0 & -t \\ -t & 0 \end{pmatrix}$$

Hence,

$$\hat{\mathcal{G}}^{-1}(\omega) = \begin{pmatrix} \omega + \mu - \Delta_{00}(\omega) & t - \Delta_{0\alpha}(\omega) \\ t - \Delta_{0\alpha}(\omega) & \omega + \mu - \Delta_{00}(\omega) \end{pmatrix}$$

The Weiss Green function $\hat{\mathcal{G}}$ is connected with the impurity Green function $\hat{\mathbf{G}}$ through suitable matrix self-consistency condition. For Bethe lattice the self-consistency condition reduces to the simplified form : $\hat{\mathbf{\Delta}}(\omega) = t^2\hat{\mathbf{G}}(\omega)$. Using Dyson's equation in matrix form the self-energy is: $\hat{\mathbf{\Sigma}}(\omega) = \hat{\mathcal{G}}^{-1}(\omega) - \hat{\mathbf{G}}^{-1}(\omega)$, i.e.

$$\begin{pmatrix} \Sigma_{00}(\omega) & \Sigma_{0\alpha}(\omega) \\ \Sigma_{0\alpha}(\omega) & \Sigma_{00}(\omega) \end{pmatrix} = \begin{pmatrix} \omega + \mu - \Delta_{00}(\omega) & t - \Delta_{0\alpha}(\omega) \\ t - \Delta_{0\alpha}(\omega) & \omega + \mu - \Delta_{00}(\omega) \end{pmatrix} - \begin{pmatrix} G_{00}(\omega) & G_{0\alpha}(\omega) \\ G_{0\alpha}(\omega) & G_{00}(\omega) \end{pmatrix}^{-1}$$

Hence the final form of the local and non-local self-energy:

$$\Sigma_{00}(\omega) = (\omega + \mu - \Delta_{00}(\omega)) - \frac{1}{2}\left[\frac{1}{G_{00}(\omega) + G_{0\alpha}} + \frac{1}{G_{00}(\omega) - G_{0\alpha}}\right] \tag{5.26}$$

$$\Sigma_{0\alpha}(\omega) = (t - \Delta_{0\alpha}(\omega)) + \frac{1}{2}\left[\frac{1}{G_{00}(\omega) - G_{0\alpha}} - \frac{1}{G_{00}(\omega) + G_{0\alpha}}\right] \tag{5.27}$$

5.2.2 Self-consistency condition for two-site Cluster Method

The solution for the two site cluster impurity problems give the following matrix Green function and self-energy:

$$\hat{\mathbf{G}}(\omega) = \begin{pmatrix} G_{00}(\omega) & G_{0\alpha}(\omega) \\ G_{0\alpha}(\omega) & G_{00}(\omega) \end{pmatrix}, \qquad \hat{\mathbf{\Sigma}}(\omega) = \begin{pmatrix} \Sigma_{00}(\omega) & \Sigma_{0\alpha}(\omega) \\ \Sigma_{0\alpha}(\omega) & \Sigma_{00}(\omega) \end{pmatrix}$$

Dividing the Brillouin zone as shown in Fig 5.1 into two parts corresponds to two cluster momentum, $\mathbf{K} = (0, 0, --)$ and $\mathbf{K} = (\pi, \pi, --)$ as shown in Fig 5.1. For k-points corresponds to $\mathbf{K} = (0, 0, --)$ is S-sector and for k-points corresponds to $\mathbf{K} = (\pi, \pi, --)$ is P-sector. Then the lattice self-energy is related to the impurity self energy $\hat{\mathbf{\Sigma}}(\omega)$ using DCA:

$$\Sigma_{DCA}(\vec{k}, \omega) = \begin{cases} \Sigma_S = \Sigma_0 + \Sigma_1 & \mathbf{k} \in S \\ \Sigma_P = \Sigma_0 - \Sigma_1 & \mathbf{k} \in P \end{cases} \tag{5.28}$$

The partial density of states correspond to the cluster momentum S, P are:

$$\rho_{S(P)}(\epsilon) = 2 \times \int_{k \in \{S,P\}} d\mathbf{k}\delta(\epsilon - \epsilon_k) \tag{5.29}$$

The Green function corresponds to cluster momentum basis:

$$\hat{\mathbf{G}}(\omega) = \begin{pmatrix} G_S(\omega) & 0 \\ 0 & G_P(\omega) \end{pmatrix}, \qquad \hat{\mathbf{\Sigma}}(\omega) = \begin{pmatrix} \Sigma_S(\omega) & 0 \\ 0 & \Sigma_P(\omega) \end{pmatrix}$$

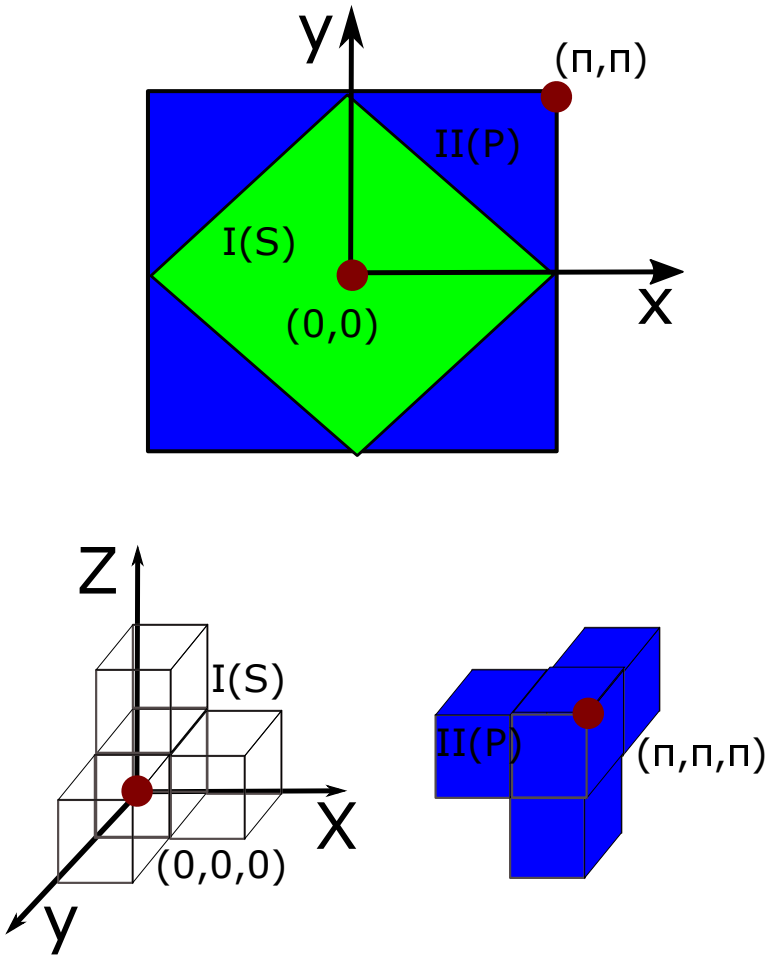

Figure 5.1: Division of Brillouin zone (a) 2-site DCA on square lattice. (b) 2-site cluster on cubic lattice, figure taken from [93]

where,

$$G_{S(P)} = \int \frac{\rho_{S(P)}(\epsilon) d\epsilon}{\omega + \mu - \epsilon - \Sigma_{S(P)}} \tag{5.30}$$

The self consistency condition is:

$$\begin{aligned} G_{00} &= (G_S + G_P)/2 \\ G_{0\alpha} &= (G_S - G_P)/2 \end{aligned} \tag{5.31}$$

The algorithm for two site cluster DMFT is shown in the flowchart (Fig 5.2):

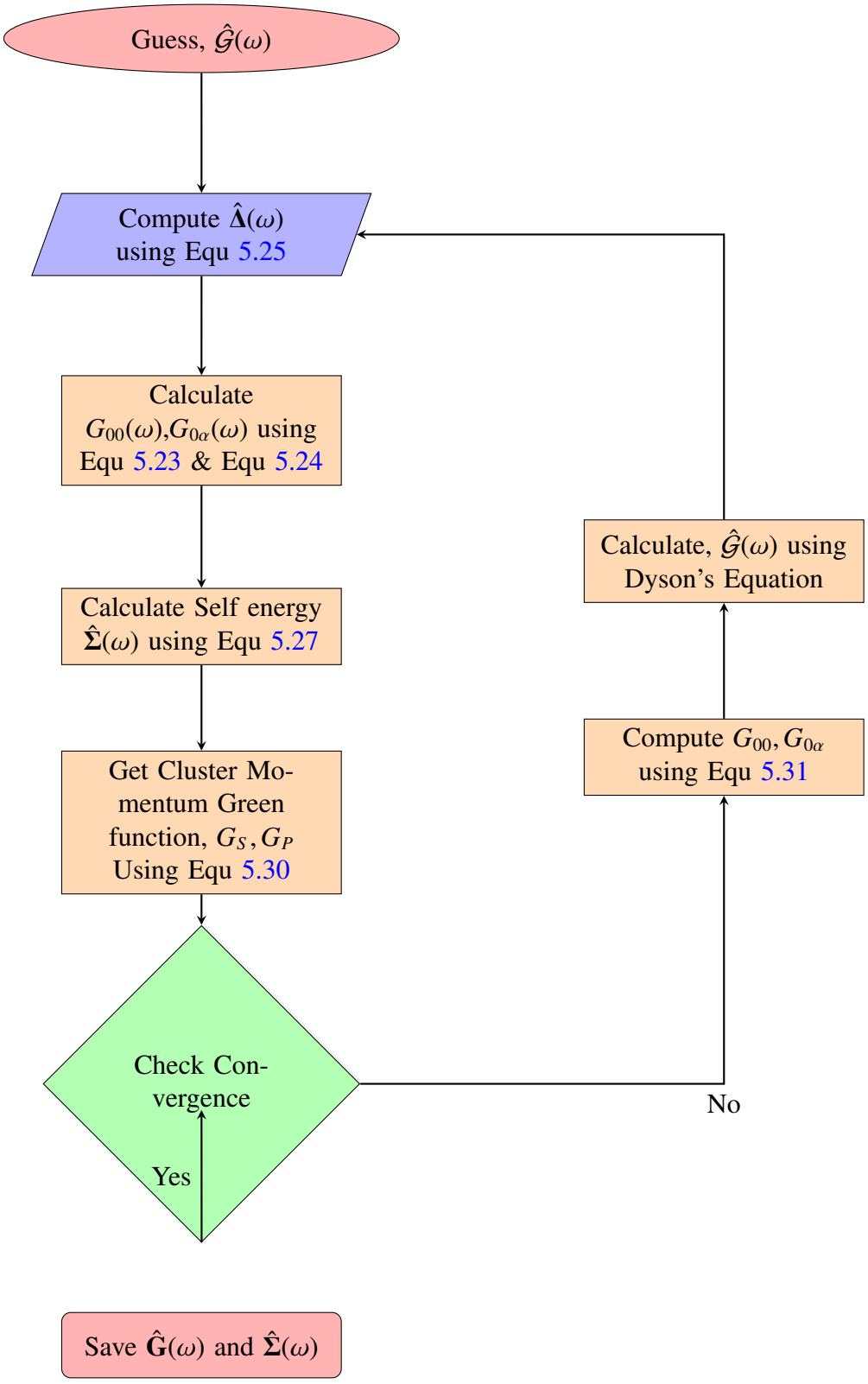

Figure 5.2: CDMFT Algorithm Flow Diagram for FKM within Alloy Analogy

5.2.3 Calculation of Vertex Function

According to the functional methods begin with the generating function with source field ϕ_σ, then the partition function in grand canonical ensemble:

$$lnZ[\phi] = lnTr[e^{-\beta(\hat{H}-\mu\hat{N})}T_\tau(e^{-c_\sigma^\dagger\phi_\sigma c_\sigma})] \tag{5.32}$$

Green function in presence of this source field is defined as:

$$G_\sigma(\phi) := -\langle c_\sigma; c_\sigma^\dagger\rangle_\phi = -\frac{\delta lnZ[\phi]}{\delta\phi_\sigma} \tag{5.33}$$

Similarly the two particle Green function ($\mathbf{\Pi}$) is obtained by functional derivative of $\mathbf{G}[\phi_\sigma]$ w.r.t. ϕ_σ, i.e.

$$\mathbf{\Pi}_\sigma = \frac{\delta\mathbf{G}[\phi]}{\delta\phi_\sigma} \tag{5.34}$$

Using the matrix notation I have:

$$\mathbf{G}\mathbf{G}^{-1} = \mathbb{I} \tag{5.35}$$

Differentiating w.r.t. ϕ I have,

$$\frac{\delta\mathbf{G}}{\delta\phi}\mathbf{G}^{-1} + \mathbf{G}\frac{\delta\mathbf{G}^{-1}}{\delta\phi} = 0 \tag{5.36}$$

$$\frac{\delta\mathbf{G}}{\delta\phi} = -\mathbf{G}\frac{\delta\mathbf{G}^{-1}}{\delta\phi}\mathbf{G} \tag{5.37}$$

Using the Dyson's equation: $\mathbf{G}^{-1} = \mathcal{G}_0^{-1} - \mathbf{\Sigma} - \phi$ one gets,

$$\frac{\delta\mathbf{G}}{\delta\phi} = \mathbf{G}.\mathbf{G} + \mathbf{G}\frac{\delta\mathbf{\Sigma}}{\delta\phi}\mathbf{G} \tag{5.38}$$

As the self-energy is functional of Green function, $\mathbf{\Sigma} := \mathbf{\Sigma}(\mathbf{G})$, using chain rule one gets,

$$\frac{\delta\mathbf{G}}{\delta\phi} = \mathbf{G}.\mathbf{G} + \mathbf{G}\left[\frac{\delta\mathbf{\Sigma}}{\delta\mathbf{G}}\frac{\delta\mathbf{G}}{\delta\phi}\right]\mathbf{G} \tag{5.39}$$

Comparing the above equation with Bethe-Salpeter equation (BSE) given as,

$$\mathbf{\Pi} = \mathbf{\Pi}_0 + \mathbf{\Pi}_0 \mathbf{\Gamma} \mathbf{\Pi} \tag{5.40}$$

one gets the irreducible particle-hole vertex function $\mathbf{\Gamma}$ corresponds to the BSE as

$$\mathbf{\Gamma} \equiv \frac{\delta \mathbf{\Sigma}(\mathbf{G})}{\delta \mathbf{G}} \tag{5.41}$$

For my case both the self-energy and Green functions are 2×2 matrix form. Consider the Green function and self-energy in symmetric (cluster momentum) basis on the diagonalized forms:

$$\hat{\mathbf{G}}(\omega) = \begin{pmatrix} G_S(\omega) & 0 \\ 0 & G_P(\omega) \end{pmatrix}, \qquad \hat{\mathbf{\Sigma}}(\omega) = \begin{pmatrix} \Sigma_S(\omega) & 0 \\ 0 & \Sigma_P(\omega) \end{pmatrix}$$

In diagonalized basis each two sector (S and P) disjoint from each other i.e. $\Sigma_S \equiv \Sigma_S(G_S)$ and $\Sigma_P \equiv \Sigma_P(G_P)$. Now,

$$\frac{\delta}{\delta \hat{\mathbf{G}}} = \begin{bmatrix} \frac{\delta}{\delta G_S} & 0 \\ 0 & \frac{\delta}{\delta G_P} \end{bmatrix}$$

Hence the vertex function is given as,

$$\begin{aligned} \hat{\mathbf{\Gamma}}(\omega) &= \frac{\delta}{\delta \hat{\mathbf{G}}} \hat{\mathbf{\Sigma}} \\ &= \begin{bmatrix} \frac{\delta}{\delta G_S} & 0 \\ 0 & \frac{\delta}{\delta G_P} \end{bmatrix} \begin{bmatrix} \Sigma_S & 0 \\ 0 & \Sigma_P \end{bmatrix} \\ &= \begin{bmatrix} \frac{\delta \Sigma_S}{\delta G_S} & 0 \\ 0 & \frac{\delta \Sigma_P}{\delta G_P} \end{bmatrix} \end{aligned} \tag{5.42}$$

Hence the vertex function is also diagonal in cluster momentum basis corresponds to S and P sector and the off-diagonal vertex function vanishes. One can argue that as Σ_S is

function of G_S only, the derivative of Σ_S with respect to G_P vanishes and vice versa i.e.,

$$\frac{\delta\Sigma_{P(S)}}{\delta G_{S(P)}} = 0 \qquad\qquad \frac{\delta\Sigma_{S(P)}}{\delta G_{P(S)}} = 0 \tag{5.43}$$

and only diagonal components survive with,

$$\Gamma_{S(P)} = \frac{\delta\Sigma_{S(P)}}{\delta G_{S(P)}} \tag{5.44}$$

5.3 Results:

I have considered the Bethe lattice of high dimensions (d) with unit half-bandwidth (2t=1) of the unperturbed density of states (DOS) of conduction electrons. Then the non-interacting DOS for conduction electrons is given as,

$$\rho_0(\epsilon) = \frac{2}{\pi D}\sqrt{D^2 - \epsilon^2} \tag{5.45}$$

I follow the self consistency condition $\hat{\mathbf{\Delta}}(\omega) = t^2\hat{\mathbf{G}}(\omega)$ for Bethe lattice and calculate the single particle spectral function ($\rho_{00}(\omega)$) and self-energy ($\hat{\mathbf{\Sigma}}(\omega)$). Then using Luttinger ward identity I calculate the Vertex function ($\hat{\mathbf{\Gamma}}(\omega)$). The average f-electrons density is: $\langle n_{if}\rangle = \langle x_i\rangle$ and the nearest-neighbour(n.n.) short range correlation is: $f_{0\alpha} = \langle x_0 x_\alpha\rangle - \langle x_0\rangle\langle x_\alpha\rangle$, where the $0, \alpha$ the n.n. sites on the lattice. In the following I show the results for three different cases:

1. Particle-hole symmetric with no short range correlation case : $\langle n_{if}\rangle = 0.5, f_{0\alpha} = 0.0$

2. Particle-hole asymmetric with no short range correlation case : $\langle n_{if}\rangle = 0.45, f_{0\alpha} = 0.0$

3. Particle-hole symmetric with short range correlation case : $\langle n_{if}\rangle = 0.5, f_{0\alpha} = -0.15$

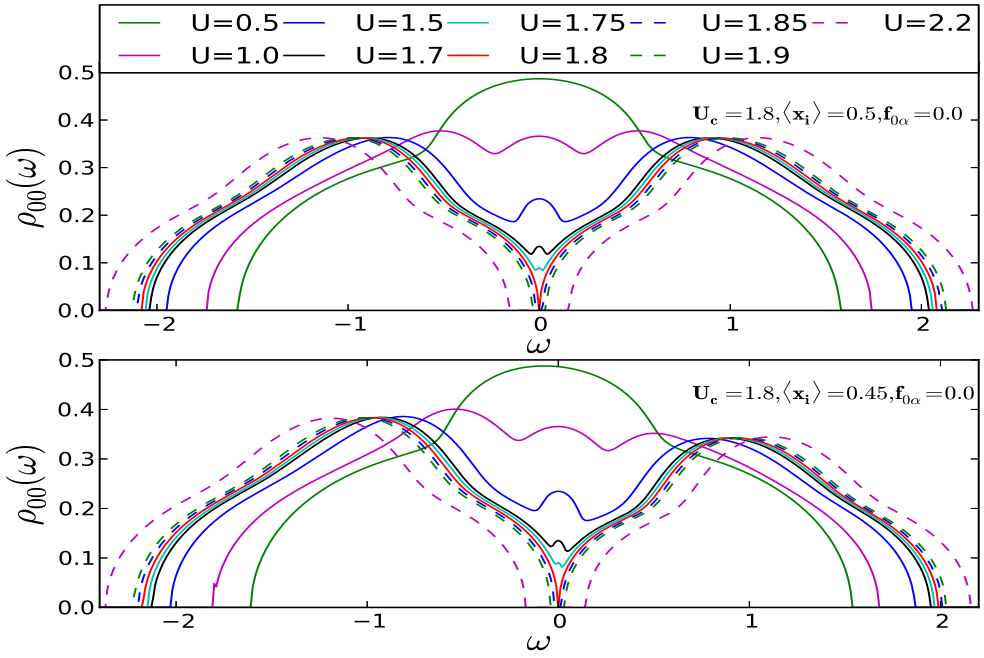

Figure 5.3: The local density of states (LDOS) of the binary-alloy disorder model for p-h symmetry (upper panel) and p-h asymmetric case (lower panel). A clear continuous band-splitting transition of the Hubbard (or Falicov-Kimball model-like) variety is seen in both cases. At $U_c = 1.8$ (red curve), the LDOS exhibits a critical $|\omega|^{1/3}$ singular behaviour in both cases.

5.3.1 Particle-hole Symmetric Case:

I begin with the $\langle n_{ic}\rangle = \langle n_{if}\rangle = 0.5$ and $f_{0\alpha} = 0.0, x_{0\alpha} = \langle x_0 x_\alpha\rangle = \langle x_0\rangle\langle x_\alpha\rangle = 0.25$. In the upper panel of Fig 5.3, I show the local DOS (LDOS) for different values of U (in range from U=0.5 to U=2.2). At the critical point ($U_c = 1.8$) the band is split into two subband which signifies the metal-insulator transition (MIT) of the Mott-Hubbard [2] type. But in contrast to the Hubbard model the band spliting occurs continuously(i.e. $\rho_{00}(\omega = 0)$ vanishes continuously at $U_c = 1.8$ with the increasing U), so continuous MIT (2nd order) happens in FKM. So one can see this as genuine quantum critical point (QCP). Comparing with the single-site exact DMFT result I see that with the incorporation of dynamical effect of 1/d corrections in our two-site C-DMFT gives more additional features in the LDOS, even with totally random case ($f_{0\alpha} = 0$) this additional features in LDOS survived. In Fig 5.6, I show the LDOS for critical point with $U = U_c = 1.80$. I also find that at QCP ($U = U_c$) the LDOS in low energy can be written as, $\rho_c(\omega) = c \mid \omega \mid^{\eta}$, where $\eta \approx \frac{1}{3}$ (shown in Fig 5.6 in log-scale plot), the similar result was found for single site DMFT with FKM. Although this result is contrast to that Hubbard model for which for the critical curve $\eta = \frac{1}{2}$.

Using CDMFT method I also calculate the spectral density of cluster momentum $K \in (0, 0, ...)$ and $(\pi, \pi, ...)$. I define K=(0,0,..) as S-channel and $K = (\pi, \pi, ..)$ as P-channel. In the upper panel Fig 5.4, I show the cluster spectral function $A(\mathbf{K} \in \{S, P\}, \omega)$ as a function of U. I find that $A(\mathbf{K} \in \{S, P\}, \omega) \geq 0$ as one expected from analytical properties of momentum spectral function. As the particle-hole symmetric case, it is obvious that $\rho_S(\omega) = A(\mathbf{K} = S, \omega) = \rho_P(-\omega) = A(\mathbf{K} = P, -\omega)$. The cluster momentum dependent spectral function also exhibits same singular features as LDOS. Notwithstanding these similarities, I stress that our extension of DMFT faithfully captures the feedback of the non-local (intra-cluster) correlations on the single-particle DOS and the self-energies (see below) in contrast to DMFT, where such 1/d feedback effects are absent.

In the upper-left panel of Fig 5.5, I show the imaginary part of the local self-energy

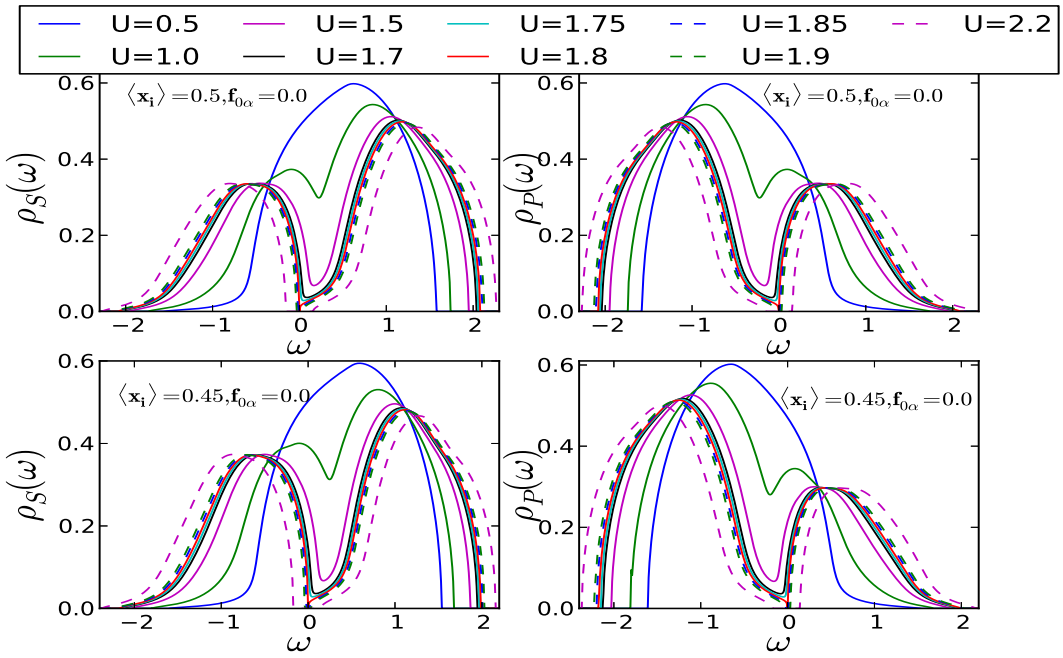

Figure 5.4: The cluster-momentum resolved one-electron spectral functions for same parameters as in Fig. 5.3. For the p-h symmetric case, the symmetry relation $\rho_S(\omega) = \rho_P(-\omega)$ is clearly satisfied as it must be (upper panel).

($\Sigma_{00}(\omega)$) for the same values of disorder strength U as above. For small U, $Im\Sigma_{00}$ weakly depends on ω, and is sizable only near $\omega = 0$. However, it has the wrong sign, i.e, a minimum, instead of a maximum characteristic of a Landau Fermi liquid, at $\omega = 0$. Thus, the metallic state is incoherent and not a Landau Fermi liquid (LFL). This is again a feature in common with DMFT studies. In DMFT, it is well known that this feature becomes more prominent as U increases, and diverges at the MIT. In CDMFT, however, $\mathrm{Im}\Sigma_{00}$ develops marked structure already at (U) = 1.0: it develops a maximum at $\omega = 0$, which progressively sharpens up with increasing U in the incoherent metallic regime. Interestingly, (i) right at (U_c) as shown in Fig 5.6 (red curve), for low energy $Im\Sigma_{00}(\omega) = c|\omega|^{1/3}$, reminiscent of what is expected in a power-law liquid, in strong contrast to what happens in DMFT, where it diverges. The real part of local self energy ($\mathrm{Re}\Sigma_{00}(\omega)$) is shown in the right panels of Fig. 5.5. For p-h symmetric case (shown in upper right panel of Fig. 5.5), $\mathrm{Re}\Sigma_{00}(\omega)$ is U/2.0 at ω=0 for all values of U. If I see $Re[\Sigma_{00}(\omega)] - \frac{U}{2}$ it changes sign according to the ω near the Fermi level and at the transition point ($U \sim U_c$) it shows

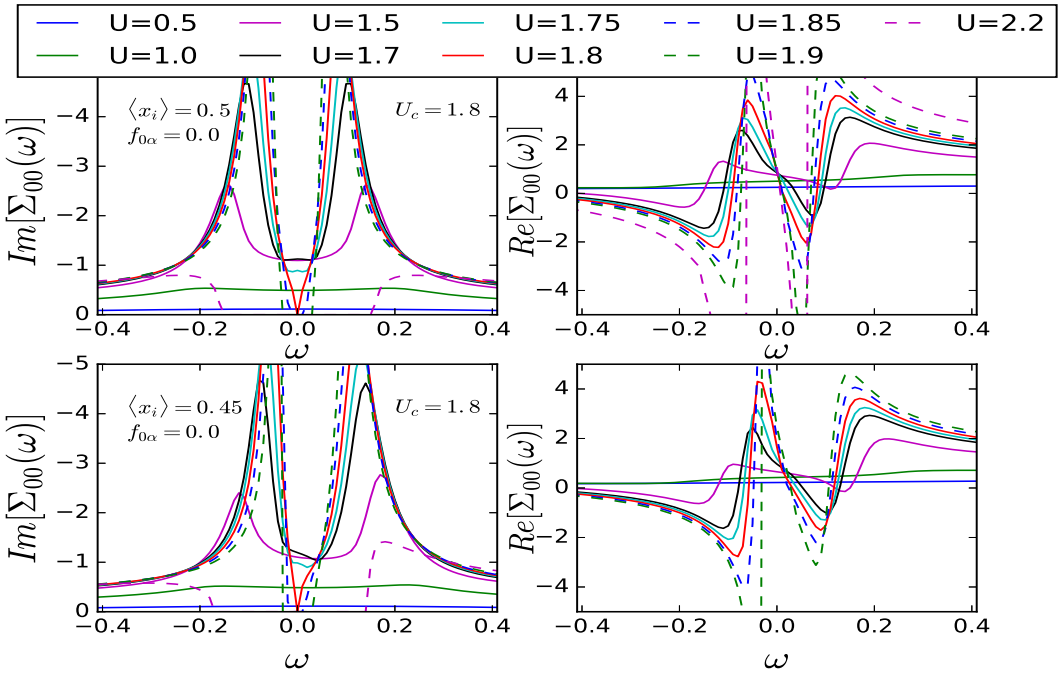

Figure 5.5: $\Sigma_{00}(\omega)$ (both real and imaginary part) vs U for the binary-ally disorder problem for the same parameters as in Fig. 5.3. For small U, our results agree with self-consistent Born approximation (constant $\mathrm{Im}\Sigma_{00}(\omega)$). As U increases, $\mathrm{Im}\Sigma_{00}(\omega)$ develops marked low-energy structure, and at $U_c = 1.8$ (red curve), $\mathrm{Im}\Sigma_{00}(\omega) \simeq |\omega|^{1/3}$, reflecting the non-perturbative nature of the "Hubbard III" quantum criticality. The $Re\Sigma_{00}(\omega)$ shows discontinuity at $\omega = 0$ at the critical U.

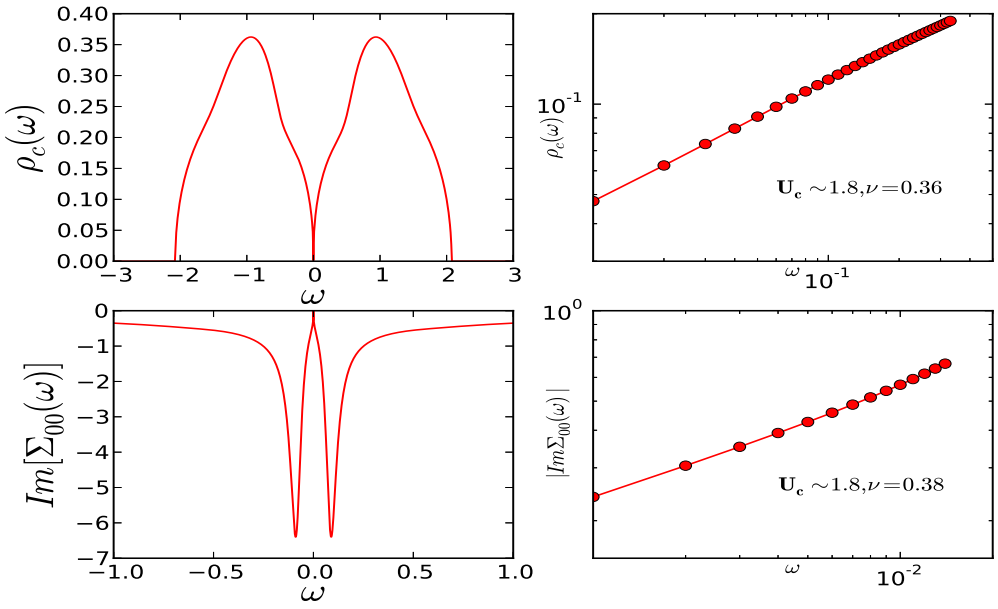

Figure 5.6: Exponent of $\rho_{00}(\omega)$ and $Im\Sigma_{00}(\omega)$ closed to the Fermi energy at critical value of U with symmetric alloy

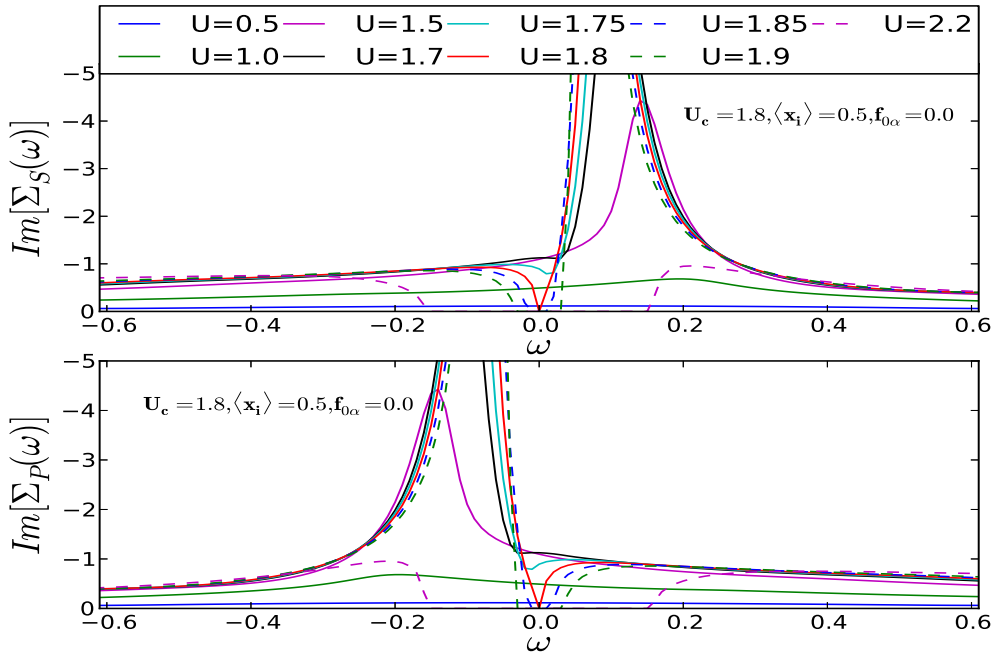

Figure 5.7: Same as Fig. 5.5, but now for the cluster-momentum resolved self-energies. It is clear that the symmetry relation $\mathrm{Im}\Sigma_S(\omega) = \mathrm{Im}\Sigma_P(-\omega)$ holds in the p-h symmetric case.

steep discontinuity at $\omega = 0$. The source of gap opening comes from the divergence of $\frac{\partial}{\partial\omega} Re\Sigma_{00}(\omega)$ at ω=0. For $U > U_c$, opening up of a "Mott" gap in the LDOS goes hand-in-hand with the divergence of $\frac{\partial}{\partial\omega} Re\Sigma_{00}(\omega)$ and vanishing $\mathrm{Im}\Sigma_{00}(\omega)$ in the gap. For $(U > U_c)$, opening up of a "Mott" gap in the LDOS goes hand-in-hand with vanishing $Im\Sigma_{00}(\omega)$ in the gap. In all cases, I also find power-law fall-off in self-energies at high energy and, more interestingly, clear isosbestic points (where $Im\Sigma_{00}(\omega)$ is independent of ω) at $\Omega = 0.2t$.

Finally, CDMFT allows a direct evaluation of the K-dependent self-energies, which I exhibit in Fig 5.7. As a cross-check, I find that $Im\Sigma(\mathbf{K} = S, \omega) = Im\Sigma(\mathbf{K} = P, -\omega)$ as I expected with particle-hole symmetry.

In Fig 5.8, I exhibit the imaginary parts of the cluster-momentum-resolved irreducible particle-hole vertex functions as functions of U. It is clear that both, $Im\Gamma(\mathbf{K},)$ with K = (0, 0,...) (called "S") and with $K = (\pi, \pi, ..)$ (called "P") show non-analyticities precisely at $\omega = 0$ at $U_c = 1.8$ (red curves). Thus, for the completely random case, I find, as expected,

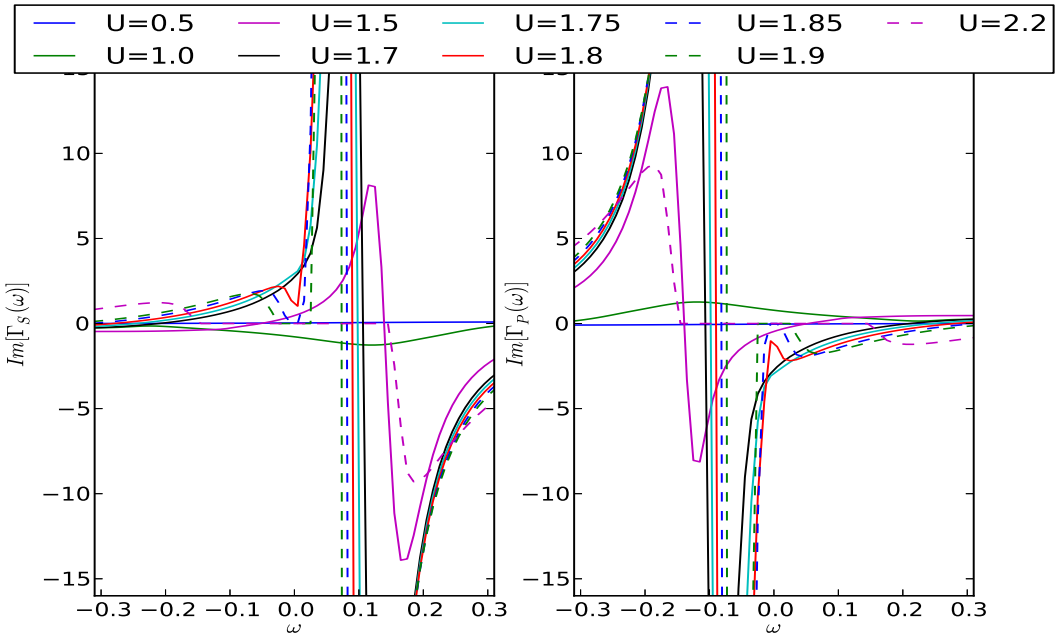

Figure 5.8: Imaginary parts of the irreducible particle-hole vertex functions in the S, P channels as a function of U for the binary-alloy disorder model. Clear non-analyticities in $\Gamma_{S,P}(\omega)$ at $\omega = 0$ occur precisely at $U_c = 1.8$ (red curve), where the continuous Hubbard band-splitting transition occurs. In addition, the results confirm the symmetry $\mathrm{Im}\Gamma_S(\omega) = -\mathrm{Im}\Gamma_P(-\omega)$.

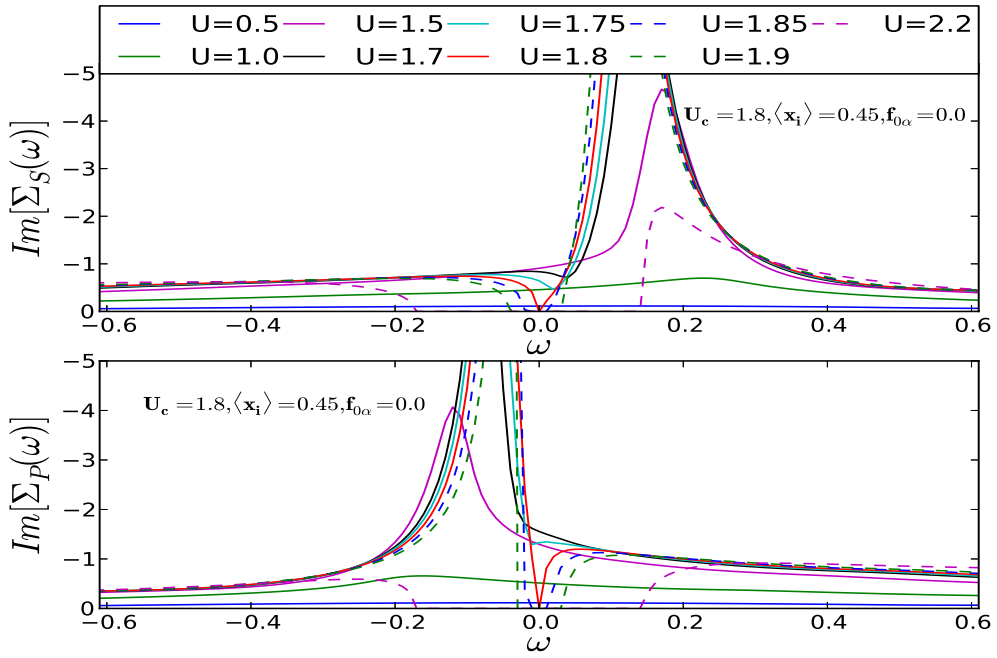

Figure 5.9: Same as in Fig. 5.7, but for the p-h asymmetric case. Though no symmetry is expected nor found here, the critical features are unaffected, since $\mathrm{Im}\Sigma_{S,P}(\omega)$ indeed exhibit the same non-analytic feature ($\simeq |\omega|^{1/3}$ behavior) for $\omega < 0(S)$ and $\omega > 0(P)$.

that the "Mott" QCP is signaled by a clear non-analyticity in the momentum-dependent (irreducible) p-h vertices at the Fermi energy ($\omega = 0$). This non-analytic feature goes hand-in-hand with a power-law variation of $Im\Sigma_{S(P)}(\omega)$ in the vicinity of the Fermi energy ($\omega = 0$). Along with spectral functions and self-energies, the vertex functions also satisfy the "symmetry" relation, $Im\Gamma(\mathbf{K} = S, \omega) = -Im\Gamma(\mathbf{K} = P, -\omega)$ for the p-h symmetric case. Clearly, the anomalous infra-red behavior of the irreducible vertices is directly related to the clear non-analytic structures in the cluster self-energies discussed above.

5.3.2 Particle-hole Asymmetric Case:

Next, I consider the "particle-hole asymmetric case" with completely random disorder i.e. $n_{ic} \neq n_{if}$ but $f_{o\alpha} = 0.0$. In the lower panel of Fig 5.3, I show the LDOS with particle-hole asymmetric case with $\langle n_{if} \rangle = \langle x_i \rangle = 0.45$. The LDOS is fully reflected the asymmetric case. At $U = U_c = 1.80$ the LDOS at $\omega = 0$ vanishes which is same as in the

p-h symmetric case. Here also MIT is associated with a genuine Quantum Critical Point (QCP). The exponent of LDOS in p-h asymmetric csae also $\frac{1}{3}$ near the Fermi energy. Hence comparing to p-h symmetric case no more extra features find in this case.

In the cluster K-dependent spectral function I find, $\rho_S(\omega) = A(\mathbf{K} = (0,0), \omega) = \rho_P(-\omega) = A(\mathbf{K} = (\pi,\pi), -\omega)$ as shown in the lower panels of Fig 5.4, which is consistent with the p-h asymmetric case. The K-dependent spectral function also show the power-law behaviour with with an exponent $\eta \approx \frac{1}{3}$ on both sides of the Fermi energy. In the lower panels of Fig 5.5, I show the imaginary and real part of the self-energy that correctly depicted the p-h asymmetry. In Fig 5.9, I show the cluster momentum resolve self-energies that exhibit the same non-analytic features ($\sim \mid \omega \mid^{\frac{1}{3}}$) for $\omega < 0(S)$ and $\omega > 0(P)$.

5.3.3 Particle-hole Symmetric Case with Short Range Order:

Additional notable features characteristic of $1/D$ effects captured by CDMFT become apparent upon repeating the above procedure for the case of finite "alloy" short-range order (SRO), namely, when $f_{0\alpha} = \langle x_0 x_\alpha \rangle - \langle x_0 \rangle \langle x_\alpha \rangle \neq 0$.

In Fig. 5.10, Fig. 5.11 and Fig. 5.12, I exhibit the cluster self-energies and p-h vertices for the case of $f_{0\alpha} = -0.15$, which represents the physical situation with short-range "antiferro" alloy correlations on the two-site cluster. Now, the MIT occurs at a critical $U_{c1} = 1.35$, smaller than for the completely random case. The reason is simple: on very general grounds, short-ranged "antiferro" alloy correlations suppress the one-electron hopping by a larger amount compared to the random case (this is also reflected in the deeper pseudogap in the incoherent metal for $f_{0\alpha} < 0$), simply because the probability for an electron to hop onto its neighbour on the cluster is reduced when there is more probability of having a local potential U on the neighbouring site. In this case, $\mathrm{Im}\Sigma(\mathbf{K}, \omega)$ shows, on first glance, a behaviour similar to the case with $f_{0\alpha} = 0$ described before. Upon closer scrutiny of Fig. 5.11, however, I find that $\mathrm{Im}\Sigma(\mathbf{K}, \omega)$ already *di-*

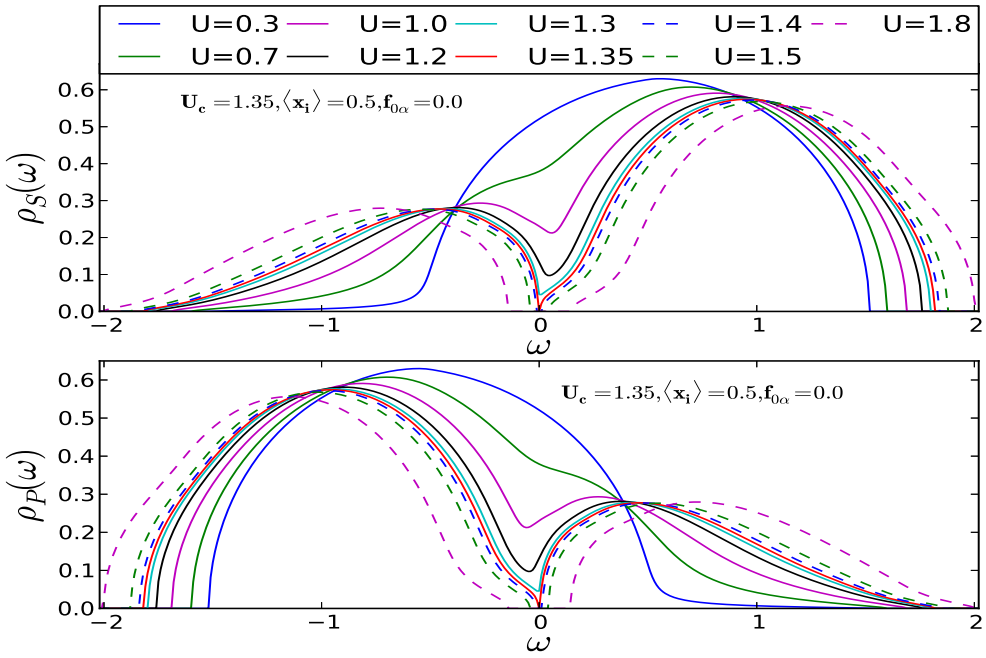

Figure 5.10: Cluster-momentum resolved one-electron spectral functions as a function of U for the short-range ordered binary alloy in the p-h symmetric case. As expected, the continuous "Hubbard" transition now obtains at a smaller $U_c = 1.35$ (red curve), due to enhanced suppression of itinerance by the "anti-ferro" alloy short-range order ($f_{0\alpha} = -0.15 < 0$). As for the totally random alloy, the symmetry relation for the spectral functions still holds. The LDOS shows very similar quantum-critical singular features at low energy at U_c.

verges for $U = 1.3$, slightly *before* Hubbard band-splitting occurs (cyan curve). Also, Fig. 5.11 also clearly shows the power-law divergence of the self-energy (cyan and red curves), with $\mathrm{Im}\Sigma_{00}(\omega) \simeq |\omega|^{-\eta}$, with $\eta = 1/3$ at the MIT. This new feature is very different from the pole-divergence of the self-energy in the Hubbard model within DMFT, but is indeed seen in the DMFT solution for the FKM when the self-energy and the vertex function are treated consistently at the local level [51]. A related non-analyticity in $\mathrm{Im}\Gamma(\mathbf{K}, \omega)$ also correspondingly occurs at precisely the same value in Fig. 5.12. Thus, in this case, I find that the irreducible p-h vertex diverges before the actual MIT occurs. Such features are also known for the $d = 2$ Hubbard model within the dynamical vertex approximation [103, 98]. However, this divergence of the vertex function is *not* associated with $(\partial\Sigma_{00}(\omega)/\partial\omega)_{\omega=0} = \infty$, where the actual "Mott" transition occurs. Thus, it is neither connected to any symmetry-breaking (which would require a divergence in the

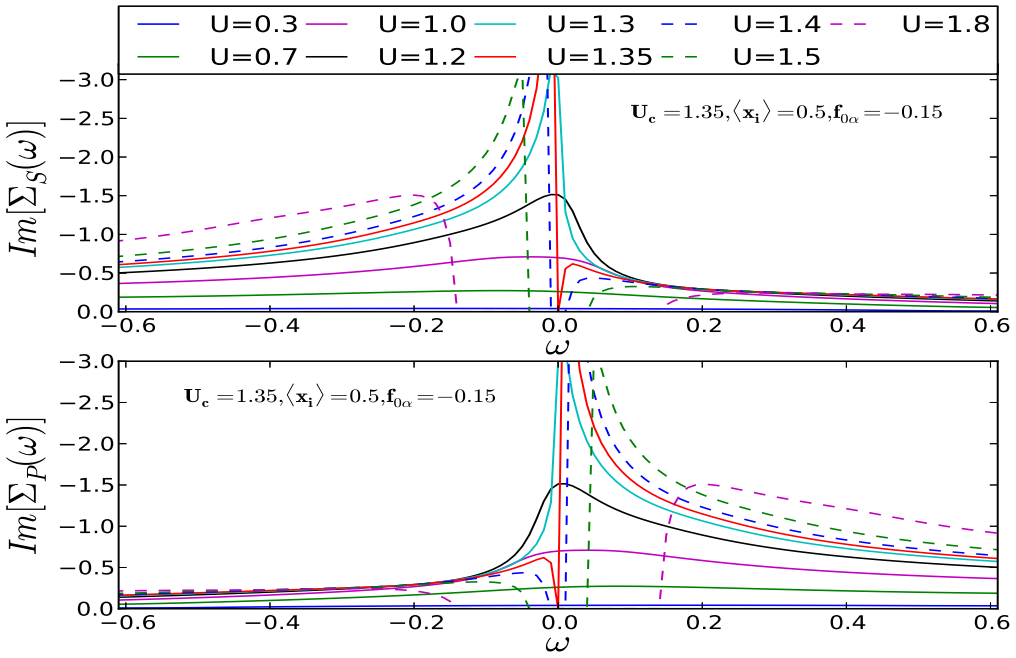

Figure 5.11: Imaginary parts of the cluster-momentum resolved one-particle self-energies as a function of U for the short-range ordered binary alloy. The symmetry relation for the cluster self-energies still holds, as does the fact that both show critical power-law behavior at U_c (see text).

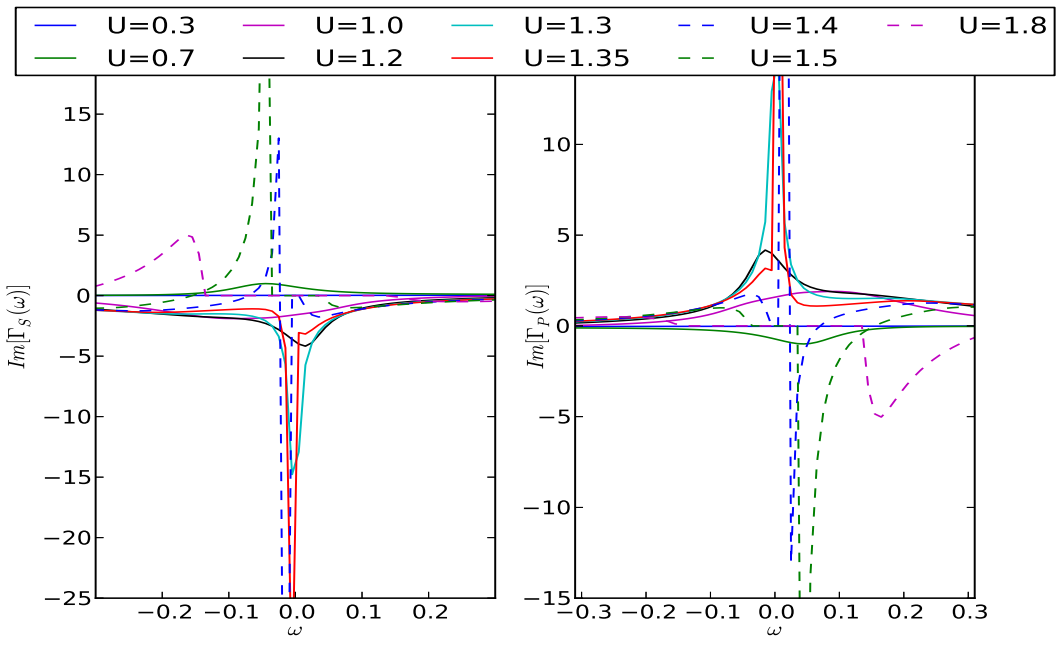

Figure 5.12: Imaginary parts of the cluster-momentum resolved irreducible p-h vertex functions for the p-h symmetric short-range ordered binary alloy as a function of U. Clear non-analyticities in both $\Gamma_{S,P}(\omega)$ occur slightly *before* the Hubbard-type band-splitting transition occurs, signifying the onset of a novel kind of localization (see text).

momentum channel), nor does it lead to non-analyticities in the one-particle response (the LDOS remains smooth for all $U < U_{c1} = 1.35$).

Thus, at the level of spectral functions and self-energies, our CDMFT for the FKM finds universal features at a quantum-critical "Mott" transition that are qualitatively similar to those found by Janis *et al* [51]. I find that the infra-red non-analytic behaviour in $\Gamma(\mathbf{K}, \omega)$ *precedes* the MIT. This was probably to be expected, since both approaches deal with quasi-local quantum criticality suited to the Mott-Hubbard problem. The advantages of our extension relate to (*i*) having a CDMFT that always respects causality [62], and (*ii*) enables computation of momentum-resolved spectral responses, even for the hitherto scantily considered cases of explicit “alloy” short-range order. Importantly, having an almost analytic cluster extension of DMFT means that I have to simply deal with N coupled nonlinear algebraic equations to compute the full CDMFT propagators for a N-site cluster, even with short-range order. This is an enormous numerical simplification when one envisages its use for *real* disordered systems, with or without strong Hubbard correlations: these issues have long been extremely well-studied using the coherent-potential approximation (CPA) and DMFT [41]. I anticipate wide uses of such a semi-analytic approach as ours in this context.

It is interesting to compare our results to those obtained by Shinaoka *et al.* [109]. Motivated by disordered and correlated systems near a MIT, they consider a disordered Hubbard model, where Hubbard correlations are treated within static Hartree-Fock, giving rise to local moments, while disorder effects over and above HF are studied by exact diagonalization techniques. Their main findings are (*i*) a “soft” gap arises even with purely local interactions, in contrast to that in an Efros-Shklovskii picture, where it arises from long-range coulomb interactions and (*ii*) while the LDOS $A(E) \simeq |E - E_F|^{\alpha}$ with $0.5 < \alpha < 1$ for $|E - E_F| > 0.1$, they see that $A(E) \simeq \exp[-(-\gamma \log|E - E_F|)^3]$ provides a much better fit for $|E - E_F| < 0.1$. In contrast, I find that the LDOS, $\rho(\omega) \simeq C|\omega|^{1/3}$ remains valid up to lowest energies at the QCP: this is similar to the situation found in single-site DMFT [29],

where precisely the same behavior is found analytically.

These differences could arise from many factors: (*a*) there are *no* localized magnetic moments in our case, since I do not have the Hubbard term, (*b*) while I focus on predominantly short-range disorder correlations, Shinaoka et al include longer range disorder correlations. It is noteworthy that a "soft power-law gap" already appears in (C)DMFT studies, and while it is conceivable that the low-energy behaviour may change upon increasing cluster size, this remains to be shown. Alternatively, if local moments *are* crucial to obtain this behaviour, one must study the disordered Hubbard model within CDMFT. This ambitious enterprise is left for future consideration.

5.4 Discussions:

Using the disordered binary alloy analogy extended to a two-site cluster, I have investigated $1/d$ effects on the continuous MIT in the "simplified" FKM (by this, I mean a FKM where the disorder is quenched, rather than annealed, so quantities like $\langle x_0 \rangle$ and $f_{0\alpha}$ are fixed and given from a binary distribution, rather than computed self-consistently, as in the true FKM). In spite of this simplification, I find that quantum critical features at the level of one-electron Green functions and self-energies are very similar to those obtained from an "Anderson-Falicov-Kimball" [51] model. This is not so surprising, since the effect of the FK term, $U \sum_i n_{if} n_{ic}$ is precisely to generate a band "splitting" for all U in the FKM as well, and a binary alloy disorder indeed has exactly a similar effect on the DOS. Thus, within DMFT or CDMFT approaches such as ours, one would expect quantitative changes in the spectral functions, but no qualitative modification of critical exponents in the LDOS exactly at the band-splitting Hubbard-like transition.

However, in strong contrast to one-electron response, the nonlocal p-h vertex shows clear divergence even before MIT Metal to Anderson localization transition in this thesis, the qualitative discussion have done in the dynamical charge susceptibility in the next chapter

6.

5.5 Summary

To summarize this chapter, I have analyzed the role of short-ranged (spatially non-local) alloy correlations on the Hubbard-like MIT in a binary disorder Anderson model at strong coupling in detail. While quantum critical features at one-electron level are exactly similar to recent DMFT results [51] for the disordered FKM, non-local vertex corrections show up a clear signature of quantum interference at strong coupling. In contrast to previous CPA studies, this is a concrete manifestation of the relevance of dynamical effects associated with $1/D$ alloy correlations near the quantum critical point associated with a continuous MIT of the Hubbard band-splitting type. It is obviously of interest to elucidate the nature and consequences of this strong coupling QCP in various transport responses. This aspect will be discussed in the following chapters.

Chapter 6

Dynamical Charge Susceptibility in FKM using CDMFT

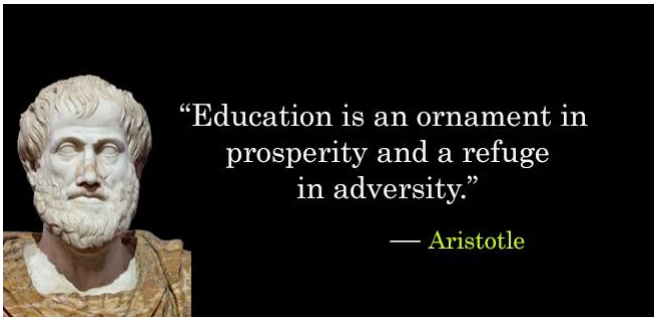

Previous chapter, I have discussed the CDMFT formalism of solving FKM. In this chapter, I will present the frequency-dependent charge susceptibility of FKM by using Cluster DMFT. Using time dependent response to a sudden local quench, I find long-time wave-function changes from a power-law to an anomalous form at strong coupling.

I have already studied MIT within an exact-to-$O(1/d)$ CDMFT for the FKM using one-electron response like Green function, Self-Energy. Additional details regarding the nature of this strong-coupling "Mott" transition can be gleaned from examination

of the two-particle response. In particular, the non-analyticities in the irreducible vertex function before the MIT made us curious to study two particle response function that included vertex correction close to the MIT. The dynamic charge susceptibility of the FKM can also be precisely computed in our approach by using the CDMFT propagators ($G_{S(P)}(\mathbf{k},\omega)$) and the irreducible p-h vertices $\Gamma_{S(P)}(\omega)$ in the Bethe-Salpeter equation (Appendix B).

6.1 Calculation of Dynamical Charge Susceptibility

The two-particle dynamical charge susceptibility [36, 38] in generally defined by,

$$\begin{aligned}\chi^{cc}(q;i\nu_l) &= \frac{1}{2s+1}\int_0^\beta d\tau e^{i\nu_l\tau}\frac{1}{V}\sum_{\mathbf{R}_i-\mathbf{R}_j} e^{\mathbf{q}(\mathbf{R}_i-\mathbf{R}_j)} \\ &\times \left[Tr_{cf}\frac{\langle e^{-\beta H}n_i^c(\tau)n_j^c(0)\rangle}{\mathcal{Z}} - Tr_{cf}\frac{\langle e^{-\beta H}n_i^c\rangle}{\mathcal{Z}}Tr_{cf}\frac{\langle e^{-\beta H}n_i^c\rangle}{\mathcal{Z}}\right] \end{aligned} \tag{6.1}$$

with $i\nu_l = 2i\pi lT$ the bosonic matsubara frequency, ω_m, ω_n are the fermionic Matsubara frequency and $n_i^c = c_i^\dagger c_i$ is the number operator for conduction electrons. In the previous chapter, I have discussed about two-particle irreducible vertex function ($\mathbf{\Gamma}_{S(P)}$) corresponding to the particle-hole(p-h) channel. The momentum-dependent cluster susceptibility corresponding to the S(P) channels is evaluated using Bethe-Salpeter Equation (BSE) is:

$$\begin{aligned}\chi_{S(P)}(\mathbf{q},i\omega_m,i\omega_n;i\nu_l) &= \chi^0_{S(P)}(\mathbf{q},i\omega_m;i\nu_l)\delta_{mn} - T\sum_{n'}\chi^0_{S(P)}(\mathbf{q},i\omega_m;i\nu_l) \\ &\times \Gamma_{S(P)}(i\omega_m,i\omega_{n'};i\nu_l)\chi_{S(P)}(\mathbf{q},i\omega_{n'},i\omega_n;i\nu_l)\end{aligned} \tag{6.2}$$

The full susceptibility is found by summing over all the fermionic Matsubara frequencies (ω_m,ω_n) given as,

$$\chi_{S(P)}(\mathbf{q},i\nu_l) = T\sum_{mn}\chi_{S(P)}(\mathbf{q},i\omega_m,i\omega_n;i\nu_l) \tag{6.3}$$

The vertex function is defined as,

$$\Gamma_{S(P)}(i\omega_n, i\omega_m; i\nu_l) = \frac{1}{T}\frac{\delta\Sigma(i\omega_m, i\omega_{m+l})}{\delta G(i\omega_n, i\omega_{n+l})} \tag{6.4}$$

Here, both a self-energy and a Green function that depend on two fermionic Matsubara frequencies, because these functions are not time-translation-invariant in imaginary time.

It is proved that both the self-energy and the Green function are nonzero on the diagonal m = n and on the diagonal shifted by l units m + l = n and irreducible dynamical charge vertex from yields,

$$\Gamma_{S(P)}(i\omega_m, i\omega_n; i\nu_{l\neq 0}) = \delta_{mn}\frac{1}{T}\frac{\Sigma_m^{S(P)} - \Sigma_{m+l}^{S(P)}}{G_m^{S(P)} - G_{m+l}^{S(P)}} \tag{6.5}$$

As, $\chi_{S(P)}$ are diagonal in S or P channel, I keep only the channel index S, with the understanding that an identical calculation holds for the P channel. Using $\Gamma_{S(P)}$ from the above equation I find,

$$\begin{aligned}\chi^S(\mathbf{q}, i\omega_m, i\omega_n; i\nu_l) &= \chi_0^S(\mathbf{q}, i\omega_m; i\nu_l)\delta_{mn} - T\chi_0^S(\mathbf{q}, i\omega_m; i\nu_l) \\ &\times \Gamma^S(i\omega_m, i\omega_m; i\nu_l)\chi^S(\mathbf{q}, i\omega_m, i\omega_n; i\nu_l)\end{aligned} \tag{6.6}$$

$$\Rightarrow \boxed{\chi^S(\mathbf{q}, i\omega_m, i\omega_n; i\nu_l) = \frac{\chi_0^S(\mathbf{q}, i\omega_m; i\nu_l)\delta_{mn}}{1 + \chi_0^S(\mathbf{q}, i\omega_m; i\nu_l)\frac{\Sigma_m^S - \Sigma_{m+l}^S}{G_m^S - G_{m+l}^S}}} \tag{6.7}$$

Replacing $\mathbf{q}$ by $X(\mathbf{q})$ with $X(\mathbf{q})$ is defined as,

$$X(\mathbf{q}) = \lim_{d\to\infty}\sum_{i=1}^{d} cos(\frac{q_i}{d}) \tag{6.8}$$

one has the full lattice susceptibility given by,

$$\begin{aligned}\chi^S(X, i\nu_l) &= T\sum_{m,n}\chi^S(X, i\omega; i\nu_l) \\ &= T\sum_{m,n}\frac{\chi_0^S(X, i\omega_m; i\nu_l)\delta_{mn}}{1+\chi_0^S(X, i\omega_m; i\nu_l)\frac{\Sigma_m^S-\Sigma_{m+l}^S}{G_m^S-G_{m+l}^S}}\end{aligned} \tag{6.9}$$

Summing over the n index:

$$\Rightarrow \boxed{\chi^S(X, i\nu_l \neq 0) = T\sum_m \frac{\chi_0^S(X, i\omega_m; i\nu_l)}{1+\chi_0^S(X, i\omega_m; i\nu_l)\frac{\Sigma_m^S-\Sigma_{m+l}^S}{G_m^S-G_{m+l}^S}}} \tag{6.10}$$

There are two possibility for two-site cluster case:

(i) For $\mathbf{q} = 0$, $X(\mathbf{q}) = 1$, the bare charge susceptibility is:

$$\chi_0^S(X = 1, i\omega_m; i\nu_l) = -\frac{G_m^S - G_{m+l}^S}{i\nu_l + \Sigma_m^S - \Sigma_{m+l}^S} \tag{6.11}$$

then one find the full dynamical charge susceptibility as,

$$\chi(1; i\nu_l \neq 0) = -T\sum_m \frac{G_m^S - G_{m+l}^S}{i\nu_l} = 0 \tag{6.12}$$

which one expected because the number operator of conduction electron is commute with the Hamiltonian, hence there is no τ dependence. Hence dynamical charge susceptibility for $l \neq 0$ is vanishes except there is a statics charge susceptibility corresponds to $l = 0$.

(ii) For second case, for generic q, $X(\mathbf{q}) = 1$, the contribution from bare bubble is given as,

$$\chi_0^S(X = 1, i\omega_m; i\nu_l) = -G_m^S G_{m+l}^S \tag{6.13}$$

Then the full dynamical charge susceptibility is:

$$\Rightarrow \boxed{\chi^S(X = 0, i\nu_l \neq 0) = -T\sum_m \frac{G_m^S G_{m+l}^S}{1 - G_m^S G_{m+l}^S\frac{\Sigma_m^S-\Sigma_{m+l}^S}{G_m^S-G_{m+l}^S}}} \tag{6.14}$$

Following the same steps for P channel one will also find the same expression for $\chi^P(X, i\nu_l \neq 0)$ with only S will be replaced by P.

6.2 Analytical Contunuation of Dynamical Charge Susceptibility

Now by performing the analytical continuation from Matsubara frequency to real frequency in the standard way one can obtained the dynamical charge susceptibility ($\chi^{S(P)}(x = 0; \nu)$) on real frequency. I will discuss this method in the following:

I know that the Fermi function $f(z) = [e^{\beta z} + 1]^{-1}$ has poles of strength $-T$ at each discrete frequency $z = i\omega_n$. So, one can write,

$$T \sum_n F(i\omega_n) = -\oint_C \frac{dz}{2\pi i} F(z) f(z) \tag{6.15}$$

where,$F(i\omega_n) = \frac{-G_m^{S(P)} G_{m+l}^{S(P)}}{1 - G_m^{S(P)} G_{m+l}^{S(P)} \frac{\Sigma_l^{S(P)} - \Sigma_{m+l}^{S(P)}}{G_m^{S(P)} - G_{m+l}^{S(P)}}}$,the contour integral C is to be taken anticlockwise around the poles at $z = i\omega_n$ as shown in Fig. 6.1.

I introduce "null" contours which allow us to distort the original contour C into the modified contour C' shown in Fig 6.2.

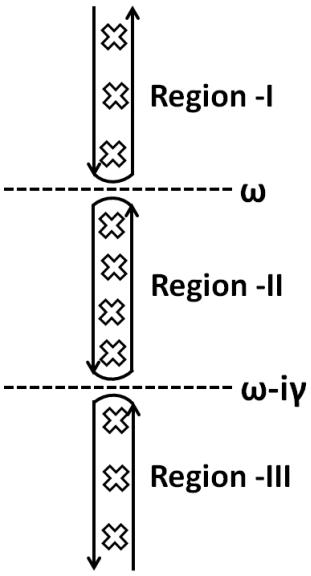

Figure 6.1: Contour integral for evaluating the Matsubara frequency summations of the charge susceptibility. The $\times'$ s mark the locations of fermionic Matsubara frequencies. The contours enclose all Matsubara frequencies, but no other poles of the system. Note that I divide the complex plane into three regions: (i) region I, where the imaginary part is greater than zero; (ii) region II, where the imaginary part lies between zero and $-i\nu_l$; and (iii) region 3, where the imaginary part is less than $-i\nu_l$.

Hence, the susceptibility becomes:

$$\chi^{S(P)}(i\nu_l) = \frac{1}{2\pi i}\int_{C_1} d\omega f(\omega)\frac{G_R^{S(P)}(\omega)G_R^{S(P)}(\omega+i\nu_l)}{1-G_R^{S(P)}(\omega)G_R^{S(P)}(\omega+i\nu_l)\frac{\Sigma_R^{S(P)}(\omega)-\Sigma_R^{S(P)}(\omega+i\nu_l)}{G_R^{S(P)}(\omega)-G_R^{S(P)}(\omega+i\nu_l)}}$$

$$+\frac{1}{2\pi i}\int_{C_2} d\omega f(\omega)\frac{G_A^{S(P)}(\omega)G_R^{S(P)}(\omega+i\nu_l)}{1-G_A^{S(P)}(\omega)G_R^{S(P)}(\omega+i\nu_l)\frac{\Sigma_A^{S(P)}(\omega)-\Sigma_R^{S(P)}(\omega+i\nu_l)}{G_A^{S(P)}(\omega)-G_R^{S(P)}(\omega+i\nu_l)}} \tag{6.16}$$

$$+\frac{1}{2\pi i}\int_{C_3} d\omega f(\omega)\frac{G_A^{S(P)}(\omega)G_A^{S(P)}(\omega+i\nu_l)}{1-G_A^{S(P)}(\omega)G_A^{S(P)}(\omega+i\nu_l)\frac{\Sigma_A^{S(P)}(\omega)-\Sigma_A^{S(P)}(\omega+i\nu_l)}{G_A^{S(P)}(\omega)-G_A^{S(P)}(\omega+i\nu_l)}}$$

When I evaluate the integral along the lines indicated in Fig. 6.2, I replace the Fermi function at $\omega - i\nu_l$ of form $f(\omega - i\nu_l)$ by $f(\omega)$ and then I can make the analytical continuation

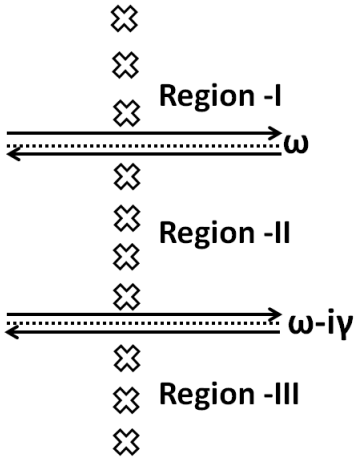

Figure 6.2: Deformation of the contours needed for evaluation of the susceptibility on the real axis. The integrations are parallel to the real axis.

$i\nu_l \rightarrow \nu + i0^+$. Then the final expression becomes,

$$\chi^{S(P)}(\nu) = \frac{1}{2\pi i}\int_{-\infty}^{\infty} d\omega \Bigg\{ f(\omega)\frac{G^{S(P)}(\omega)G^{S(P)}(\omega+\nu)}{1 - G^{S(P)}(\omega)G^{S(P)}(\omega+\nu)\frac{\Sigma^{S(P)}(\omega)-\Sigma^{S(P)}(\omega+\nu)}{G^{S(P)}(\omega)-G^{S(P)}(\omega+\nu)}}$$

$$- f(\omega+\nu)\frac{G^{S(P)*}(\omega)G^{S(P)*}(\omega+\nu)}{1 - G^{S(P)*}(\omega)G^{S(P)*}(\omega+\nu)\frac{\Sigma^{S(P)*}(\omega)-\Sigma^{S(P)*}(\omega+\nu)}{G^{S(P)*}(\omega)-G^{S(P)*}(\omega+\nu)}} \tag{6.17}$$

$$- [f(\omega) - f(\omega+\nu)]\frac{G^{S(P)*}(\omega)G^{S(P)}(\omega+\nu)}{1 - G^{S(P)*}(\omega)G^{S(P)}(\omega+\nu)\frac{\Sigma^{S(P)*}(\omega)-\Sigma^{S(P)}(\omega+\nu)}{G^{S(P)*}(\omega)-G^{S(P)}(\omega+\nu)}} \Bigg\}$$

Here, I replace the retarded green function $G_R^{S(P)}$ by $G^{S(P)}$ and the advanced green function($G_A^{S(P)}$) by the complex conjugate of the retarded Green function($G^{S(P)*}$) and similarly holds for self-energy ($\Sigma^{S(P)}(\omega)$).

6.3 Results and Discussions

In Fig 6.3, I show the imaginary part of full cluster-local dynamical charge susceptibility as U increases. From small U up to $U \simeq 1.2$, Im$\chi_{ch}(\omega)$ varies linearly with ω in

the infra-red, with a maximum at intermediate energy, followed by a high-energy fall-off. However, closer scrutiny of the strong-coupling ($U \geq 1.4$) regime reveals that this behaviour undergoes a qualitative change at low energies: now $\mathrm{Im}\chi_{ch}(\omega) \simeq \omega^{1-\kappa}$, with $0 < \kappa(U) < 1$. It is important to notice that the configurationally averaged DOS does *not* show any non-analyticities in this regime, and the system is close to, but not in the "Mott" insulating regime. A closer look at the behaviour of the cluster self-energies and irreducible vertex functions in this regime shows that both begin to acquire non-trivial energy dependence at low energy when U is close to the critical value needed for the "Mott" transition to occur. In fact, as described in the previous chapter, (see both Im $\Gamma_{S(P)}(\omega)$ start exhibiting strong ω-dependence, especially near $\omega = 0$, when $U \geq 1.4$, and clear non-analyticities accompanied by anomalous power-law variation near $\omega = 0$ when one is very close to the transition in the range $1.7 < U < 1.8$. Thus, it is clear that the anomalous low-energy behaviour of the collective charge fluctuations is linked to the strong ω-dependence and impending non-analytic behaviour in the cluster irreducible vertex as the MIT as approached from the metallic side. Thus, while the fact that the vertex diverges *before* the actual MIT does not lead to non-analyticity in the one-electron spectral functions, it does qualitatively modify the collective density fluctuations, reflecting in an anomalously overdamped critical form. I am unaware of such a connection existing within earlier DMFT studies [38] and this qualitatively new feature has not previously been noticed, to our best knowledge.

One interpretation of this unusual feature is the following. Close to the Hubbard band splitting ("Mott") transition, one generically expects formation of excitons. A simple way to understand this is in terms of the "holon-doublon" mapping of the model, which is a partial particle-hole transformation where $c^\dagger \rightarrow c^\dagger, d \rightarrow d^\dagger$. Now $U \sum_i n_{i,c} n_{i,d} \rightarrow -U \sum_i (n_{i,c} n_{i,d} - n_{i,c})$, whereby the c, d fermions experience an on-site *attraction*, leading to formation of local "pair" bound states (these are excitons in the original model) of the type $\langle c_i^\dagger d_i^\dagger \rangle$. Quite generally, in a Hubbard model, one expects these bosons to Bose-condense. On first glance, our results are quite similar to those in upshot thereof is the well-known

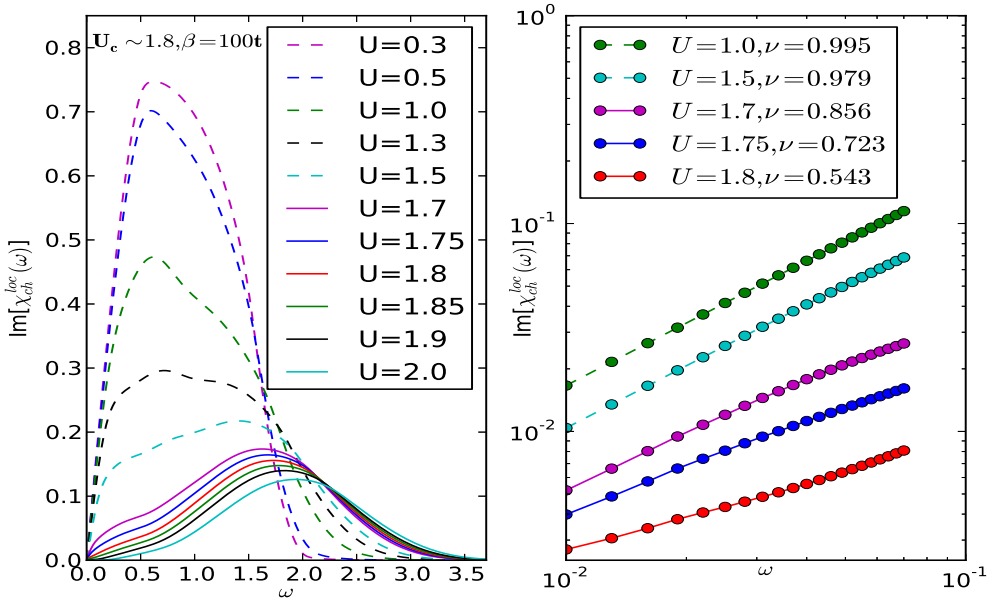

Figure 6.3: The imaginary part of the local component of the full dynamical charge susceptibility for the p-h symmetric binary alloy disorder model in the totally random case ($f_{0\alpha} = 0$). Up to $U_1 = 1.4$, $\mathrm{Im}\chi^{loc}_{ch}(\omega) \simeq \omega$, similar to its DMFT counterpart. However, for $1.5 \leq U \leq U_c = 1.8$, $\mathrm{Im}\chi^{loc}_{ch}(\omega) \simeq \omega^{\nu}$ where $\nu = 1 - \kappa$ and $0 < \kappa(U) < 1$ and κ reduces with increasing U, reaching a value $\kappa = 0.5$ at U_c (red curve). This has very unusual consequences for the long-time response to a "sudden" local quench at strong coupling (see text).

fact that this is nothing else but antiferromagnetic magnetic order, now interpreted as a Bose condensate of spin excitons. In our simplified FKM or binary-alloy case, however, such a BEC is explicitly forbidden by the fact that the *local* Z_2 gauge symmetry, associated with $[n_{i,d}, H] = 0$ for all i, cannot be spontaneously be broken by Elitzur's theorem. This still leaves open the possibility of having inter-site excitonic pairing of the c-fermions on the two-site cluster. Without global broken symmetry, such a state would be a dynamically fluctuating excitonic liquid. One would expect that a phase transition to a "solid" of such excitonic pairs will eventually occur, perhaps as a Berezinskii-Kosterlitz-Thouless (BKT) transition [8], but this is out of scope of the present work. However, having strong inter-site excitonic liquid fluctuations could cause the irreducible charge vertices to exhibit precursor features, and it could be that our finding above is a signal of such an impending instability. More work is certainly needed to put this idea on a stronger footing, but this requires a separate investigation.

6.3.1 Response to a Sudden Local Quench

Finally, one would expect emergence of anomalous features in vertex functions and charge fluctuations close to the MIT to have deeper ramifications. Specifically, I now address the question outlined in the Introduction: "Can we study the long-time response of the FKM to a sudden local quench, and can such an endeavour provides deeper insight into the "strong" localization aspect inherent in a continuous "Mott" transition?" In other words, if I introduce a local, suddenly switched-on potential in the manner of a deep-core hole potential in metals [40], how would the long-time response of the "core-hole" spectrum evolve with U? In the famed instance of a Landau Fermi liquid metal, the seminal work of Anderson [6], Nozieres and de Dominicis [88] (AND) leads to the result that at long times, the core-hole propagator, related to the wave function overlap between the ground states without and with the suddenly switched potential, goes like a power-law: $\rho_h(t)|_{t\to\infty} \simeq t^{-\alpha}$ with $\pi\alpha$ $=\tan^{-1}(V_h\rho_c(0))$ being the (s-wave for a local scalar potential) scattering phase

shift. It has also long been shown that [84] the deep reason for this feature is that the particle-hole fluctuation spectrum, $\rho_{ph}(\omega)$ (related to the collective charge fluctuation response), in a Fermi gas is linear in energy. Explicit evaluation of the core-hole response when $e-e$ interactions in the Landau Fermi liquid sense are present is a much more involved and delicate matter [51]. It is clear that qualitative change(s) in the low-energy density fluctuation spectrum must qualitatively modify the long-time response to such a sudden quench.

Answering this question in our case of the FKM is a subtle matter, since the c-fermion spectral function is *not* that of a Landau Fermi liquid, but describes an incoherent non-Landau Fermi liquid state. As long as $\mathrm{Im}\chi_{ch}(\omega) \simeq \omega$ holds, however, I expect that the long-time response will be similar to that evaluated by Janis [51] using rather formal Wiener-Hopf techniques. Ultimately, the long-time response still behaves in a qualitatively similar way to that for the free Fermi gas, except that the exponent in the power law is modified by interactions (thus, $\mathrm{Im}\chi_{ch}(\omega) \simeq \omega$ still holds, but with sizable renormalization). In my case, I thus expect that $\rho_h(t)|_{t\to\infty} \simeq t^{-\alpha}$ still holds for $U < 1.3$, since I do find $\mathrm{Im}\chi_{ch}(\omega) \simeq \omega$ in this regime in the infra-red. However, the qualitative change to the form $\mathrm{Im}\chi_{ch}(\omega) \simeq \omega^{1-\kappa}$ with $0 < \kappa < 1$ in the infra-red for $U \geq 1.4$ must also qualitatively modify the long-time overlap and the "core-hole" response.

Rather than resort to a direct computation of the long-time response within CDMFT, I will find it more instructive to consider this issue by using the low-energy results gleaned from CDMFT as inputs into an elegant approach first used in the context of the seminal X-ray edge problem by Schotte *et al.* [104] and by Müller-Hartmann *et al* [84]. To this end, I have to identify the collective charge fluctuations encoded in $\chi_{ch}(\omega)$ with a bath of bosonic particle-hole excitations in the incoherent metal. Generally, using the linked cluster expansion, the spectral function of the localized "core-hole" is (for detail calculation see Appendix C)

$$S_h(\omega) = \frac{1}{2\pi}\int_{-\infty}^{\infty} dt e^{i\omega t} exp[V_h^2 \int_0^{\infty} dE Im\chi_{ph}(E)\frac{e^{-iEt}-1}{E^2}] \tag{6.18}$$

where V_h is the "suddenly switched" core-hole potential. As long as $\mathrm{Im}\chi_{ph}(E) \simeq E$, I estimate, similar to the well-known result, that the core-hole spectral function behaves like $S_h(\omega) \simeq \omega^{-\alpha}$ with $\alpha = (1/\pi)tan^{-1}(V_h\rho_{00}(0))$, with $\rho_{00}(0)$ being the CDMFT LDOS at the Fermi energy (in a full computation, this exponent will change a bit because $\rho_{00}(\omega)$ has sizable frequency dependence close to $\omega = 0$ at strong coupling in the metal as found in Results, but the qualitative features will survive). However, when $U \geq 1.4$, having $\mathrm{Im}\,\chi_{ch}(\omega) \simeq \omega^{1-\kappa}$ must modify this well-known behavior. In this regime I find (see also Ref. [84]) the following leading contribution to the core-hole spectral function

$$S_h(\omega) \simeq \frac{V_h^2}{E_F}(\frac{E_F}{\omega})^{1+\kappa} exp[-\pi V_h^4(\frac{E_F}{\omega})^{2(1-\kappa)}] \tag{6.19}$$

which is qualitatively distinct from the well-known form, and corresponds to a long-time wave function overlap having a very non-standard form: $\rho_h(t)|_{t\to\infty} \simeq e^{-t^{1-\kappa}}$. This qualitative modification of the long-time wave function overlap is a strong manifestation of a novel type of localization at work. It would be tempting to associate this with a many-body localized regime, especially since the Landau quasiparticle picture is also violated within this strong-coupling regime, but more work is called for to clinch this issue. The basic underlying reason for this novel behaviour is the same as the one leading to generation of the anomalous exponent κ in the p-h fluctuation spectrum, *i.e*, strong ω-dependence and incipient non-analyticity in the irreducible p-h vertex close to the MIT.

6.4 Summary

I can safely summarize that in strong contrast to the one-electron response, inclusion of *non-local* irreducible p-h vertex in computation of the dynamic charge susceptibility does

lead to qualitatively new effects at strong coupling. I have shown that $\mathrm{Im}\chi_{ch}(\omega) \simeq \omega^{1-\kappa}$ with $0 < \kappa < 1$ to occur precisely in the same regime where the non-local vertex shows strong frequency dependence and signs of an impending non-analyticity (the latter occurs either at the MIT, or precedes it, see above). This feature is quite anomalous, indicating that a novel collectively fluctuating state of the electronic fluid, characterized by infra-red critical *bosonic* p-h modes, sets in before the MIT occurs. Naturally, one expects that this feature will drastically modify the charge responses in the strong coupling limit: in fact, related effects should reveal themselves in optical response of the disordered electron fluid. I leave detailed elucidation of such points for future work.

Chapter 7

DC Conductivity Tensor and Quantum Criticality at the Continuous MIT

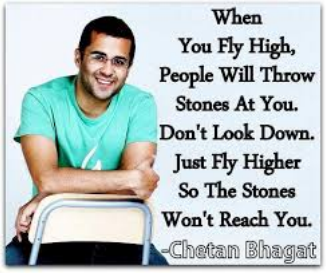

The phase diagram of Mott-like transition in the FKM is well reproduced by both single-site DMFT as well as Cluster DMFT in the previous chapters. The main task in this chapter is to perform a detailed study of the dc conductivity tensor (both longitudinal and transverse) throughout the CDMFT or DMFT phase diagram, identify different regimes, try to find evidence of quantum critical behaviour at finite temperatures and to compare the results to experiments.

The weak localization (WL) of non-interacting electrons due to disorder is now well understood within the scaling formalism [3] as a genuine quantum phase transition. In spite of its extensive successes [67], further experimental developments [60, 11] present compelling evidence for a different kind of quantum criticality that requires non-

trivial extensions of the WL paradigm. It has long been suggested, both experimentally [33] and more recently, theoretically [74] that electron-electron interactions in a disordered system can cause a metal-insulator transition (MIT) in $D = 2$ dimensions. Another possibility is that the experiments may be probing the "strong localization" region of a disorder model, *i.e*, in a regime $k_F l \leq 1$, opposite to that where WL theory works.

Binary disordered alloy which is isomorphic to the Falicov-Kimball Model (FKM) shows continuous metal-insulator transition (MIT) at strong disorder. That motivate us to study quantum critical behaviour in binary disordered alloy or equivalent FKM with disorder strength (U) as an tuning parameter. This chapter is divided into three sections. In section I, I discuss the quantum criticality of longitudinal dc conductivity across the MIT. In section II, I present the quantum criticality of transverse dc conductivity (or Hall conductivity). In the third section I analysis the experimental data of disordered NbN.

7.1 DC Conductivity in FKM

7.1.1 General Formalism for Calculation of conductivity:

The Kubo formula in Appendix D relates the response function to the corresponding current-current correlation function. Each current takes the general form:

$$j_a(\mathbf{q}) = \sum_{\sigma} \sum_{k} \gamma_a(\mathbf{k} + \mathbf{q}/\mathbf{2}) c^{\dagger}_{\mathbf{k}+\mathbf{q}\sigma} c_{\mathbf{k}\sigma} \tag{7.1}$$

where $\gamma_a(\mathbf{k})$ is the current vertex function. The Bethe-Salpeter equation (BSE) for any current-current correlation is shown in fig 7.1. There is no vertex correction in current current correlation whereever,

$$\sum_{k} \gamma_a(\mathbf{k} + \mathbf{q}/\mathbf{2}) G_{n\sigma}(\mathbf{k}) G_{n+l\sigma}(\mathbf{k} + \mathbf{q}) = 0 \tag{7.2}$$

For optical conductivity $\mathbf{q} = 0$ and vertex correction is zero. Hence the only contribution

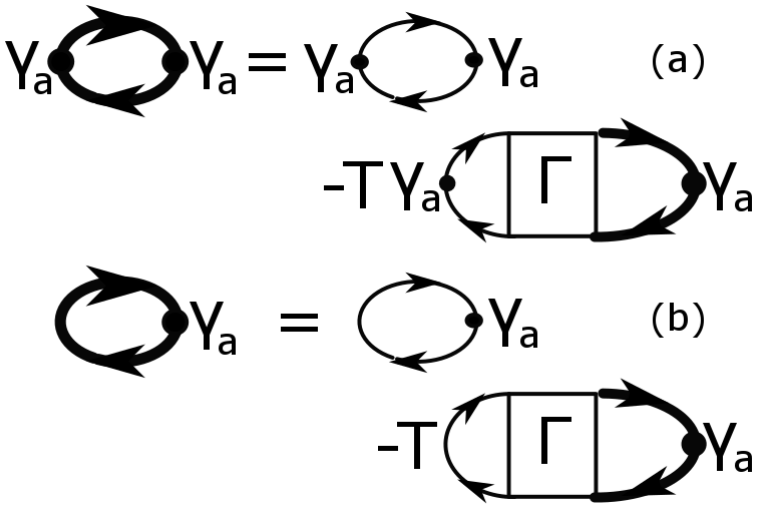

Figure 7.1: Bethe-Salpeter equations (BSE) for current-current correlation functions described by the vertex function γ_a . Panel (a) depicts the BSE equation for the interacting correlation function, while panel (b) is the supplemental equation needed to solve for the correlation function. The symbol Γ stands for the local dynamical irreducible charge vertex function. In situations where Eq. 7.2 is satisfied, there are no charge vertex corrections, and the correlation function is simply given by the first diagram on the right hand side of panel (a).

comes from the bare bubble. Hence the current current correlation within our CDMFT approach is:

$$\chi^{nn}(i\nu_l) = \sum_{a\in S,P} \sigma_0 \sum_{a\in S,P} \sum_{\sigma} \sum_{n} \sum_{k} v^2(\mathbf{k}) G^a_{n\sigma}(\mathbf{k}) G^a_{n+l}(\mathbf{k}) \tag{7.3}$$

Change the momentum summation into energy integral I have,

$$\chi^{nn}(i\nu_l) = \sigma_0 \sum_{a\in S,P} \sum_{\sigma} \sum_{n} \int_{-\infty}^{\infty} d\epsilon \rho^a(\epsilon) v^2(\epsilon) G^a_{n\sigma}(\epsilon) G^a_{n+l}(\epsilon) \tag{7.4}$$

After doing the analytical continuation as was done for dynamical charge susceptibility I get the $\chi^{nn}(\omega)$ on the real frequency. Now the optical conductivity$\sigma(\omega)$ is given by,

$$\begin{aligned} \sigma(\omega) &= \frac{Im\chi^{nn}(\omega)}{\omega} \\ &= \sigma_0 \sum_{\sigma} \sum_{a\in S,P} \int d\epsilon \rho^a(\epsilon) \int d\nu A^a_{\sigma}(\epsilon,\nu) A^a_{\sigma}(\epsilon,\omega+\nu) \times \frac{f(\nu) - f(\omega+\nu)}{\omega} \end{aligned} \tag{7.5}$$

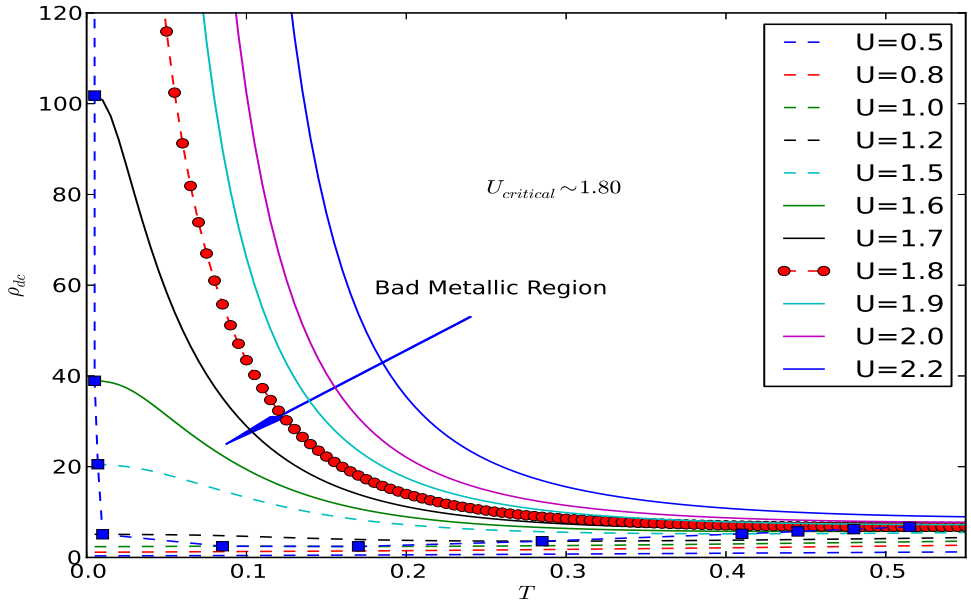

Figure 7.2: The *dc* resistivity for various U/t across the continuous "Mott" transition in the binary-alloy disorder model. When $0.90 \leq U/t < 1.8$, an intermediate "bad insulator" regime separates the high-T incoherent metal from the $T \to 0$ very bad metal, beyond which a split-band ("Mott") insulator obtains.

Using optical sum rule (i.e. integral of optical conductivity over frequency) I have,

$$\frac{d}{d\epsilon}[v^2(\epsilon)\rho(\epsilon)] + \epsilon\rho(\epsilon) = 0 \tag{7.6}$$

Solving the above equation with the boundary condition $v^2(\epsilon) \to 0$ for hypercubic lattice one get $v^2(\epsilon) = \frac{1}{2}$ and infinite coordination Bethe lattice [24, 125] $v^2(\epsilon) = (4 - \epsilon^2)/3$. I have used more exact calculation of $v^2(\epsilon)$ as given in Appendix E. Taking the limit $\nu \to 0$ I have the dc conductivity as,

$$\begin{aligned} \sigma_{dc}(T) &= \lim_{\omega \to 0} \sigma(\omega) \\ &= \sigma_0 \sum_{\mathbf{a} \in \mathbf{S},\mathbf{P}} \int_{-\infty}^{+\infty} d\epsilon v^2(\epsilon) \rho_0^{\mathbf{a}}(\epsilon) \int_{-\infty}^{+\infty} d\nu A_{\mathbf{a}}^2(\epsilon, \nu)(\frac{-df}{d\nu}) \end{aligned} \tag{7.7}$$

where $\sigma_0 = \frac{\pi e^2}{\hbar D a} \simeq (10^{-3} - 10^{-2})(2/D)(\mu\Omega).\text{cm}-1$

7.1.2 Results and Discussions

In Fig.7.2, I show $\rho_{xx}(U/t, T)$ as U/t is raised from small to large values across a critical value, $(U/t)_c = 1.80$, where a *continuous* MIT occurs in the FKM within CDMFT [47]. Several features clearly stand out: (1) at high T, $\rho_{xx}(T) \approx AT$ with small A, and always attains bad-metallic limiting values $\forall\ U/t \geq 0.5$. This behavior persistis up to rather low $T \sim 0.01 - 0.02t$, below which it levels off to a T-independent value, as expected of a weakly disordered metal. Thus, the metallic state is *never* a strict Landau Fermi liquid (2) Remarkably, $\forall\ U/t \geq 0.90$, $\rho_{xx}(T)$ develops a minimum at intermediate-to-low T, and further, $\rho_{xx}(T \to 0) > (2-3)\hbar/e^2$, exceeding the Mott-Ioffe-Regel (MIR) limit. This describes a *re-entrant* "transition" from "bad insulator" to bad-metal at very low T. Both $\rho_{xx}(T) \simeq T$ and bad-metallicity are found for the FKM in DMFT [38], though I find much cleaner linear-in-T behaviour up to much lower T here (3) Even more surprisingly, in the regime $0.90 \leq U/t \leq 1.80$, $\rho_{xx}(T)$ crosses over smoothly from a high-T bad-metallic behaviour to a progressively wider intermediate-to-low T window where it shows progressively insulating behaviour, followed by a second "re-entrant transition" to an extremely bad metal with $\rho_{xx}(T \to 0) \simeq O(20-250)\hbar/e^2$, before the $T \to 0$ "Mott" insulating state obtains as a divergent resistivity. These features are very different from expectations based on WL approaches, and cry out for deeper understanding.

Theoretically, two-site CDMFT reliably captures arbitrarily strong, repeated scattering processes off spatially separated scatterers on the cluster length scale $l \simeq k_F^{-1}$. Thus, it works best in the MIR regime, where $k_F l \simeq O(1)$, opposite to the weak-scattering regime, where $k_F l \gg 1$. Hence, quantum criticality in this regime has no reason tobe of the WL type, since no $(1/k_F l)$-expansion is now tenable. Rather, as in the locator expansion [28], one expects criticality associated with "strong localization". To unearth the nature and effects of underlying quantum criticality, I analyze our results by performing a detailed scaling analysis, which I now describe. In Fig.7.3, I show $\log(\rho_{xx}(T)/\rho_{xx}^{(c)}(T))$ versus T, where $\rho_{xx}^{c}(T)$ is the *critical* resistivity just at $(U/t)_c = 1.80$ where the MIT occurs. Beauti-

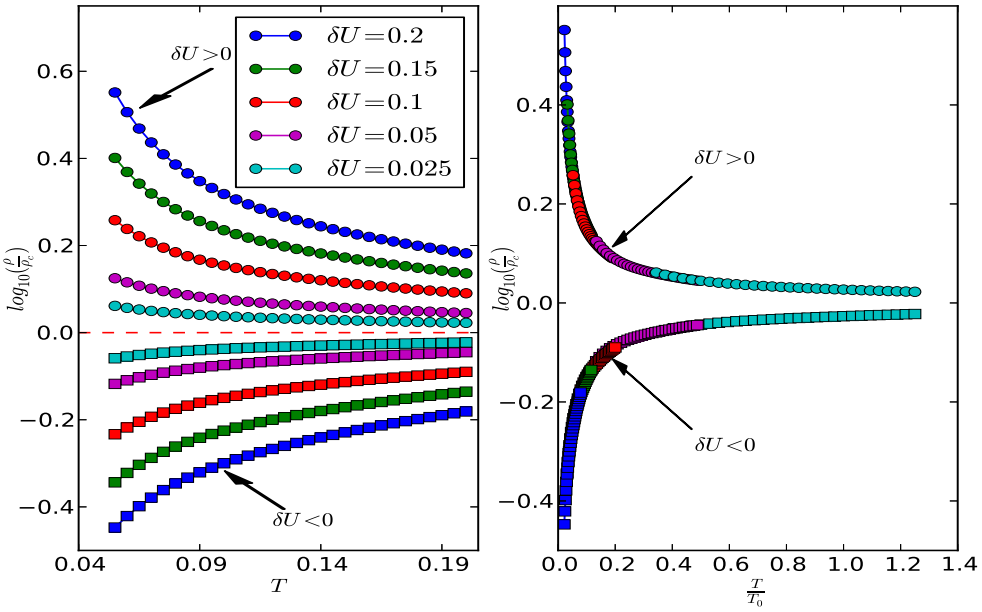

Figure 7.3: Log(ρ/ρ_c) vs T (left panel) and Log(ρ/ρ_c) vs $T/T_0(U/t)$ (right panel) for same parameters as in Fig. 7.2. Beautiful mirror symmetry around $(U/t)_c = 1.8$ and collapse of the $T \to 0$ "metallic" and insulating curves on to two universal scaling trajectories is clear.

ful "mirror" symmetry of the curves about that for $(U/t)_c$ is testimony to the genuine quantum criticality underlying the resistivities. Interestingly, in stark contrast to the Hubbard model (within DMFT) where $\rho^{(c)}_{xx}(T)$ is bad-metallic but quasilinear in T, $\rho^{(c)}_{xx}(T)|_{(U/t)_c}$ in the FKM is insulator-like up to very low T and reaches extremely high values $O(200)\hbar/e^2$, attesting to very different underlying behavior. To further unveil the novel quantum criticality, I show $\log(\rho(T)/\rho_c(T))$ as a function of T and T/T_0 in Fig. 7.3, with $T_0(U)$ chosen using standard procedure [60, 74] to make the insulating and metallic curves collapse onto two master curves. This unbiased procedure has the advantage of directly explicitly yielding $z\nu$, the product of the critical exponents associated with diverging spatial and temporal correlations at the Mott QCP, directly from the U-dependence of a low-energy scale, $T_0(U)$, which vanishes precisely at the MIT. Remarkably, as Fig.7.3(right panel), clearly shows, I find that the "metallic" and insulating curves cleanly collapse on to two universal scaling curves for a wide range of $|U - U_c|$. In Fig.7.4(left panel), I also confirm that $T_0(\delta U) \simeq c_1|\delta U|^{z\nu}$ with $z\nu = 1.3$. Further, by plotting the dc conductivity at $T \to 0$

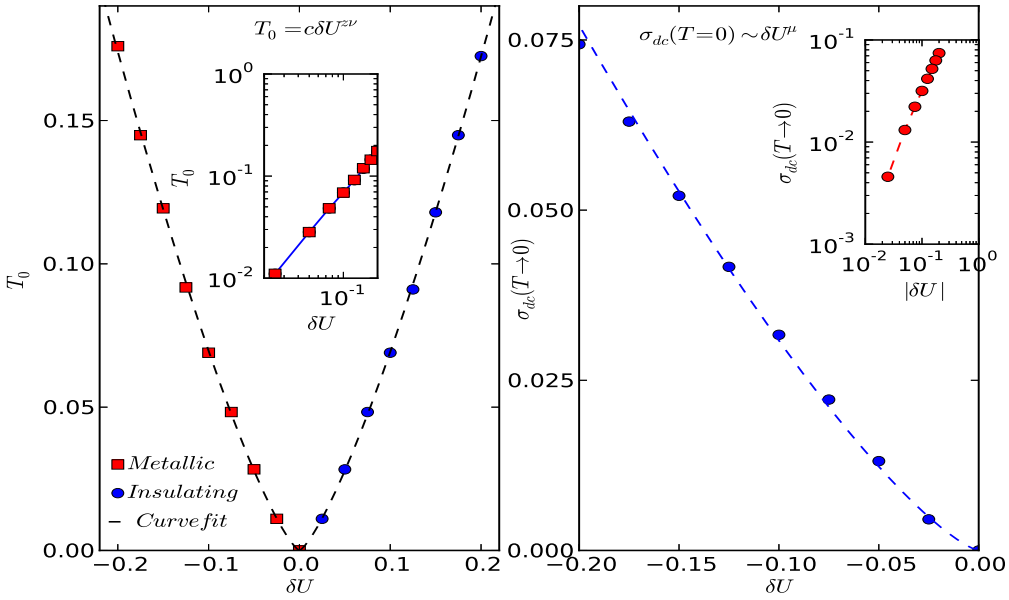

Figure 7.4: The parameter $T_0(U/t)$ vs $\delta U = (|U - U_c|$ (left panel) and conductivity $\sigma_{xx}(T \to 0)$ vs δU (right panel). Insets show that $T_0(\delta U) = (\delta U)^{1.32} \simeq (\delta U)^{4/3}$ and $\sigma_{xx}(T \to 0) = (U_c - U)^{1.31} \simeq (U_c - U)^{4/3}$, testifying to clear quantum critical behavior (see text).

as a function of U in Fig.7.4(right panel), I also find that $\sigma_{xx}(U, T \to 0) \simeq |U_c - U|^{1.3}$ as the MIT is approached from the metallic side. More confirmation of quantum critical behavior is shown in Fig. 7.5, where I exhibit $\log(\rho(T)/\rho_c(T))$ as a function of the scaling variable, $(\delta U)/T^{1/z\nu}$: the fact that the scaling curves for both insulating and metallic phases have the same scaling form on either side of the MIT testifies to robust quantum critical scaling. Since the critical behavior of the dc conductivity at the MIT reflects the critical divergence of the only relevant length scale, namely the localization length, $\xi(U)$, via $\sigma_{xx} \simeq e^2/\hbar\xi$ [17], and since $\xi(U) \simeq |U - U_c|^{-\nu}$, I directly extract $\nu = 1.3 \simeq 4/3$ and $z = 1$. It is interesting to note that $\nu = 4/3$ is characteristic of a percolation mechanism for transport. This intriguing possibility indeed holds qualitatively in the FKM as follows: as shown by Pastor *et al.* [92], one can define a configuration averaged charge-glass susceptibility, $\chi^{[2]}$, which is also singular in the disordered "Mott" insulating phase of the FKM. Noticing that inter-site correlations already effectively arise in our two-site CDMFT (near the transition on the metallic side, these read $H_{res} \simeq J_1 \sum_{\langle i,j \rangle} \sigma_i^z \sigma_j^z +$ 4th-order Ising "ring"

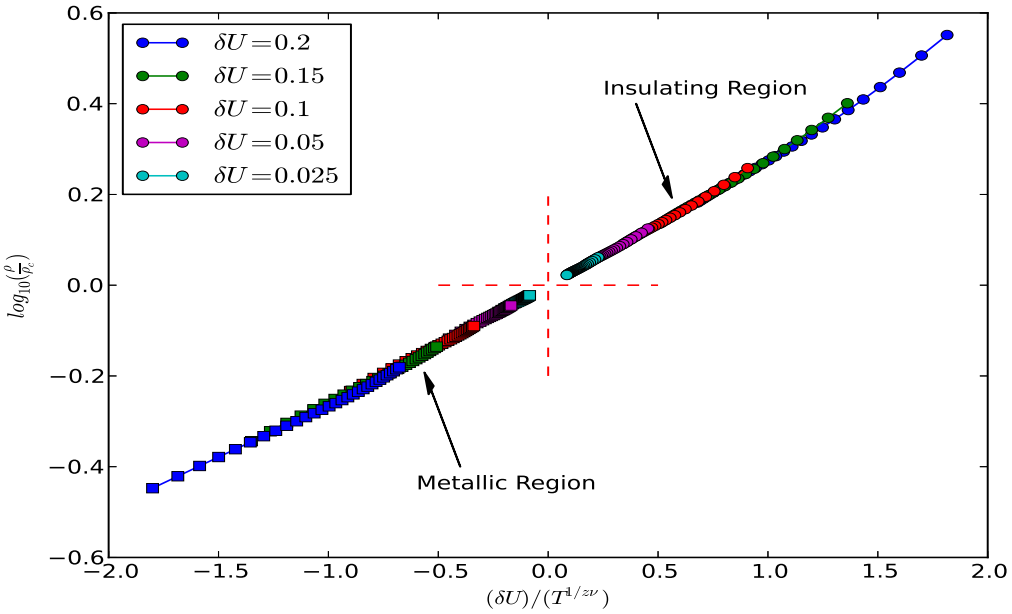

Figure 7.5: Log(ρ/ρ_c) vs the scaling parameter $(\delta U)/T^{1/z\nu}$ on both sides of the MIT. Both metallic and insulating branches exhibit the same scaling form on either side of U_c. Continuity of the scaling curve across U_c clearly bares "Mott" quantum criticality.

exchange for the FKM, with $\sigma_i^z = (n_{i,c} - n_{i,d})/2$ and $J_1 \simeq 4t^2/U$) at sizable $U \leq U_c$, one expects an *effective* inter-site term, $H' \simeq j \sum_{\langle i,j \rangle} n_{i,c} n_{j,c}$ with a modified $j \neq J$ to persist somewhat in to the very bad metallic regime. Since the glass transition is also signaled by the equation $(1 - j\chi^{[2]}) = 0$, $\chi^{[2]}$will already diverge before the MIT. Thus, our finding of $\nu = 4/3$ maybe due to onset of an *electronic* glassy dynamics near the MIT. Percolative transport is a strong possibility in glassy systems. Though our results suggest such an emerging scenario near the MIT, clinching this link requires deeper analysis alike that by Pastor *et al.*, which I leave for future work. Moreover, noticing that the Harris criterion, $\nu > 2/D$, always holds for $D \geq 2$ in our case also implies that *intrinsic* disorder effects in the FKM cannot lead to droplet formation (which requires $\nu < 2/D$ [55] for a second-order transition) [55]. Thus, the quantum criticality is “clean”. Interestingly, along with the extended "mirror" symmetry, our $z\nu \simeq 1.3$ is qualitatively consistent with $z\nu \simeq 1.6$ for the $2D$-electron gas (2DEG) in Si near the MIT [60] and $z\nu \simeq 1.5$ for Bi films. Our computed $z\nu = 1.3$ is vey different from $z\nu = 0.67$ for the one-band Hubbard model within

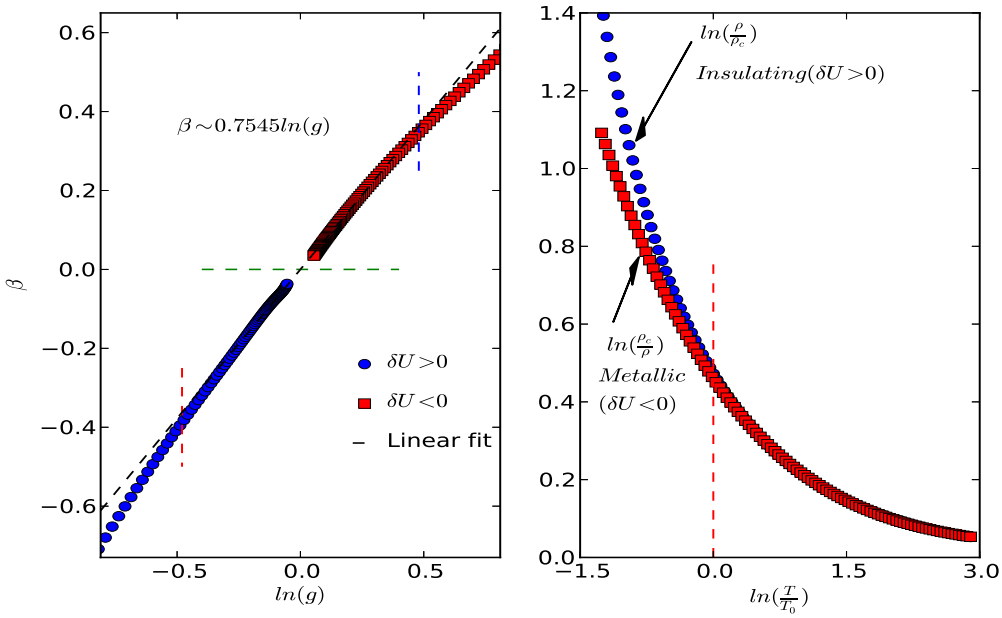

Figure 7.6: The conductivity β function vs log(g) (left panel) and ln(ρ/ρ_c) (insulating) and ln(ρ_c/ρ) (metallic) vs ln(T/T_0) (right panel). Left panel shows that $\beta(g) = log(g)$ clearly holds over an extended regime in U/t on both sides of U_c, testifying to clear "Mott" quantum criticality. Right panel establishes the symmetry relation ln($\rho(\delta U)/\rho_c$) =ln($\sigma_{xx}(-\delta U)/\sigma_c$) around U_c.

DMFT. The latter value is consistent with data for $2D$-organics [117]. Thus, one may conclude that MITs in the 2DEG in Si and Bi films, among others, are better understood by a "strong localization" limit in a physical picture where strong disorder is more relevant than local Hubbard correlations.

Further, upon plotting the transport *beta*-function (or Gell-Mann Low function), defined by $\beta(g) = \frac{d[log(g)]}{d[log(L)]} = \frac{d[log(g)]}{d[log(T)]}$ (since $L \simeq T^{-z}$ with $z = 1$ as above) versus log(g) in Fig. 7.6(left panel) [67], I find that $\beta(g) \simeq log(g)$ over a wide range of U, from the insulator, through U_c, extending deep into the "metallic" phase. In fact, it persists up to $(U/t) \simeq 0.90$, showing now that the intermediate-to-low-T pseudogap feature in $\rho_{xx}(T)$ in Fig. 7.2 is a manifestation of this underlying Mott quantum criticality. It is clear that this scaling is natural deep in the insulator, where $\rho_{xx}(T) \simeq \exp(E_g/k_BT)$. Its persistence deep into the metallic regime shows that the appearance of the very low-T "re-entrant metal" is due to the same physical processes which cause Mott insulating behavior, and pro-

vides deeper insight into the origin of this anomalous state. Specifically, this means that this QCP arises from strong-coupling physics, and is out of scope of perturbative weak-coupling schemes, as alluded to earlier. This has additional deep implications as follows. (i) Consequent to the above, I find that the "symmetry" relation linking ρ and σ_{xx} on two sides of the MIT, $\frac{\rho(\delta U)}{\rho_c} = \frac{\sigma_{xx}(-\delta U)}{\sigma^c_{xx}}$, also holds over an extended region around U_c, as shown in the right panel of Fig. 7.6.(ii) I also find that $log(\rho/\rho_c)$ is a universal function of the "scaling parameter" $\frac{\delta U}{T^{1/z\nu}}$ as shown in Fig. 7.5. (iii) Further, this also allows us to explicitly construct $\beta(g)$ for a specific microscopic model (known to be a hard task) [28] as follows: In scaling approaches to WL [67], $\beta(g)$ depends explicitly (only) on g, and that the probability distribution of g, $P(g)$, is sharply peaked at its mean value. This assumption breaks down at "strong" localization, where one expects a broad distribution, *i.e*, $P(g)$ is broad. It has been argued, based on insight from a locator expansion [28], that it is $P(\log(g))$, or more generally $P[\log\phi(g)]$ with $\phi(g) = a/g + b + cg + ...$ as $g \to 0$ that is sharply peaked in this case. Then it turns out that $\beta(g) \simeq \log[\phi(g)/\phi(g_c)]$, with g_c the critical conmductivity. Comparing this with our results, I now explicitly find that $\phi(g) \simeq 1/g$ for the FKM.

7.1.3 Comparison with the single-site DMFT result

Most, but not all, novel features found in our two-site CDMFT study of transport are already visible in single-site DMFT.

To obtain these features, I simply use the exact DMFT spectral function, $A(\mathbf{k}, \omega) = -1/\pi \mathrm{Im} G(\mathbf{k}, \omega)$ with $G(\mathbf{k}, \omega)^{-1} = \omega - \epsilon_{\mathbf{k}} - \Sigma(\omega)$ for Bethe lattice. I insert the $A(\mathbf{k}, \omega)$ in the Kubo formula for the current-current correlation function. It is well known that this is literally exact, since irreducible vertex corrections in the Bethe-Salpeter equations for conductivities rigorously drop out in this limit.

In particular, at first glance, Figs 7.7, 7.8, 7.9, 7.10 cleanly exhibit all features seen in two-site CDMFT calculations. Upon closer inspection, however, some important distinctions

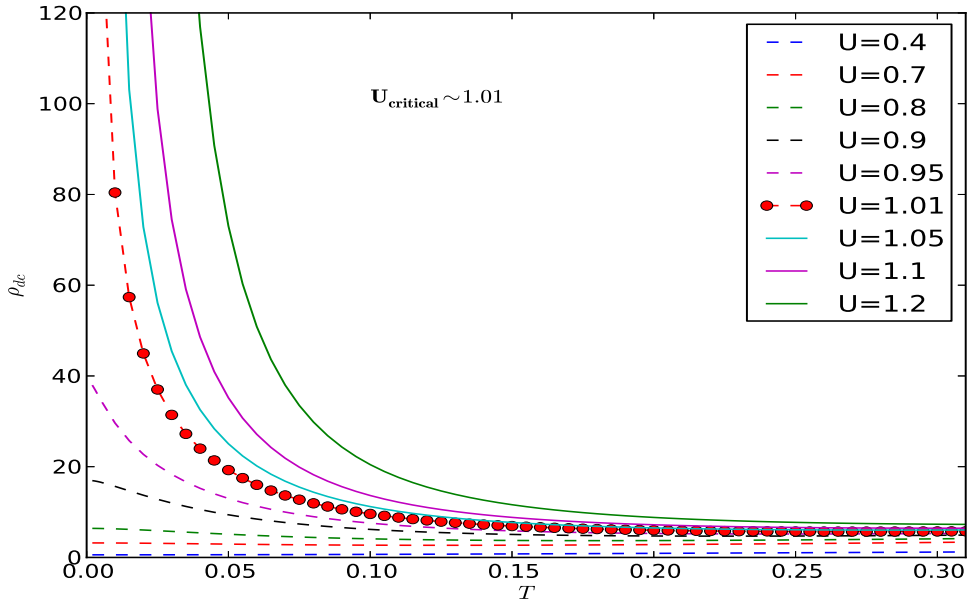

Figure 7.7: *dc* resistivity as a function of U/t in single-site DMFT. Though the trend is similar to that in CDMFT, $\rho_{dc}(U_c, T)$ is $O(40\hbar/e^2)$, much smaller than $O(250\hbar/e^2)$ seen in the CDMFT.

between DMFT and CDMFT results arise.

(*i*) The *dc* resistivity follows a similar trend with U/t. However, it attains values $O(40)\hbar/e^2$ just before the MIT, in contrast to the much larger values $O(250)\hbar/e^2$ in CDMFT.

(*ii*) Though similar scaling of $T_0(\delta U)$ and $\beta(g)$ of comparable good quality is seen in DMFT results as well, the DMFT finding of $z\nu = 1.2$ (shown in Fig 7.9) is different from $z\nu = 4/3$ found in CDMFT. The latter is the expected value for a classical percolation regime associated with onset of electronic *glassy* dynamics near the MIT. Thus, our results point toward the need for a cluster extension of DMFT to access onset of a dynamical glassy regime in transport close to the MIT.

(*iii*) finally, since $(z\nu)_{DMFT} = 1.2 > 2/D$ for $D \geq 2$ satisfies the Harris criterion as well, no droplet formation can occur, and the quantum criticality I find is "clean".

Thus, all conclusions found in CDMFT remain valid, and the only important difference is that the glassy dynamics strongly hinted at in CDMFT is absent in DMFT.

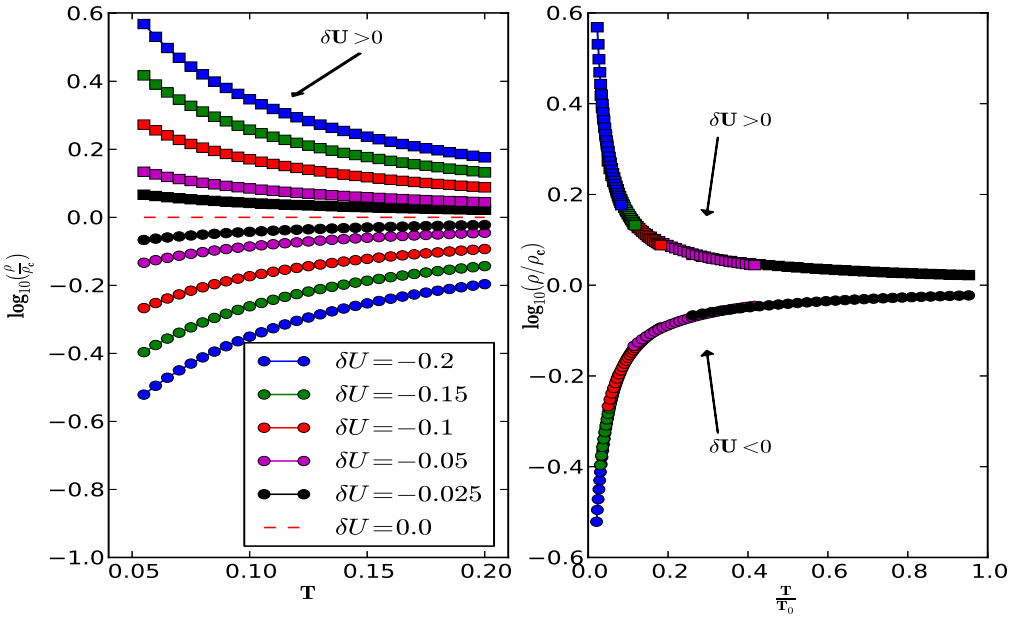

Figure 7.8: Log(ρ/ρ_c) versus T (left panel) and versus T/T_0 (right panel) exhibiting clear mirror symmetry about $U_c^{DMFT}/t = 1.01$. This is very similar to CDMFT results, indicating that no qualitative changes occur for the scaling features upon use of DMFT.

7.1.4 Comparison with the Quantum Criticality in Hubbard Model

Our findings provide clinching support for clear manifestations of an unusual quantum criticality associated with the continuous Mott-like MIT. Perfect mirror symmetry, along with $\beta(g) \simeq -ln(g)$ and its persistence deep into the "metallic" regime all indicate similarities with Mott criticality in the Hubbard model (HM). But while such features appear above the finite-T end-point (T^*) of the line of first-order Mott transitions in the HM, they persist down to $T = 0$ in the FKM, underlining a genuine “Mott” QCP. I can understand this qualitatively as follows: observe that the Landau quasiparticle picture is already destroyed above $T_{LFL} < T^*$ in the HM [117]. I am then left with a bad-metal where absence of coherent $\downarrow$-spin recoil in the HM prevents the lattice Kondo effect, making it possible to "map" the HM onto two coupled FKMs (one for each spin species) [31]. This qualitatively explains why the “Mott” criticality features I find for the FKM resemble those seen for the HM, even though $(z\nu)^{FKM} \simeq 1.3 \simeq 2(z\nu)^{HM} \simeq 0.67$. I am presently unable to explain this difference. Experimentally, I posit that this QCP leaves its imprint in $\rho_{xx}(T)$

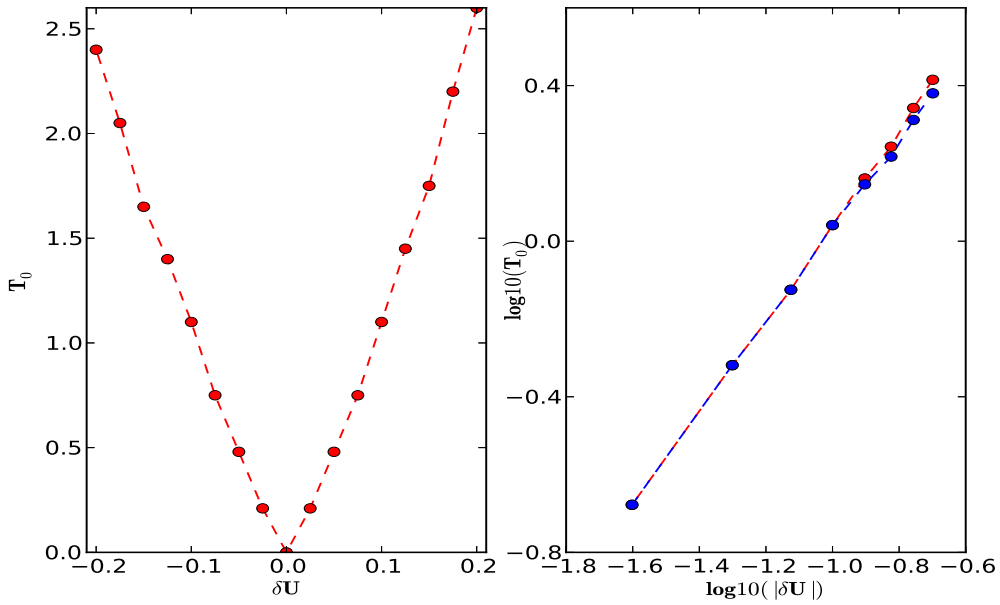

Figure 7.9: $T_0(\delta U)$ as a function of δU on normal (left panel) and on log-log scale (right panel). Though behavior qualitatively very similar to CDMFT results obtains, the exponent product $z\nu = 1.2$ (right panel) in contrast to $z\nu = 4/3$ in CDMFT. This means that onset of glassy dynamics does not get reflected in single-site theories.

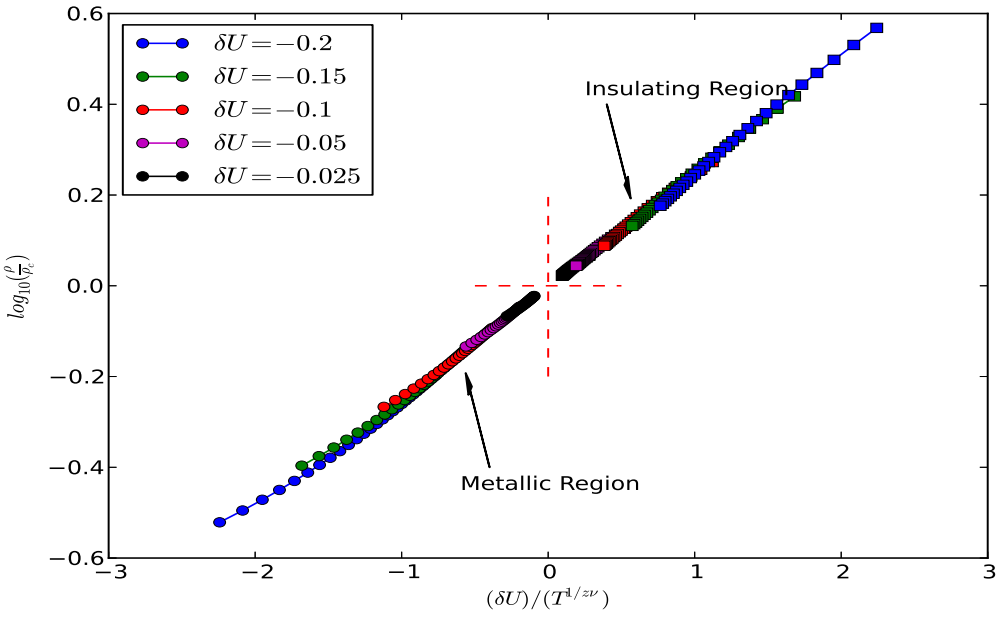

Figure 7.10: Log(ρ/ρ_c) versus the scaling parameter $\frac{\delta U}{T^{1/z\nu}}$ for the metallic and insulating phases in DMFT. Continuity across the MIT and ideentical form of the scaling function on both sides of the MIT testify to Mott quantum criticality in the FKM within DMFT as well.

as a "bad insulator" at intermediate T, followed by an anomalously bad metal as $T \to 0$: this is also distinct from the Hubbard case, where a bad-metallic $\rho^c_{xx}(T) \simeq AT$ obtains at the critical point. Finally, within (C)DMFT, the quantum disordered phase in the FKM is known to possess a finite residual entropy $O(\ln 2)$ per site. Along with infra-red branch-cut continuum spectral functions [47] in earlier work, our findings are reminiscent of "hologhraphic duality" scenarios [101]. Thus such novel quantum criticality, originally proposed for QCPs associated with Kondo-destruction approaches to ($T = 0$) melting of quasiclassical order, may also hold for "Mott" quantum criticality associated with a *continuous* metal-insulator transition.

7.2 Magneto-transport in the FKM

In this section, I study the Hall conductivity and Hall constant using the exact-to-$O(1/D)$ cluster propagators $G_{\mathbf{K}}(\omega)$ for each of the 2-site cluster momenta $\mathbf{K} = (0,0), (\pi,\pi)$ to compute the full conductivity tensor, $\sigma_{ab}(T)$, with $a, b = x, y$. I neglect the vertex corrections to the Bethe-Salpeter equation (BSE) for all the intra-cluster momenta since they are negligible even within CDMFT, as can be seen, for example, within a cluster-to-orbital mapping [119, 48]. Thus, this constitutes an excellent approximation for computation of transport coefficients.

7.2.1 Expression for Hall conductivity and Hall constant

Explicit expression for the dc conductivity given in equation 7.7. The Hall conductivity is a more delicate quantity to compute [65]. Fortunately, absence of vertex corrections comes to the rescue and I find the expression for the Hall conductivity,

$$\sigma_{xy}(T) = \sigma_{xy,0} B \sum_{\mathbf{K}} \int d\epsilon v^2(\epsilon) \rho_0^{\mathbf{K}}(\epsilon) \epsilon \int d\omega A^3_{\mathbf{K}}(\epsilon, \omega) (\frac{df}{d\omega}) \tag{7.8}$$

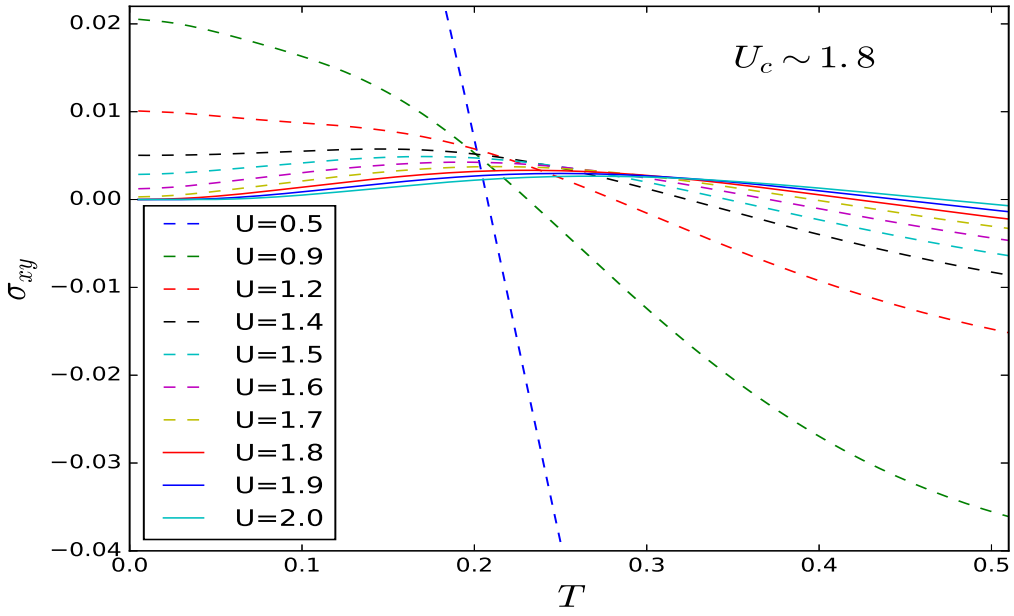

Figure 7.11: Hall Conductivity(σ_{xy}) as a function of temperature(T) for different U

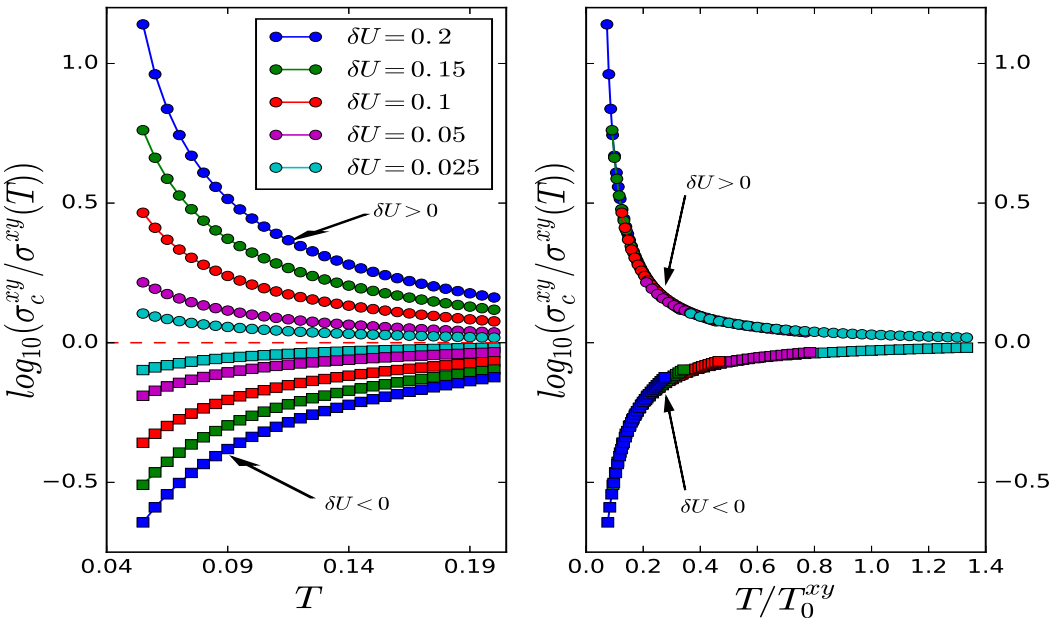

Figure 7.12: (a) In left panel, $log_{10}(\frac{\sigma_c^{xy}}{\sigma^{xy}(T)})$ as a function of temperature T for $\delta U = \pm 0.025, 0.05, 0.1, 0.15, 0.2$; σ_c^{xy} is the "separatrix". (b)In right panel, scaling the data along T-axis by scaled temperature T_0^{xy}.

with $\sigma_{xy,0} = -\frac{2\pi^2|e|^3a}{3\hbar^2}(1/2D^2)$, and B the magnetic field. Now, the Hall constant is defined as,

$$R_H(T) = \frac{\sigma_{xy}}{B\sigma_{xx}^2} \tag{7.9}$$

and the Hall angle is:

$$cot\theta_H = \frac{\sigma_{xx}}{\sigma_{xy}} \tag{7.10}$$

7.2.2 Results and Discussions:

I show the off-diagonal conductivity, $\sigma_{xy}(U,T)$ as a function of U from small- to large U across the continuous MIT occurring at $U_c = 1.8$. First, I show results for the temperature-dependent off-diagonal conductivity, $\sigma_{xy}(T)$ as a function of U across the continuous Mott transition.

I use Equation 7.8 to compute $\sigma_{xy}(T,U)$. In Fig. 7.11 I show $\sigma_{xy}(T,U)$ as a function of temperature (T) for different disorder values (U). A clear change of slope at low $T < 0.05t$ occurs around $U \simeq 1.3$, which seems to correlate with the bad-metal-to-bad-insulator crossover in the dc resistivity in our earlier section. Close to the MIT, $\rho_{dc}(T)$ diverges approximately like $\exp(E_g/k_BT)$ as $T \to 0$ in this regime, $R_H(T \to 0)$ diverges as it must, since the MIT is accompanied by loss of carriers due to gap opening. A clear change of slope (for $T < 0.05t$) occurs around $U = 1.3$, and $\sigma_{xy}(T) \simeq T^{1.2}$ around U_c. The dc resistivity $\rho_{xx}(T)$ shows extremely bad-metallic behaviour at lowest T, beautiful mirror symmetry and novel "Mott-like" scaling precisely in this regime. It is obviously of interest to inquire whether the novel features seen in $\rho_{xx}(U,T)$ are also reflected in magneto-transport near the "Mott" QCP. To facilitate this possibility, I show $log_{10}(\frac{\sigma_c^{xy}}{\sigma^{xy}(T)})$ versus T in the left panel of Fig.7.12, finding that the family of $1/\sigma^{xy}(U,T)$ curves also exhibit a near-perfect "mirror" symmetry over an extended region around $1/\sigma^{xy}_{(c)}(U,T)$, strongly presaging quantum critical behaviour. To unearth this feature, I also show $log_{10}(\frac{\sigma_c^{xy}}{\sigma^{xy}(T)})$ versus T/T_0^{xy} in the right panel of Fig.7.12, where I have repeated the unbiased method

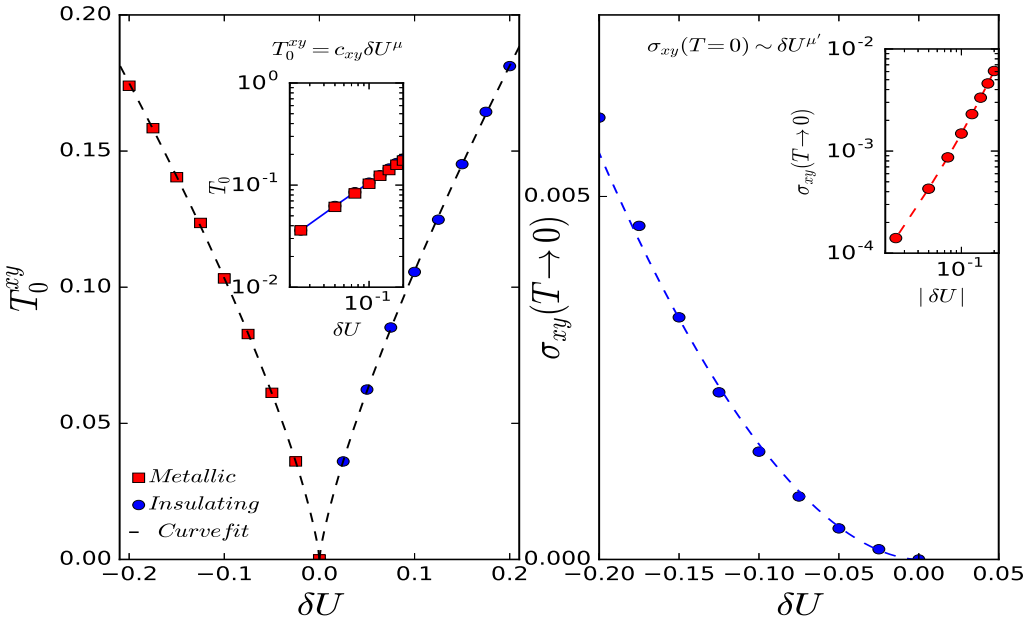

Figure 7.13: (a) In left panel, scaling parameter T_0^{xy} as a function of control parameter $\delta U = U - U_c$; the inset illustrates power law dependence of scaling parameter $T_0^{xy} = c \mid \delta U \mid^{\mu}$. (b)In right panel, $\sigma_{xy}(T \to 0)$ as a function of control parameter $\delta U = U - U_c$; the inset illustrates power law dependence of $\sigma_{xy}(T \to 0) = c \mid \delta U \mid^{\mu'}$.

of introducing a $T_0^{xy}(U)$ to rescale all metallic and insulating curves on to two universal curves. Remarkably, as for the ρ_{xx}-scaling, I find, as shown in the left panel of Fig.7.13, that T_0^{xy} vanishes precisely at the MIT. Clear scaling behaviour I find testifies to a remarkable fact: the novel scaling features found earlier in *dc* resistivity are also clearly manifest in the off-diagonal resistivity.

Even clearer characterization of the quantum critical features obtains when I compute the γ-function [108] (this is the analogue of the well-known β-function for the longitudinal conductivity) for $\sigma_{xy}(U,T)$, defined by $\gamma(g_{xy}) = \frac{d[ln(g_{xy})]}{d[ln(T)]}$, with $g_{xy} = \sigma^{xy}(T)/\sigma_c^{xy}$. As shown in Fig.7.14, it is indeed remarkable that it clearly varies as $\ln(g_{xy})$, and is continuous through $\delta U = 0$. This shows that it has precisely the same form on both sides of the MIT, which is exactly the feature needed for genuine quantum criticality. These features resemble those found for QC scaling in ρ_{xx} [46], showing that, like $\beta(g)$, $\gamma(g_{xy}) \simeq \ln(g_{xy})$ deep into the metallic phase. Thus, I have found that the *full dc* conductivity tensor reflects

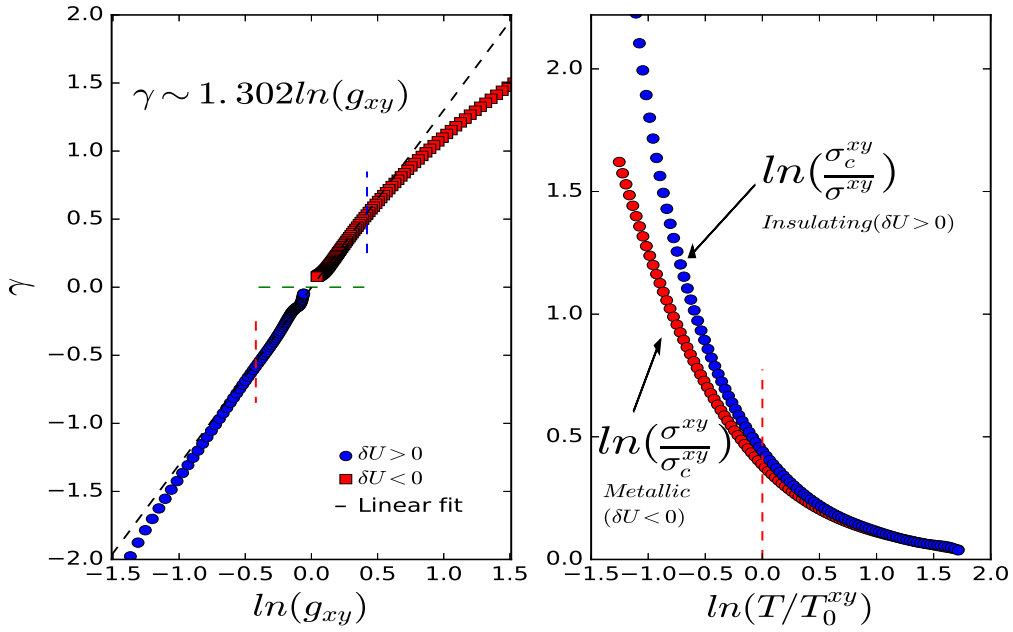

Figure 7.14: (a) In left panel, γ-function shows linear in $ln(g_{xy})$ behaviour close to the transition. Squares are for metallic branch ($\delta U < 0$) and circles ones are for insulating branch ($\delta U > 0$) ; vertical dashed indicate the region where mirror symmetry of curved is found. (b) In right panel, reflection symmetry of scaled curved close to the transition.

the strong coupling nature of the "Mott" QCP, attesting to its underlying non-perturbative origin in Mott-like (strong scattering) physics.

That $\gamma(g_{xy}) \simeq \ln g_{xy}$ holds on both sides of the MIT implies that its two branches must display "mirror symmetry" over an extended range of g_{xy}. In Fig.7.14, left panel, I indeed see that magneto-transport around the QCP exhibits well-developed reflection symmetry (bounded by dashed vertical lines), It is also manifest in the right panel of Fig.7.14, where $\sigma_c^{xy}/\sigma^{xy}(\delta U) = \sigma^{xy}(-\delta U)/\sigma_c^{xy}$; *i.e*, they are mapped onto each other under reflection around U_c, precisely as found earlier for the *dc* resistivity. As a final check, I also show (see Fig. 7.15) that log $(\sigma_c^{xy}/\sigma^{xy}(T)$ is a universal function of the "scaling variable" $\delta U/T^{1/\mu}$. Thus, our study explicitly shows the novel quantum criticality in magneto-transport at the "Mott" QCP (associated with a *continuous* Mott transition) in the FKM at strong coupling.

In an Anderson model framework, scaling of σ_{xy} is long known [108]. Our findings

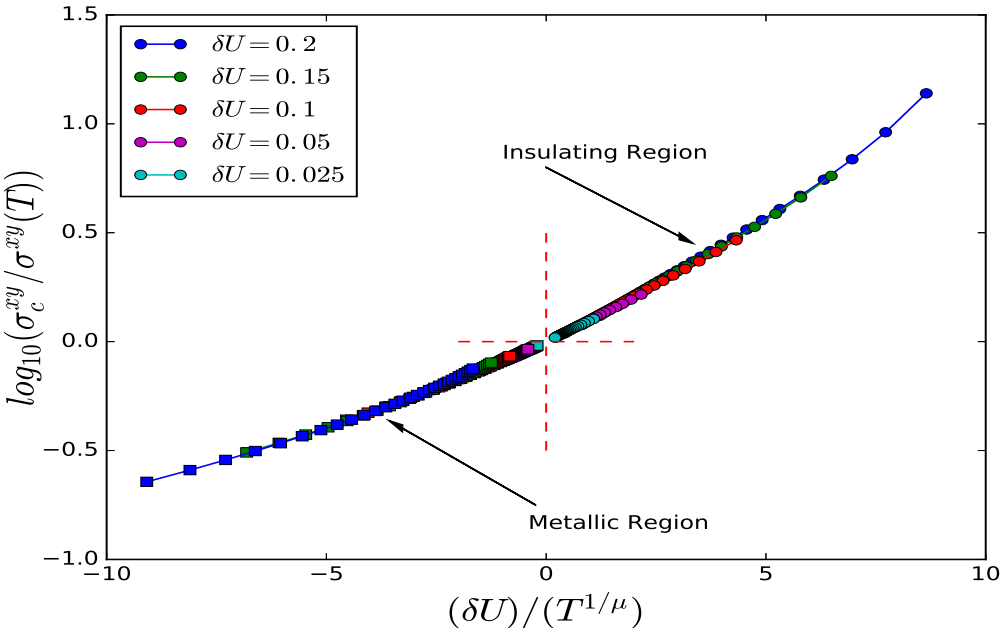

Figure 7.15: $log_{10}(\frac{\sigma_c^{xy}}{\sigma^{xy}(T)})$ vs $(\delta U)/T^{\frac{1}{\mu}}$, where $\delta U = U - U_c$.

are very distinct from expectations for an Anderson-like transition: observe that I find $T_0^{xy}(\delta U) \simeq c_{xy}|\delta U|^{\mu}$ (in left panel of Fig. 7.13) with $\mu \simeq 0.75 = 3/4$ (in inset) on both sides of U_c, as required for genuinely quantum critical behaviour. This strongly contrasts with the $T_0^{xx}(\delta U) \simeq c|\delta U|^{z\nu}$ with $z\nu = 1.32 \simeq 4/3$ found for the *dc* resistivity [46]. Further, in the right panel of Fig.7.13, I also show that $\sigma_{xy} = \sigma_{0,xy}(U_c - U)^{\mu'}$ with $\mu' = 1.8$ (in inset), quite distinct from $\nu \simeq 4/3$ found earlier for $\sigma_{xx}(U)$.

Along with our finding of $\sigma_{xx}(T) \simeq T$ and $\sigma_{xy}(T) \simeq T^{1.2}$ at the MIT, these findings have very interesting consequences: (*i*) the Hall constant is critical at the MIT. I find $R_H^{-1} \simeq \sigma_{xx}^2/\sigma_{xy} \simeq (U_c - U)^{0.8}$, whereas R_H is non-critical [108] at the Anderson MIT, (*ii*) R_H is also strongly T-dependent and divergent at the MIT, varying like $R_H(T) \simeq T^{-0.8}$, whereas $R_H \simeq (nec)^{-1}$ in an Anderson disorder model. Concomitantly, the Hall *angle* also exhibits anomalous behaviour: (*iii*) $\tan\theta_H(T) \simeq T^{0.2}$ and $\tan\theta_H(U) \simeq (U_c - U)^{1/2}$ in the quantum critical region. Our results are distinct from expectations from a Landau FL and Anderson-MIT views. At an Anderson MIT [108], $R_H = (nec)^{-1}$ is T-independent and non-critical at the MIT. In the metallic phase, use of semiclassical ideas dictates that

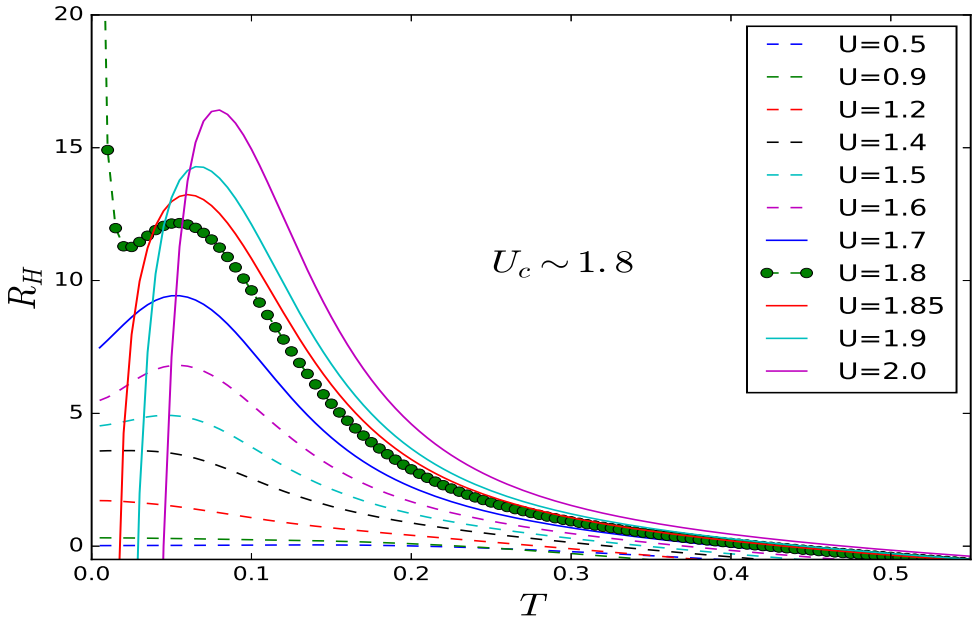

Figure 7.16: Hall co-efficient R_H as a function of temperature T for different U.

both $\beta(g)$ and $\gamma(g_{xy})$ scale like $(d-2) - A/g$, and the quantum correction to the Hall conductance is twice as big as for the Ohmic conductance. The stringent assumption under which this holds is that the inverse Hall constant (related to $h(L) = L^{d-2}/R_H B$ in Abrahams *et al.*) scales *classically* like $h(L) \simeq L^{d-2}$ for small B (large h). It is precisely this assumption that breaks down when one considers the Mott MIT, where R_H *is* critical at the MIT (see above). They are also different from expectations in a correlated LFL: a strongly T-dependent R_H close to a Mott MIT in a Hubbard model framework is long known [66]. However, in a DMFT framework, $R_H(T)$ exhibits a recovery of correlated Landau-Fermi liquid behaviour below a low-T lattice coherence scale. Moreover, the MIT there is a first-order transition. In the FKM, the metallic state remains bad-metallic and incoherent down to lowest T, and the MIT is continuous. The Mott-like character of the associated QCP is revealed by the observation of $\beta(g) \simeq \log(g)$ and $\gamma(g_{xy}) \simeq \log(g_{xy})$.

In Fig.7.16, I show $R_H(U,T)$ versus Temperature (T). Both are indeed markedly T-dependent. For an Anderson MIT, R_H would be non-critical. In a LFL metal, one expects $\sigma_{xx}(T) = 1/\rho_{dc}(T) = AT^2$, while $\sigma_{xy}(T) \simeq T^{-4}$ at low T. In that case, I end up with a T-independent

R_H and $\cot\theta_H(T) = cT^2$. This is the expected behaviour for a LFL, where a single relaxation rate governs the T-dependent relaxation of longitudinal and Hall currents. Very different T-dependences I find here testify to the breakdown of this intimate link between LFL quasi-particles and this conventional behaviour, and that the results I find are direct consequences of the destruction of LFL quasi-particles at strong coupling. They render semiclassical Boltzmann arguments (based on validity of $k_F l >> 1$) inapplicable at the outset.

7.3 Experimental Results: Disordered NbN

I now turn to experiments to investigate how our theory stands this stringent test. Recent work on NbN [23] most clearly reveals ill-understood signatures of localization incompatible with weak localization predictions. In NbN, the effect of intentional charge disorder is to cause a random variation in the local atomic potential, which increases as $k_F l$ is reduced by increasing the disorder level. Following Freericks *et al.* [38], I posit that the FKM is a suitable effective model for materials like Ta_xN and Nb_xN, where carriers interact locally with randomly distributed charge disorder. I have reanalyzed Chand *et al.*'s data on NbN in light of the above results to test how our strong coupling view performs relative to data. To make meaningful contact with data on NbN, I make a reasonable assumption that increasing U/t in the FKM corresponds to *decreasing* $k_F l$, since the scattering strength should increase with U/t, reducing $k_F l$ to $O(1)$ [23] near the MIT. I find: as shown in Fig. 7.17(a), that (*i*) $\log(\rho_{xx}(T)/\rho_c)$ on the (bad) metallic side scales with $T/T_0(k_F l)$ exactly as predicted by our theory [46]. Further, the data analysis shows (Fig. 7.17(b)) that $T_0(k_F l) \simeq (k_f l - (k_f l)_c)^{z\nu}$ with $z\nu \simeq 1.3$, again in excellent accord with theory if I identify decreasing $k_F l$ with increasing U in our model. (*ii*) interestingly, our $\rho_{xx}(T), R_H(T)$ results reproduce the detailed T-dependence seen in data [23] with only one adjustable parameter (U). (*iii*) even more remarkably, I find that $(\Delta R_H/R_H)/(\Delta\rho_{xx}/\rho_{xx})$, shown in Fig. 7.17(c), achieves values between 0.5 and 0.7 close to the MIT (between $1.5 \leq U \leq 1.9$) in our

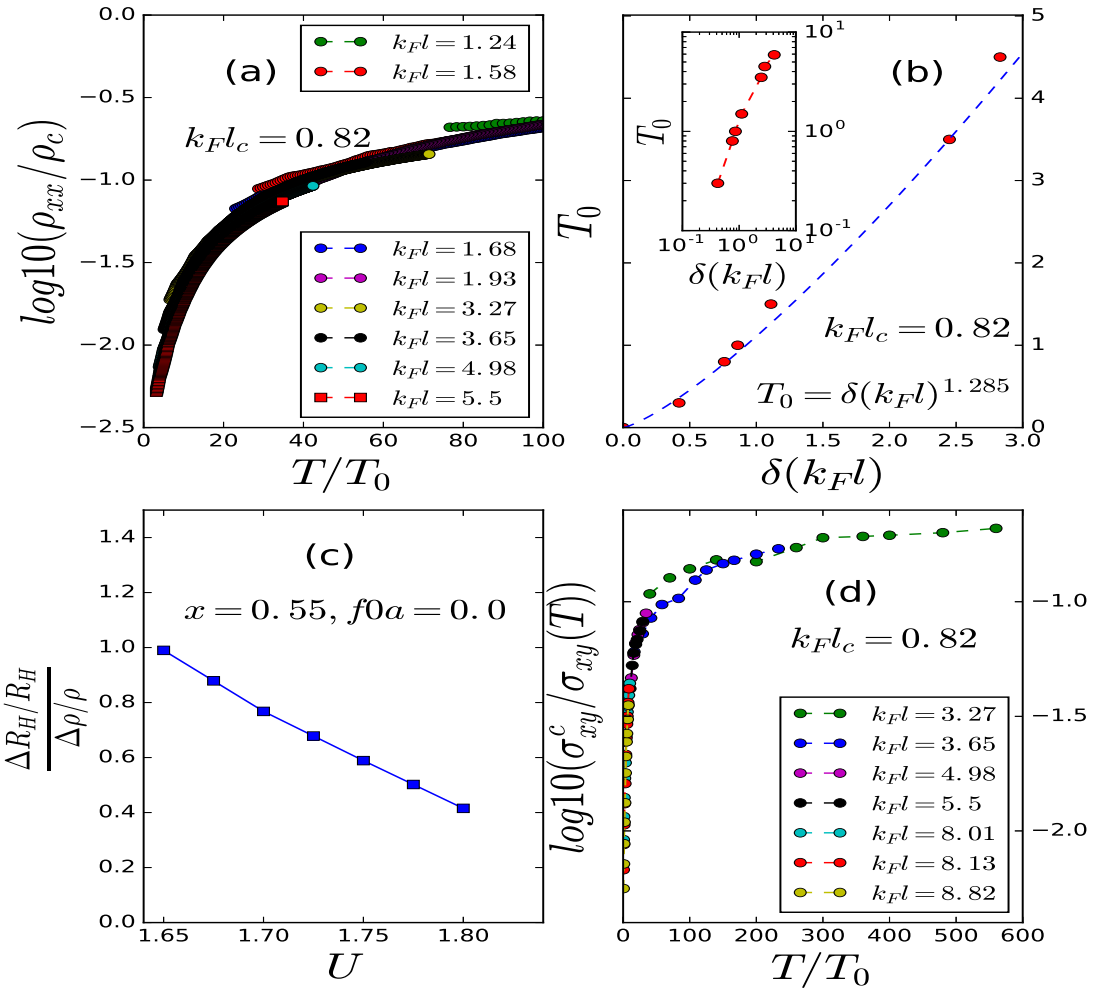

Figure 7.17: (a) Resistivity data from Chand *et al.* [23], replotted as $\log(\rho_{xx}(T)/\rho_c)$ versus T/T_0 with $T_0(\delta k_F l) \simeq |\delta k_F l|^{1.3}$ in Panel (b), in excellent accord with theory [46]. In Panel (c), I show that the theoretical ratio $\frac{\Delta R_H/R_H}{\Delta\rho/\rho}$ is in the range of 0.5 – 0.7 near the Mott QCP, again in good qualitative accord with the value of 0.69 from Hall data [23]. In Panel (d), I show clear scaling of the *experimentally* extracted $\log(\sigma^{(c)}_{xy}/\sigma_{xy}(T))$ in very good accord with theory for the same sample set used for Panel (a). The $\sigma_{xy}(T)$ is constructed from the experimental dc resistivity and Hall constant (R_H). The R_H at the critical $k_F l$ is calculated from extrapolation of the experimental Hall constant (R_H) down to $(k_F l)_c = 0.82$, as shown in Fig. 7.18

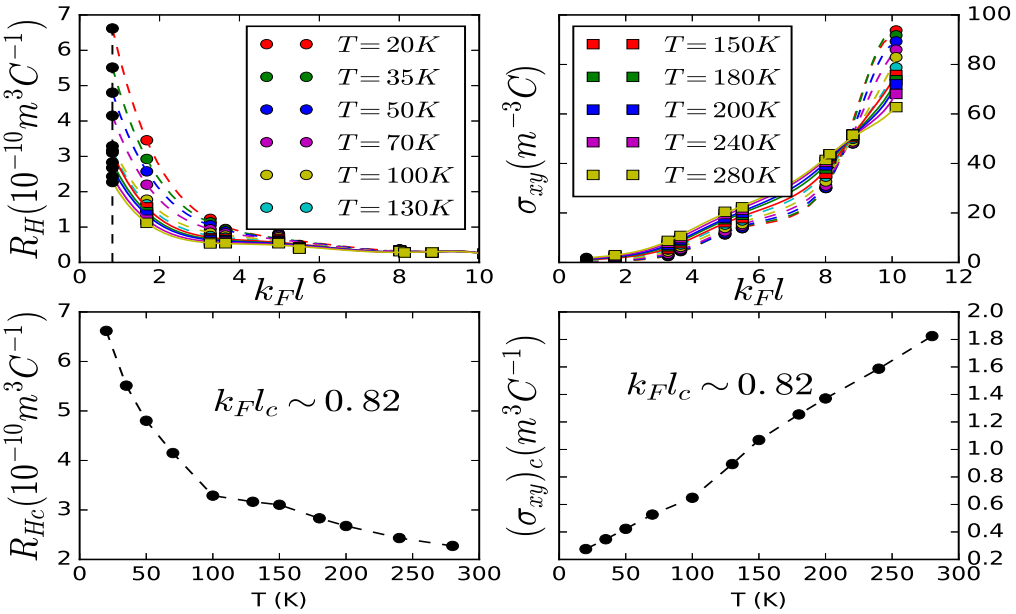

Figure 7.18: (a) In top-left panel, Hall constant R_H as a function of k_Fl for various temperature T, black circles are the values of R_H after extrapolating the curves upto critical $k_Fl = 0.82$ (b) In top-right panel, Hall conductivity σ_{xy} calculated from the Hall constant (R_H) and dc resistivity (ρ_{xx}) as a function of k_Fl for various temperature T (c) In bottom-left panel, Hall constant R_H as a function temperature (T) at the critical $k_Fl = 0.82$ calculated from the extrapolation, (d) In bottom-right panel, Hall conductivity σ_{xy} as a function temperature (T) at the critical $k_Fl = 0.82$

model, in very good accord with 0.69 extracted in experiment. Finally, in Fig. 7.17(d), I uncover quantum critical scaling in $1/\sigma_{xy}(T)$ as a function of k_Fl from data on NbN, which is expected in our model, since both σ_{xx}, σ_{xy} exhibit such novel scaling behaviour. Since R_H is difficult to extract reliably in very bad-metallic samples (with $k_Fl < 3.0$) close to the MIT, I resorted to a careful extrapolation of the Hall conductivity (σ_{xy}) and Hall constant (R_H) to smaller values of k_Fl.

In Fig. 7.18, I show the results of a careful fitting of the experimental data down to $k_Fl \simeq O(1)$ (in fact, the critical $(k_Fl)_c$ is now consistent with 0.82, which is the critical value for the longitudinal dc conductivity). Using these extrapolated fits to the dc conductivity tensor as a function of k_Fl, I constructed Fig. 7.17(d) in the main text. This makes our analysis consistent with a single $(k_Fl)_c \simeq 0.82$ for *both* $\sigma_{xx}(k_Fl, T)$ and $\sigma_{xy}(k_Fl, T)$.

Taken together, earlier results of Chand *et al.* [23], now suitably reanalyzed in light of our CDMFT results, receive comprehensive explication within a "strong localization" view adopted here, lending substantial support to the view that the novel findings in NbN are representative of strong scattering effects near a continuous MIT, and involve microscopic processes beyond perturbative-in-$(1/k_F l)$ approaches.

7.4 Summary

Thus, to conclude this chapter, I have presented clear evidence of novel quantum critical behaviour in dc resistivity as well as magneto-transport near a continuous MIT by a careful scaling analysis of CDMFT results for the diagonal and off-diagonal conductivity for the FKM in the strong localization limit. I find that the loss of the quasiparticle pole structure at strong coupling ($k_F l \simeq 1$) leads to a rather distinct "Mott"-like quantum criticality, necessitating substantial modification of the quasiclassical Drude-Boltzmann transport schemes to study (longitudinal and transverse)-transport. The resulting quantum criticality I find is closer to that expected from the opposite limit of strong localization based on a real-space locator expansion [5, 28], as manifested in $\beta(g_{xx}) \simeq \ln(g_{xx})$ or $\gamma(g_{xy}) \simeq \ln(g_{xy})$. Comprehensive and very good explication of recent data on NbN lend substantial experimental support to this Mott-like view. I suggest that strongly disordered electronic systems that show a bad-metallic resistivity and sizeable T-dependent Hall constant would be promising candidates to unearth such novel quantum-critical at a continuous MIT. Finally, the similarity of QC scaling in resistivity to the Mott QC scaling in the Hubbard model [117] above the finite-T critical end-point suggests that related features discussed above may also manifest in wider classes of strongly correlated Mott materials.

Chapter 8

Thermal Transport in FKM within Alloy Analogy

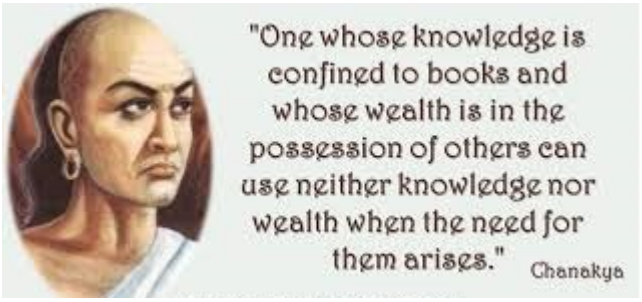

In this chapter, I will discuss the thermal transport close to the continuous metal-insulator transition in the FKM within alloy analogy using CDMFT technique. I will study quantum critical scaling of thermopower, thermal conductivity and Lorentz number and unearth the deeper reasons of the quantum critical behaviour. I will discuss the thomson coefficient and the Wiedemann-Franz law in the incoherent metals in details. At the end, I will compare our findings with single site DMFT results.

In the disorder driven MIT the core interest of study is to investigate how the dc conductivity tensor (both longitudinal and transverse conductivity) behaves near the quantum critical point (QCP). However, there is recent interest developed which

shows physical knowledge of the transport properties of the materials partly accomplished through the study of thermoelectric properties. Thermoelectric materials have numerous applications in designing new devices in the field of physics and engineering such as, power generation or refrigeration devices. Motivated by the practical application of the thermoelectric materials I study thermal properties of the disorder system near the MIT.

8.1 Definition of Thermal Transport Co-efficient

There is no single thermo-electric coefficient like dc conductivity or Hall conductivity. The definition of different thermal coefficient is different so one must be very careful when define this coefficients. The forces responsible for the thermoelectric effects are mainly temperature gradient (ΔT) and electric field (E). But all the thermal averaging assumes a constant temperature, so the calculation of thermal conductivity can be done for $\Delta T \to 0$, so that correlation function can be evaluated at a single temperature. The electric field also be weak so that one can write the induced currents to linear order of ΔT and E.

If the conductor is maintain in a constant temperature so that the temperature difference at the both ends of the conductor is zero (i.e. $\Delta T = 0$), then electric current flowing through the conductor is proportional to the induced electric field E i.e.,

$$\langle j \rangle = \sigma_{dc} E \tag{8.1}$$

where, σ_{dc} is the d.c. conductivity.

Now consider an open circuit but a temperature gradient is applied i.e. $\Delta T \neq 0$. Then electrons would flow from high-T end to the low-T end. This gives rise to the depletion of electrons at the high-T end and at the same time electrons would store at the low T-end. As a result a electric field E will generate in the open circuit from the low-T end to

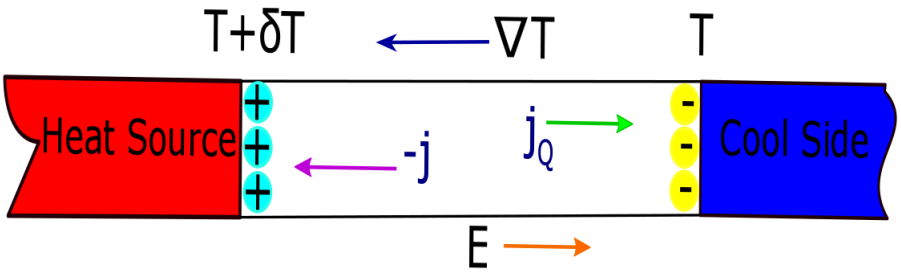

Figure 8.1: The Seebeck effect : Due to the temperature gradient ∇T an electric field **E** induced, **E** opposes the thermal flow of electrons

the high-T end. This electric field opposes the thermal flows of electrons from high-T to low-T end. This electric field E is proportion to the temperature gradient ΔT for small ΔT i.e.

$$E = S\,\Delta T \tag{8.2}$$

The quantity S is termed as thermoelectric power or thermopower.

Again, in the open circuit ($\langle j \rangle$=0), the heat current j_Q flowing through the conductor is proportional to the temperature gradient ΔT (with small ΔT). According to the Fourier's law heat current (j_Q) can be written as,

$$\langle j_Q \rangle = K(-\Delta T) \tag{8.3}$$

where K is the thermal conductivity. At low temperature the contribution of phonon is negligible compared to electron contribution. As $T \to 0$, σ_{dc} approaches a constant value and K becomes linear in T in metals. Then one can check the Wiedemann Franz law which states that the ratio of K and σ_{dc} is directly proportional to T i.e.

$$\frac{K}{\sigma_{dc} T} = L_0 \tag{8.4}$$

where, L_0 is the proportionality constant which takes the value $\frac{e^2\pi^2}{3k_B^2}$ for metal. The Wiedemann Franz law is valid at very low temperature ($\leq$ 10K) as well as at very high tempera-

ture (room T) because in this region the electrons are scattered elastically. At intermediate temperature, the Lorentz number depends on temperature (T).

In the circuit shown in Fig. 8.1, if electric current is driven through the circuit at an constant temperature T and heat will be absorbed at one end and released at the other end. Then the Peltier coefficient (Π) can be defined as the ratio of the heat current density ($\langle \mathbf{j_Q} \rangle$) and electric current density ($\langle \mathbf{j} \rangle$) i.e.

$$\langle \mathbf{j_Q} \rangle = \Pi \langle j \rangle \tag{8.5}$$

Similarly, the Thomson's effect is defined as the production or absorption of heat when electrons flows through a conductor with a temperature gradient ∇T. Thomson's coefficient τ is defined as the ratio of heat current $\langle j_Q \rangle$ and negative electric current $\langle j \rangle$ multiply temperature gradient i.e.,

$$\langle \mathbf{j_Q} \rangle = -\tau \nabla T \langle j \rangle \tag{8.6}$$

Using Kelvin's law the relation between three thermoelectric coefficients S, Π, τ as,

$$\begin{aligned} \Pi &= S\,T \\ \tau &= T\frac{dS}{dT} \end{aligned} \tag{8.7}$$

8.2 Calculation of Thermal Coefficient Using Onsager Relation

According to the linear response theory, the response of a quantum system linearly depends on applied forces. Thus using linear response theory, both electronic current ($\langle \mathbf{j} \rangle$) and heat current ($\langle \mathbf{j_Q} \rangle$) can be written as linear in $\mathbf{E}$ and ΔT of the form:

$$\langle \mathbf{j} \rangle = L_{11}\mathbf{E} - \frac{L_{12}}{\mid e \mid T}\Delta T \tag{8.8}$$

and,

$$\langle \mathbf{j_Q} \rangle = \frac{L_{21}}{e}\mathbf{E} - \frac{L_{22}}{eT}\Delta T \tag{8.9}$$

The coefficients L_{ij} are known as Onsager Coefficients. In general L_{ij} are tensors. For isotropic case considered here L_{ij} are scalar quantities. Using Ohm's law (8.1) in Eq. (8.8), I obtain:

$$\sigma_{dc} = L_{11} \tag{8.10}$$

Putting $\langle j \rangle = 0$ in equation (8.8) the thermopower (S) according to equation (8.2) is given as,

$$S = \frac{L_{12}}{\mid e \mid T L_{11}} \tag{8.11}$$

Similarly, using equation (8.3) expression for thermal conductivity (K) yields

$$K = \frac{L_{22}L_{11} - L_{21}L_{12}}{e^2 T L_{11}} \tag{8.12}$$

and from equation (8.4) for Lorentz number (L_0) the expression as,

$$L_0 = \frac{L_{22}L_{11} - L_{21}L_{12}}{(k_B T L_{11})^2} \tag{8.13}$$

Therefore the transport properties of the system can be determined immediately once one know the Onsager coefficients. It is also mention that in the absence of magnetic field the Onsager relation $L_{12} = L_{21}$ holds. Substituting the Onsager coefficient by transport coefficient in equations (8.8) and (8.9) I obtain the final expression for electric and heat current as,

$$\langle \mathbf{j} \rangle = \sigma_{dc}\mathbf{E} - \sigma_{dc} S \Delta T \tag{8.14}$$

and,

$$\frac{\langle \mathbf{j_Q} \rangle}{T} = S \langle \mathbf{j} \rangle - \frac{K \Delta T}{T} \tag{8.15}$$

Here, $\langle \mathbf{j_Q} \rangle / T$ is the entropy current density will go to zero as $T \to 0$ according to the third

law of thermodynamics.

Onsager coefficients $L_{lm}, l, m = 1, 2$ can be computed from the corresponding current correlation in the zero frequency limit:

$$L_{11} = \lim_{\nu \to 0} Re \frac{i}{\nu} \bar{L}_{11}(\nu) \tag{8.16}$$

$\bar{L}_{11}(\nu)$ is obtained from the analytical continuation of $\bar{L}_{11}(i\nu_l)$ to the real axis with,

$$\bar{L}_{11}(i\nu_l) = \frac{\pi}{\beta} \int_0^\beta d\tau e^{i\nu_l \tau} \langle T_\tau j_\alpha^\dagger(\tau) j_\beta(0) \rangle \tag{8.17}$$

where, $\nu_l = \frac{2\pi l}{\beta}$ is the bosonic Matsubara frequency. Similarly for the others Onsager coefficients:

$$\begin{aligned} L_{12} &= L_{21} = \lim_{\nu \to 0} Re \frac{i}{\nu} \bar{L}_{12}(i\nu_l), \\ \bar{L}_{12}(i\nu_l) &= \frac{\pi}{\beta} \int_0^\beta d\tau e^{i\nu_l \tau} \langle T_\tau j_\alpha^\dagger(\tau) j_{Q\beta}(0) \rangle \end{aligned} \tag{8.18}$$

and

$$\begin{aligned} L_{22} &= \lim_{\nu \to 0} Re \frac{i}{\nu} \bar{L}_{22}(i\nu_l), \\ \bar{L}_{22}(i\nu_l) &= \frac{\pi}{\beta} \int_0^\beta d\tau e^{i\nu_l \tau} \langle T_\tau j_{Q\alpha}^\dagger(\tau) j_{Q\beta}(0) \rangle \end{aligned} \tag{8.19}$$

Here, j_α, j_β are the electrical currents whose general expression is:

$$\mathbf{j} = \sum_{q\sigma} \mathbf{v}_q c_{q\sigma}^\dagger c_{q\sigma} \tag{8.20}$$

Similarly, $j_{Q\alpha}, j_{Q\beta}$ are the heat current with general expression:

$$\mathbf{j_Q} = \sum_{q\sigma} (\epsilon_q - \mu) \mathbf{v}_q c_{q\sigma}^\dagger c_{q\sigma} + \frac{U}{2} \sum_{qq'\sigma} W(q - q') [\mathbf{v}_q + \mathbf{v}'_q] c_{q\sigma}^\dagger c_{q'\sigma} \tag{8.21}$$

The detailed derivation of the electric current and heat current in equations 8.20 and 8.21 are given in Appendix F. The subscripts α, β represents the spatial dimension of the current vectors.

In absence of vertex corrections to transport coefficients, the L_{lm} can finally be expressed in terms of the cluster propagators, $G(\mathbf{K}, \omega)$. L_{11} is same as I derived for the *dc* conductivity $\sigma_{xx}(T)$ earlier in Chapter 7,

$$L_{11} = \sum_{a=S,P} \frac{T\sigma_0}{e^2} \int d\epsilon \rho_a(\epsilon) \int d\omega (\frac{-df(\omega)}{d\omega}) A_a^2(\epsilon, \omega) \tag{8.22}$$

The Onsager co-efficient relevant for heat transport is most conveniently given in the two-site cluster bonding-anti-bonding basis (S, P channels [47]) as the sum of the "kinetic" and "potential" contributions as sketched above, $L_{12} = L_{12}^k + L_{12}^p$. Then following Freericks *et al.* [37] for our two-site CDMFT, this reads (for details see the Appendix F),

$$L_{12} = \sum_{a=S,P} \frac{T\sigma_0}{e^2} \int d\epsilon \rho_a(\epsilon) \int d\omega (-\frac{df(\omega)}{d\omega}) \omega A_a^2(\epsilon, \omega) \tag{8.23}$$

while L_{22} is given by

$$L_{22} = \sum_{a=S,P} \frac{T\sigma_0}{e^2} \int d\epsilon \rho_a(\epsilon) \int d\omega (-\frac{df(\omega)}{d\omega}) \omega^2 A_a^2(\epsilon, \omega) \tag{8.24}$$

As for the conductivity tensor, it turns out that thermal transport co-efficients can be precisely evaluated within our two-site CDMFT. This is because the irreducible cluster resolved particle-hole vertex corrections rigorously drop out from the Bethe-Salpeter equations (BSE) for all current-current correlation functions [48]. This enormous simplification permits a precise computation of thermal transport within CDMFT without any further approximation. Further, having explicit closed-form analytical expressions for the cluster propagators, $G(\mathbf{K}, \omega)$, minimizes the computational cost, even within CDMFT.

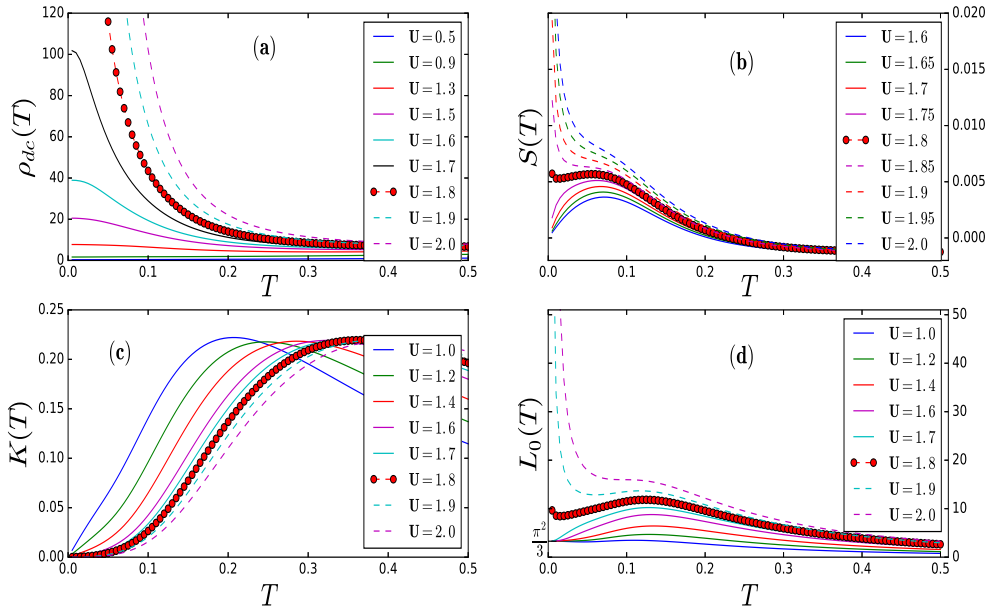

Figure 8.2: *dc* resistivity $\rho_{dc}(T)$ (a), thermopower $S_{el}(T)$ (b), thermal conductivity $K_{el}(T)$ (c) and Lorenz number $L_0(T)$ (d) for the FKM as functions of U/t. At the Mott QCP (bold red circles) at $(U/t)_c = 1.8$, both $S_{el}(T), L_0(T)$ attain finite values, cleanly separating metallic and insulating behavior. Concomitantly, $\rho_{dc}(T \to 0)$ diverges and $K_{el}(T) \simeq T^{1+\nu}$ with $\nu \simeq 4/3$ [46].

8.3 Results within Cluster DMFT

In this section, I show the result of the thermal transport with two site CDMFT approach. For convenience consider non-interacting electrons half-bandwidth as unity i.e. 2t=1. Since I aim to correlate specific features in electrical and thermal transport with each other, I start by recapitulating *dc* resistivity.

In Fig. 8.2(a), I exhibit the *dc* resistivity, $\rho_{dc}(U,T)$ as a function of U as the system is driven through a continuous MIT at $U_c = 1.8$ [46]. It is clear that at intermediate $0.95 < U < 1.8$, clear pseudogap signatures appear in $\rho_{dc}(T)$ over a progressively wider T-range, between the high-T incoherent metal and a low-T bad metal, before the MIT occurs for $U \geq 1.8$. This feature is associated with proximity to the "Mott" quantum critical point (QCP) occuring between a $T = 0$ very bad metal and a "Mott" insulator at U_c. I am interested in how this Mott quantum criticality manifests in thermal transport.

In Fig. 8.2(b), I show how the electronic contribution to the thermopower varies across the continuous MIT. Several features stand out: (*i*) for weak-to-intermediate $U < 0.9$, $S_{el}(T) \simeq AT$ at low $T < 0.025t$ is small (not shown), as expected for a weakly correlated metal, and goes hand-in-hand with $\rho_{dc}(T) \simeq const$ at low T. (*ii*) In the intermediate-to-strong coupling ($0.9 < U < 1.7$) regime, where one is in the increasingly bad-metallic low-T regime, $S_{el}(T)$ is still linear-in-T, but is significantly enhanced by factors of $O(50-100)$ over its weakly correlated values. $S_{el}(T)$ also exhibits a broad peak around $T^* \simeq 0.04t$, before continuously falling off to achieve the Heikes value [22] at very high T. It is very interesting that $S_{el}(U,T) = A(U)T$ with $A(U)$ increasing with U holds throughout this very bad metallic regime, even as $\rho_{dc}(T \to 0) \simeq 100\hbar/e^2$. This is the regime in which no quasiclassical Boltzmann view of transport is tenable, since application of Drude-Boltzmann ideas would necessarily yield $k_F l < 1$ (where no $1/k_F l$-expansion is possible). Since thermopower features result solely from a non-Landau quasiparticle cluster propagator within CDMFT, this implies that this low-T enhancement in $S_{el}(T)$ involves non-Landau-FL quasiparticle (branch-cut continuum) excitations. Just before

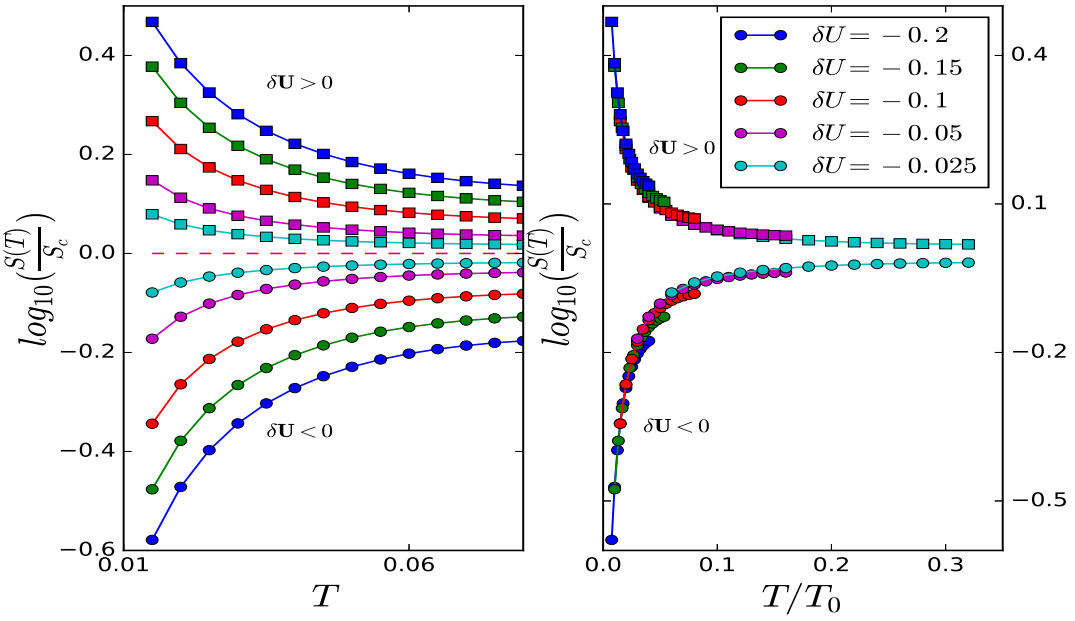

Figure 8.3: Mott Quantum critical scaling in thermopower $S_{el}(U/t, T)$ across the MIT. Log$(S_{el}(T)/S_c)$ vs T exhibits almost perfect "mirror symmetry" around $(U/t)_c$ (left panel). Collapse of metallic and insulating curves onto two "universal" curves upon scaling T axis by T_0^{th}(right panel). This is evidence that Mott quantum critical scaling in electrical transport [46] extends to thermal transport as well.

the MIT, $S_{el}(T \to 0)$ is still linear in T, but is enhanced by a factor of about 100 relative to its small U value. (*iii*) Finally, precisely at the QCP $U = 1.8$, clear anomalies obtain: $S_{el}(T)$ increases with decreasing T right down to $T \to 0$, but achieves a *finite* value. For $U > 1.8$, opening of the "Mott" gap in the one-electron density-of-states [47] produces a divergent $S_{el}(T \to 0)$. This is not a violation of the Nernst theorem, since $\rho_{dc}(T \to 0)$ simultaneously diverges.

It is clear from Fig. 8.2(b) that $S_{el}(U, T \to 0)$ curves fan out to either metallic or insulating values, except at the "Mott" QCP, where S_{el} is finite. This suggests that, like electrical transport [46], thermal transport should also exhibit characteristic quantum critical features. To unravel this novel possibility, I repeat earlier procedure [46] for thermopower by making the metallic and insulating curves fall on to two "universal" curves by scaling both with a U-dependent scale, $T_0^{th}(U)$. In the left panel of Fig. 8.3, I exhibit $\log(S_{el}(T)/S_{el}^{(c)})$ versus T. Remarkably, this bares clear signatures of "mirror" symmetry, exactly as in

electrical transport. This strongly presages novel "Mott" quantum critical features in thermal transport as well. More clinching support for such criticality is seen in right panel of Fig. 8.3, where I show $\log(S_{el}(T)/S_{el}^{(c)})$ versus $T/T_0^{th}(U)$ as done earlier [46]. Remarkably, I find (*i*) clear "mirror" symmetry between metallic and insulating curves around the critical $S_{el}(U_c)$, and (*ii*) $T_0^{th}(\delta U) = c_{th}|\delta U|^{\eta}$ with $\eta = 1$ (in Fig. 8.4 left panel). To further cement this unusual idea, I also show in the right panel of Fig. 8.4 the "beta"-function (or the Gell-Mann Low function) for thermopower, $\beta_{th}(s) = d[\log(s)]/d[\log(T)]$ versus s, with $s = (S_{el}(T)/S_c(T))$ and $S_c(T)$ being the critical thermopower right at the MIT (red circled curve in Fig. 8.2(b)). Remarkably, I find $\beta_{th}(s) \simeq \log(s)$ near the MIT, exactly as found before for the *dc* conductivity. This conclusively establishes novel quantum-critical scaling of the thermopower at the "strong localization" MIT as well.

Appearance of such quantum-critical scaling in thermopower at the MIT is very surprising, and calls for deeper analysis. Since $S_{el}(T)$ measures "mixed" electrical current-energy current correlations, these features must originate from long-time behavior of $\langle j_e(\tau) j_Q(0)\rangle$. Let us look more closely at this term. The energy current, in contrast to the electrical current, involves *three* sites, and reads [128]

$$j_{i,Q} = t^2(ic^{\dagger}_{i-\delta}c_{i+\delta} + h.c) - \frac{U}{2}(j_{i-\delta,i} + j_{i,i+\delta})(n_{i,d} - \frac{1}{2}) \tag{8.25}$$

where I have relabelled $c \rightarrow c_{\uparrow}, d \rightarrow c_{\downarrow}$, δ denotes nearest neighbors of site$i$, and $j_{i,i+\delta}$ is the electrical current operator. For the FKM, I have $[n_{i,d}, H] = 0$ for all i, and thus $n_{i,d} = 0, 1$ only. The expression for $j_{i,Q}$ now simplifies to a revealing form

$$j_{i,Q} = t^2(ic^{\dagger}_{i-\delta}c_{i+\delta} + h.c) \pm \frac{U}{4}(j_{i-\delta,i} + j_{i,i+\delta}) \tag{8.26}$$

for $(+,-)$ corresponding to $n_{i,d} = 0, 1$. Thus, for the FKM, I find that $j_{i,Q}$ is directly related to the electrical current operator, providing direct insight into the underlying reason for emergence of very similar quantum critical scaling responses in $\rho_{dc}(T)$ [46] and $S_{el}(T)$

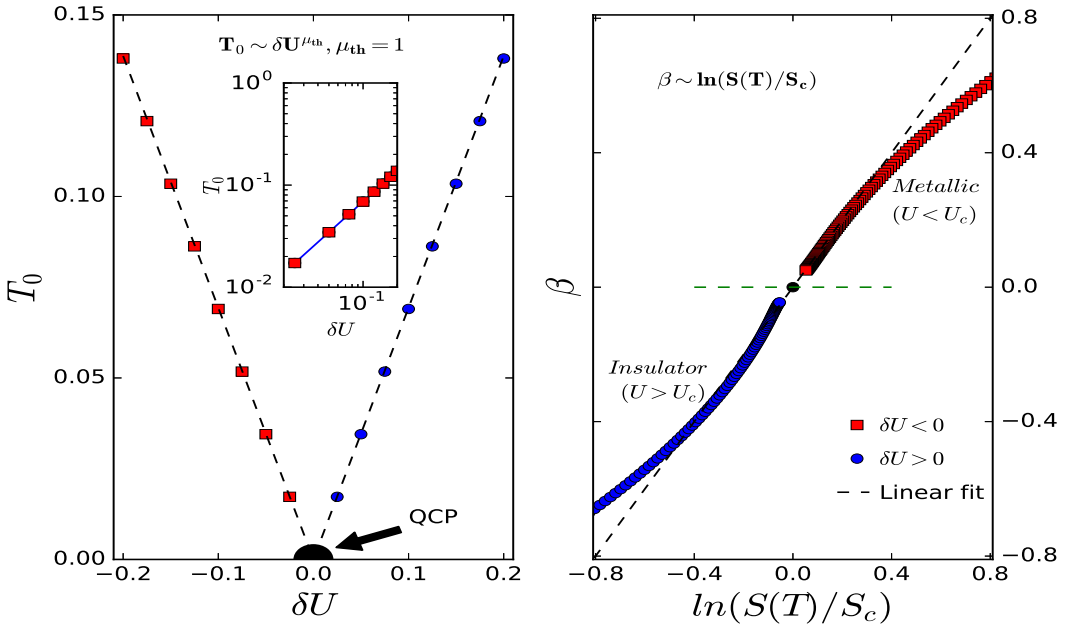

Figure 8.4: $T_0^{th}(\delta U) = c|\delta U|^{\mu_{th}}$ with $\mu_{th} = 1$ (left panel). The "beta function" varies like $\beta(s) \simeq \log(s)$ with $s = S_{el}(T)/S_c$ close to the MIT and is continuous across U_c (right panel)

above. Simply put, energy current correlations mirror those of the electrical current.

Armed with these positive features, I now study the electronic contribution to the thermal conductivity, $K_{el}(T)$, in Fig. 8.2(c). In the small U regime, $K_{el}(T) \simeq A_2 T$ is linear in T, as would be expected for a weakly correlated metal, with transport being determined by a LFL of "dirty" quasiparticles. This is the regime where $\rho_{dc}(T \to 0) \simeq const$, and formally corresponds to the weak scattering regime where $k_F l >> 1$ holds (this is thus the regime where self-consistent Born approximation (SCBA) applies). As I enter the intermediate-to-strong scattering regime with $0.95 < U < 1.8$, progressive bad metallicity in resistivity goes hand-in-hand with emergence of a low-energy scale in $K_{el}(T)$, where its power-law-in-T ($K_{el}(T) \simeq T^n, n > 1$) behaviour at intermediate-T crosses over to a linear-in-T variation as $T \to 0$. Precisely at $U_c = 1.8$, I find $K_{el}(T) \simeq T^{1+\nu}$. This behavior is characteristic of heat conductivity arising from non-fermionic excitations. In our case, such collective modes can only be of electronic origin: these are the low-energy particle-hole fluctuations, which remain low-energy excitations in the insulator when charge degrees of

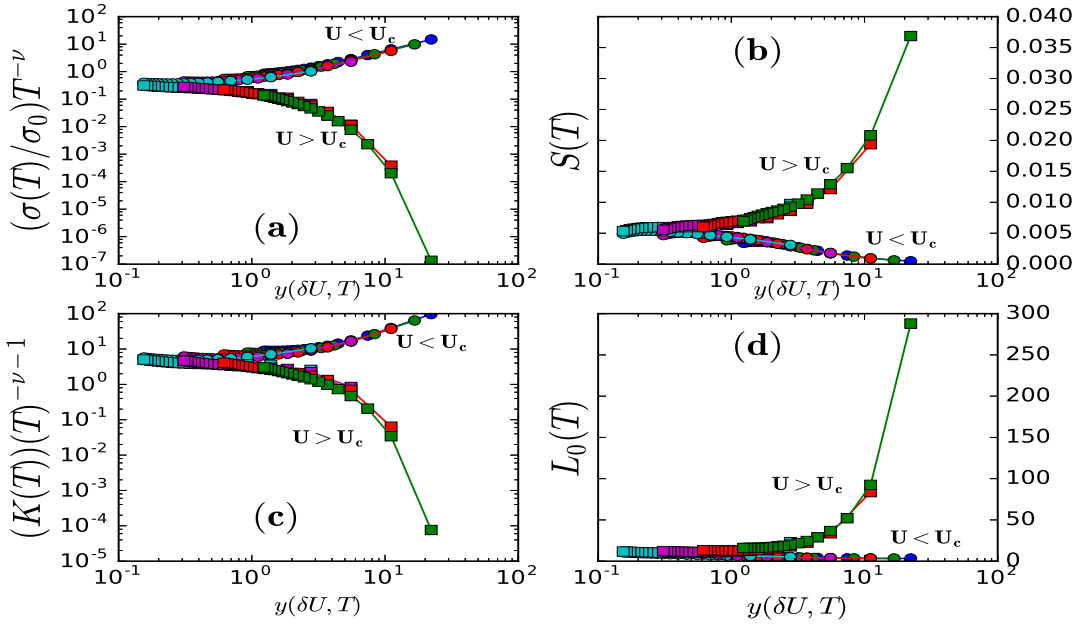

Figure 8.5: Quantum critical scaling in scaled electrical conductivity $T^{-\nu}\sigma_{dc}(T)$ (panel (*a*)), thermopower $S_{el}(T)$ (panel (*b*)), scaled thermal conductivity, $T^{-1-\nu}K_{el}(T)$(*panel*(c)) and Lorenz number (panel (*d*)) when plotted as functions of the "scaling variable" $y(U,T) = |U - U_c|/U_cT$, demonstrating clean quantum critical scaling in electrical as well as thermal transport at the Mott QCP.

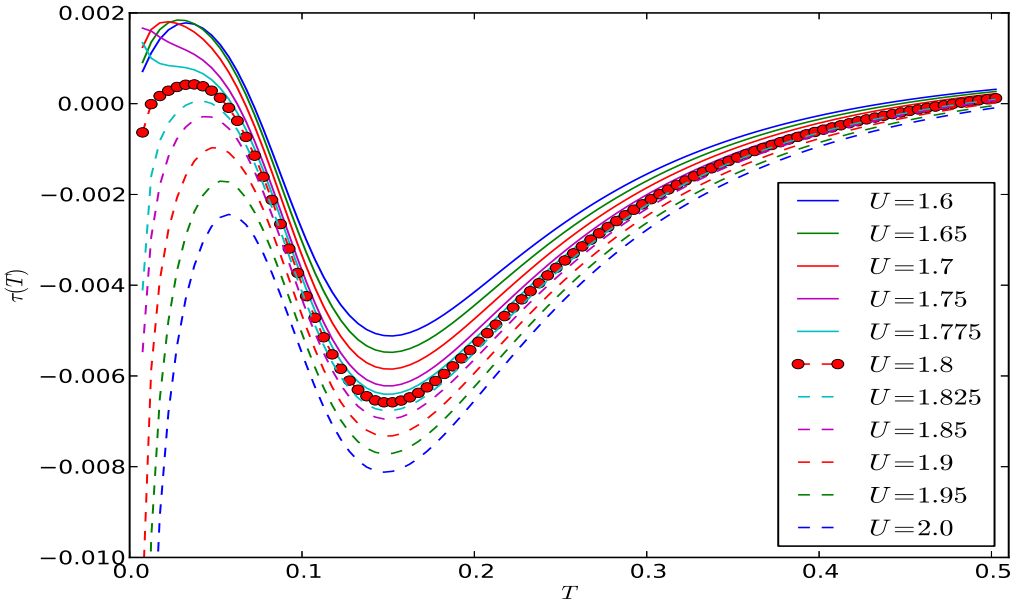

Figure 8.6: Thomson Co-efficient $\tau_{th}(T)$ for FKM as a function of U/t

freedom are frozen out at low energies. Upon closer inspection, I see that the linear-in-T contribution gives way to a power-law behavior ($K_{el}(T) \simeq T^{1+\nu}, 0 < \nu < 1$) right down to $T = 0$ for $U = 1.8$ within our numeric, *precisely* where the MIT occurs. This finding is completely consistent with breakdown of the LFL quasiparticle description in the quantum critical region associated with the MIT.

Even more insight into the breakdown of the LFL quasiparticle description close to the MIT is provided by examination of the T-dependent Lorenz number, $L_0(T) = K_{el}(T)/T\sigma_{xx}(T)$, as a function of U. In Fig. 8.2(d), I exhibit $L_0(U,T)$ across the MIT. Throughout the metallic phase, including the very bad metal, $L_0(T \to 0) = \frac{\pi^2}{3}$ (in units of $k_B = 1 = e$), even though $L_0(T)$ exhibits significant T-dependence up to the lowest T, especially for $U > 1.4$, implying no breakdown of the WF law in the metallic phase. Precisely at the MIT, however, $L_0(T \to 0) \simeq 10$, indicating breakdown of the WF law exactly at the MIT. In the insulator ($U > 1.8$), $L_0(T \to 0)$ diverges, as it must, since $K_{el}(T) \simeq T^3$ while $\rho_{dc}(T) \simeq \exp(E_g/k_BT)$. Our finding is remarkable because, whilst the resistivity shows clear precursor features of impending proximity to the MIT via progressive enhancement

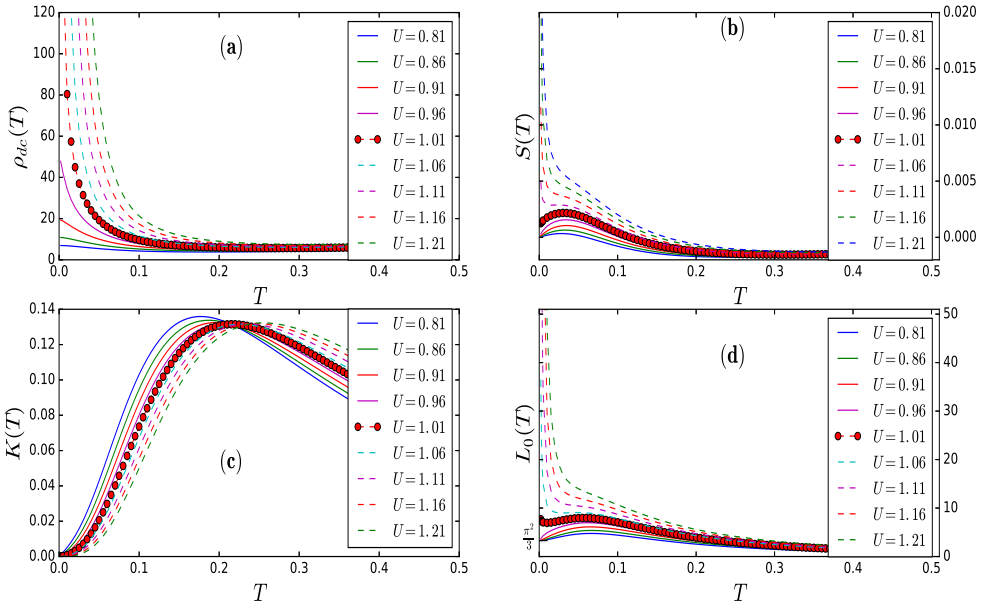

Figure 8.7: Results similar to those in Fig. 8.2, but now using single-site DMFT.

of bad-insulating and very bad metallic regimes beginning from $U = 0.95$, both $S_{el}(T)$ and $K_{el}(T)$ continue to display apparently conventional behavior right up to the MIT. Further, spectral responses clearly show non-Landau-FL metallicity [47], and while one may argue for a non-WF behavior at any $T \neq 0$, our results indicate no breakdown of the WF law at $T = 0$.

Remarkably, upon proper rescaling, it now turns out that $\sigma_{xx}(T), S_{el}(T), K_{el}(T)$ and $L_0(T)$ all exhibit clear quantum-critical scaling features. At the QCP, I find (not shown) that $K_{el}(T) \simeq T^{7/3} = T^{1+\nu}$ with $\nu = 4/3$. Recalling that $\nu = 4/3$ is precisely the correlation length exponent I find for the *dc* conductivity [46], this suggests an alternative way to exhibit quantum critical scaling that bares the link between electrical and thermal transport.

In Fig. 8.5, I find that $T^{-4/3}\sigma_{xx}(T)/\sigma_0, S_{el}(T), T^{-7/3}K_{el}(T)$ and $L_0(T)$ exhibit clear collapse of the metallic and insulating curves onto two clear branches when plotted as a function of the "scaling variable" $y = |U - U_c|/U_cT$, *i.e*, as a function of the distance from the "Mott" QCP. Since $\sigma_{xx}(U) \simeq (U_c - U)^{4/3}$ as found earlier [46], $\nu = 4/3$ and $z = 1$, as expected for the FKM. Further, $z\nu = 4/3 > (2/d)$ implies that the Harris criterion holds,

a implying a genuinely *clean* QCP. Again, these features reflect the finding above, where energy current correlations simply mirror the electrical current correlations for the FKM, providing direct microscopic rationale for closely related quantum-critical transport in both. I am aware of only one previous study [126, 78] where this issue was studied phenomenologically, by using the *experimental* conductivity as an input into the Kubo formula for the L_{lm}. In contrast, our results emerge from a truly microscopic CDMFT formulation for the FKM, and our finding of $z = 1$ is very different from $z = 3$ and $\nu = 1$ (latter taken from experimental conductivity data). It is also different from $z = d$ found [58, 55] for scaling in the non-interacting disorder model. Together with Mott-like criticality in transport [46], these differences reflect the qualitatively distinct "strong coupling" nature of the QCP in the FKM.

Finally, using the Kelvin formula, I now show the Thomson co-efficient as a function of U/t across the MIT. In Fig. 8.6, I show $\tau_{th}(U/t, T)$. In the metallic phase, right up to $(U/t) = 1.7$, the Thomson co-efficient exhibits a weak T-dependence at high T, changes sign at a low-to-intermediate $T_1 \simeq O(0.08t)$, passes through a maximum around $0.5T_1$ before vanishing linearly at lowest T. Exactly at the MIT, qualitative changes occur: $\tau_{th}(U > U_c, T)$ now exhibits two distinct regimes where $d\tau_{th}(T)/dT$ changes sign (around $1.13t$ and $0.05t$)before asymptoting to a *finite* negative value in the insulator. Remarkably, much alike the way in which the γ-co-efficient of the usual specific heat at constant volume diverges upon approach to the MIT, I find that the γ-co-efficient of the "specific heat of electricity", defined as $\gamma_e = (dS_{el}(T)/dT)$, progressively increases with U/t right up to the MIT, diverging at the "Mott" QCP.

8.4 Single-Site DMFT Results for Thermal Transport

Here, I compare our result with single site DMFT [35] result. The spectral function, $A(\mathbf{k}, \omega) = -\frac{1}{\pi} ImG(\mathbf{k}, \omega)$ with $G(\mathbf{k}, \omega)^{-1} = \omega - \epsilon_k - \Sigma(\omega)$. Inserting $A(\mathbf{k}, \omega)$ in Kubo-

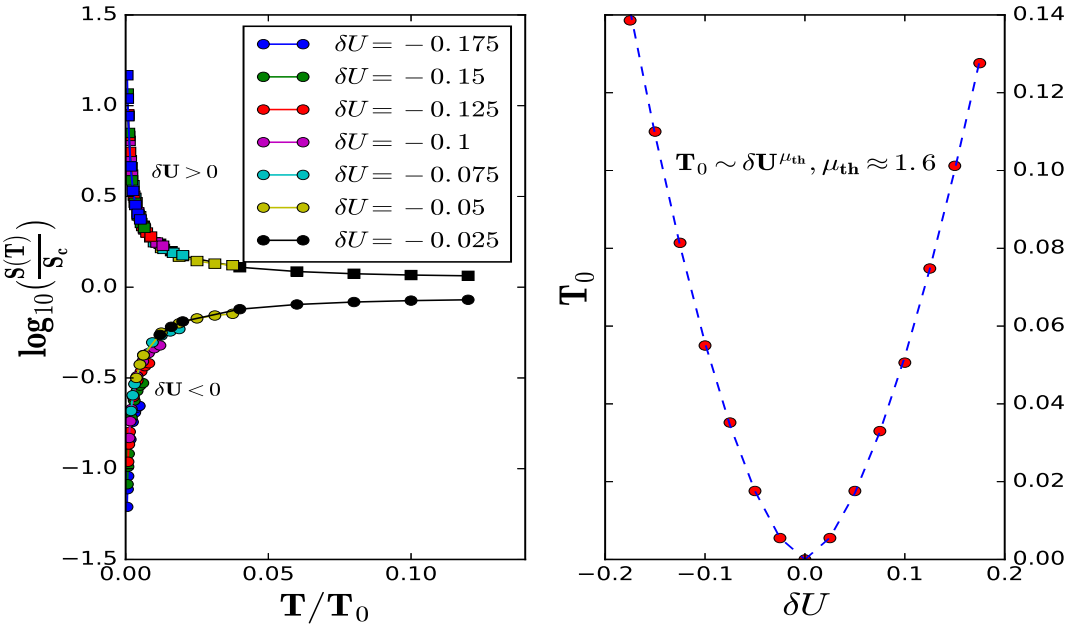

Figure 8.8: (a) In left panel, $log(S_{el}(T)/S_c)$ vs T/T_0 and (b) in right panel, $T_0^{th}(\delta U)$ vs δU within single-site DMFT.

Greenwood formula I calculate current-current correlation function [38, 37]. It is well known that for single-site DMFT irreducible vertex correction vanishes in the Bethe-Salpeter equation, so only the bare bubble contributes.

I now show single-site DMFT results for electrical and thermal transport. In *dc* resistivity across the MIT, shown in Fig. 8.7 (which now occurs at a $(U/t)_c^{DMFT} = 1.1$), I see features very similar to those found in CDMFT. However, (*i*) $\rho_{dc}(T)$ at U_c now attains values $O(40)\hbar/e^2$, much smaller than the $O(200)\hbar/e^2$ found in CDMFT. Correspondingly, $S_{el}(T)$, $K_{el}(T)$ and $L_0(T)$ exhibit very similar behavior to that found in CDMFT, as shown in Fig. 8.7. At first sight, one may thus conclude that no qualitative difference exists between DMFT and CDMFT results.

However, closer inspection of DMFT results, obtained by performing the same scaling analysis as the one done in the main text, reveals crucial differences between DMFT and CDMFT results. Comparing scaling for $S_{el}(T)$ within DMFT in Fig. 8.8 to those obtained from CDMFT in Fig. 8.3 and Fig. 8.4 in the reveals that (*i*) scaling holds over a much

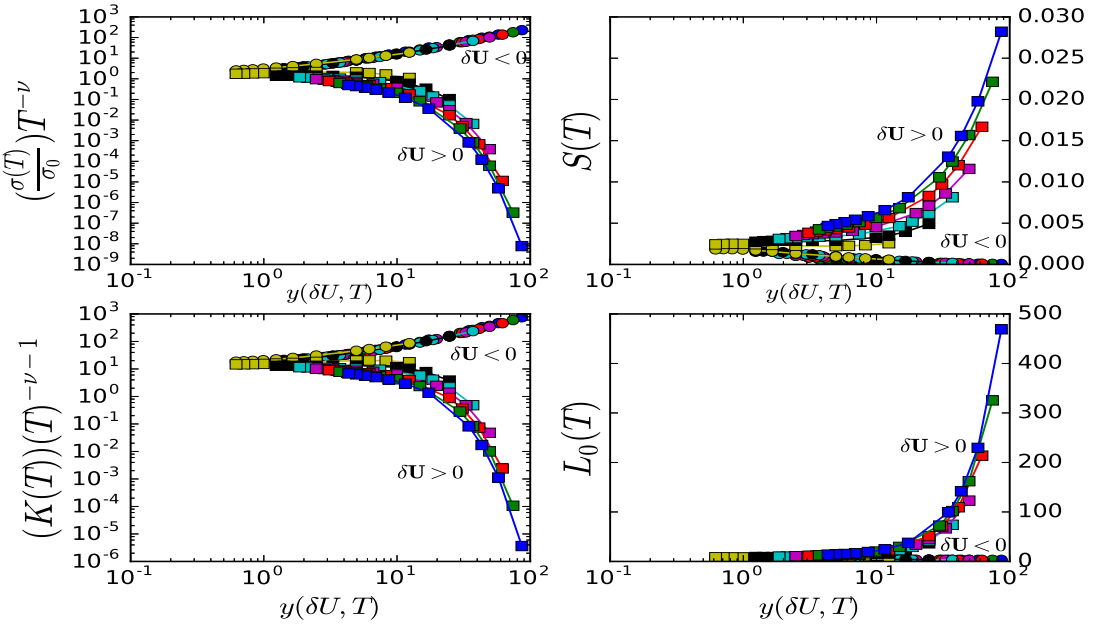

Figure 8.9: Results similar to those obtained in Fig. 8.5, but now using single-site DMFT.

narrower window in DMFT compared with CDMFT, and (*ii*) $\mu_{th}^{DMFT} = 1.2$, compared to $\mu_{th} = 1$ in CDMFT. It is thus more difficult to discern clean extended scaling behavior from DMFT results, and CDMFT clearly performs better in this respect.

Moreover, repeating the analysis leading to Fig. 8.5, I exhibit the results in Fig. 8.9. It is now clear that the scaling features in $S_{el}(T), L_0(T), T^{-\nu}\sigma_{xx}(T)$ and $T^{-1-\nu}K_{el}(T)$ are of much poorer quality than those obtained from two-site CDMFT results.

Comparing with CDMFT results, several features stand out. These reveal very interesting differences between DMFT and CDMFT results, and I use these to propose that extensions of DMFT to include short-range spatial correlations seem to be *necessary* to discuss novel quantum critical scaling in thermal transport at the MIT.

Thus, while critical features in electrical transport may be adequately captured by single-site DMFT as above (though the critical exponents z and ν are, as expected, different), I find that description of energy transport, and, in particular, much better elucidation of quantum critical thermal transport, requires cluster extensions capable of properly dis-

tinguishing between non-local aspects entering the distinct microscopic processes which underlie energy transport, as opposed to charge transport.

8.5 Discussions

What is the microscopic origin of boson-like collective modes that can provide a distinct channel for heat conduction which simultaneously blocks charge transport? It is most instructive to invoke the analogy with the Hubbard model, where one-electron excitations in the Mott insulator are frozen out at low energies $\omega < \Delta_{MH}$, the Mott-Hubbard gap in the one-electron DOS. Were one to consider the Hubbard model, dynamical *bosonic* spin fluctuations, originating from second-order-in-(t/U) virtual one-electron hopping processes, would be the natural low-energy excitations. However, in the FKM-like binary alloy model I consider, identifying $c \rightarrow c_{\uparrow}, d \rightarrow c_{\downarrow}$ leads to an Ising super-exchange to second order in a (t/U) expansion when $U >> t$ in the "Mott" insulator. It is important, exactly as in the Hubbard case, that it is the virtual hopping of a c-fermion between neighboring sites (from 0 to α and back in our two-site cluster [47]) that is necessary to generate such a boson-like mode. Since this is *not* a real low energy charge fluctuation, it cannot cause real charge transport. But it does lead to a gain $O(-t^2/U)$ in super-exchange energy; *i.e*, energy is *not* conserved, and so these virtual charge fluctuations indeed cause energy transport. Physically, this n.n hopping in a gapped "Mott" insulator involves creation of a particle-hole pair (a holon-doublon composite on neighboring sites). At low energy, this local "exciton" is effectively a bosonic mode that disperses on the scale of $J \simeq t^2/U$. These bosons are thus *not* necessarily linked to any broken symmetry, but naturally emerge in a "Mott" insulator. In our CDMFT, the dynamical effects of such "excitonic" inter-site correlations on the cluster length scale *are* fed back into the cluster self-energy, and thus the basic process leading to energy transport but not charge transport *is* included in CDMFT. This is also the reason why CDMFT performs much better that single site DMFT when I study quantum critical scaling in thermal transport. The underlying reason for this in-

ability of DMFT results to properly describe quantum critical scaling of thermal transport can be understood heuristically as follows: in CDMFT approach, I have argued that thermal transport involves microscopic electronic processes associated with virtual hopping between a given site to its neighbors and back. Such second-order-in-hopping processes block charge transport, but allow energy transport, since such processes involve a gain of "super-exchange" (of Ising form for the FKM) energy. In single site DMFT, this process is $O(1/d)$, and so is not adequately captured. But precisely such a process *is* captured in our CDMFT, since the dynamical effects of inter-site (intracluster) correlations *are* fed back into CDMFT self-energies by construction [47]. These "bosons" are thus natural candidates that can account for our finding of $K_{el}(T) \simeq T^{1+\nu}$ in the proximity of the MIT.

Very interestingly, a series of careful experiments on two-dimensional electron gases (2DEGs) show remarkable features [87]: (*i*) in the low-n_s regime where $\rho >> h/e^2$, the activated T-dependence of $\rho_{dc}(T)$ shows a remarkable "slowing down" to an extremely bad metallic state, even as $\rho_{dc}(T \rightarrow 0) \simeq 250h/e^2$, (*ii*) in the *same* n_s-regime, the thermopower shows hugely enhanced values (two orders of magnitude above the Mott value) and, perhaps even more remarkably, exhibits linear-in-T behavior reminiscent of normal metals precisely below 1.0 K. It may be possible to apply our high-D approach, which focuses on short-ranged correlations, to these mesoscopic systems *if* one could model the system as a 2DEG influenced by strong scattering from atomic-sized (strong) scattering charged centers. In light of our calculations, the dichotomy between the T-dependence of $\rho_{dc}(T)$ and $S_{el}(T)$ can be interpreted as follows: a real charge excitation is blocked in the "strong-disorder" limit of the FKM near the MIT due to blocking effects associated with Mottness, explaining the extraordinarly high $\rho_{dc}(T \rightarrow 0)$ below 1.0 K. But a collective particle-hole (or holon-doublon composite in Hubbard model lore) excitations are real low-energy electronic collective modes that naturally arise in this regime, and lead to a hugely enhanced S_{el}. It is interesting that our strong-coupling approach seems to rationalize the very unusual experimental observations in a single picture which emphasizes proximity to a (Mott-like) localization transition. That such observations maybe subtle

manifestations of novel phase fluctuation effects is not inconsistent with our view either, since it follows directly from the number-phase uncertainty principle that increasing proximity to electronic localization will necessary generate large phase fluctuation-dominated state(s).

It is interesting to compare our CDMFT technique of studying thermal transport to the recent work on thermal transport by Finkel'stein and Schwiete [106, 105]. Based on perturbative renormalization group (RG) calculation they studied the quantum criticality using $2+\epsilon$ expansion and calculate the critical exponent corresponds to different universality classes. This theory describes the system with both disorder as well as interaction and treat the system as disordered Fermi liquid with disorder induced renormalized Landau parameter.

Despite the great success of this approach, there are certain limitations in compare with the CDMFT approach - (a) In this theory (perturbative RG), low temperature excitations which are adiabatically connected to a non-interacting (but disordered) electronic systems, hence excitations are fermionic in nature and collective excitations play a subleading role, while in CDMFT approach fermionic like excitations are absence and the collective excitations play prominent role (b) perturbative RG is unable to detect any metastable states (like glassy dynamics) arising due to the competition between disorder and interaction whereas our approach can easily describe those features.

8.6 Summary

To summarize, I have showed clear quantum-critical scaling features in $S_{el}(T), K_{el}(T)$ and $L_0(T)$ at the MIT strongly testifies to robust quantum critical scaling of thermal transport at a continuous MIT. Ours is a truly microscopic approach, and is best valid in the strong localization regime ($k_F l \simeq 1$), where a Hubbard-like band-splitting type of MIT obtains. This is the limit opposite to the well-studied weak localization (WL) case, where

a perturbative-in-$1/k_F l$ expansion is possible: at strong localization, the criticality is better rationalized in terms of a locator expansion [28], and exhibits signatures expected of a continuous "Mott" quantum criticality. Moreover, I am also able to connect these critical features in a very transparent way to those observed in electrical conductivity by analysing the structure of underlying correlations, thereby providing a direct rationalization for our findings. In view of the fact that the one-band Hubbard model exhibits "quantum critical" scaling in *dc* transport near the finite- but low T end-point of the line of first-order Mott transitions, it would also be interesting to study the possibility of related features in thermal transport for such cases in future if the finite-T critical end-point of the Mott transition could be driven to sufficiently low T.

Chapter 9

Optical Conductivity and Dielectric Response in FKM

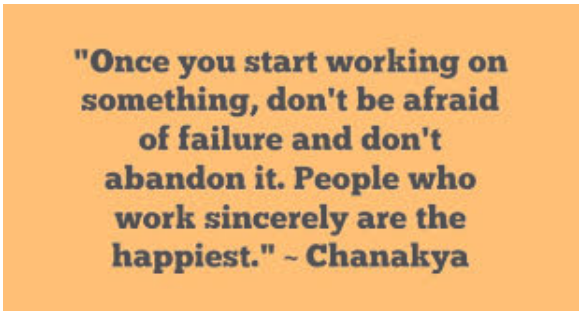

In this chapter, I will investigate the optical response of the Falicov-Kimball model (FKM) across the continuous metal-insulator transition (MIT) in detail using results from a cluster extension of dynamical mean field theory (CDMFT). Exploiting rigorous sum rules, I will characterize polarization fluctuations and the related singularity in the Hilbert space metric tensor at the MIT. Surprisingly, I will find that all "Universal Dielectric Response" UDR naturally emerges in the quantum critical region associated with the continuous MIT, followed by a superlinear power-law increase in their optical responses over exceptionally broad frequency regimes.

Optical conductivity has long been used to characterize elementary excitations in condensed matter. Response of matter to *ac* electromagnetic fields is usually encoded in the complex conductivity [10], $\sigma(\omega)$ or the complex dielectric constant, $\epsilon(\omega)$.

Optical studies have been especially valuable in strongly correlated electronic matter [50] and, as a particular example, have led to insights into breakdown of traditional concepts in cuprates [120].

Such studies have also led to much progress in understanding of complex charge dynamics in disordered matter. In the seventies, pioneering work of Jonscher [54] showed a universal dielectric response (UDR) of disordered quantum matter to *ac* electromagnetic fields, wherein $\sigma(\omega) \simeq \omega^{\alpha}$ with $\alpha \leq 1$ in the sub-GHz regime. More recently, in a remarkable study, Lunkenheimer *et al.* [72] find an astonishingly similar response in a wide class of disordered matter: among others, doped, weakly and strongly correlated semiconductors exhibit UDR, followed by a superlinear power-law increase in $\sigma(\omega)$, bridging the gap between classical dielectric and infra-red regions. That this behavior is also common to dipolar and ionic liquids as well as to canonical glass formers suggests involvement of a deeper, more fundamental and common element, related to onset of a possibly intrinsic, glassy dynamics in emergence of UDR. In the context of correlated quantum matter (such as the Mott insulator $LaTiO_3$ and $Pr_{0.65}(Ca_{0.8}Sr_{0.2})_{0.35}MnO_{0.35}$ (PCSMO) [72]), such unconventional "glassy" dynamics must emerge near the doping-induced MIT as a consequence of substitutional and/or intrinsic disorder due to inhomogeneous electronic phase(s) near the MIT. The microscopic origin of electronic processes leading to these observations, however, is an open and challenging issue, and remains largely unaddressed theoretically, to our best knowledge. In this chapter, I will present the optical conductivity and universal dielectric response in the FKM within CDMFT approximation.

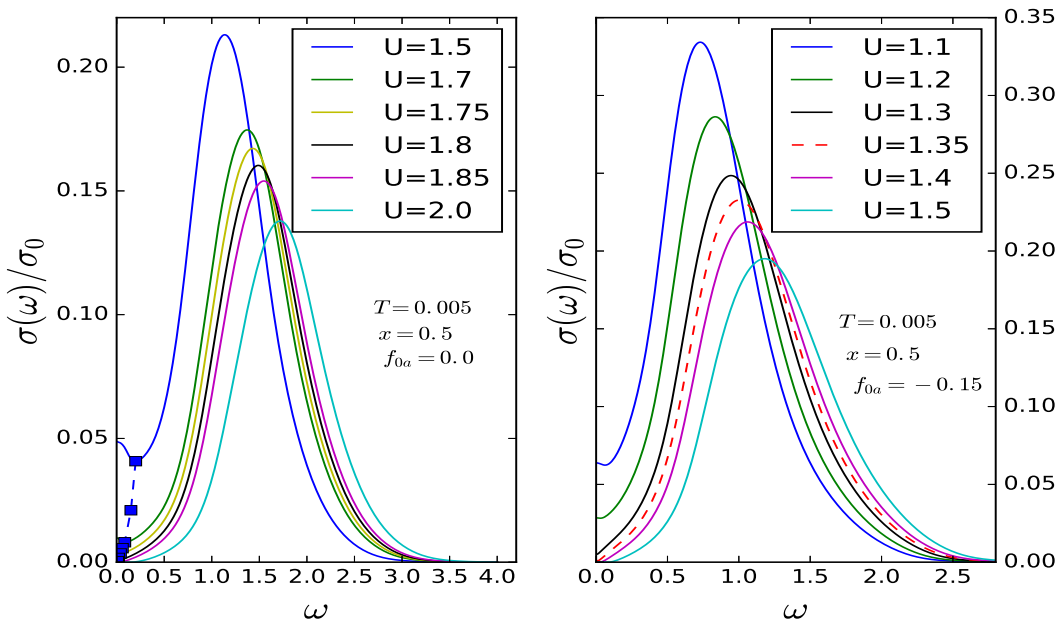

Figure 9.1: In the left panel (A) the real part of optical conductivity ($\sigma(\omega)$) as function of frequency (ω) for different disorder strength U with short range order $f_{0\alpha} = 0$. The bump has observed in the bad metallic region in the low frequency. In the right panel (B) the real part of optical conductivity ($\sigma(\omega)$) as function of frequency (ω) for different disorder strength U with short range order $f_{0\alpha} = -0.15$.

9.1 Relation between Optical conductivity and Dielectric Response

The expression for the optical conductivity$\sigma(\omega)$ (the detailed calculation is given in Chapter 7) is given by,

$$\begin{aligned}\sigma(\omega) &= \frac{Im\chi^{nn}(\omega)}{\omega} \\ &= \sigma_0 \sum_{\sigma} \int d\epsilon \rho(\epsilon) \int d\nu A_\sigma(\epsilon,\nu) A_\sigma(\epsilon,\omega+\nu) \times \frac{f(\nu)-f(\omega+\nu)}{\omega} \end{aligned} \tag{9.1}$$

I can consider $v^2(\epsilon)$ is equal to 1/2. For more exact calculation of $v^2(\epsilon)$ is given in Appendix E. Now, the real part of the conductivity is related with the imaginary part of the dielectric response (known as dielectric loss) by,

$$\sigma(\omega) = \omega\epsilon_0 Im[\epsilon(\omega)] \tag{9.2}$$

where, ϵ_0 is the permittivity of free space. So using equation 9.2 one can calculate the dielectric response.

9.2 Results for Optical Conductivity

In Fig. 9.1, I show the real part of the optical conductivity near and across the MIT ($1.6 \leq U/t \leq 2.0$), computed from Eq. 9.1 as a function of U/t for (a) the completely disordered case in Panel A (short-range order parameter $f_{0\alpha} = 0$ in our earlier work [47]) and (b) the short-range ordered case in Panel B ($f_{0\alpha} \neq 0$). Several features stand out clearly: In Case (a), (1) $\sigma(\omega)$ shows a bad-metallic low-energy bump (shown in Fig 9.2) centered at $\omega = 0$, whose weight decreases continuously as the MIT is approached (at $U/t = 1.8$). It is important to note that low-energy spectral weight is continuously transferred from the bad-metallic and mid-infra-red (MIR) regions to high energies $O(U)$ across the MIT. This

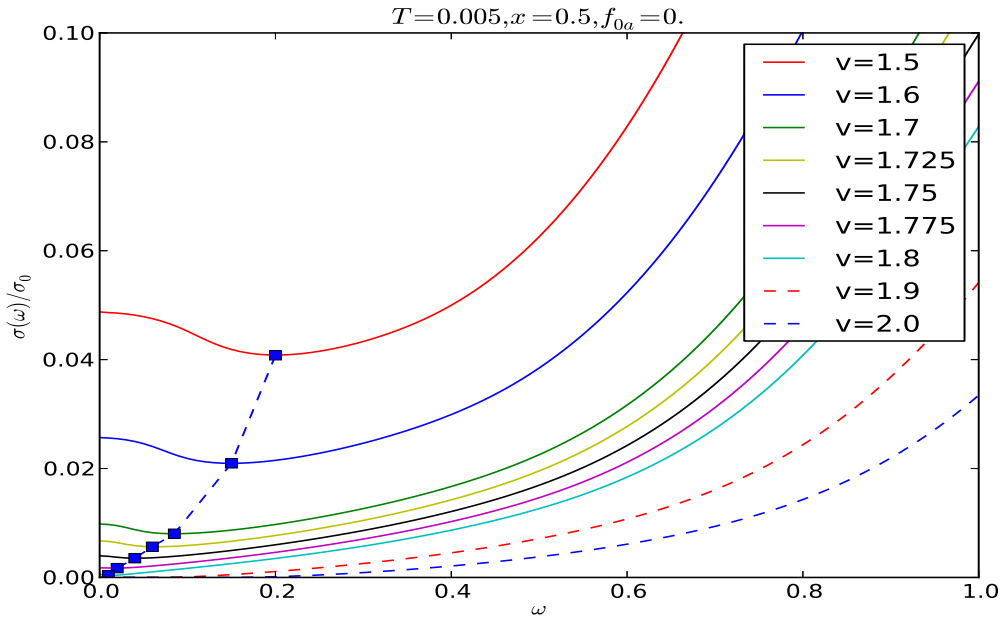

Figure 9.2: The low frequency view of the left panel of Fig 9.1, the bump at the low frequency are very prominent

is characteristic of a correlation-driven MIT and the continuous depletion of low-energy weight is a consequence of the continuous MIT in the FKM. In Case (*b*), I exhibit the effect of "anti-ferro alloy" (AF-A) short range order (SRO). Apart from the fact that the MIT now occurs at $(U/t) \simeq 1.35$ [47], the above features seem to be reproduced in this case as well. Looking more closely, however, I see marked changes in the low- and mid-infra-red energy range: the "bad metallic" bump centered at $\omega = 0$ is suppressed by SRO, and $\sigma(\omega)$ rises faster with ω in the MIR. These changes are to be expected, since AF-A SRO reduces the effective kinetic energy, increases U/t and leads to reduction low-energy spectral weight in optics.

9.3 Universal Dielectric Response

Having investigated the optical conductivity, I now turn to the UDR near the MIT. Since the FKM is isomorphic to the binary-alloy Anderson disorder problem, I inquire how

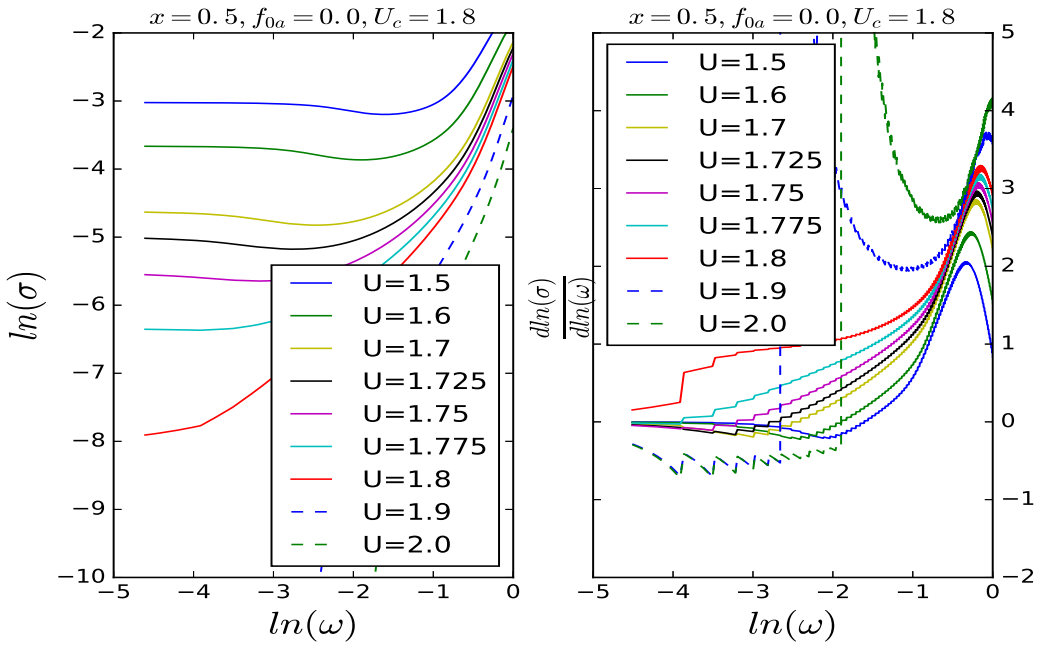

Figure 9.3: (a) In left panel, $log(\sigma(\omega))$ vs $log(\omega)$ for different disorder strengths (U) (b) In right panel, $\frac{dlog(\sigma)}{dlog(\omega)}$ vs $log(\omega)$ for different disorder strengths (U).

CDMFT performs in the context of the remarkable universality in dielectric response in disordered quantum matter alluded to before [72]. In Figs. 9.3 9.4, I show $\log(\sigma(\omega))$ and $\log(\sigma(\omega)/\omega)$ versus $\log(\omega)$ as functions of U/t to facilitate meaningful comparison with data of Lunkenheimer *et al.* [72]. It is indeed quite remarkable that *all* the basic features reported for disordered matter are faithfully reproduced by our CDMFT calculation. Specifically, (*i*) for $1.5 < (U/t) < 1.8$, a "dc" conductivity regime at lowest energy (up to $10^{-4} - 10^{-3}t$) smoothly goes over to a sublinear-in-ω regime (UDR, in the region $(10^{-2} - 10^{-1})t$) followed by a superlinear-in-ω regime (around $(10^{-1})t$, connecting up smoothly into the "boson" peak. These regimes are especially visible around $(U/t) = 1.8$, precisely where the MIT occurs. (*ii*) Moreover, corroborating behavior is also clearly seen in Fig. 9.4, where I exhibit the dielectric loss function $\log(\sigma(\omega)/\omega)$ vs ω on a log-log scale. It is clearly seen that a shallow minimum separates the UDR and superlinear regimes at approximately $\ln(\omega) = -0.8$ (in the meV region) in the very bad-metallic state close to the MIT. This is in excellent accord with results for both $LaTiO_3$ and PCSMO [72]. Moreover, the energy dependence of the optical conductivity also seems to be

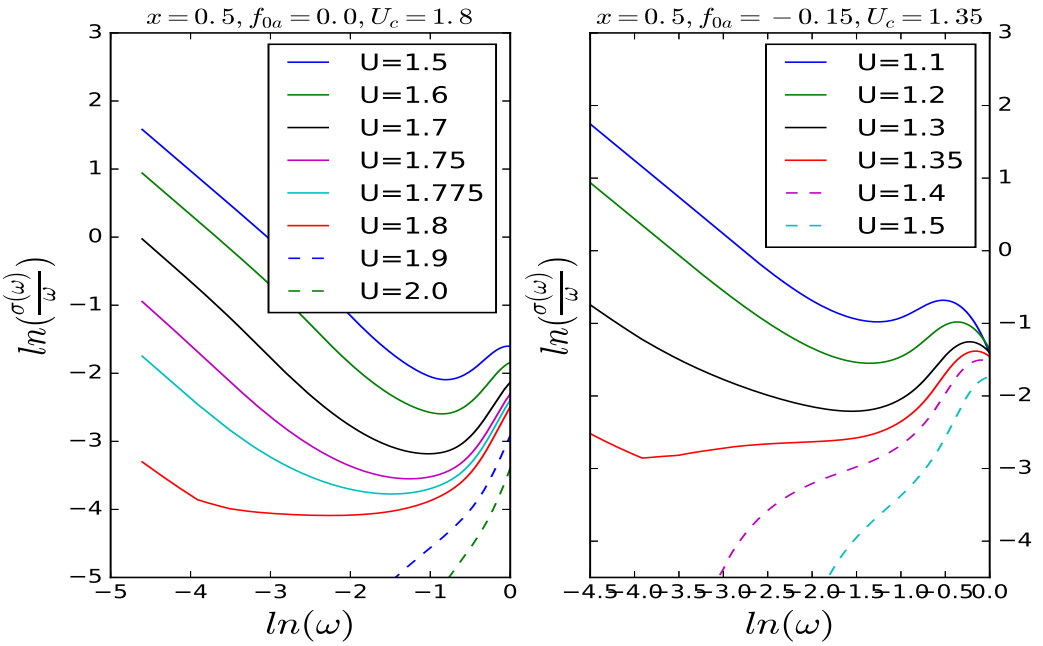

Figure 9.4: (a) In left panel, dielectric loss $log(\sigma(\omega)/\omega)$ vs $log(\omega)$ for different disorder strengths (U) with short range order $f_{0\alpha}$=0.0 (b) In right panel, dielectric loss $log(\sigma(\omega)/\omega)$ vs $log(\omega)$ for different disorder strengths (U) with short range order $f_{0\alpha}$=-0.15

in good qualitative accord with data when I compare our results with Figures(1),(2) and (3) of Lunkenheimer *et al.* [72]. Finally, in Fig. 9.4(b), I also show that short-range spatial correlations do not qualitatively modify these conclusions, attesting to their robustness against finite short-range order.

This accord is quite remarkable, and begs a microscopic clarification in terms of basic electronic processes at work near the MIT. It was conjectured that the similarities in responses of electronic systems with those of canonical glass formers suggests that the apparent universality is linked to glassy dynamics as a common underlying element. Interestingly, thanks to the mapping between the FKM and the binary-alloy Anderson model, this possibility arises in the FKM near the MIT due to the following reasons: (*i*) from our previous *dc* transport study [46], I find $z = 1$ and $\nu = 4/3$. The latter is characteristic of percolative transport that naturally arises in glassy systems. (*ii*) More importantly, it has also been shown [92] (for the Anderson disorder problem) that electronic glassy behavior *precedes* an insulating phase. Given the formal equivalence between the FKM and

the binary-alloy disorder problem, their arguments are also fully valid for the FKM. An analysis literally similar to that of Dobrosavljevic *et al.* can thus also be carried out for the FKM, whence I also expect an *intrinsic* electronic glassy phase near the continuous MIT. Thus, these arguments now pin the novel universal dielectric responses I observe to the onset of an electronic glassy dynamics near the continuous MIT in the FKM. It also rationalizes the finding [72] of very similar dielectric responses in a wide variety of disordered matter in a natural way by positing that glassy dynamics is the basic factor at work across widely different classes of disordered systems.

Theoretically, it is very interesting that such features appear near a correlation-driven MIT in the FKM, since this is a band-splitting type Mott (rather than pure Anderson localization) transition. It supports views [28, 46] that the (binary-alloy) disorder problem at strong coupling (with $k_F l \simeq O(1)$) is characterized by a different "Mott"-like quantum criticality as made manifest by the finding that $\beta(g) \simeq \ln(g)$ even deep in the (bad) metallic phase. This is reasonable, as it is long known [125] that the coherent potential approximation (CPA), the best mean-field theory for the Anderson disorder problem, is equivalent to the Hubbard III band-splitting view of the Mott transition (the latter becomes exact for the FKM in $d = \infty$ [124]). Various aspects of manganite physics have also been successfully modeled by an effective FKM, where the c-fermions represent effectively spinless fermions strongly scattered by a disordered "liquid" of effectively localized Jahn-Teller polarons [97]. Thus, our model can serve as a simplest effective model for PCSMO [72]. Application to $LaTiO_3$ would require using a full Hubbard model very close to half-filling, where even modest disorder would generally be expected to be relevant. Aside from material specificities, I believe that non-perturbative aspects related to strong intrinsic disorder scattering in the FKM lead to onset of strongly correlated glassy dynamics near the MIT. I find that it is this specific aspect that is at the heart of the "universal" dielectric response.

9.4 Summary

To summarise, I have shown the optical conductivity and dielectric response of the FKM using our newly developed CDMFT technique and made some critical analysis about universal dielectric response of materials with different types of disorder. This work is in progress. I hope I will provide this work completely at the time of final thesis submission.

Chapter 10

Conclusion and Future Directions

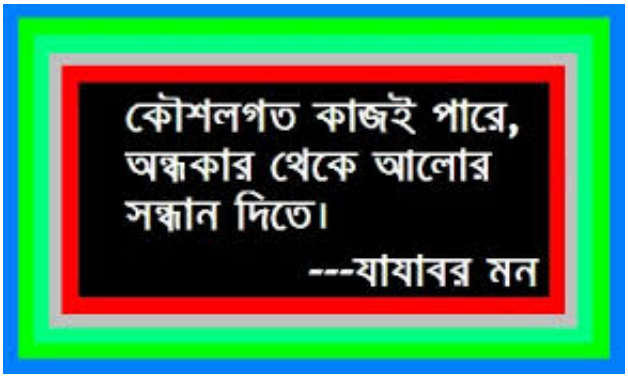

In this chapter, I give some concluding remarks of my thesis. I also discuss future directions and open issues.

In this thesis, I have made a detailed study of the simplified interacting model, "Falicov-Kimball Model (FKM)" which is also isomorphic to binary disorder alloy. I have solved this model using a novel and almost analytic cluster scheme (Cluster DMFT). This model showed continuous metal-insulator transitions (MITs), which are rare and are characteristic of disordered systems. Using both DMFT and Cluster DMFT technique I have surveyed metallic and insulating phases of this model and have investigated how the single particle and two-particle response function behave near the MIT. Surprisingly, I have found the irreducible two particle vertex exhibits clear non-analyticities

before the transition. After that, I have enquired the frequency dependent charge susceptibility in this model and using time-dependent response to a sudden local quench as a diagnostic, I have found that the long-time wave-function overlap changes from a power-law to an anomalous form at strong coupling.

Falicov-Kimball Model or equivalent binary disorder model shows continuous metal-insulator transition at zero temperature. This intrigated me to inquire about, and study quantum criticality associated with continuous MITs. Using our recently developed exact-to-order 1/D cluster-DMFT technique, I have presented an exact description of the quantum criticality across the metal-insulator transition (MIT) for the FKM. I have showed dc resistivity exhibits striking features of quantum criticality with clear mirror symmetry between metallic and insulating branch of the scaled resistivity driven by unusual form of the beta-function (or Gell-Mann-Low function in field theory) of the form $\beta(g) \sim log(g)$, with g is a scaled conductance. I have also studied magnetotransport and the issue of Mott quantum criticality reflected in magneto-transport across the continuous MIT, which has long been an interesting issue in the literature. I have tested my theoretically determined quantum critical exponents with the experimentally determined (on Nb vacancies disorder NbN) critical exponents. I have explicitly showed that like dc resistivity, hall conductivity and thermal transport coefficients also showed quantum critical behaviour close to the MIT but with different with critical exponents. This gave us the idea of two relaxation time in spinfull FKM with Hubbard like interaction [14]. At the end, I have studied the optical conductivity and dielectric response in this model using CDMFT technique. I have found that the model shows "Universal Dielectric Response" (UDR), followed by a super-linear power-law increase in their optical responses over exceptionally broad frequency regimes as experiment predicted.

10.1 Future Work

Our finding demonstrate the Mott-like metal-insulator transition (MIT) in binary disorder alloy which is known as disorder induced MIT. The semi-analytical cluster schemes discussed here can be used as an advanced approximation along with CPA for disordered binary alloys in the context of ab-initio electronic structure calculations for disordered systems. It could be more interesting if one can apply this technique to real 2D/3D systems like topological insulator, Weyl semimetal etc to explore the effect of disorder. Entropy is an important quantity to study classical (Landau) phase transition. So one can also study the entropy in the FKM and show how it behaves across or near the MIT.

Hubbard model showed MIT of the first order (discontinuous) induced by strong electron-electron interactions. Recent studies showed the quantum criticality ("hidden") in Hubbard model across the MIT. Therefore, one can survey the quantum criticality in a system which treats both strong electron-electron interactions and disorder on equal footing. There are many works of such studies using CPA+DMFT technique where they used self-consistently perturbation theory (Iterated Perturbation Theory) to take into account e-e interactions. But the Iterated Perturbation Theory (IPT) is best applicable for single-site DMFT. It is very complicated to formulate perturbation theory within cluster DMFT. The best possible way is to map the Hamiltonian to a multi-orbital (like bonding and antibonding orbital for two sites cluster) model and then solve the Hamiltonian using multi-orbital IPT+DMFT. Another possible impurity solver is the Continuous Time Quantum Monte Carlo (CT-QMC) which is very good in case of cluster DMFT and it is numerically exact upto some statistical error (monte carlo error). But the problem with this technique is that it provides single-particle propagators on Matsubara frequency (finite temperature). So to find the spectral function, one needs to use the Analytic continuation technique which is very poor. The most widely used method to study disorder and interaction is the Typical Medium Theory [26].

Appendix A

Technique of Equation of Motion for Calculating Green Function

Here, I will discuss in details the Equation of Motion technique [13] for fermions in both zero and non-zero temperature. The technique is used in this thesis to calculate the Green function of the impurity solver while applying DMFT (both single-site and cluster) to Falicov-Kimball Model.

A.1 Equation of motion for fermions at T = 0 (real time)

The real time retarded Green's function is defined as:

$$\begin{aligned} \langle \hat{A}(t); \hat{B}(t') \rangle &\equiv -i\theta(t-t')\langle [\hat{A}(t), \hat{B}(t')]_+ \rangle \\ &= G^{AB}(t-t') \end{aligned} \tag{A.1}$$

Let us assume that $t' = 0$, then I can write:

$$\begin{aligned} \langle \hat{A}(t); \hat{B} \rangle &= -i\theta(t)\langle [\hat{A}(t), \hat{B}]_+ \rangle \\ &= G^{AB}(t) \end{aligned} \tag{A.2}$$

Now,

$$\begin{aligned} \frac{dG^{AB}(t)}{dt} &= -i\frac{d\theta(t)}{dt}\langle [\hat{A}(t), \hat{B}]_+ \rangle - i\theta(t)\frac{d}{dt}\langle [\hat{A}(t), \hat{B}]_+ \rangle \\ &= -i\delta(t)\langle [\hat{A}(t), \hat{B}]_+ \rangle - i\theta(t)\langle \frac{d\hat{A}(t)}{dt}\hat{B} + \hat{B}\frac{d\hat{A}(t)}{dt} \rangle \\ &= -i\delta(t)\langle [\hat{A}(t), \hat{B}]_+ \rangle + \theta(t)\langle [\hat{H}, \hat{A}(t)]\hat{B} + \hat{B}[\hat{H}, \hat{A}(t)] \rangle \end{aligned} \tag{A.3}$$

In last line I used Heisenberg Equation of Motion:

$$\boxed{\frac{d\hat{X}}{dt} = \frac{i}{\hbar}[\hat{H}, \hat{A}(t)]}$$

with $\hbar = 1$.

$$\begin{aligned} \frac{dG^{AB}(t)}{dt} &= -i\delta(t)\langle [\hat{A}(t), \hat{B}]_+ \rangle + \theta(t)\langle [[\hat{H}, \hat{A}(t)], \hat{B}]_+ \rangle \\ &= -i\delta(t)\langle [\hat{A}(t), \hat{B}]_+ \rangle - i(-i\theta(t)\langle [[\hat{A}(t), \hat{H}], \hat{B}]_+ \rangle) \\ &= -i\delta(t)\langle [\hat{A}(t), \hat{B}]_+ \rangle - i\langle [\hat{A}(t), \hat{H}]; \hat{B} \rangle \end{aligned} \tag{A.4}$$

Now by Fourier transform of Equ. A.4 into $\omega^+ \equiv +i\eta; \eta \to 0 - space$, I get:

$$\begin{aligned} -i\omega \int dt e^{i(\omega+i\eta)t}\frac{d}{dt}\langle \hat{A}(t); \hat{B} \rangle &= -i\int dt e^{i\omega^+ t}\delta(t)\langle [\hat{A}(t), \hat{B}]_+ \rangle \\ &- i\int dt e^{i\omega^+ t}\langle \hat{A}(t), \hat{H}]; \hat{B} \rangle \end{aligned} \tag{A.5}$$

$$\Rightarrow -i\omega \int dt \langle \hat{A}; \hat{B} \rangle_{\omega^+} = -i\langle [\hat{A}, \hat{B}]_+ \rangle - i\langle [\hat{A}, \hat{H}]; \hat{B} \rangle \tag{A.6}$$

Here I have used,

$$\begin{aligned} \int dt e^{i(\omega+i\eta)t} \langle \hat{A}(t); \hat{B} \rangle &= \frac{e^{i\omega t - \eta t}}{i\omega} \langle \hat{A}(t); \hat{B} \rangle |_{t=-\infty}^{t=\infty} - \int dt \frac{e^{i\omega t}}{i\omega} \frac{d}{dt} \langle \hat{A}(t); \hat{B} \rangle \\ &= -\int dt \frac{e^{i\omega t}}{i\omega} \frac{d}{dt} \langle \hat{A}(t); \hat{B} \rangle \end{aligned} \tag{A.7}$$

The first term vanishes as the upper limit $t \to \infty$, the $e^{-\eta t} \to 0$ and the $\theta(t)$ discards the lower limit $t \to -\infty$. Hence the final expression for the Fermion in frequency space at zero temperature is given as:

$$\boxed{\omega \langle \hat{A}; \hat{B} \rangle_\omega = \langle [\hat{A}, \hat{B}]_+ \rangle + \langle [\hat{A}, \hat{H}]; \hat{B} \rangle_\omega} \tag{A.8}$$

A.2 Equation of motion for fermions at T ≠ 0 (imaginary time)

I will now formulate the equation of motion for fermions at finite temperature. The imaginary time Green function is defined as:

$$\begin{aligned} \langle \hat{A}(\tau); \hat{B}(\tau') \rangle &\equiv -\theta(\tau - \tau') \langle [\hat{A}(\tau), \hat{B}(\tau')]_+ \rangle \\ &= G^{AB}(\tau - \tau') \end{aligned} \tag{A.9}$$

Let us assume that $\tau' = 0$, then I can write:

$$\begin{aligned} \langle \hat{A}(\tau); \hat{B} \rangle &= -\theta(\tau) \langle [\hat{A}(\tau), \hat{B}]_+ \rangle \\ &= G^{AB}(\tau) \end{aligned} \tag{A.10}$$

Now, the imaginary time evolution for the Heisenberg operator can be written as,

$$\hat{O}(\tau) = e^{\frac{\hat{K}\tau}{\hbar}} \hat{O}(0) e^{\frac{-\hat{K}\tau}{\hbar}} \tag{A.11}$$

where, $\hat{K}$ is the grand canonical Hamiltonian of the system,

$$\hat{K} = \hat{H} - \mu \hat{N} \tag{A.12}$$

Then the equation of motion corresponding to $\hat{O}(\tau)$ as,

$$\frac{d\hat{O}(\tau)}{d\tau} = \frac{1}{\hbar} [\hat{K}, \hat{O}(\tau)] \tag{A.13}$$

As before for simplicity I considered, $\hbar = 1$. I have,

$$\begin{aligned}
\frac{dG^{AB}(\tau)}{d\tau} &= -\frac{d\theta(\tau)}{d\tau}\langle[\hat{A}(\tau),\hat{B}]_+\rangle - \theta(\tau)\frac{d}{d\tau}\langle[\hat{A}(\tau),\hat{B}]_+\rangle \\
&= -\delta(\tau)\langle[\hat{A}(\tau),\hat{B}]_+\rangle - \theta(\tau)\langle\frac{d\hat{A}(\tau)}{d\tau}\hat{B} + \hat{B}\frac{d\hat{A}(\tau)}{d\tau}\rangle \\
&= -\delta(\tau)\langle[\hat{A}(\tau),\hat{B}]_+\rangle + \theta(\tau)\langle[\hat{K},\hat{A}(\tau)]\hat{B} + \hat{B}[\hat{K},\hat{A}(\tau)]\rangle \\
&= -\delta(\tau)\langle[\hat{A}(\tau),\hat{B}]_+\rangle + \theta(\tau)\langle[[\hat{K},\hat{A}(\tau)],\hat{B}]_+\rangle \\
&= -\delta(\tau)\langle[\hat{A}(\tau),\hat{B}]_+\rangle - (-\theta(\tau)\langle[[\hat{A}(\tau),\hat{K}],\hat{B}]_+\rangle) \\
&= -\delta(\tau)\langle[\hat{A}(\tau),\hat{B}]_+\rangle - \langle[\hat{A}(\tau),\hat{K}];\hat{B}\rangle
\end{aligned} \tag{A.14}$$

Now, in term of Matsubara frequency, $\omega_n = \frac{2n\pi}{\beta}$ for fermions. Using the above equation I have,

$$\begin{aligned}
\int_0^\beta d\tau e^{i\omega_n\tau}\frac{d}{d\tau}\langle\hat{A}(\tau);\hat{B}\rangle &= \int_0^\beta d\tau e^{i\omega_n\tau}\delta(\tau)\langle[\hat{A}(\tau),\hat{B}]_+\rangle \\
&- \int_0^\beta d\tau e^{i\omega_n\tau}\langle\hat{A}(\tau),\hat{K}];\hat{B}\rangle
\end{aligned} \tag{A.15}$$

$$\Rightarrow -i\omega_n\langle\hat{A};\hat{B}\rangle_{\omega_n} = \langle[\hat{A},\hat{B}]_+\rangle - \langle[\hat{A},\hat{K}];\hat{B}\rangle \tag{A.16}$$

Here, I have used,

$$\int_0^\beta d\tau e^{i\omega_n\tau}\langle\hat{A}(\tau);\hat{B}\rangle = \frac{e^{i\omega_n\tau}}{i\omega_n}\langle\hat{A}(\tau);\hat{B}\rangle\,|_{\tau=0}^{\tau=\beta} - \int d\tau\frac{e^{i\omega_n\tau}}{i\omega_n}\frac{d}{d\tau}\langle\hat{A}(\tau);\hat{B}\rangle \tag{A.17}$$

Now,

$$\begin{aligned}
e^{i\omega_n\tau}\langle\hat{A}(\tau);\hat{B}\rangle\,|_{\tau=0}^{\tau=\beta} &= e^{i\omega_n\beta}\langle\hat{A}(\beta);\hat{B}\rangle - \langle\hat{A};\hat{B}\rangle \\
&= 0
\end{aligned} \tag{A.18}$$

Thus,

$$\int_0^\beta d\tau e^{i\omega_n\tau}\langle\hat{A}(\tau);\hat{B}\rangle = -\int d\tau \frac{e^{i\omega_n\tau}}{i\omega_n}\frac{d}{d\tau}\langle\hat{A}(\tau);\hat{B}\rangle \tag{A.19}$$

and finally,

$$\boxed{-i\omega_n\langle\hat{A};\hat{B}\rangle_{\omega_n} = \langle[\hat{A},\hat{B}]_+\rangle - \langle[\hat{A},\hat{K}];\hat{B}\rangle} \tag{A.20}$$

This is the equation of motion formalism for fermions in Matsubara frequency (or finite temperature).

Appendix B

Derivation of Bethe-Salpeter Equation

The generating function [107] with source field ϕ_σ in the grand canonical ensemble is given as,

$$lnZ[\phi] = lnTr[e^{-\beta(\hat{H}-\mu\hat{N})}T_\tau(e^{-\psi^\dagger_{\bar{\sigma}}(\bar{1})\phi_{\bar{\sigma}}(\bar{1},\bar{2})\psi_{\bar{\sigma}}(\bar{2})})] \tag{B.1}$$

Where, $\psi^\dagger_{\bar{\sigma}}(\bar{1})$ is the creation operator at position and imaginary time $(\mathbf{r_1}, \tau_1)$ and $\psi_{\bar{\sigma}}(\bar{2})$ is the anhilliation operator at position and imaginary time $(\mathbf{r_2}, \tau_2)$. Now, the Green function in the presence of ϕ_σ is:

$$G_\sigma(1,2;\phi) = -\langle\psi_\sigma(1);\psi^\dagger_\sigma(2)\rangle_\phi = -\frac{\delta lnZ[\phi]}{\delta\phi_\sigma(2,1)} \tag{B.2}$$

The physical correlation function is obtained in the limit of $\{\phi\} = 0$. In the usual practice ϕ is kept finite in the intermediate steps of the calculation and at the end put $\{\phi\} = 0$. Now, using the Dyson's equation one obtains the self-energy in the presence of the source field ϕ as,

$$\begin{aligned}(G_0^{-1} - \phi)G &= 1 + \Sigma G;\\ G^{-1} &= G_0^{-1} - \phi - \Sigma\end{aligned} \tag{B.3}$$

Now, the two-particle response function (four-point) can be obtained from the function (Π) single-particle (two-point) propagator given as,

$$\begin{aligned}\Pi(1,2,3,4;\{\phi\}) &= -\langle\psi_\sigma(1)\psi^\dagger_\sigma(2);\psi_\sigma(3)\psi^\dagger_\sigma(4)\rangle_\phi \\ &= \frac{\delta G(1,2;\phi)}{\delta\phi(4,3)}\Big|_{\{\phi\}=0} = -\frac{\delta^2 lnZ[\phi]}{\delta\phi(4,3)\delta\phi(2,1)}\Big|_{\{\phi\}=0}\end{aligned} \tag{B.4}$$

Now, using the matrix notation one can use the propagator G as,

$$GG^{-1} = 1 \tag{B.5}$$

Differentiating with respect to the source field ϕ, I find,

$$\frac{\delta G}{\delta\phi}G^{-1} + G\frac{\delta G^{-1}}{\delta\phi} = 0 \tag{B.6}$$

Using Dyson's equation $G^{-1} = G_0^{-1} - \phi - \Sigma$, I can write as,

$$\frac{\delta G}{\delta\phi} = -G\frac{\delta G^{-1}}{\delta\phi}G = G.G + G\frac{\delta\Sigma}{\delta\phi}G \tag{B.7}$$

Using chain rule one can have, $\frac{\delta\Sigma}{\delta\phi} = \frac{\delta\Sigma}{\delta G}\frac{\delta G}{\delta\phi}$. Substituting this into the equation B.7 I have,

$$\frac{\delta G}{\delta\phi} = G.G + G\Big[\frac{\delta\Sigma}{\delta G}\frac{\delta G}{\delta\phi}\Big]G \tag{B.8}$$

If I rearrange slightly I have,

$$\frac{\delta G}{\delta\phi} = G.G + GG\Big[\frac{\delta\Sigma}{\delta G}\frac{\delta G}{\delta\phi}\Big] \tag{B.9}$$

Now, the interacting two particle function $\Pi = \frac{\delta G}{\delta\phi}$ and the non-interacting two particle function $\Pi_0 = G.G$. The two-particle irreducible particle-hole vertex function is defined as:

$$\Gamma = \frac{\delta\Sigma}{\delta G} \tag{B.10}$$

So using equation B.9 one can write the two-particle function analogous to the Dyson-like equation for single-particle function, given of the form:

$$\boxed{\Pi = \Pi_0 + \Pi_0 \Gamma \Pi} \tag{B.11}$$

This equation is known as Bethe-Salpeter Equation (BSE) which is used to calculate the two-particle response function.

Appendix C

Response to a Sudden Local Quench (Loschmidt Echo)

Here, I will show in details the many-electron response on the core hole due to the switching on a sudden local potential [73] (known as Loschmidt echo). The Green function of the core-hole is given as,

$$G_h(t) = -i\langle T d(t) d^\dagger(0)\rangle \tag{C.1}$$

where $d^\dagger$, d are the creation and annihilation operator of the core-hole, respectively. The very useful way to study the core-hole spectrum is by the linked cluster expansion. The Loschmidt echo is given as,

$$\rho(t) = \langle T exp[-i\int_0^t dt_1 V(t_1)]\rangle = exp[\sum_{l=1}^{\infty} F_l(t)] \tag{C.2}$$

$$F_l(t) = \frac{(-1)^l}{l}\int_0^t dt_1 ... \int_0^t \langle T V(t_1)...V(t_1)\rangle_{connected} \tag{C.3}$$

The first term $F_1(t)$ is linear in t and is a self energy term given as,

$$F_1(t) = -i\int_0^t dt_1 \langle V(t_1)\rangle = \frac{-it}{\mathcal{N}}\sum_k V(\mathbf{k},\mathbf{k}) n_F(\epsilon(\mathbf{k})) \tag{C.4}$$

The exact self-energy of the core-hole is of the form:

$$E_i = -\frac{2\hbar^2}{m}\sum_l (2l+1)\int_0^{k_F} kdk\delta_l(k) \tag{C.5}$$

The factor $V(\mathbf{k},\mathbf{k})$ is the first term in an expansion which should give Fumi's result E_i when all terms are summed. The second term $F_2(t)$ is given as:

$$\begin{aligned} F_2(t) &= \frac{(-i)^2}{2}\int_0^t dt_1\int_0^t dt_2\langle|T_t V(t_1)V(t_2)|\rangle \\ &= \frac{(-i)^2}{2\mathcal{N}^2}\int_0^t dt_1\int_0^t dt_2\sum_{\boldsymbol{k}_1\boldsymbol{k}_2\sigma}\sum_{\boldsymbol{k}_3\boldsymbol{k}_4\sigma'} V(\boldsymbol{k}_1,\boldsymbol{k}_2)V(\boldsymbol{k}_3,\boldsymbol{k}_4) \\ &\times \langle T_t C^\dagger_{\boldsymbol{k}_1\sigma}(t_1)C_{\boldsymbol{k}_2\sigma}(t_1)C^\dagger_{\boldsymbol{k}_3\sigma'}(t_2)C_{\boldsymbol{k}_4\sigma'}(t_2)\rangle \end{aligned} \tag{C.6}$$

Evaluating the time integrals directly I have,

$$\begin{aligned} F_2(t) &= \frac{(-i)^2}{2\mathcal{N}^2}\int_0^t dt_1\int_0^t dt_2\sum_{\boldsymbol{k}_1\boldsymbol{k}_2\sigma} V(\boldsymbol{k}_1,\boldsymbol{k}_2)V(\boldsymbol{k}_2,\boldsymbol{k}_1) \\ &\times G(\boldsymbol{k}_1,t_1-t_2)G(\boldsymbol{k}_2,t_1-t_1) \\ &= \frac{(-i)^2}{2\mathcal{N}^2}\int_0^t dt_1\int_0^t dt_2\sum_{\boldsymbol{k}_1\boldsymbol{k}_2\sigma}|V(\boldsymbol{k}_1,\boldsymbol{k}_2)|^2 e^{i(t_1-t_2)(\epsilon_2-\epsilon_1)} \\ &\times [\Theta(t_1-t_2)-n_1][\Theta(t_2-t_1)-n_2] \end{aligned} \tag{C.7}$$

Hence,

$$F_2(t) = \frac{1}{\mathcal{N}^2}\sum_{\boldsymbol{k}_1\boldsymbol{k}_2\sigma}|V(\boldsymbol{k}_1,\boldsymbol{k}_2)|^2\Big[\frac{itn_1}{\epsilon_1-\epsilon_2}-\frac{n_1(1-n_2)}{(\epsilon_1-\epsilon_2)^2}(1-e^{it(\epsilon_1-\epsilon_2)})\Big] \tag{C.8}$$

The factor $\frac{1}{2}$ in front vanished, because each term in the final result appear twice. The first term is linear in t, is dropped as it only contributes to the self-energy. So, with the remaining term the expression for the $F_2(t)$ is:

$$F_2(t) = -\frac{2}{N^2}\sum_{\boldsymbol{k}_1\boldsymbol{k}_2}|V(\boldsymbol{k}_1,\boldsymbol{k}_2)|^2\frac{n_F(\epsilon_{\boldsymbol{k}_1})[1-n_F(\epsilon_{\boldsymbol{k}_2})]}{(\epsilon_1-\epsilon_2)^2}(1-e^{it(\epsilon_{\boldsymbol{k}_1}-\epsilon_{\boldsymbol{k}_2})}) \tag{C.9}$$

Re-write this with the assumption that the hole potential $V(\mathbf{k}, \mathbf{k}')$ only depends on the difference of its momentum $V(\mathbf{k} - \mathbf{k}')$ and with the changing variable $\mathbf{k}_1 = \mathbf{k}_2 + \mathbf{q}$ I have the second order contribution of the diagram is:

$$F(t) = \int_{-\infty}^{\infty} \frac{g(\omega)}{\omega^2}(e^{-i\omega t} - 1)d\omega \tag{C.10}$$

We take $g(\omega)$ to be of the form,

$$g(\omega) = 2V_0^2\omega^\alpha\theta(\omega)\theta(\xi - \omega) \qquad \text{where, } \alpha < 1$$

Inserting $g(\omega)$ into equation(1) we have,

$$F(t) = 2V_0^2 \int_0^{\xi} \frac{1}{\omega^{2-\alpha}}(e^{-i\omega t} - 1)d\omega \tag{C.11}$$

For t small ($t \ll \frac{1}{\xi}$),
we can expand the exponential to first order as $\omega t < 1$, then from equation(2) we have,

$$\begin{aligned} F(t) &= 2V_0^2 \int_0^{\xi} \frac{-i\omega t}{\omega^{2-\alpha}} d\omega \\ &= -\frac{2V_0^2 it}{\alpha}\omega^\alpha|_0^\xi \\ &= -\frac{2V_0^2 it\xi^\alpha}{\alpha} \end{aligned} \tag{C.12}$$

For large t ($t >> \frac{1}{\xi}$),
For that $\omega t > 1$, hence the exponential term will oscillate quickly and we can qualitatively ignore that term. Then the integration is not valid at $\omega = 0$. So we use a lower cut-off to avoid the divergence at $\omega = 0$. Hence we have,

$$\begin{aligned} F(t) &\approx -2V_0^2 \int_{\frac{1}{t}}^{\xi} \frac{d\omega}{\omega^{2-\alpha}} \\ &= \frac{2V_0^2}{(1-\alpha)}[\xi^{\alpha-1} - t^{1-\alpha}] \\ &\approx -\frac{2V_0^2}{(1-\alpha)}t^{1-\alpha} \end{aligned} \tag{C.13}$$

Now, the Loschmidt echo $\rho(t)$ is define by,

$$\rho(t) = e^{-i\epsilon_h t} exp[F(t)] \tag{C.14}$$

Putting the value of F(t) for large t limit we have,

$$\begin{aligned} \rho(t) &= e^{-i\epsilon_h t} exp[-\frac{2V_0^2 t^{1-\alpha}}{1-\alpha}] \\ &\approx exp[-\frac{2V_0^2 t^{1-\alpha}}{1-\alpha}] \end{aligned} \tag{C.15}$$

Hence, at $t \to \infty, \rho(t)$ vanishes exponentially which is the signature of many body localized states. Now, the hole spectrum is given by,

$$S(\nu) = \frac{1}{2\pi} \int_{-\infty}^{\infty} dt e^{i\nu t} exp[F(t)] \tag{C.16}$$

So for $t \to \infty$ i.e. for $\nu \to 0$ the hole spectrum is given by,

$$S(\nu) = \frac{1}{2\pi} \int_{-\infty}^{\infty} dt e^{i\nu t} exp[-\frac{2V_0^2 t^{1-\alpha}}{1-\alpha}] \tag{C.17}$$

Now for Fermi liquid metallic case,

$$g(\omega) = 2V_0^2 \omega \theta(\omega) \theta(\xi - \omega)$$

For large t ($t >> \frac{1}{\xi}$),

$$F(t) \approx -2V_0^2 log(\xi t) \qquad\qquad t \gg \frac{1}{\xi} \tag{C.18}$$

Now, the Loschmidt echo $\rho(t)$ for $t \to \infty$ is define by,

$$\rho(t) = e^{-i\epsilon_h t} (\xi t)^{-2V_0^2} \tag{C.19}$$

Which vanishes at large t in power law.

Appendix D

Linear Response Theory

D.1 General Kubo Formula

Linear Response Theory states that the response to a weak external perturbation is proportional to the perturbation, and therefore all one needs to understand is the proportionality constant.

Among the numerous applications of the linear response formula, one can mention charge and spin susceptibilities of e.g. electron systems due to external electric or magnetic fields.

Consider a quantum system described by the (time independent) Hamiltonian H_0.Then expectation value of a physical quantity, described by the operator A, can be evaluated as,

$$\langle A \rangle = \frac{1}{Z_0} Tr[\rho_0 A] = \frac{1}{Z_0} \sum_n \langle n \mid A \mid n \rangle e^{-\beta E_n} \tag{D.1}$$

where, ρ_0 is the density operator given by,

$$\rho_0 = e^{-\beta H_0} = \sum_n \mid n \rangle \langle n \mid e^{-\beta E_n} \tag{D.2}$$

and $Z_0 = Tr[\rho_0]$ is the partition function, $\{\mid n\rangle\}$ is the complete sets of eigenstates corresponds to the unperturbed Hamiltonian H_0.

Suppose now that at some time, $t = t_0$, an external perturbation is applied to the system, driving it out of equilibrium.Then Hamiltonian is,

$$H(t) = H_0 + H'(t)\theta(t - t_0) \tag{D.3}$$

$\{\mid n(t)\rangle\}$ is the complete sets of eigenstates corresponds to the Hamiltonian $H(t)$.

$$\langle A(t)\rangle = \frac{1}{Z_0} Tr[\rho(t)A] = \frac{1}{Z_0} \sum_n \langle n(t) \mid A \mid n(t)\rangle e^{-\beta E_n} \tag{D.4}$$

$$\rho(t) = \sum_n \mid n(t)\rangle\langle n(t) \mid e^{-\beta E_n} \tag{D.5}$$

The time dependence of the states $\mid n(t)\rangle$ is of course governed by the Schrödinger equation,

$$i\partial_t \mid n(t)\rangle = H(t) \mid n(t)\rangle \tag{D.6}$$

Since $H'(t)$ is to be regarded as a small perturbation, it is convenient to utilize the interaction picture representation $\mid n_I(t)\rangle$. Then,

$$\mid n(t)\rangle = e^{-iH_0 t} \mid n_I(t)\rangle = e^{-iH_0 t}\hat{U}(t, t_0) \mid n_I(t_0)\rangle \tag{D.7}$$

where by definition, $\mid n_I(t_0)\rangle = e^{iH_0 t_0} \mid n(t_0)\rangle =\mid n\rangle$

To linear order in $H'(t)$, $\hat{U}(t, t_0) = 1 - i\int_{t_0}^{t} dt' H'(t)$.Inserting these into equation(4) I have,

$$\begin{aligned}
\langle A(t)\rangle &= \langle A\rangle_0 - i\int_{t_0}^{t} dt' \frac{1}{Z_0} \sum_n e^{-\beta E_n} \langle n(t_0) \mid \hat{A}(t)\hat{H}'(t) - \hat{H}'(t)\hat{A}(t) \mid n(t_0)\rangle \\
&= \langle A\rangle_0 - i\int_{t_0}^{t} dt' \langle [\hat{A}(t), \hat{H}'(t')]\rangle_0
\end{aligned}$$

Then,

$$\boxed{\delta\langle A(t)\rangle = \langle A(t)\rangle - \langle A\rangle_0 = int_{t_0}^{\infty} dt' C^R_{AH'}(t,t')e^{-\eta(t-t')}} \tag{D.8}$$

where,

$$\boxed{C^R_{AH'}(t,t')e^{-\eta(t-t')} = -i\theta(t-t')\langle[\hat{A}(t),\hat{H}'(t')]\rangle_0} \tag{D.9}$$

D.2 Kubo Formula for Conductivity

Consider a system of charged particles, electrons say, which is subjected to an external electromagnetic field. The electromagnetic field induces a current, and the conductivity is the linear response coefficient.

$$J^{\alpha}_e(\mathbf{r},t) = \int dt' \int dr' \sum_{\beta} \sigma^{\alpha\beta}(\mathbf{r}t,\mathbf{r}'t')E^{\beta}(\mathbf{r}',t') \tag{D.10}$$

Where, $\sigma^{\alpha\beta}(\mathbf{r}t,\mathbf{r}'t')$ is the conductivity tensor. The electric field $\mathbf{E}$ is given by,

$$\mathbf{E}(\mathbf{r},t) = -\Delta_r\phi_{ext}(\mathbf{r},t) - \partial_t\mathbf{A}(\mathbf{r},t) \tag{D.11}$$

The perturbing term in the Hamiltonian due to the external electromagnetic field is given by upto the linear order of the external potential,

$$H_{ext} = -e\int d\mathbf{r}\rho(\mathbf{r})\phi_{ext}(\mathbf{r},t) + e\int d\mathbf{r}\mathbf{J}(\mathbf{r}).\mathbf{A}(\mathbf{r},t) \tag{D.12}$$

Let $\mathbf{A}_0$ denote the vector potential in the equilibrium, i.e. prior to the onset of the perturbation $\mathbf{A}_{ext}$, and let $\mathbf{A}$ denote the total vector potential. Then I have,

$$\mathbf{A} = \mathbf{A}_0 + \mathbf{A}_{ext} \tag{D.13}$$

The current operator has two components the diamagnetic term and the paramagnetic

term:

$$\mathbf{J}(\mathbf{r}) = \mathbf{J}^{\Delta}(\mathbf{r}) + \frac{e}{m}\mathbf{A}(\mathbf{r})\rho(\mathbf{r}) \tag{D.14}$$

I choose gauge in such a way that the scalar external potential is zero i.e. $\phi_{ext} = 0$. Since, ∂_t becomes $-i\omega$ in the frequency domain I have, $\mathbf{A}_{ext}(\mathbf{r},\omega) = \frac{1}{i\omega}\mathbf{E}_{ext}(\mathbf{r},\omega)$, the external perturbation in frequency domain:

$$H_{ext}(\omega) = \frac{e}{i\omega}\int d\mathbf{r}\mathbf{J}(\mathbf{r}).\mathbf{E}_{ext}(\mathbf{r},\omega) \tag{D.15}$$

In frequency domain I have,

$$\mathbf{J}_e^{\alpha}(\mathbf{r},\omega) = \int d\mathbf{r}' \sum_{\beta} \sigma^{\alpha\beta}(\mathbf{r},\mathbf{r}',\omega)E^{\beta}(\mathbf{r}',\omega) \tag{D.16}$$

The total current is:

$$\begin{aligned} \mathbf{J} &= \mathbf{J}^{\Delta} + \frac{e}{m}(\mathbf{A}_0 + \mathbf{A}_{ext})\rho \\ \mathbf{J}_0 &= \mathbf{J}^{\Delta} + \frac{e}{m}\mathbf{A}_0\rho \end{aligned} \tag{D.17}$$

Since I am interested in the linear response , thus neglecting the term proportional to $\mathbf{E}_{ext}.\mathbf{A}_{ext}$ the perturbative Hamiltonian,

$$H_{ext}(\omega) = \frac{e}{i\omega}\int d\mathbf{r}\mathbf{J}_0(\mathbf{r}).\mathbf{E}_{ext}(\mathbf{r},\omega) \tag{D.18}$$

The expectation value of the current I write,

$$\langle\mathbf{J}(\mathbf{r},\omega)\rangle = \langle\mathbf{J}_0(\mathbf{r},\omega)\rangle + \langle\frac{e}{m}\mathbf{A}_{ext}(\mathbf{r},\omega)\rho(\mathbf{r})\rangle \tag{D.19}$$

For the last term in equation(20) I use that to linear order in $\mathbf{A}_{ext}$ the expectation value can

be evaluated in the equilibrium state,

$$\langle \frac{e}{m}\mathbf{A}_{ext}(\mathbf{r},\omega)\rangle \approx \frac{e}{m}\mathbf{A}_{ext}(\mathbf{r},\omega)\langle\rho(\mathbf{r})\rangle_0 = \frac{e}{i\omega m}\mathbf{E}_{ext}(\mathbf{r},\omega)\langle\rho(\mathbf{r})\rangle_0 \tag{D.20}$$

Thus the expectation value of current reads:

$$\langle \mathbf{J}(\mathbf{r},\omega)\rangle = \langle \mathbf{J}_0(\mathbf{r},\omega)\rangle + \frac{e}{m}\langle\rho(\mathbf{r})\rangle_0 \mathbf{A}_{ext}(\mathbf{r},\omega) \tag{D.21}$$

where first term is:

$$\langle \mathbf{J}_0(\mathbf{r},\omega)\rangle = \int d\mathbf{r}' \sum_\beta \mathbf{\Pi}^R(\omega)\frac{e}{i\omega}\mathbf{E}^\beta(\mathbf{r}',\omega) \tag{D.22}$$

Now, $\mathbf{J}_e = -e\langle\mathbf{J}\rangle$ Hence the final expression for the conductivity tensor is

$$\sigma^{\alpha\beta}(\mathbf{r},\mathbf{r}',\omega) = \frac{ie^2}{\omega}\mathbf{\Pi}^R_{\alpha\beta}(\mathbf{r},\mathbf{r}',\omega) + \frac{e^2 n(\mathbf{r})}{i\omega m}\delta(\mathbf{r}-\mathbf{r}')\delta_{\alpha\beta}, \tag{D.23}$$

In the time domain retarded current-current correlation function is given by,

$$\mathbf{\Pi}^R_{\alpha\beta}(\mathbf{r},\mathbf{r}',t-t') = -i\theta(t-t')\langle[\hat{J}^\alpha_0(\mathbf{r},t),\hat{J}^\beta_0(\mathbf{r}',t')]\rangle_0 \tag{D.24}$$

Appendix E

Calculation of Fermi Velocity ($\langle v^2 \rangle(\epsilon)$)in the Conductivity Expression

The expression for the optical conductivity as derived in the Chapter 7 is given in the limit $d \to 0$ as,

$$\sigma(\omega) = \sigma_0 \int_{-\infty}^{\infty} d\epsilon \tilde{\rho}(\epsilon) \int_{-\infty}^{\infty} d\nu A(\epsilon, \nu) A(\epsilon, \omega + \nu) \frac{f(\nu) - f(\omega + \nu)}{\omega} \tag{E.1}$$

where, $A(\epsilon, \omega)$ is the spectral function, $f(\omega)$ is the Fermi-function, $\sigma_0 = \frac{2\pi e^2}{\hbar^2} \frac{N}{V}$, and

$$\tilde{\rho}(\epsilon) := \frac{1}{N} \sum_k \mid \mathbf{v_k} \mid^2 \delta(\epsilon - \epsilon_{\mathbf{k}}) := \langle \mid \mathbf{v} \mid^2 \rangle(\epsilon) \rho(\epsilon) \tag{E.2}$$

where, $\rho(\epsilon)$ is the non-interacting density of state (DOS) is given as,

$$\rho(\epsilon) = \frac{1}{N} \sum_{\mathbf{k}} \delta(\epsilon - \epsilon_{\mathbf{k}}) \tag{E.3}$$

with $\epsilon_{\mathbf{k}}$ is the non-interacting dispersion relation. For hyper-cubic lattice it is given as, $\epsilon_{\mathbf{k}}^{hc} = -2t \sum_{\alpha=1}^{d} cos(k_\alpha)$ which for the proper scaling $t = t^* / \sqrt{2d}$ leads to a Gaussian DOS

for $d \to \infty$,

$$\rho^{hc}(\epsilon) = \frac{1}{\sqrt{2\pi}t^8} Exp[-\frac{\epsilon^2}{2t^{*2}}] \tag{E.4}$$

In the hyper-cubic lattice in $d \longrightarrow \infty$, the momentum dependence of the Fermi velocity $\mathbf{v_k}$ becomes irrelevant, for unit hopping (t) and unit lattice spacing one can show that, $\tilde{\rho}^{hc}(\epsilon) = \rho^{hc}(\epsilon)$.

Now, my aim is calculate the value of $\tilde{\rho}(\epsilon)$ or $\langle v^2 \rangle(\epsilon)$ for any arbitrary lattice structure (given DOS ($\rho(\epsilon)$)) using the DOS of hyper-cubic lattice ($\rho^{hc}(\epsilon)$) at $d \to \infty$ following the method developed in [16].

Let us start with the non-interacting Hamiltonian as,

$$H_0 = \sum_{i,\sigma} \sum_{\delta} t_\delta c^\dagger_{\mathbf{R}_i\sigma} c^\dagger_{\mathbf{R}_i+\delta,\sigma} = \sum_{\mathbf{k},\sigma} \epsilon(\mathbf{k}) n_{\mathbf{k},\sigma} \tag{E.5}$$

where, the hopping distance $\| \delta \| = \sum_{\alpha=1}^{d} \mid \delta_\alpha \mid$ is:

$$\epsilon(\mathbf{k}) = \sum_{D=1}^{\infty} \epsilon_D(\mathbf{k}), \tag{E.6}$$

with $\epsilon_D(\mathbf{k}) = \sum_{\|\delta\|=D} t_\delta e^{i\delta.\mathbf{k}}$ With some algebra one can derive the recursion relation for $\epsilon_D(\mathbf{k})$ as,

$$\epsilon(\mathbf{k}) = \sum_{D=1}^{\infty} \frac{t^*_D}{\sqrt{D!}} He_D(\epsilon^{hc}_k) =: \mathcal{F}(\epsilon^{hc}_{\mathbf{k}}) \tag{E.7}$$

Using the orthogonality of the Hermite polynomials, the hopping matrix elements can be expressed in terms of the transformation function $\mathcal{F}(x)$ as,

$$t^*_D = \frac{1}{\sqrt{2\pi D!}} \int_{-\infty}^{\infty} d\epsilon \mathcal{F}(\epsilon) He_{D(\epsilon)} e^{-\frac{\epsilon^2}{2}} \tag{E.8}$$

Specializing on the case of a monotonic transformation function $\mathcal{F}(x)$, one can write the $\rho(\epsilon)$ as,

$$\rho(\epsilon) = \frac{1}{\mathcal{F}'(\mathcal{F}^{-1}(\epsilon))} \rho^{hc}(\mathcal{F}^{-1}(\epsilon)) \tag{E.9}$$

Here, $\mathcal{F}'(x)$ is the derivative of $\mathcal{F}(x)$. From the above equation one can find,

$$\mathcal{F}^{-1}(\epsilon) = \sqrt{2} erf^{-1}(2 \int_{-\infty}^{\epsilon} d\epsilon' \rho(\epsilon') - 1). \tag{E.10}$$

Then, the Fermi-velocity $\mathbf{v_k} = \nabla \epsilon_{\mathbf{k}}$ can be computed as,

$$\mathbf{v_k} = \mathcal{F}'(\mathcal{F}^{-1}(\epsilon)) \mathbf{v_k}^{hc} = \frac{\rho^{hc}(\sqrt{2} erf^{-1}(2 \int_{-\infty}^{\epsilon} d\epsilon' \rho(\epsilon') - 1))}{\rho(\epsilon)} \mathbf{v_k}^{hc} \tag{E.11}$$

For practical used the general formalism proceed as follows:

1. calculate $\mathcal{F}^{-1}(\epsilon)$ from arbitrary DOS ($\rho(\epsilon)$) using Equation E.10.

2. Obtain $\mathcal{F}(x)$ by inverting the function $\mathcal{F}^{-1}(\epsilon)$.

3. Finally, calculate $\langle v^2 \rangle(\epsilon)$ or $\tilde{\rho}(\epsilon)$ using equation E.11 for the arbitrary DOS ($\rho(\epsilon)$).

Appendix F

Calculation of the transport coefficients: L_{11}, L_{12}, L_{21} and L_{22}

Transport properties are calculated using Kubo-Greenwood formalism. Here, I will give in details the calculation [38] of transport coefficients: $L_{11}, L_{12}, L_{21}, L_{22}$ for Falicov-Kimball Model (FKM). It is noted that the calculation of L_{11} have provided in detail in Chapter 7 and $L_{12} = L_{21}$. Therefore here I will present the calculations of L_{12} and L_{22} only using Freericks *et all.* [37].

The electron (particle) current operator is given as,

$$\mathbf{j} = \sum_{q\sigma} \mathbf{v}_q c^{\dagger}_{q\sigma} c_{q\sigma}, \tag{F.1}$$

where the velocity operator is $\mathbf{v}_q = \nabla_q \epsilon(q)$ and the Fourier transform of the creation operator is $c^{\dagger}_q = \sum_j \exp[iq \cdot \mathbf{R}_j] c^{\dagger}_j / \mathrm{N}$. The heat current operator is:

$$\begin{aligned} \mathbf{j}_Q &= \sum_{q\sigma} (\epsilon_q - \mu) \mathbf{v}_q c^{\dagger}_{q\sigma} c_{q\sigma} \\ &+ \frac{U}{2} \sum_{qq'\sigma} W(q - q')[\mathbf{v}_q + \mathbf{v}_{q'}] c^{\dagger}_{q\sigma} c_{q'\sigma}, \end{aligned} \tag{F.2}$$

where $W(q) = \sum_j \exp(-iq \cdot \mathbf{R}_j) w_j/N$. The heat current can be broken into two pieces: (i) first term is the kinetic-energy part $\mathbf{j}_Q^K$ and (ii) second term is the potential energy $\mathbf{j}_Q^P$.

Now, at zero frequency the Onsager coefficients are defined as,

$$\begin{aligned} L_{11} &= \lim_{\nu\to 0} \mathrm{Re} \frac{i}{\nu} \bar{L}_{11}(\nu), \\ \bar{L}_{11}(i\nu_l) &= \pi T \int_0^\beta d\tau e^{i\nu_l \tau} \langle T_\tau j_\alpha^\dagger(\tau) j_\beta(0) \rangle, \end{aligned} \tag{F.3}$$

where $\nu_l = 2\pi T l$ is the Bosonic Matsubara frequency, the τ-dependence of the operator is with respect to the full Hamiltonian. Similar definitions hold for the other coefficients:

$$\begin{aligned} L_{12} &= \lim_{\nu\to 0} \mathrm{Re} \frac{i}{\nu} \bar{L}_{12}(\nu), \\ \bar{L}_{12}(i\nu_l) &= \pi T \int_0^\beta d\tau e^{i\nu_l \tau} \langle T_\tau j_\alpha^\dagger(\tau) j_{Q\beta}(0) \rangle, \end{aligned} \tag{F.4}$$

and

$$\begin{aligned} L_{22} &= \lim_{\nu\to 0} \mathrm{Re} \frac{i}{\nu} \bar{L}_{22}(\nu), \\ \bar{L}_{22}(i\nu_l) &= \pi T \int_0^\beta d\tau e^{i\nu_l \tau} \langle T_\tau j_{Q\alpha}^\dagger(\tau) j_{Q\beta}(0) \rangle. \end{aligned} \tag{F.5}$$

In all of these equations, the subscripts α and β denote the respective spatial index of the current vectors.

One can divide the heat current into two pieces, one corresponding to the kinetic energy and one corresponding to the potential energy. This allows me to write $L_{12} = L_{12}^K + L_{12}^P$. The derivation for the kinetic energy piece follows exactly like the derivation for L_{11} except there is an extra factor of $\epsilon - \mu$ that appears. The integral over ϵ can then be performed straightforwardly producing

$$\begin{aligned} L_{12}^K = \lim_{\nu\to 0} \frac{T\sigma_0}{e^2} \delta_{\alpha\beta} \int_{-\infty}^{\infty} d\omega \frac{f(\omega) - f(\omega+\nu)}{\nu} \\ \times \quad \mathrm{Re}\Big\{ - \frac{[\omega - \Sigma(\omega)]G(\omega) - [\omega + \nu - \Sigma(\omega+\nu)]G(\omega+\nu)}{\nu + \Sigma(\omega) - \Sigma(\omega+\nu)} \end{aligned}$$

$$+ \quad \frac{[\omega - \Sigma^*(\omega)]G^*(\omega) - [\omega + \nu - \Sigma(\omega + \nu)]G(\omega + \nu)}{\nu + \Sigma^*(\omega) - \Sigma(\omega + \nu)}\Big\}. \tag{F.6}$$

Evaluating the limit $\nu \to 0$ is simple. The final result is

$$\begin{aligned} L_{12}^K &= \frac{T\sigma_0}{e^2}\int_{-\infty}^{\infty} d\omega \left(-\frac{df(\omega)}{d\omega}\right)\{[\omega - \mathrm{Re}\Sigma(\omega)]\tau(\omega) \\ &- 2\mathrm{Im}\Sigma(\omega)\mathrm{Im}[(\omega + \mu - \Sigma(\omega))G(\omega)]\}, \end{aligned} \tag{F.7}$$

with $\tau(\omega)$ defined as,

$$\tau(\omega) = \frac{\mathrm{Im}G(\omega)}{\mathrm{Im}\Sigma(\omega)} + 2 - 2\mathrm{Re}\{[\omega + \mu - \Sigma(\omega)]G(\omega)\}. \tag{F.8}$$

Replacing the momentum-dependent operator $W(q - q')$ by its Fourier transform. Simplifying the expression for $\bar{L}_{12}^P$ I have,

$$\begin{aligned} \bar{L}_{12}^P(i\nu_l) &= \frac{\pi T U}{2}\int_0^\beta d\tau e^{i\nu_l\tau} \sum_{qq'\sigma\sigma'} \frac{1}{N}\sum_j \mathbf{v}_{q\alpha}\mathbf{v}_{q'\beta} \\ &\times \Big[e^{-iq'\cdot\mathbf{R}_j}\langle T_\tau w_j c_{q\sigma}^\dagger(\tau)c_{q\sigma}(\tau)c_{q'\sigma'}^\dagger(0)c_{j\sigma'}(0)\rangle \\ &+ e^{iq'\cdot\mathbf{R}_j}\langle T_\tau w_j c_{q\sigma}^\dagger(\tau)c_{q\sigma}(\tau)c_{j\sigma'}^\dagger(0)c_{q'\sigma'}(0)\rangle\Big]. \end{aligned} \tag{F.9}$$

Noting that the w_j operator commutes with the Fermionic operators, allows us to use Wick's theorem to rewrite the terms in the square bracket as

$$\begin{aligned} \frac{1}{N}\sum_j \Big[&-e^{-iq\cdot\mathbf{R}_j}\langle T_\tau w_j c_{q\sigma}^\dagger(\tau)c_{j\sigma}(0)\rangle G_{q\sigma}(\tau) \\ &+ e^{iq\cdot\mathbf{R}_j}\langle T_\tau w_j c_{q\sigma}(\tau)c_{j\sigma}^\dagger(0)\rangle G_{q\sigma}(-\tau)\Big]\delta_{qq'}\delta_{\sigma\sigma'}, \end{aligned} \tag{F.10}$$

The correlation functions in Eq. (F.10) can be evaluated by taking the derivative with respect to the components of an infinitesimal field $-\sum_j h_j w_j$. These correlation functions have a factor of $\exp[-\beta H]$ in the numerator and a factor of Z in the denominator. In addition, the τ-dependence of the operators arises from factors of $\exp[\pm\tau H]$. Since the

operator w_j commutes with all Fermionic operators, it is easy to verify that the expression in Eq. (F.10) becomes

$$-\frac{1}{N}\sum_j \Big[G_{q\sigma}(\tau)\left(T\frac{\partial}{\partial h_j}+\langle w_j\rangle\right)G_{q\sigma}(-\tau) + G_{q\sigma}(-\tau)\left(T\frac{\partial}{\partial h_j}+\langle w_j\rangle\right)G_{q\sigma}(\tau)\Big]\delta_{qq'}\delta_{\sigma\sigma'}, \tag{F.11}$$

which follows by first removing the w_j operator through the derivative, then expressing the Fermionic operator at site j through a Fourier transform, and finally evaluating the Fermionic averages. Substituting this result into Eq. (F.9) I have,

$$\begin{aligned}\bar{L}^P_{12}(i\nu_l) &= -\frac{\pi T^2 U}{2N}\sum_n\sum_{q\sigma}\sum_j \mathbf{v}_{q\alpha}\mathbf{v}_{q\beta} \\ &\times \Big(\{[T\frac{\partial}{\partial h_j}+\langle w_j\rangle]G_{q\sigma}(i\omega_n)\}G_{q\sigma}(i\omega_{n+l}) \\ &+ G_{q\sigma}(i\omega_n)[T\frac{\partial}{\partial h_j}+\langle w_j\rangle]G_{q\sigma}(i\omega_{n+l})\Big).\end{aligned} \tag{F.12}$$

The derivatives need to be computed. Writing the momentum-dependent Green's function as a Fourier transform

$$G_{q\sigma}(i\omega_n) = \frac{1}{N}\sum_{i-j} e^{iq\cdot(\mathbf{R}_i-\mathbf{R}_j)}G_{ij\sigma}(i\omega_n), \tag{F.13}$$

and using the identity

$$G_{ij\sigma}(i\omega_n) = \sum_{kl} G_{ik\sigma}(i\omega_n)G^{-1}_{kl\sigma}(i\omega_n)G_{lj\sigma}(i\omega_n), \tag{F.14}$$

allows us to compute the derivative as

$$\begin{aligned}\frac{\partial}{\partial h_j}G_{q\sigma}(i\omega_n) &= \frac{1}{N}\sum_{i-j} e^{iq\cdot(\mathbf{R}_i-\mathbf{R}_j)}G_{ij\sigma}(i\omega_n) \\ &\times \frac{\partial\Sigma_{jj\sigma}(i\omega_n)}{\partial h_j}G_{jj\sigma}(i\omega_n).\end{aligned} \tag{F.15}$$

But in a homogeneous phase, the derivative of the local self energy with respect to the local field, and the local Green's function are both independent of the site j, so I finally have,

$$\frac{\partial G_{q\sigma}(i\omega_n)}{\partial h} = G_{n\sigma}\frac{\partial \Sigma_{n\sigma}}{\partial h}G_{q\sigma}(i\omega_n). \tag{F.16}$$

Since the self energy depends only on G_n and w_1, the derivative can be computed by taking partial derivatives and using the chain rule

$$\frac{\partial \Sigma_{n\sigma}}{\partial h} = \frac{\frac{\partial \Sigma_{n\sigma}}{\partial w_1}\frac{\partial w_1}{\partial h}}{1 - G_{n\sigma}^2\frac{\partial \Sigma_{n\sigma}}{\partial G_{n\sigma}}}. \tag{F.17}$$

Each of the derivatives in Eq. (F.17) can be found directly

$$\frac{\partial \Sigma_{n\sigma}}{\partial w_1} = \frac{U}{1 + G_{n\sigma}(2\Sigma_{n\sigma} - U)}, \tag{F.18}$$

$$\frac{\partial w_1}{\partial h} = \frac{w_1(1 - w_1)}{T}, \tag{F.19}$$

and

$$1 - G_{n\sigma}^2\frac{\partial \Sigma_{n\sigma}}{\partial G_{n\sigma}} = \frac{(1 + G_{n\sigma}\Sigma_{n\sigma})(1 + G_{n\sigma}[\Sigma_{n\sigma} - U])}{1 + G_{n\sigma}(2\Sigma_{n\sigma} - U)}. \tag{F.20}$$

Substituting these derivatives into Eq. (F.17) and performing some straightforward simplifications that involve the quadratic equation that the self energy satisfies finally yields

$$[T\frac{\partial}{\partial h} + \langle w\rangle]G_{q\sigma}(i\omega_n) = \frac{\Sigma_{n\sigma}}{U}G_{q\sigma}(i\omega_n). \tag{F.21}$$

Now I can perform the analytic continuation. First I substitute Eq. (F.21) into Eq. (F.12) and I note that the sum over j cancels the factor of $1/N$

$$\begin{aligned}\bar{L}_{12}^{P}(i\nu_l) &= -\frac{\pi T^2}{2}\sum_n\sum_{q\sigma}\mathbf{v}_{q\alpha}\mathbf{v}_{q\beta} \\ &\times [\Sigma_\sigma(i\omega_n) + \Sigma_\sigma(i\omega_{n+l})]G_{q\sigma}(i\omega_n)G_{q\sigma}(i\omega_{n+l}).\end{aligned} \tag{F.22}$$

Next, I rewrite the sum over Matsubara frequencies as a contour integral and perform the

analytic continuation in the exact same way as before. If I then evaluate L_{12}^P I find

$$\begin{aligned} L_{12}^P &= \lim_{\nu\to 0} -\frac{T\sigma_0}{2e^2\nu}\int_{-\infty}^{\infty} d\omega \int_{-\infty}^{\infty} d\epsilon \rho(\epsilon) \\ &\times \mathrm{Re}\Big[f(\omega)\{[\Sigma(\omega)+\Sigma(\omega+\nu)]G_q(\omega)G_q(\omega+\nu) \\ &- [\Sigma^*(\omega)+\Sigma(\omega+\nu)]G_q^*(\omega)G_q(\omega+\nu)\} \\ &+ f(\omega+\nu)\{[\Sigma^*(\omega)+\Sigma(\omega+\nu)]G_q^*(\omega)G_q(\omega+\nu) \\ &- [\Sigma^*(\omega)+\Sigma^*(\omega+\nu)]G_q^*(\omega)G_q^*(\omega+\nu)\}\Big]. \end{aligned} \tag{F.23}$$

Now the integral over ϵ can be performed and the limit $\nu \to 0$ can be taken. It becomes

$$\begin{aligned} L_{12}^P &= \frac{T\sigma_0}{e^2}\int_{-\infty}^{\infty} d\omega \left(-\frac{df(\omega)}{d\omega}\right)\Big[\mathrm{Re}\Sigma(\omega)\tau(\omega) \\ &+ 2\mathrm{Im}\Sigma(\omega)\mathrm{Im}[\{\omega+\mu-\Sigma(\omega)\}G(\omega)]\Big]. \end{aligned} \tag{F.24}$$

Adding together Eqs. (F.7) and (F.24) yields the Jonson-Mahan result of

$$L_{12} = \frac{T\sigma_0}{e^2}\int_{-\infty}^{\infty} d\omega \left(-\frac{df(\omega)}{d\omega}\right)\tau(\omega)\omega. \tag{F.25}$$

Now, I will do the derivation for the coefficient L_{22}. Like before, I separate this into pieces corresponding to the kinetic energy and the potential energy: $L_{22} = L_{22}^{KK} + L_{22}^{KP} + L_{22}^{PK} + L_{22}^{PP}$. Due to the symmetry, I have $L_{22}^{KP} = L_{22}^{PK}$. The kinetic energy piece is simple to calculate. Like in our derivation for L_{12}^K, the steps are identical to the derivation for L_{11} except I have an extra factor of $(\epsilon-\mu)^2$. Performing the integration over ϵ and collecting terms finally yields

$$\begin{aligned} L_{22}^{KK} &= \frac{T\sigma_0}{e^2}\int_{-\infty}^{\infty} d\omega \left(-\frac{df(\omega)}{d\omega}\right) \\ &\times \Big\{[\omega-\mathrm{Re}\Sigma(\omega)]^2\tau(\omega) + \mathrm{Im}G(\omega)\mathrm{Im}\Sigma(\omega) \\ &- 2[\mathrm{Im}\Sigma(\omega)]^2 + 2[\mathrm{Im}\Sigma(\omega)]^2\mathrm{Re}\{[\omega+\mu-\Sigma(\omega)]G(\omega)\} \\ &- 4[\omega-\mathrm{Re}\Sigma(\omega)]\mathrm{Im}\Sigma(\omega)\mathrm{Im}\{[\omega+\mu-\Sigma(\omega)]G(\omega)\}\Big\}. \end{aligned} \tag{F.26}$$

The derivation for $L_{22}^{KP} = L_{22}^{PK}$ is identical to that of L_{12}^{P} except I have an extra factor of $(\epsilon - \mu)$. Performing the integration over ϵ then produces

$$\begin{aligned} L_{22}^{KP} &= \frac{T\sigma_0}{e^2}\int_{-\infty}^{\infty} d\omega\left(-\frac{df(\omega)}{d\omega}\right) \\ &\times \Big\{[\omega - \mathrm{Re}\Sigma(\omega)]\mathrm{Re}\Sigma(\omega)\tau(\omega) - \mathrm{Im}G(\omega)\mathrm{Im}\Sigma(\omega) \\ &+ 2[\mathrm{Im}\Sigma(\omega)]^2 - 2[\mathrm{Im}\Sigma(\omega)]^2\mathrm{Re}\{[\omega + \mu - \Sigma(\omega)]G(\omega)\} \\ &+ 2[\omega - 2\mathrm{Re}\Sigma(\omega)]\mathrm{Im}\Sigma(\omega)\mathrm{Im}\{[\omega + \mu - \Sigma(\omega)]G(\omega)\}\Big\}. \end{aligned} \tag{F.27}$$

The final term I must evaluate is L_{22}^{PP}. I proceed by an alternate method based on the equation of motion (EOM) technique. The EOM for the Fermionic creation and annihilation operators (in the momentum basis) are

$$\frac{\partial}{\partial\tau}c_{q\sigma}^{\dagger}(\tau) = [\epsilon(q) - \mu]c_{q\sigma}^{\dagger}(\tau) + U\sum_k W(k)c_{q+k\sigma}^{\dagger}(\tau), \tag{F.28}$$

and

$$\frac{\partial}{\partial\tau}c_{q\sigma}(\tau) = -[\epsilon(q) - \mu]c_{q\sigma}(\tau) - U\sum_k W(k)c_{q-k\sigma}(\tau). \tag{F.29}$$

These EOMs can be employed to express the correlation function of the heat-current operators in terms of derivatives with respect to imaginary time as shown below

$$\begin{aligned} &\bar{L}_{22}^{PP}(i\nu_l) = \frac{\pi T U^2}{4}\int_0^{\beta} d\tau e^{i\nu_l\tau}\sum_{qq'q''q'''\sigma\sigma'} \\ &(\mathbf{v}_{q\alpha} + \mathbf{v}_{q'''\alpha})(\mathbf{v}_{q'\beta} + \mathbf{v}_{q''\beta}) \\ &\times \langle T_\tau W(q - q''')W(q' - q'')c_{q\sigma}^{\dagger}(\tau)c_{q'''\sigma}(\tau) \\ &c_{q'\sigma'}^{\dagger}(0)c_{q''\sigma'}(0)\rangle \\ &= \pi T\int_0^{\beta} d\tau e^{i\nu_l\tau}\sum_{qq'\sigma\sigma'}\mathbf{v}_{q\alpha}\mathbf{v}_{q'\beta}\lim_{\tau'\to\tau^-}\lim_{\tau'''\to\tau''^-\to 0^+} \\ &\langle T_\tau[\{\frac{1}{2}(\partial_\tau - \partial_{\tau'}) - (\epsilon_{q'} - \mu)\}c_{q'\sigma}^{\dagger}(\tau)c_{q'\sigma}(\tau')] \\ &\times [\{\frac{1}{2}(\partial_{\tau''} - \partial_{\tau'''}) - (\epsilon_q - \mu)\}c_{q\sigma'}^{\dagger}(\tau'')c_{q\sigma'}(\tau''')]\rangle. \end{aligned} \tag{F.30}$$

Now each of the operator averages can be expressed in terms of Green's functions, since

the velocity factors guarantee there will be no vertex corrections. Noting further, that the integrals will only contribute if $\alpha = \beta$ finally yields

$$\begin{aligned}
\bar{L}_{22}^{PP}(i\nu_l) &= \pi T \int_0^\beta d\tau e^{i\nu_l \tau} \sum_{q\sigma} v_{q\alpha}^2 \\
&\times \Big[\frac{1}{2} \partial_\tau G_{q\sigma}(\tau) \partial_\tau G_{q\sigma}(-\tau) - \frac{1}{4} \partial_\tau^2 G_{q\sigma}(\tau) G_{q\sigma}(-\tau) \\
&\quad - \frac{1}{4} G_{q\sigma}(\tau) \partial_\tau^2 G_{q\sigma}(-\tau) \\
&\quad + (\epsilon_q - \mu) \{ G_{q\sigma}(\tau) \partial_\tau G_{q\sigma}(-\tau) - \partial_\tau G_{q\sigma}(\tau) G_{q\sigma}(-\tau) \} \\
&\quad - (\epsilon_q - \mu)^2 G_{q\sigma}(\tau) G_{q\sigma}(-\tau) \Big].
\end{aligned} \tag{F.31}$$

I need to be able to produce expressions for the derivatives of the Green functions. I do so by first writing the Green's function as a Fourier series over the Matsubara frequencies, and then taking the derivative into the Matsubara summation. Since I am interested only in $0 < \tau < \beta$, this procedure has no convergence issues. Likewise, one is also able to take the second derivative in this fashion. I find for $0 < \tau < \beta$

$$\begin{aligned}
\partial_\tau G_{q\sigma}(\tau) &= -(\epsilon_q - \mu) G_{q\sigma}(\tau) \\
&\quad - T \sum_m e^{-i\omega_m \tau} \frac{\Sigma_{m\sigma}}{i\omega_m + \mu - \Sigma_{m\sigma} - \epsilon_q}, \\
\partial_\tau^2 G_{q\sigma}(\tau) &= +(\epsilon_q - \mu)^2 G_{q\sigma}(\tau) \\
&\quad + (\epsilon_q - \mu) T \sum_m e^{-i\omega_m \tau} \frac{\Sigma_{m\sigma}}{i\omega_m + \mu - \Sigma_{m\sigma} - \epsilon_q} \\
&\quad + T \sum_m e^{-i\omega_m \tau} \frac{i\omega_m \Sigma_{m\sigma}}{i\omega_m + \mu - \Sigma_{m\sigma} - \epsilon_q},
\end{aligned} \tag{F.32}$$

with similar formulae for $G_{q\sigma}(-\tau)$. Substituting the derivatives from Eq. (F.32) into Eq. (F.31), and then simplifying the result finally produces

$$\begin{aligned}
\bar{L}_{22}^{PP}(i\nu_l) &= -\frac{\pi T^2}{4} \sum_n \sum_{q\sigma} v_{q\alpha}^2 \\
&\times \Big[\{ \Sigma_\sigma(i\omega_n) + \Sigma_\sigma(i\omega_{n+l}) \}^2 G_{q\sigma}(i\omega_n) G_{q\sigma}(i\omega_{n+l}) \\
&\quad + \Sigma_\sigma(i\omega_{n+l}) G_{q\sigma}(i\omega_n) + \Sigma_\sigma(i\omega_n) G_{q\sigma}(i\omega_{n+l}) \Big].
\end{aligned} \tag{F.33}$$

Performing the analytic continuation and simplifying I have,

$$\begin{aligned} L_{22}^{PP} &= \frac{T\sigma_0}{e^2}\int_{-\infty}^{\infty} d\omega\left(-\frac{df(\omega)}{d\omega}\right) \\ &\times \Big\{[\mathrm{Re}\Sigma(\omega)]^2\tau(\omega) - 2[\mathrm{Im}\Sigma(\omega)]^2 + \mathrm{Im}\Sigma(\omega)\mathrm{Im}G(\omega) \\ &+ 2[\mathrm{Im}\Sigma(\omega)]^2\mathrm{Re}\{[\omega+\mu-\Sigma(\omega)]G(\omega)\} \\ &+ 4\mathrm{Re}\Sigma(\omega)\mathrm{Im}\Sigma(\omega)\mathrm{Im}\{[\omega+\mu-\Sigma(\omega)]G(\omega)\}\Big\}. \end{aligned} \tag{F.34}$$

Summing together Eq. (F.26), twice Eq. (F.27), and Eq. (F.34) gives:

$$L_{22} = \frac{T\sigma_0}{e^2}\int_{-\infty}^{\infty} d\omega\left(-\frac{df(\omega)}{d\omega}\right)\tau(\omega)\omega^2. \tag{F.35}$$

I can also generalize the original Jonson-Mahan argument to prove relations between L_{21} and L_{11} and between L_{22} and L_{12}. I begin with the generalized two-particle correlation function

$$\begin{aligned} &F_{\alpha\beta}(\tau,\tau',\tau'',\tau''') = \\ &\sum_{qq'\sigma\sigma'} \mathbf{v}_{q\alpha}\mathbf{v}_{q'\beta}\langle T_\tau c^\dagger_{q\sigma}(\tau)c_{q\sigma}(\tau')c^\dagger_{q'\sigma'}(\tau'')c_{q'\sigma'}(\tau''')\rangle. \end{aligned} \tag{F.36}$$

In the infinite-dimensional limit, the two-particle correlation function is expressed by just its bare bubble because the irreducible charge vertex has a different symmetry than $\mathbf{v}_q$. Hence, I have

$$\begin{aligned} &F_{\alpha\beta}(\tau,\tau',\tau'',\tau''') \\ &= -\sum_{q\sigma}\mathbf{v}^2_{q\alpha}\delta_{\alpha\beta}G_{q\sigma}(\tau'''-\tau)G_{q\sigma}(\tau'-\tau''). \end{aligned} \tag{F.37}$$

But

$$G_{q\sigma}(\tau) = \int d\omega A(k,\omega)e^{-\omega\tau}[1-f(\omega)], \tag{F.38}$$

for $\tau > 0$ and

$$G_{q\sigma}(\tau) = \int d\omega A(k,\omega) e^{-\omega\tau}[-f(\omega)], \tag{F.39}$$

for $\tau < 0$. Substituting into Eq. (F.37), then have

$$\begin{aligned} F_{\alpha\beta}(\tau,\tau',\tau'',\tau''') = \frac{\delta_{\alpha\beta}}{2d} \int d\epsilon \rho(\epsilon) \int d\omega \int d\omega' \\ \times \quad A(\epsilon,\omega)A(\epsilon,\omega') e^{\omega(\tau-\tau''')-\omega'(\tau'-\tau'')} f(\omega)[1-f(\omega')]. \end{aligned} \tag{F.40}$$

Using this function I can construct the relevant "polarization operators". Recalling the EOM in Eqs. (F.28) and (F.29) shows that

$$\lim_{\tau'\to\tau^-} \frac{1}{2}\left(\frac{\partial}{\partial\tau} - \frac{\partial}{\partial\tau'}\right) \sum_{q\sigma} \mathbf{v}_q c^\dagger_{q\sigma}(\tau) c_{q\sigma}(\tau') = \mathbf{j}_Q(\tau). \tag{F.41}$$

The Jonson-Mahan theorem will hold for any Hamiltonian that satisfies Eq. (F.41). The "polarization operators" then become

$$\bar{L}_{11} = \pi T \int_0^\beta e^{i\nu_l\tau} F(\tau,\tau^-,0,0), \tag{F.42}$$

for the conductivity,

$$\bar{L}_{12} = \pi T \int_0^\beta e^{i\nu_l\tau} \frac{1}{2}\left(\frac{\partial}{\partial\tau} - \frac{\partial}{\partial\tau'}\right) F(\tau,\tau',0,0), \tag{F.43}$$

(in the limit where $\tau' \to \tau^-$) for the thermopower, and

$$\begin{aligned} \bar{L}_{22} \quad = \quad \pi T \int_0^\beta e^{i\nu_l\tau} \frac{1}{4}\left(\frac{\partial}{\partial\tau} - \frac{\partial}{\partial\tau'}\right)\left(\frac{\partial}{\partial\tau''} - \frac{\partial}{\partial\tau'''}\right) \\ \times \quad F(\tau,\tau',\tau'',\tau'''), \end{aligned} \tag{F.44}$$

(in the limit where $\tau' \to \tau^-$, $\tau''' \to \tau''^-$, and $\tau'' \to 0^+$) for the thermal conductivity. Because of Eq. (F.40), the analytic continuation is trivial (one first converts from imaginary time to Matsubara frequencies and then performs the Wick rotation to the real frequency

axis), and using the identity

$$f(\omega) - f(\omega + \nu) = -f(\omega)[1 - f(\omega + \nu)][e^{-\beta\nu} - 1], \tag{F.45}$$

then I can easily compute that

$$L_{12} = \frac{T\sigma_0}{e^2} \int d\epsilon \rho(\epsilon) \int d\omega \left(-\frac{df(\omega)}{d\omega} \right) A^2(\epsilon, \omega)\omega, \tag{F.46}$$

and,

$$L_{22} = \frac{T\sigma_0}{e^2} \int d\epsilon \rho(\epsilon) \int d\omega \left(-\frac{df(\omega)}{d\omega} \right) A^2(\epsilon, \omega)\omega^2, \tag{F.47}$$

Bibliography

[1] Electron correlations in narrow energy bands. *Proceedings of the Royal Society of London A: Mathematical, Physical and Engineering Sciences 276*, 1365 (1963), 238–257.

[2] Electron correlations in narrow energy bands. ii. the degenerate band case. *Proceedings of the Royal Society of London A: Mathematical, Physical and Engineering Sciences 277*, 1369 (1964), 237–259.

[3] Abrahams, E., Anderson, P. W., Licciardello, D. C., and Ramakrishnan, T. V. Scaling theory of localization: Absence of quantum diffusion in two dimensions. *Phys. Rev. Lett. 42* (Mar 1979), 673–676.

[4] Abrahams, E., Kravchenko, S. V., and Sarachik, M. P. Metallic behavior and related phenomena in two dimensions. *Rev. Mod. Phys. 73* (Mar 2001), 251–266.

[5] Anderson, P. W. Absence of diffusion in certain random lattices. *Phys. Rev. 109* (Mar 1958), 1492–1505.

[6] Anderson, P. W. Infrared catastrophe in fermi gases with local scattering potentials. *Phys. Rev. Lett. 18* (Jun 1967), 1049–1051.

[7] Anderson, P. W. Local moments and localized states. *Rev. Mod. Phys. 50* (Apr 1978), 191–201.

[8] Apinyan, V., and Kopeć, T. K. Excitonic phase transition in the extended three-dimensional falicov–kimball model. *Journal of Low Temperature Physics 176*, 1 (Jul 2014), 27–63.

[9] Ashcroft, N., and Mermin, N. *Solid state physics*. Science: Physics. Saunders College, 1976.

[10] Ashcroft, N. W., and Mermin, N. D. Solid state physics.

[11] Baenninger, M., Ghosh, A., Pepper, M., Beere, H. E., Farrer, I., and Ritchie, D. A. Low-temperature collapse of electron localization in two dimensions. *Phys. Rev. Lett. 100* (Jan 2008), 016805.

[12] Bardeen, J., Cooper, L. N., and Schrieffer, J. R. Theory of superconductivity. *Phys. Rev. 108* (Dec 1957), 1175–1204.

[13] Barman, H. *Diagrammatic perturbation theory based investigations of the Mott transition physics*. PhD thesis, Ph. D. Thesis, Theoretical science unit, Jawaharlal Nehru centre for advanced scientific research, Bangalore, India, 2013.

[14] Barman, H., Laad, M. S., and Hassan, S. R. Realization of a "two relaxation rates" in the hubbard-falicov-kimball model. *arXiv:1611.07594* (2016).

[15] Belitz, D., and Kirkpatrick, T. R. The anderson-mott transition. *Rev. Mod. Phys. 66* (Apr 1994), 261–380.

[16] Blümer, N., and Dongen, P. G. J. V. Transport properties of correlated electrons in high dimensions. *arXiv:0303204* (2003).

[17] Bogdanovich, S., Sarachik, M. P., and Bhatt, R. N. Scaling of the conductivity with temperature and uniaxial stress in si:b at the metal-insulator transition. *Phys. Rev. Lett. 82* (Jan 1999), 137–140.

[18] Brandt, U., and Mielsch, C. Thermodynamics and correlation functions of the falicov-kimball model in large dimensions. *Zeitschrift für Physik B Condensed Matter 75*, 3 (Sep 1989), 365–370.

[19] Brandt, U., and Mielsch, C. Thermodynamics of the falicov-kimball model in large dimensions ii. *Zeitschrift für Physik B Condensed Matter 79*, 2 (Jun 1990), 295–299.

[20] Brandt, U., and Mielsch, C. Free energy of the falicov-kimball model in large dimensions. *Zeitschrift für Physik B Condensed Matter 82*, 1 (Feb 1991), 37–41.

[21] Brandt, U., and Urbanek, M. P. Thef-electron spectrum of the spinless falicov-kimball model in large dimensions. *Zeitschrift für Physik B Condensed Matter 89*, 3 (Oct 1992), 297–303.

[22] Chaikin, P., and Beni, G. Thermopower in the correlated hopping regime. *Physical Review B 13*, 2 (1976), 647.

[23] Chand, M., Mishra, A., Xiong, Y. M., Kamlapure, A., Chockalingam, S. P., Jesudasan, J., Bagwe, V., Mondal, M., Adams, P. W., Tripathi, V., and Raychaudhuri, P. Temperature dependence of resistivity and hall coefficient in strongly disordered nbn thin films. *Phys. Rev. B 80* (Oct 2009), 134514.

[24] Chung, W., and Freericks, J. K. Charge-transfer metal-insulator transitions in the spin-$\frac{1}{2}$ falicov-kimball model. *Phys. Rev. B 57* (May 1998), 11955–11961.

[25] DobrosavljeviÄĞ, V., Pastor, A. A., and NikoliÄĞ, B. K. Typical medium theory of anderson localization: A local order parameter approach to strong-disorder effects. *EPL (Europhysics Letters) 62*, 1 (2003), 76.

[26] Dobrosavljević, V., Pastor, A. A., and Nikolić, B. K. Typical medium theory of anderson localization: A local order parameter approach to strong-disorder effects. *EPL (Europhysics Letters) 62*, 1 (2003), 76.

[27] Dobrosavljevic, V., Trivedi, N., and Valles, J. *Conductor Insulator Quantum Phase Transitions*. OUP Oxford, 2012.

[28] Dobrosavljević, V., Abrahams, E., Miranda, E., and Chakravarty, S. Scaling theory of two-dimensional metal-insulator transitions. *Phys. Rev. Lett. 79* (Jul 1997), 455–458.

[29] Dongen, P. v., Majumdar, K., Huscroft, C., and Zhang, F.-C. Quantum critical point in a periodic anderson model. *Phys. Rev. B 64* (Oct 2001), 195123.

[30] Drude, P. Zur elektronentheorie der metalle. *Annalen der Physik 306*, 3 (1900), 566–613.

[31] Edwards, D. M. The breakdown of fermi liquid theory in the hubbard model: Ii. *Journal of Physics: Condensed Matter 5*, 2 (1993), 161.

[32] Falicov, L. M., and Kimball, J. C. Simple model for semiconductor-metal transitions: Smb_6 and transition-metal oxides. *Phys. Rev. Lett. 22* (May 1969), 997–999.

[33] Field, S. B., and Rosenbaum, T. F. Critical behavior of the hall conductivity at the metal-insulator transition. *Phys. Rev. Lett. 55* (Jul 1985), 522–524.

[34] Fisk, Z., and Webb, G. Saturation of the high-temperature normal-state electrical resistivity of superconductors. *Physical Review Letters 36*, 18 (1976), 1084.

[35] Freericks, J. K., Demchenko, D. O., Joura, A. V., and Zlatić, V. Optimizing thermal transport in the falicov-kimball model: The binary-alloy picture. *Phys. Rev. B 68* (Nov 2003), 195120.

[36] Freericks, J. K., and Miller, P. Dynamical charge susceptibility of the spinless falicov-kimball model. *Phys. Rev. B 62* (Oct 2000), 10022–10032.

[37] Freericks, J. K., and Zlatić, V. Thermal transport in the falicov-kimball model. *Phys. Rev. B 64* (Dec 2001), 245118.

[38] Freericks, J. K., and Zlatić, V. Exact dynamical mean-field theory of the falicov-kimball model. *Rev. Mod. Phys. 75* (Oct 2003), 1333–1382.

[39] Furukawa, T., Miyagawa, K., Taniguchi, H., Kato, R., and Kanoda, K. Quantum criticality of mott transition in organic materials. *Nature Physics 11*, 3 (2015), 221.

[40] Gefen, Y., Berkovits, R., Lerner, I. V., and Altshuler, B. L. Anderson orthogonality catastrophe in disordered systems. *Phys. Rev. B 65* (Feb 2002), 081106.

[41] Georges, A., Kotliar, G., Krauth, W., and Rozenberg, M. J. Dynamical mean-field theory of strongly correlated fermion systems and the limit of infinite dimensions. *Rev. Mod. Phys. 68* (Jan 1996), 13–125.

[42] Goldenfeld, N. *Lectures on Phase Transitions and the Renormalization Group*. Frontiers in physics. Avalon Publishing, 1992.

[43] Gruner, G. Density waves in solids. *Frontiers in Physics Perseus Pub.* (2000).

[44] Gull, E. *Continuous-time quantum Monte Carlo algorithms for fermions*. PhD thesis, 2008.

[45] Gutzwiller, M. C. Effect of correlation on the ferromagnetism of transition metals. *Phys. Rev. Lett. 10* (Mar 1963), 159–162.

[46] Haldar, P., Laad, M. S., and Hassan, S. R. Quantum critical transport at a continuous metal-insulator transition. *Phys. Rev. B 94* (Aug 2016), 081115.

[47] Haldar, P., Laad, M. S., and Hassan, S. R. Real-space cluster dynamical mean-field approach to the Falicov-Kimball model: An alloy-analogy approach. *Phys. Rev. B 95* (Mar 2017), 125116.

[48] Haule, K., and Kotliar, G. Optical conductivity and kinetic energy of the superconducting state: A cluster dynamical mean field study. *EPL (Europhysics Letters) 77*, 2 (2007), 27007.

[49] HusseyâĂŰ, N., Takenaka, K., and Takagi, H. Universality of the mott–ioffe–regel limit in metals. *Philosophical Magazine 84*, 27 (2004), 2847–2864.

[50] Imada, M., Fujimori, A., and Tokura, Y. Metal-insulator transitions. *Rev. Mod. Phys. 70* (Oct 1998), 1039–1263.

[51] Janiš, V., and Pokorný, V. Critical metal-insulator transition and divergence in a two-particle irreducible vertex in disordered and interacting electron systems. *Phys. Rev. B 90* (Jul 2014), 045143.

[52] Janis, V. A lattice model for x-ray emission and absorption: the edge singularity. *Journal of Physics: Condensed Matter 5*, 35 (1993), L425.

[53] Jarrell, M., and Krishnamurthy, H. R. Systematic and causal corrections to the coherent potential approximation. *Phys. Rev. B 63* (Mar 2001), 125102.

[54] Jonscher, A. K. Dielectric relaxation in solids. *J. Phys. D: Appl. Phys. 32* (1999), R57.

[55] Kirkpatrick, T. R., and Belitz, D. Stable phase separation and heterogeneity away from the coexistence curve. *Phys. Rev. B 93* (Apr 2016), 144203.

[56] Kotliar, G., Savrasov, S. Y., Haule, K., Oudovenko, V. S., Parcollet, O., and Marianetti, C. A. Electronic structure calculations with dynamical mean-field theory. *Rev. Mod. Phys. 78* (Aug 2006), 865–951.

[57] Kotliar, G., and Vollhardt, D. Strongly correlated materials: Insights from dynamical mean-field theory. *Physics Today 57* (2004), 53.

[58] Kramer, B., Bergmann, G., and Bruynseraede, Y. Localization, interaction, and transport phenomena. *Springer Series in Solid-State Sciences 61* (1985), p. 99.

[59] Kravchenko, S. V., Mason, W. E., Bowker, G. E., Furneaux, J. E., Pudalov, V. M., and D'Iorio, M. Scaling of an anomalous metal-insulator transition in a two-dimensional system in silicon at b=0. *Phys. Rev. B 51* (Mar 1995), 7038–7045.

[60] Kravchenko, S. V., Mason, W. E., Bowker, G. E., Furneaux, J. E., Pudalov, V. M., and D'Iorio, M. Scaling of an anomalous metal-insulator transition in a two-dimensional system in silicon at b=0. *Phys. Rev. B 51* (Mar 1995), 7038–7045.

[61] Laad, M. S., and Craco, L. Cluster coherent potential approximation for the electronic structure of disordered alloys. *Journal of Physics: Condensed Matter 17*, 30 (2005), 4765.

[62] Laad, M. S., and van den Bossche, M. Non-local effects in the fermion dynamical mean-field framework; application to the two-dimensional falicov-kimball model. *Journal of Physics: Condensed Matter 12*, 10 (2000), 2209.

[63] Landau, L. D. The theory of a fermi liquid. *Sov. Phys. JETP 3*, 920 (1957).

[64] Landau, L. D. Landau theory of fermi liquids reformulated. *Sov. Phys. JETP 8*, 70 (1959).

[65] Lange, E. Memory-function approach to the hall constant in strongly correlated electron systems. *Phys. Rev. B 55* (Feb 1997), 3907–3928.

[66] Lange, E., and Kotliar, G. Magnetotransport in the doped mott insulator. *Phys. Rev. B 59* (Jan 1999), 1800–1807.

[67] Lee, P. A., and Ramakrishnan, T. V. Disordered electronic systems. *Rev. Mod. Phys. 57* (Apr 1985), 287–337.

[68] Limelette, P., Georges, A., Jérome, D., Wzietek, P., Metcalf, P., and Honig, J. Universality and critical behavior at the mott transition. *Science 302*, 5642 (2003), 89–92.

[69] Limelette, P., Wzietek, P., Florens, S., Georges, A., Costi, T., Pasquier, C., Jérome, D., Mézière, C., and Batail, P. Mott transition and transport crossovers in the organic compound κ-(b e d t- t t f) 2 c u [n (c n) 2] c l. *Physical review letters 91*, 1 (2003), 016401.

[70] Lorentz, H. A., and Zeeman, P. in recognition of the extraordinary service they rendered by their researches into the influence of magnetism upon radiation phenomena. *was awarded the Nobel Prize* (1902).

[71] Luitz, D. J., Laflorencie, N., and Alet, F. Many-body localization edge in the random-field heisenberg chain. *Phys. Rev. B 91* (Feb 2015), 081103.

[72] Lunkenheimer, P., and Loidl, A. Response of disordered matter to electromagnetic fields. *Phys. Rev. Lett. 91* (Nov 2003), 207601.

[73] Mahan, G. *Many-Particle Physics*. Physics of Solids and Liquids. Springer, 2000.

[74] Mahmoudian, S., Tang, S., and Dobrosavljević, V. Quantum criticality at the anderson transition: A typical medium theory perspective. *Phys. Rev. B 92* (Oct 2015), 144202.

[75] Maier, T., Jarrell, M., Pruschke, T., and Hettler, M. H. Quantum cluster theories. *Rev. Mod. Phys. 77* (Oct 2005), 1027–1080.

[76] Marder, M. *Condensed Matter Physics*. Wiley, 2010.

[77] Metzner, W., and Vollhardt, D. Correlated lattice fermions in $d = \infty$ dimensions. *Phys. Rev. Lett. 62* (Jan 1989), 324–327.

[78] Milde, F., Römer, R. A., and Schreiber, M. Energy-level statistics at the metal-insulator transition in anisotropic systems. *Phys. Rev. B 61* (Mar 2000), 6028–6035.

[79] Mills, R., and Ratanavararaksa, P. Analytic approximation for substitutional alloys. *Phys. Rev. B 18* (Nov 1978), 5291–5308.

[80] Miranda, E., and DobrosavljeviÄĞ, V. Disorder-driven non-fermi liquid behaviour of correlated electrons. *Reports on Progress in Physics 68*, 10 (2005), 2337.

[81] Mooij, J. H. Electrical conduction in concentrated disordered transition metal alloys. *physica status solidi (a) 17*, 2 (1973), 521–530.

[82] Mott, N. F. *Proc. Roy. Soc. (London) A197*, 269 (1949).

[83] Mott, N. F. *Metal-Insulator Transition*. Taylor and Francis, London, 1990.

[84] Müller-Hartmann, E., Ramakrishnan, T. V., and Toulouse, G. Localized dynamic perturbations in metals. *Phys. Rev. B 3* (Feb 1971), 1102–1119.

[85] Musso, D. Introductory notes on holographic superconductors. *PoS Modave2013* (2013), 004.

[86] Nandkishore, R., and Huse, D. A. Many-body localization and thermalization in quantum statistical mechanics. *Annual Review of Condensed Matter Physics 6*, 1 (2015), 15–38.

[87] Narayan, V., Pepper, M., and Ritchie, D. A. Thermoelectric and electrical transport in mesoscopic two-dimensional electron gases. *Comptes Rendus Physique 17*, 10 (2016), 1123 – 1129.

[88] NOZIÈRES, P., and DE DOMINICIS, C. T. Singularities in the x-ray absorption and emission of metals. iii. one-body theory exact solution. *Phys. Rev. 178* (Feb 1969), 1097–1107.

[89] Onnes, H. K. âĂIJfor his investigations on the properties of matter at low temperatures which led, inter alia, to the production of liquid heliumâĂİ. *was awarded the Nobel Prize* (1913).

[90] Paalanen, M., and Bhatt, R. Transport and thermodynamic properties across the metal-insulator transition. *Physica B: Condensed Matter 169*, 1 (1991), 223 – 230.

[91] Paalanen, M. A., Graebner, J. E., Bhatt, R. N., and Sachdev, S. Thermodynamic behavior near a metal-insulator transition. *Phys. Rev. Lett. 61* (Aug 1988), 597–600.

[92] Pastor, A. A., and Dobrosavljević, V. Melting of the electron glass. *Phys. Rev. Lett. 83* (Nov 1999), 4642–4645.

[93] Pavarini, E., Koch, E., Vollhardt, D., and Lichtenstein, A. The lda+dmft approach to strongly correlated materials modeling and simulation vol. 1.

[94] Piróth, A., and Sólyom, J. *Fundamentals of the Physics of Solids: Volume 1: Structure and Dynamics*. Springer Berlin Heidelberg, 2007.

[95] Piróth, A., and Sólyom, J. *Fundamentals of the Physics of Solids: Volume II: Electronic Properties*. Fundamentals of the Physics of Solids. Springer Berlin Heidelberg, 2008.

[96] Popović, D., Fowler, A. B., and Washburn, S. Metal-insulator transition in two dimensions: Effects of disorder and magnetic field. *Phys. Rev. Lett. 79* (Aug 1997), 1543–1546.

[97] Ramakrishnan, T. V., Krishnamurthy, H. R., Hassan, S. R., and Pai, G. V. Theory of insulator metal transition and colossal magnetoresistance in doped manganites. *Phys. Rev. Lett. 92* (Apr 2004), 157203.

[98] Rohringer, G., Valli, A., and Toschi, A. Local electronic correlation at the two-particle level. *Phys. Rev. B 86* (Sep 2012), 125114.

[99] Rowlands, D. A., Staunton, J. B., and Györffy, B. L. Korringa-kohn-rostoker nonlocal coherent-potential approximation. *Phys. Rev. B 67* (Mar 2003), 115109.

[100] Sachdev, S. *Quantum Phase Transitions*. Cambridge University Press, 2001.

[101] Sachdev, S. Holographic metals and the fractionalized fermi liquid. *Phys. Rev. Lett. 105* (Oct 2010), 151602.

[102] Sato, Y., Kawasugi, Y., Suda, M., Yamamoto, H. M., and Kato, R. Critical behavior in doping-driven metal–insulator transition on single-crystalline organic mott-fet. *Nano letters 17*, 2 (2017), 708–714.

[103] Schäfer, T., Rohringer, G., Gunnarsson, O., Ciuchi, S., Sangiovanni, G., and Toschi, A. Divergent precursors of the mott-hubbard transition at the two-particle level. *Phys. Rev. Lett. 110* (Jun 2013), 246405.

[104] Schotte, K. D., and Schotte, U. Tomonaga's model and the threshold singularity of x-ray spectra of metals. *Phys. Rev. 182* (Jun 1969), 479–482.

[105] Schwiete, G., and Finkel'stein, A. M. Renormalization group analysis of thermal transport in the disordered fermi liquid. *Phys. Rev. B 90* (Oct 2014), 155441.

[106] Schwiete, G., and Finkel'stein, A. M. Thermal transport and wiedemann-franz law in the disordered fermi liquid. *Phys. Rev. B 90* (Aug 2014), 060201.

[107] Sénéchal, D., Tremblay, A.-M., and Bourbonnais, C. *Theoretical methods for strongly correlated electrons*. Springer Science & Business Media, 2006.

[108] Shapiro, B., and Abrahams, E. Scaling theory of the hall effect in disordered electronic systems. *Phys. Rev. B 24* (Oct 1981), 4025–4030.

[109] Shinaoka, H., and Imada, M. Soft hubbard gaps in disordered itinerant models with short-range interaction. *Phys. Rev. Lett. 102* (Jan 2009), 016404.

[110] Si, Q., Kotliar, G., and Georges, A. Falicov-kimball model and the breaking of fermi-liquid theory in infinite dimensions. *Phys. Rev. B 46* (Jul 1992), 1261–1264.

[111] Siegrist, T., Jost, P., Volker, H., Woda, M., Merkelbach, P., Schlockermann, C., and Wuttig, M. Disorder-induced localization in crystalline phase-change materials. *Nature materials 10*, 3 (2011), 202.

[112] Simonian, D., Kravchenko, S. V., and Sarachik, M. P. Reflection symmetry at a b=0 metal-insulator transition in two dimensions. *Phys. Rev. B 55* (May 1997), R13421–R13423.

[113] Šklovskij, B., and Ėfros, A. *Electronic Properties of Doped Semiconductors: Serge Luryi].* Springer series in solid-state sciences. Springer London, Limited, 1984.

[114] Slater, J. C. Magnetic effects and the hartree-fock equation. *Phys. Rev. 82*, 538 (1951).

[115] Sólyom, J. *Fundamentals of the Physics of Solids: Volume 3 - Normal, Broken-Symmetry, and Correlated Systems*. Theoretical Solid State Physics: Interaction Among Electrons. Springer Berlin Heidelberg, 2010.

[116] Soven, P. Coherent-potential model of substitutional disordered alloys. *Phys. Rev. 156* (Apr 1967), 809–813.

[117] Terletska, H., Vučičević, J., Tanasković, D., and Dobrosavljević, V. Quantum critical transport near the mott transition. *Phys. Rev. Lett. 107* (Jul 2011), 026401.

[118] Thouless, D. Electrons in disordered systems and the theory of localization. *Physics Reports 13*, 3 (1974), 93 – 142.

[119] Tomczak, J. M., and Biermann, S. Optical properties of correlated materials: Generalized peierls approach and its application to vo_2. *Phys. Rev. B 80* (Aug 2009), 085117.

[120] van der Marel, D., Molegraaf, H. J. A., Zaanen, J., Nussinov, Z., Carbone, F., Damascelli, A., Eisaki, H., Greven, M., Kes, P. H., and Li, M. Quantum critical behaviour in a high-tc superconductor. *Nature 425* (September 2003), 271–274.

[121] VAN DONGEN, P. G. J. Exact mean field theory for correlated lattice fermions in high dimensions. *Modern Physics Letters B 05*, 13 (1991), 861–869.

[122] van Dongen, P. G. J. Exact mean-field theory of the extended simplified hubbard model. *Phys. Rev. B 45* (Feb 1992), 2267–2281.

[123] van Dongen, P. G. J., and Vollhardt, D. Exact mean-field hamiltonian for fermionic lattice models in high dimensions. *Phys. Rev. Lett. 65* (Sep 1990), 1663–1666.

[124] van Dongen, P. G. J., and Vollhardt, D. Exact mean-field hamiltonian for fermionic lattice models in high dimensions. *Phys. Rev. Lett. 65* (Sep 1990), 1663–1666.

[125] Velický, B. Theory of electronic transport in disordered binary alloys: Coherent-potential approximation. *Phys. Rev. 184* (Aug 1969), 614–627.

[126] Villagonzalo, C., Römer, R., and Schreiber, M. Transport properties near the anderson transition. *Ann. Phys. [Leipzig] 08*, SI (1999), 269–272.

[127] Zlati, V., Freericks, J.-K., LemaÅĎski, R., and Czycholl, G. Exact solution of the multicomponent falicov-kimball model in infinite dimensions. *Philosophical Magazine Part B 81*, 10 (2001), 1443–1467.

[128] Zotos, X., Naef, F., and Prelovsek, P. Transport and conservation laws. *Phys. Rev. B 55* (May 1997), 11029–11032.